The Role of Hsp20 in Alzheimer's Disease

By

Ryan Thomas Cameron

A thesis submitted in fulfilment of the requirements for the Degree of

Doctor of Philosophy

In

Molecular & Cellular Biology

Institute of Cardiovascular & Medical Sciences

College of Medical, Veterinary & Life Sciences

University of Glasgow

Scotland

September 2013

This thesis is dedicated to

my Wife & Son...

Table of Contents

Abstract

Alzheimer's disease is the most common of the degenerative brain diseases and is characterised by impairment of cognitive function. Patients with this disorder lose the ability to encode new memories. Eventually, both declarative and non-declarative memory is significantly impaired, resulting in the capacity for reasoning, abstraction and language becoming progressively reduced. Alzheimer's disease and other dementias have devastating effects on families and caregivers, and is an increasing burden in an ageing society. It is estimated that 36 million people worldwide are living with dementia and this figure is expected to double every 20 years. The worldwide costs of dementia in 2010 were estimated to be $604 billion, an exorbitant figure that represents 1% of global GDP (World Alzheimer Report 2011).

Alzheimer's disease is the fourth leading cause of death in industrialised nations, preceded by cardiovascular disease, cancer and stroke. As yet there are currently no disease-modifying drugs approved to treat Alzheimer's disease. The therapeutics that are available only temporarily alleviate symptoms of cognitive impairment, however, they do not halt the inevitable progression of the disease. As such, major scientific efforts are underway in order to develop drugs which can help stabilise the disease. The publication of the "Amyloid Hypothesis" by Dennis Selkoe in 1991 helped to focus research efforts towards a causative protein involved in the disease, the amyloid β protein (Aβ).

Aggregation and deposition of the Aβ protein is fundamental in the aetiology of Alzheimer's disease and its importance has been demonstrated by a number familial heterogeneous mutations in the amyloid precursor protein that promote increased Aβ deposition, resulting in early onset phenotypes. There are several other aspects involved in disease progression such as neuroinflammation and aberrant neuronal signalling, however, therapies targeting amyloid β aggregation have the potential to slow or even halt further neurodegeneration and anti-Aβ therapies are regarded as a logical approach to treating Alzheimer's disease.

Several endogenous pathways exist to prevent protein misfolding and subsequent aggregation following stressful cellular conditions. One pathway includes the amateur chaperones of the small heat-shock protein family, which have recently garnered interest due to their ability to inhibit the aggregation of amyloid-like proteins. In particular, Hsp20 was previously identified as having the ability to inhibit the aggregation of Aβ and could

attenuate subsequent toxicity associated with Aβ peptides. Hsp20 was of particular interest to the Baillie group as it has well established cardio-protective functions, which are triggered by the phosphorylation of a serine residue (S16) at a consensus protein kinase A/G site. Hsp20 "activity" can therefore be readily modulated via inhibition of second messenger signal degradation by phosphodiesterases.

The first part of this thesis investigated the interaction between Hsp20 and Aβ using Peptide Array technology. This technique allowed rapid characterisation of interacting domains and pinpointed key residues that mediated the protein-protein interaction. Using this approach, I demonstrated that the domain within Hsp20 that interacted with Aβ included the consensus PKA phosphorylation site (R-R-X-S). Upon introduction of a phospho-serine residue or a phospho-mimetic substitution, I was able to show that the binding of Aβ was enhanced. Reciprocal peptide array experiments highlighted that Hsp20 bound to a domain within Aβ, which is key to the aggregation of the Aβ peptide and is required to produce the higher order toxic Aβ species. The Peptide Array data was then verified using full-length recombinant proteins and several Hsp20 mutants were developed including a phospho-mimetic. The phospho-mimetic Hsp20 was shown to outperform the wild-type variant in several assays such as, *in vitro* pull-down assays, Aβ aggregation measured using nuclear magnetic resonance spectroscopy, and also a novel Aβ aggregation assay which can differentiate between two distinct aggregation pathways, namely fibrillisation and oligomerisation. These data demonstrated for the first time how the interaction between Hsp20 and Aβ may be modulated by cell signalling cascades.

I then moved to investigate the cytotoxicity of Aβ in order to investigate whether increasing Hsp20 expression in neuronal-like cells would confer protection against Aβ-mediated toxicity. This was initially carried out using a standard MTT-based cell viability assay, before utilising a real-time cell monitoring device to develop a novel Aβ toxicity assay. In both assays, increasing Hsp20 expression was shown to be cytoprotective. The wild-type variant of Hsp20 was found to be more effective in cell-based assays due to increased levels of phosphorylated Hsp20. The real-time Aβ toxicity monitoring assay also gave me a platform for testing agents with potential neuroprotective properties.

Given that increasing levels of phosphorylated Hsp20 could attenuate Aβ-mediated cytotoxicity, I logically was drawn to study ways that this event could be targeted therapeutically. Several drugs that target cAMP- and cGMP-dependent phosphodiesterases have been shown to be effective in alleviating symptoms of Alzheimer's disease in rodent

models have also been studied here in cellular systems. These included the "blockbuster" PDE5 inhibitor Viagra® (sildenafil), two novel compounds which selectively inhibit PDE9, which were developed by the pharmaceutical company Lundbeck specifically as Alzheimer's treatments, and rolipram, a well established cognitive enhancer that was developed originally as an anti-depressant. All of these compounds were shown to "activate" endogenous Hsp20 to varying degrees in neuronal-like cells and the levels of Hsp20 activation was found to correlate with both the level of induced Hsp20/Aβ co-localisation, and subsequent attenuation of Aβ-mediated cytotoxicity. This suggests that this endogenous protection pathway can be targeted by currently available therapeutics in order to reduce the neurotoxic effects of Aβ.

Finally, we wanted to develop novel agents of our own that could promote Hsp20 phosphorylation. To do this, *in silico* docking of all FDA approved drugs against the catalytic domain of PDE4 was undertaken in an attempt to find a novel compound with the potential to reposition as an Alzheimer's treatment. Using this methodology we discovered an angiotensin converting enzyme inhibitor, moexipril to be a PDE4 inhibitor in the low micro molar range. Unfortunately, moexipril works as an ACE inhibitor in the low nano molar range making repositioning unviable. However, moexipril treatment was more effective than rolipram in reversing Aβ toxicity and I speculate that this may be due to the sub-family selective nature of its (moexipril) PDE4 inhibition. Furthermore, the lack of emetic side effects associated with moexipril makes this compound an ideal starting point for the development of isoform selective and/or non-emetic PDE4 inhibitor.

In summary, these studies describe a novel endogenous mechanism for combating the toxic effects of the Aβ protein, which underpins the development and progression of Alzheimer's disease. Given that the interaction between Hsp20 and Aβ can be manipulated via cAMP/cGMP signalling, the interaction could be targeted therapeutically. As there are currently no effective drugs on the market for stabilising Alzheimer's disease, I believe that the data presented here opens up a potential new avenue that could lead to the development of a new class of AD drugs.

Author's Declaration

I hereby declare that the work presented within this thesis has been conducted by myself, unless otherwise cited or acknowledged. The work is entirely of my own composition and has not been submitted, in whole or in part, for any other degree at the University of Glasgow or any other institution.

Ryan Cameron

September 2013

Acknowledgements

I would like to express my eternal gratitude to my supervisor, Prof George Baillie for giving me the opportunity to work on such an exciting and fulfilling project. I would also like to thank him for his guidance and enthusiasm throughout my PhD project, I have thoroughly enjoyed the experience.

I would also like to thank all the past and present members of the Gardiner Lab for all their technical knowledge and assistance throughout my PhD, with particular mention for Ruth Macleod and Jane Findlay for peptide arrays, Lucien Gibson and Helen Edwards for the Hsp20 constructs and Jon Day for his assistance with phosphodiesterase activity assays.

I would like to thank Prof Manuela Zaccolo for hosting me in my rotation year and teaching me all aspects of FRET for measuring second messenger signalling pathways. I would also like to thank Dr Brian O Smith for his assistance with the NMR studies and Stephen Quinn and Carlos Penedo for forming such a successful collaboration for studying Aβ aggregation.

I am forever indebted to the Biotechnology and Biological Sciences Research Council for funding my 4 year PhD studentship and also to the University of Glasgow for providing such a fantastic setting for both my undergraduate studies and postgraduate research.

I would like thank my family and friends for their outstanding support over the last 8 years, as I embarked on this radical career change. I have never looked back. A massive thanks to my Mum and Dad, your help and assistance over the years is greatly appreciated. Most of all I would like to thank my loving and supportive wife, who has been an inspiration to me throughout this period, especially when I have been difficult more often than not. Your words of "encouragement" have been a relentless source of motivation. Finally, thank you to my amazing baby boy Connor, your smiles give me the strength to strive further, I am truly blessed.

Conabor Praecurrere...

List of Figures

List of Tables

Abbreviations

Aβ – Amyloid β

Aβscr - Amyloid β scrambled

AD – Alzheimer's disease

ADDL – Amyloid derived diffusible ligand

APP – Amyloid precursor protein

cAMP - 3',5'-cyclic adenosine monophosphate

cDNA – Complementary DNA

CFP – Cyan fluorescent protein

cGMP - 3',5'-cyclic guanosine monophosphate

CNG – Cyclic nucleotide-gated channel

DMSO - Dimethyl sulfoxide

ECL – Enhanced chemiluminescence

Epac – Exchange protein activated by cAMP

FAD – Familial Alzheimer's disease

FRET – Förster/fluorescence resonance energy transfer

FSK - Forskolin

Hsp20 - Heat shock protein 20

HUGO – Human Genome Organisation

IBMX – 3-isobutyl-1-methylxanthine

IC_{50} – Inhibitory concentration 50%

LTP – Long-term potentiation

MTT - 3-(4,5-dimethylthiazol-2-yl)-2,5-diphenyltetrazolium bromide

mRNA – Messenger RNA

NO – Nitric Oxide

PDE - Phosphodiesterase

PKA - Protein kinase A

PKG – Protein kinase G

sHSP – Small heat shock protein

siRNA - Small interfering RNA

WT - Wild-type

YFP – Yellow fluorescent protein

Publications

Quinn SD, Dalgarno PA, **Cameron RT**, Hedley GJ, Hacker C, Lucocq JM, Baillie GS, Samuel ID, Penedo JC (2014) *Real-time probing of β-amyloid self-assembly and inhibition using fluorescence self-quenching between neighbouring dyes.* Mol Biosyst. 2014 Jan;10(1):34-44.

Cameron, R. T., R. G. Coleman, et al. (2013) *Chemical informatics uncovers a new role for moexipril as a novel inhibitor of cAMP phosphodiesterase-4 (PDE4).* Biochem Pharmacol 85(9): 1297-305.

Zarros, A., **R. T. Cameron**, et al. (2013) *Evaluating the suitability of postnuclear supernatants as in vitro models for assessing cadmium- and other xenobiotic-induced neurotoxicity on crucial enzymatic parameters.* Biol Trace Elem Res 152(3): 297-9.

Cameron, R.T., and Baillie, G.S. (2012) *cAMP-specific phosphodiesterase: modulation, inhibition and activation. In: Botana, L.M. and Loza, M. (eds.) Therapeutic Targets: Modulation, Inhibition, and Activation.* John Wiley & Sons Ltd, Hoboken, N.J. ISBN 9780470587195

H.V. Edwards, **R.T. Cameron**, G.S. Baillie (2011) *The emerging role of Hsp20 as a multifunctional protective agent.* Cellular Signalling 23 (2011) 1447–1454

Conferences

xCELLigence (Roche) Global User Conference
Stockholm, Sweden, June 20-21, 2012

xCELLigence (Roche) UK User Conference
University of Glasgow, UK, June 18-19, 2012

SULSA Annual Research Symposium 2012
University of Edinburgh, UK, June 11, 2012

Tenovus Scotland 30th Anniversary Symposium – Molecular Mechanisms of Disease
University of Glasgow, UK, June 6-7, 2012

Gordon Research Conference - Cyclic Nucleotide Phosphodiesterases - A Molecular Exploration of Cyclic-Nucleotide Action
Renaissance Tuscany, Italy, May 20-25, 2012

Signalling 2011: A Biochemical Society Centenary Celebration
University of Edinburgh, UK, June 8-10, 2011
1st Prize in Poster Competition

Peptide Arrays as Tools for Study of Protein Interactions,
London, UK, March 15-16, 2011
1st Prize in Poster Competition

1 Introduction

1.1 Alzheimer's disease

Alzheimer's disease (AD) is the most common form of dementia in the elderly and accounts for between 50-75% of all cases. By 2030 it is estimated that more than 65 million people will be living with dementia, with projections almost doubling every 20 years (Alzheimer's report 2009). AD is a progressive neurological disease, which results in the loss of neurons, mainly in the cortex and the hippocampus (Nussbaum and Ellis 2003). The clinical symptoms of the disease include erosion of memory, reduction in decision-making ability and a decline in cognitive capacity. AD is regarded as a disorder of cognitive awareness, one of the fundamental components of human consciousness (Carter, Simms et al. 2010).

In addition to its role in neuro-degeneration, AD is the fourth leading cause of death in industrialised nations, preceded by cardiovascular disease, cancer and stroke. It affects all ethnic groups and occurs slightly more in females than males (Nussbaum and Ellis 2003). AD has become the most socially disruptive disease of the ageing population and has an associated socio- and economic- burden, which has resulted in major efforts by the scientific community to develop therapeutic agents to prevent the progression of the disease. However, as yet, there are no currently available drugs that can halt or even stabilise disease progression, though there is hope, as a number of potential treatments are currently undergoing clinical trials.

1.2 Discovery of Alzheimer's disease

Senile dementia had been shown since the 1800's to be associated with an obvious atrophy in the brain when compared with aged matched control brains. Historically, cerebral atrophy has been a consistent characteristic of demented brains and was associated with a gradual strangulation of the blood supply that resulted in a stroke-like pathology (Berchtold and Cotman 1998). Using an improved silver staining method, Bielschowsky (1903) visualised cellular components of neurons and was able to identify thread-like structures, which he named neurofibrils. In 1907, Alois Alzheimer also using Bielschowsky's silver staining method described a new pathology in a woman who had died at the age of 51 after developing clinically unusual dementia. The novel pathological features observed by Alzheimer included tangles of fibrils within the cytoplasm of neurons

which accompanied neuronal cell death and a widespread plaque-like pathology similar to what had previously been described for senile dementia. At that time, the pathological presentations of the disease were distinct from any previously described because of the age of onset, rapid progression of the disease, unique neuropathological features and the severity of the lesions. In the years following Alzheimer's findings, several cases of pre-senile dementia were reported also presenting neuropathological features such as plaques and neurofibrillar tangles and several of these reports referred to the condition as "Alzheimer's Disease". However, official endorsement is often attributed to the most eminent psychiatrist in the world at that time, Emil Kraepelin (Berchtold and Cotman 1998).

The source and constitution of plaques and neurofibrillary tangles (NFTs) remained controversial for several decades, however, some advances were made in 1927 when the substance in plaques was identified as "amyloid" due to green birefringence of polarized light following Congo red staining (Divry 1927). Amyloids were already familiar with pathologists, with accumulation associated with age, chronic infection and chronic inflammation. With the onset of electron microscopy in the 1950's ultrastructural studies of amyloid showed that plaques consisted of a central fibrillar core, whereas neurofibrillary tangles found in both senile dementia and AD represented neurofilaments joined together in a helical fashion. It was proposed that these twisted tubules interfered with normal neuronal function resulting in neuronal cell death (Berchtold and Cotman 1998).

Despite ultrastructural analysis of plaques and NFTs suggesting cellular elements being involved, their constituent materials were not elucidated until the 1980's. A study by Glenner & Wong (1984), isolated highly enriched amyloid fibres from meningeal vessels of AD patients. Using gel electrophoresis, they identified a unique protein band in the AD patients that was not present in aged matched controls. A protein of around 4.2 kDa was partially sequenced and residues 1-24 were identified. At that time the protein identified, named β-amyloid (Aβ) due to its partial β-pleated sheet structure, shared no homology with any protein sequence known (Glenner and Wong 1984). Further studies demonstrated that the protein was a monomer of about 40 residues. The self aggregating 4kDa monomer also termed A_4 readily formed dimers A_8, tetramers A_{16} and hexadecamers A_{64} (Masters, Multhaup et al. 1985; Masters, Simms et al. 1985). Another study which isolated the low molecular weight oligomers from amyloid plaques highlighted an amino acid composition which was approximately 50% hydrophobic. Plaque fibres were highly insoluble and resistant to a number of proteinases. In addition, antibodies raised against the low

molecular weight component of amyloid, selectively labelled plaques and vascular deposits from AD brains but did not stain NFTs. This gave rise to the suggestion that plaques and NFTs were distinct in their constituent parts (Selkoe, Abraham et al. 1986). The core component of NFTs was later found to be the microtubule-associated protein tau (Goedert, Wischik et al. 1988; Wischik, Novak et al. 1988; Wischik, Novak et al. 1988).

The peptide isolated from the plaques of AD patients was shown to be homologous to the peptide seen in aged Down's syndrome (DS) patients, a disease characterised by trisomy of chromosome 21. It was known that all DS patients over the age of 40 had almost 100% penetrance of Alzheimer's related cerebral dysfunction and neuropathological lesions. Therefore trisomy 21 was seen as an early human model for AD and suggested that genetic defects initiating AD, whether acquired or hereditary, would localise to chromosome 21 (Glenner and Wong 1984). Southern blotting experiments using cDNA from the amyloid peptide sequence found that trisomy 21 patients had 1.5-fold increase in gene dosage relative to normal patients (Podlisny, Lee et al. 1987). Indeed, subsequent cloning using cDNA probes based on the amyloid peptide sequence, identified the amyloid precursor protein (APP) which localised to human chromosome 21 and implied direct genetic linkage between AD and DS (Kang, Lemaire et al. 1987), (Tanzi, Gusella et al. 1987),(Goldgaber, Lerman et al. 1987) (Robakis, Ramakrishna et al. 1987). Further evidence of genetic linkage between AD and neuropathological lesions in trisomy 21 was highlighted in a rare case of DS where the distal location of chromosome 21q resulted in the patient being diploid for the APP gene. This individual showed no signs of dementia or deposition of amyloid upon their death at the age of 78 (Prasher, Farrer et al. 1998).

1.2.1 Amyloid Precursor Protein

APP is a type 1 trans-membrane glycoprotein with homologous proteins found in *C. elegans*, *Drosophila,* and highly conserved among mammals. APP is expressed in a variety of different tissues but is most abundant in the brain. There are three main splice variants that encode the Aβ peptide, APP695, APP751 and APP770. The latter two isoforms contain an extracellular Kunitz domain with protease inhibitor properties. The APP695 variant does not contain the Kunitz domain and is the form found predominantly in neurons (Zheng and Koo 2006).

APP is sequentially processed by three main proteases known as α-, β-, γ-secretases. Cleavage by α- and β-secretase occurs in the extracellular domain, resulting in the release

of large soluble APP derivatives known as sAPPα and sAPPβ respectively. This process results in membrane-tethered α- and β- C-terminal fragments (CTFs). The main neuronal β-secretase is a transmembrane aspartyl protease known as β-site APP cleavage enzyme (BACE1). Cleavage at the α-site can be facilitated by several zinc metalloproteinases resulting in non-amyloidogenic processing of APP. Following the extracellular cleavage of APP at the c-terminal end of Aβ, γ-secretase is responsible for the processing of CTFs to produce either Aβ, in co-ordination with BACE1 cleavage, or a 3kDa product known as P3 in co-ordination with α-secretase. γ-secretase cleavage is facilitated by a complex of proteins that includes; presenilin, nicastrin, anterior pharynx defective (APH1) and presenilin enhancer (PEN2). Finally, a neutral endopeptidase known as neprilysin can degrade monomeric Aβ peptides prior to aggregation (Zheng and Koo 2006) (Figure 1.1).

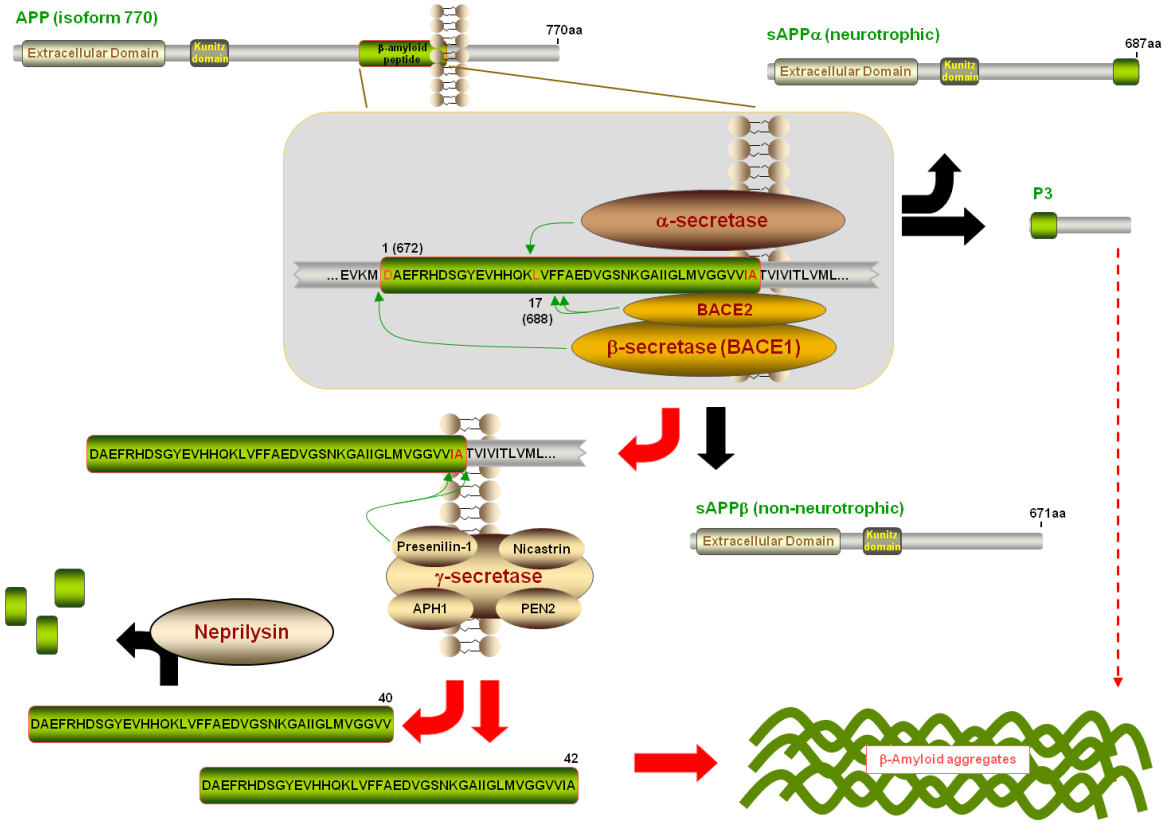

Figure 1.1 – Amyloid Precursor Protein Processing.
The sequential proteolytic degradation of APP which results in the release soluble APP peptides involved in signalling and the generation of Aβ peptides which ultimately lead to the progression of AD. Black arrows represent non-amyloidogenic processing of APP, red arrows represent amyloidogenic pathway.

Soon after the discovery of the APP gene, an autosomal dominant form of cerebral amyloid angiopathy (CAA), known as human hereditary cerebral haemorrhage with amyloidosis of the Dutch type (HCHWA-D), pointed towards a polymorphism in the APP gene. This mutation results in missense, where glutamic acid at position 693 (APP770 numbering) is substituted for glutamine (E693Q) (Van Broeckhoven, Haan et al. 1990).

Since this initial discovery, several other familial AD (FAD) associated with intra-Aβ mutations have been discovered including, E693K (Italian) (Tagliavani et al. 1999), E693G (Arctic) (Kamino, Orr et al. 1992), D694N (Iowa) (Grabowski, Cho et al. 2001), and A692G (Flemish) (Hendriks, van Duijn et al. 1992). While the Flemish mutation induces a two-fold increase in $A\beta_{1-40}$ and $A\beta_{1-42}$ production due to reduced α-secretase activity (Figure 1.2) the Dutch and Iowa mutations do not alter levels of $A\beta_{1-40}$ or $A\beta_{1-42}$ relative to wild-type APP but are associated with accelerated fibril formation and increased pathogenicity from the resulting Aβ peptides (Haass, Hung et al. 1994), (Wisniewski, Ghiso et al. 1991; De Jonghe, Zehr et al. 1998), (Van Nostrand, Melchor et al. 2001).

Several other FAD associated missense mutations in APP have been characterised that induce changes in APP processing resulting in increased Aβ production (Figure 1.2). The most notable of these are the KM670/671NL (Swedish) mutation and mutations at valine 717 which includes V717I (London) and V717F (Indiana) which frame the Aβ sequence (Mullan, Crawford et al. 1992), (Goate, Chartier-Harlin et al. 1991), (Murrell, Farlow et al. 1991). The Swedish double mutation at the β-secretase cleavage site results in a 6-8-fold increase in secreted Aβ peptide levels compared to wild-type APP. This increase in Aβ production is associated with a shift away from α-secretase towards β-secretase cleavage, as both proteases directly compete for the APP substrate within the same cellular compartment. Increased β-secretase shifts the equilibrium towards amyloidogenic over the non-amyloidogenic processing of APP (Citron, Vigo-Pelfrey et al. 1994), (Haass, Lemere et al. 1995). Mutations in the vicinity of the γ-secretase cleavage site also result in increased $A\beta_{1-42}$ production over the less toxic $A\beta_{1-40}$. Intriguingly, an increase in the ratio of $A\beta_{1-42}$ to $A\beta_{1-40}$ has been shown to inversely correlate with the age of AD onset (De Jonghe, Esselens et al. 2001).

In addition to missense mutations in APP that increase deposition of amyloid, there have been familial mutations characterised in components of the processing machinery that can promote increased production of $A\beta_{1-42}$ peptides leading to aggressive early onset forms of AD. These include presenilins (Citron, Westaway et al. 1997) and neprilysin (Iwata, Higuchi et al. 2005). In light of the large number of mutations in FAD that are all directly associated with increased production of Aβ peptides and increased amyloid deposition, the "Amyloid hypothesis" was developed by Dennis Selkoe, an early pioneer in AD research (Selkoe 1991).

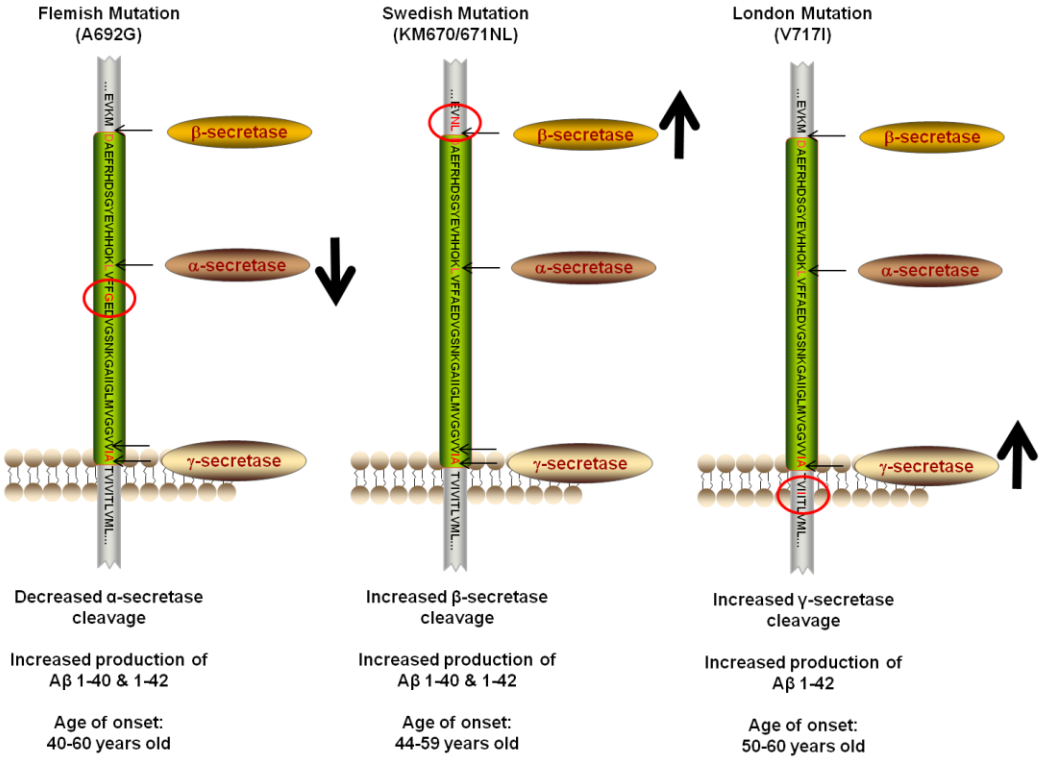

Figure 1.2 – Familial APP mutations that alter APP processing.
Examples of APP mutations which alter its interactions with secretases leading to increased production of Aβ peptides. Familial mutations in the APP gene ultimately result in early onset AD.

1.2.2 The Amyloid Hypothesis

The amyloid cascade hypothesis was originally developed by Selkoe in 1991 and supported by Hardy & Allsop (1991). Both groups recognised that the deposition of amyloid is the key event in the aetiology of AD neuropathology (Summarised in figure 1.3) (Hardy and Allsop 1991; Selkoe 1991). Prior to the discovery of Aβ and cloning of APP, scientists believed that amyloid deposition was a "tombstone" event rather than a causative factor of AD. There are several key factors which support the causative role of Aβ in the development of AD. First, is the localisation of the *APP* gene to chromosome 21 with AD penetrance almost 100% in aged DS patients and this not being apparent in a rare form of DS (discussed previously). Secondly, synthetic Aβ peptides are toxic to hippocampal and cortical neurons *in vivo* and *in vitro* (Pike, Walencewicz et al. 1991; Lambert, Barlow et al. 1998; Hoshi, Sato et al. 2003; Deshpande, Mina et al. 2006). Thirdly, FAD associated mutations, which increase production of Aβ through altered processing (figure 1.2), all result in early onset AD (Wisniewski, Ghiso et al. 1991; De Jonghe, Zehr et al. 1998; Van Nostrand, Melchor et al. 2001). Fourth, familial mutations within presenilin 1 and 2 alter the ratio of $A\beta_{1\text{-}42}$ to $A\beta_{1\text{-}40}$ resulting in aggressive forms of AD (Bentahir, Nyabi et al. 2006) (Kumar-Singh, Theuns et al. 2006). Fifth, transgenic

mice carrying mutant human APP display a gradual increase in Aβ accumulation over time and have behavioural phenotypes similar to those seen in AD patients (Ashe 2005). Lastly, co-expression of mutant APP with mutant tau accelerates tau hyperphosphorylation leading to the development of neurofibrillary tangles (Oddo, Caccamo et al. 2003; Walsh and Selkoe 2007).

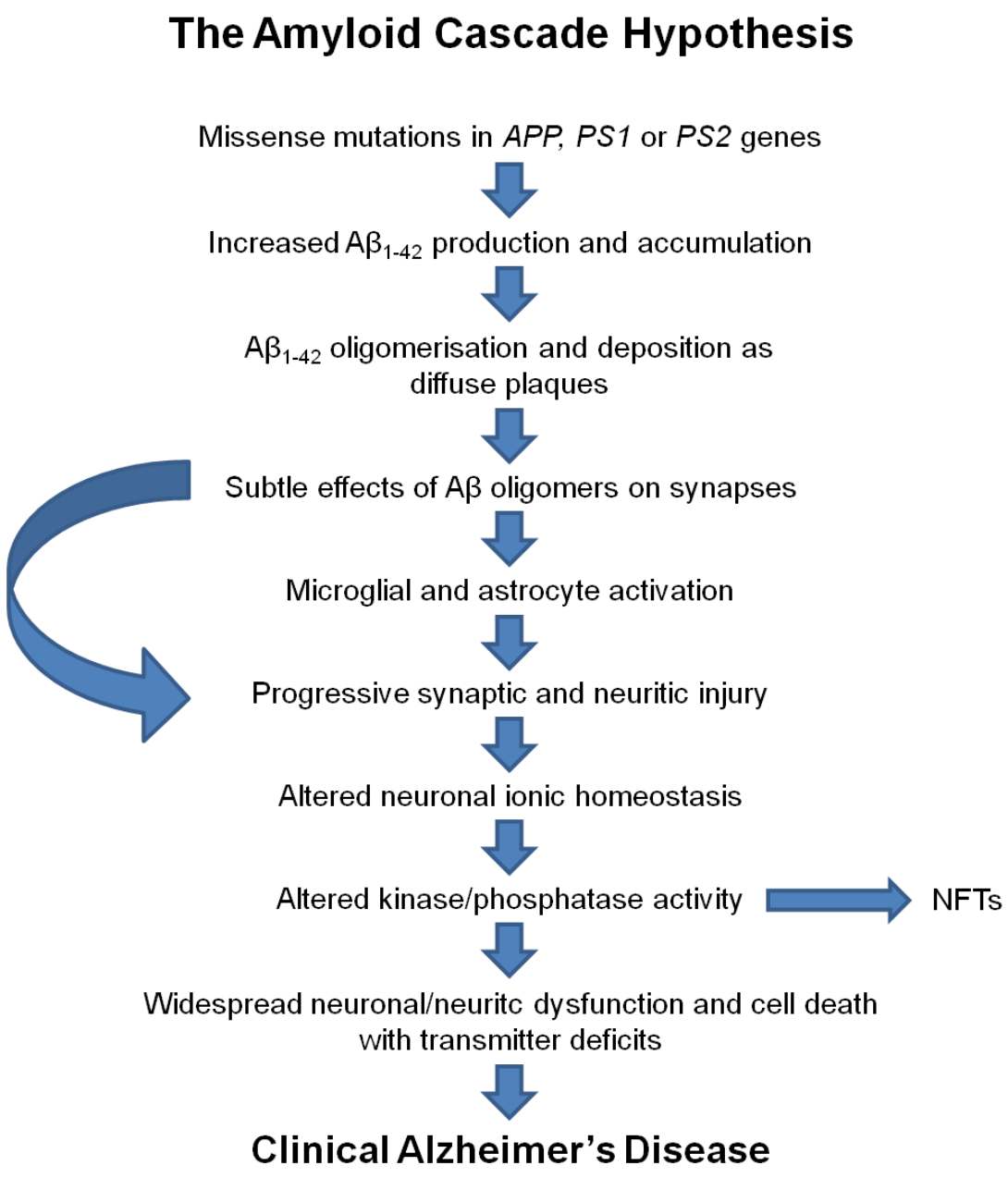

Figure 1.3 – The Amyloid Cascade Hypothesis.
The amyloid cascade hypothesis describes the sequence of events initiated by Aβ that ultimately proceeds to neuronal cell death and cognitive impairment associated with AD. Adapted from (Hardy and Selkoe 2002).

Despite convincing evidence supporting the amyloid hypothesis, controversy surrounds the model, as there are several aspects that are not consistent with Aβ being the key causative

agent in AD progression. The main factor against the amyloid hypothesis is that the number of insoluble fibrillar plaques in the brain does not fully correlate with the severity of dementia. Instead, loss of synaptic density is the strongest marker for cognitive impairment. Surprisingly, in several studies, amyloid plaques are apparent in control samples from humans who display no evidence of cognitive decline (Katzman 1986; DeKosky and Scheff 1990; Terry, Masliah et al. 1991; Dickson, Crystal et al. 1995). Other investigations have also found stronger correlation with soluble Aβ peptide density and synaptic loss/severity of cognitive impairment suggesting that insoluble fibrils may not be the key mediators of toxicity (McLean, Cherny et al. 1999; Wang, Dickson et al. 1999).

A major sticking point for the amyloid hypothesis is the lack of a way to isolate specific neurotoxic species of Aβ and characterise their effects *in vivo*. Early studies have demonstrated that aggregation of Aβ is essential to induce cytotoxic effects. Freshly prepared synthetic $A\beta_{1-42}$ peptide is monomeric and has neurotrophic effects on hippocampal neurons whereas $A\beta_{1-42}$ peptide aged for several days at physiological conditions, results in its aggregation and subsequent neurotoxicity (Pike, Walencewicz et al. 1991). Similar studies have been carried out on $A\beta_{1-40}$ and the consensus is that experimental protocols that fail to induce the peptides to form amyloid deposits also demonstrate a lack of neurotoxicity. These results suggest that conformation of the Aβ peptides is the key determinant of neurotoxicity. It was also noted that differences in Aβ peptide preparation is likely to account for major variations in the peptide's potency (Busciglio, Lorenzo et al. 1992). Another twist has been introduced more recently by studies which propose soluble oligomeric species of Aβ as being the main driver of neurotoxicity and synaptic dysfunction (Hardy and Selkoe 2002) as opposed to monomeric or insoluble amyloid fibrils.

Soluble intermediate species of synthetic Aβ are made up of several distinct conformations that have differential neurotoxic effects on cultured neurons. These include, higher molecular weight complexes known as Aβ-derived diffusible ligands (ADDLs), oligomers composed of 15-20 monomers (AβOs), protofibrils, and dodecameric oligomers Aβ*56 (Walsh, Lomakin et al. 1997; Lambert, Barlow et al. 1998; Kayed, Head et al. 2003; Lesne, Koh et al. 2006). The toxic effects of ADDLs, AβOs and Aβ fibrils were tested in parallel on human cortical neurons. The majority of ADDLs and AβOs were found to rapidly localise to synapses, while the remaining populations were found to co-localise with cellular membranes, suggesting that soluble Aβ species may initiate toxicity at multiple cellular locations. The acute toxic effect of AβOs resulted in the activation of

mitochondrial death pathways, caspase activation and nuclear condensation. Whereas ADDLs required five times longer to induce similar toxic effects and Aβ fibrils required chronic incubation for ten days to trigger this response (Deshpande, Mina et al. 2006).

Various endogenous Aβ species have been isolated from the human brain but their precise assemblies have not been fully characterised. Using a variety of size exclusion techniques, it has been shown that both control and AD patient's brains contain a continuous distribution of Aβ species ranging from monomers to high molecular weight species over 100 kDa (Roher and Kuo 1999). However, while low-n SDS-stable oligomers have been detected in the supernatant of AD brain tissue (McLean, Cherny et al. 1999), higher molecular weight SDS-stable Aβ species have not been reported in CSF or soluble extracts of the human brain. This suggests that SDS-stable low-n oligomers of Aβ are the smallest intermediate of insoluble amyloid deposits and may be the earliest mediators of neuronal dysfunction (Walsh and Selkoe 2007).

Other issues with the amyloid hypothesis are related to the transgenic mouse models of AD. Despite increased Aβ deposition in these models, there appears to be lack of coincidental neuronal loss. This is thought to be mainly due to species differences in neuronal susceptibility to Aβ accumulation, a lack of the human tau protein in mice, and also the lack of a human-like inflammatory response, which also plays a pivotal role in the progression of the disease (Hardy and Selkoe 2002). In order to address the issues with transgenic mouse models of AD, a triple transgenic model was developed by inserting two transgenes containing the APP Swedish mutant and a tau mutant (P301L) into an embryo that was homozygous with a presenilin 1 mutant (M146V). This was the first AD mouse model to develop concomitantly senile plaques and neurofibrillary tangles. Synaptic dysfunction in this mouse progressed in an age-related manner but it was also shown that, in agreement with the amyloid hypothesis, extracellular Aβ deposition preceded tangle formation. Additionally, deficits in synaptic plasticity occurred prior to extracellular accumulation and such deficits were associated with intraneuronal accumulation of Aβ (Oddo, Caccamo et al. 2003).

One of the advantages of developing the amyloid hypothesis was to focus AD research towards targets with therapeutic potential based on the understanding of the disease process (Hardy and Selkoe 2002). Despite some drawbacks with the hypothesis, alternative hypotheses that explain the pathogenesis of the disease have not been as robust. Therapies targeting Aβ amyloidogenesis have the potential to slow or even prevent further

neurodegeneration and the development of anti-Aβ therapeutics is regarded as a logical approach to treating AD (Hardy and Selkoe 2002; Walsh and Selkoe 2007). The National Institute on Aging (NIA) is currently supporting a number clinical trials that target the Aβ peptide in order to treat AD; these include immunotherapies such as intravenous immunoglobulin treatment using antibodies raised against Aβ (passive immunisation) (Relkin, Szabo et al. 2009); resveratrol, a polyphenol found in red wine which prevents Aβ aggregation (Ge, Qiao et al. 2012); carvediol, a β-blocker which lowers oligomeric Aβ levels (Wang, Ono et al. 2010), and thalidomide, a tumour necrosis factor TNFα inhibitor which down-regulates BACE1 and reduces Aβ generation (He, Cheng et al. 2013). Several more can be found at www.nia.nih.gov/alzheimers/clinical-trials.

1.3 Small Heat Shock Proteins

Small heat shock proteins (sHSPs) are a diverse class of molecular chaperones whose main role is to maintain protein homeostasis by binding proteins in their non-native confirmations to prevent aggregation (Haslbeck, Franzmann et al. 2005). sHSPs also undertake essential functions in a wide range of physiological processes and the ability of the each member of the family to form homo- and hetero-meric complexes underpins the large number of protein-protein interactions into which the sHSPs are known to enter. sHSPs have emerged as key therapeutic targets for a number of human diseases and can affect the rate of aging in tissue and entire organisms. Their regulation may have therapeutic implications for cancer, cardiovascular and neurodegenerative diseases (Kampinga and Garrido 2012).

1.3.1 Discovery

The heat shock response was originally discovered serendipitously in 1964 by the Italian geneticist Ferruccio Ritossa. While studying nucleic acid synthesis in chromosomes of the *Drosophila melanogaster* salivary glands, he noticed rapid transcriptional activity (observed as new chromosomal "puffs") in response to elevated temperatures (Ritossa 1964). The biological significance of this response was not realised at the time, however, a correlation between chromosomal puffs and protein synthesis was discovered in *Drosophila* in 1974 by Tissieres et al. By injecting radio-labelled [^{35}S] methionine into *D. melanogaster* and concomitantly increasing temperatures above optimal growth conditions (from 23°C to 37.5°C for 20 minutes), visualisation of several proteins bands that were rapidly upregulated (Tissieres, Mitchell et al. 1974) was possible. Mild heat shock

treatment was later shown to provide protection against thermal killing and increase survival of whole animals or various cell cultures of *Drosophila* (Mitchell 1979). The proteins up-regulated following heat shock were not identified until 1982 when Ignolia et al. characterised the primary amino acid sequence of 4 small heat shock proteins from *Drosophila* and found they were highly homologous and shared over 50% sequence similarity. Furthermore, the domains that shared the highest homology were found to be orthologous to mammalian α-crystallin protein, the most widely studied sHSP and a major constituent of the human eye lens (Ingolia and Craig 1982; Horwitz 2003).

Although HSP levels had been shown to correlate with thermo-tolerance, evidence of sHSPs promoting thermo-protection directly was not established until 1989 when Landry et al. demonstrated, through ectopic and constitutive expression of Hsp27, that Chinese hamster and mouse cells were protected against heat induced cell death without the need for prior heat shock pre-conditioning to upregulate endogenous HSPs (Landry, Chretien et al. 1989). A further study revealed that expression of Hsp27 increased the stability of stress fibres during induced hyperthermia and could partially protect against actin depolymerisation following treatment with cytochalasin D (Lavoie, Gingras-Breton et al. 1993).

sHSPs had been suggested to maintain the conformation of native proteins following their induction by heat shock (Figure 1.4). They were confirmed as molecular chaperones when murine Hsp25, human Hsp27 and bovine αB-crystallin were shown to regulate folding and prevent aggregation of two proteins, citrate synthase and α-glucosidase *in vitro*. All recombinant sHSPs stabilised the target proteins under heat shock conditions and even promoted full functional re-folding following urea-induced denaturation. The mechanism was shown to be similar to Hsp90 mediated chaperone function; however the sHSPs did not require ATP to drive the refolding process (Jakob, Gaestel et al. 1993).

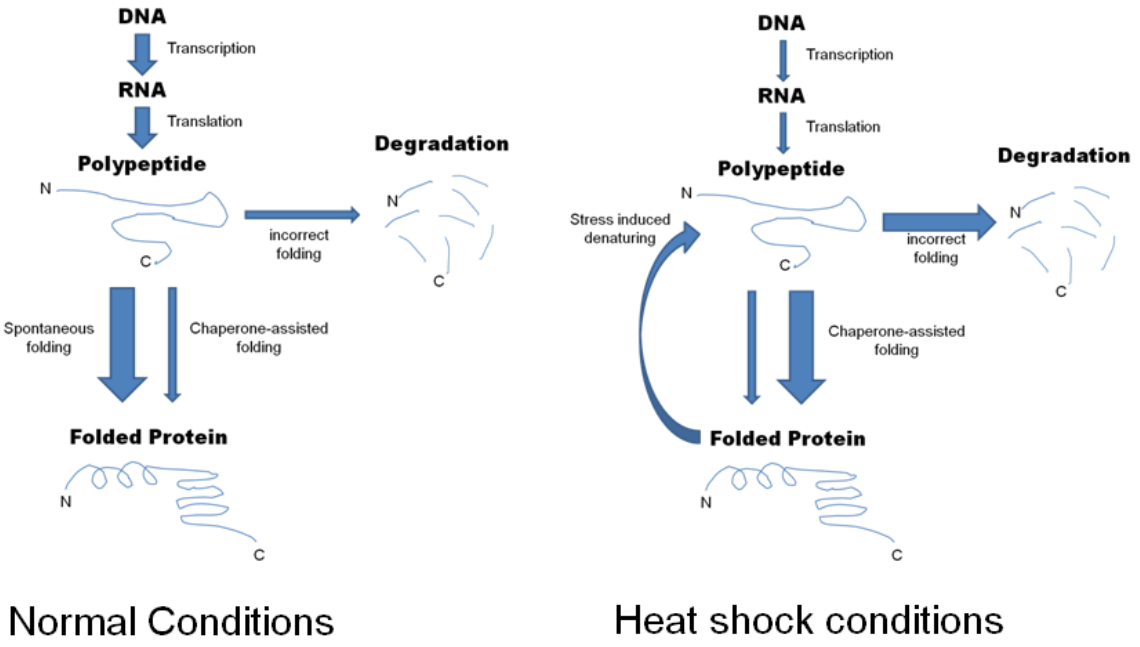

Figure 1.4 – Simplified Protein folding pathway.
Under normal physiological conditions the majority of protein folding occurs spontaneously. However, upon heat stress proteins lose their native conformation which increases the levels of proteins tagged for degradation. Under these conditions transcription and translation of proteins is suppressed to allow heat shock protein levels to increase and stabilise denatured proteins. This allows the cell to function and protects against cell death until conditions are back at optimum.

sHSPs are the most widespread family of molecular chaperones and are found throughout all kingdoms. Phylogenetic analysis uncovered early evolutionary divergence. Bacteria, Archea and single-celled eukaryotes typically contain one or two sHSPs. In higher organisms the number of sHSPs is higher, there are 4 in *Drosophila Melanogaster*, 16 in *Caenorhabditis elegans*, and 19 in *Arabidopsis thaliana* (Haslbeck, Franzmann et al. 2005). Up until 2001, 9 α-crystallin related sHSPs had been identified in humans and these were given the formal names HspB1-HspB9 ascribed by the HUGO Gene Nomenclature Committee (Kappe, Verschuure et al. 2001). Following completion of the human genome project, human Hsp27 protein sequence was used to extensively search for any remaining sHSP from predicted coding gene sequences. 10 sHSP related genes were identified in total, including all previously characterised sHSPs, and also a novel protein known previously as outer dense fiber protein 1 (ODF1). The spread of the 10 sHSP genes over 9 different chromosomes is evidence of ancient duplications that have created the human sHSP family of proteins (Kappe, Franck et al. 2003). A summary of all 10 sHSPs is given in Table 1.1.

1.3.2 sHSP expression profile

Some of the sHSP family show restricted tissue expression, whereas others (including Hsp27, αB-crystallin, Hsp22 and Hsp20 (Table 1.1)) are expressed ubiquitously. The expression profile of Hsp27, αB-crystallin, Hsp22 and Hsp20 has been studied extensively in developing pigs (from foetuses until adulthood). Initial studies looking at Hsp27 and αB-crystallin found strong expression of αB-crystallin in the eye lens, as expected, but also in the heart and skeletal muscle, while Hsp27 was expressed more strongly in heart and muscle tissue. Furthermore modulation of expression is observed in several tissues throughout development. In the lens, no change of expression of αB-crystallin was observed from foetal stage to the 3 year old adult as a constant level of expression is required to ensure normal vision. In whole brain, liver, kidney and lung, αB-crystallin expression increases with age, while Hsp27 increased only in the kidneys at later developmental stages (Tallot, Grongnet et al. 2003). In a related study by the same group, expression of Hsp20 and Hsp22 was found in porcine lens, brain, heart, liver, kidney, lung, skeletal muscle, stomach and colon. Hsp20 expression levels were found to increase with age in heart, kidney, hippocampus and striatum. Hsp22 expression remained constant in the heart but increased with age in the stomach, liver, kidney, hippocampus and striatum. Each tissue had a distinct expression profile of sHSPs that was modulated throughout development. Such data suggests that the individual roles of the different sHSPs in driving key functions at various stages of mammalian ageing (Verschuure, Tatard et al. 2003) are important for regulated development.

Table 1.1 - The human small heat shock proteins (HSPB family)

Protein Name	Alternative name	Molecular mass (kD)	Tissue Expression Profile	Function	Diseases
HSPB1	Hsp27	22.3	Ubiquitous	Cytoskeleton stabilization; chaperone and pro-refolding functions; anti-apoptotic function; anti-oxidant function	Neuropathy, Cancer, Ischemia/Reperfusion
HSPB2	MKBP	20.2	Skeletal and cardiac muscle	Chaperone activity toward DMPK; enhance kinase activity of DMPK, maintaining myofibrillar integrity; anti-apoptotic function	Myopathy, Ischemia/Reperfusion
HSPB3	HspL27	17.0	Skeletal, cardiac and smooth muscle	Maintaining myofibrillar integrity	
HSPB4	αA-crystallin	19.9	Eye Lens	Chaperone and pro-refolding functions; maintaining the proper refractive index in the lens	Cataract
HSPB5	αB-crystallin	20.2	Ubiquitous	Chaperone and pro-refolding functions; cytoskeleton stabilization; maintaining the proper refractive index in the lens; anti-apoptotic function	Neuropathy, Myopathy, Ischemia/Reperfusion, Cancer, cataract
HSPB6	Hsp20	17.1	Ubiquitous	Smooth muscle relaxation; cardioprotection; anti-aggregation; anti-apoptotic function	Neuropathy, Ischemia/Reperfusion
HSPB7	cvHsp	18.6	Skeletal and cardiac muscle	Maintaining myofibrillar integrity; SC35 speckle resident; anti-aggregation	
HSPB8	H11, Hsp22	21.6	Ubiquitous	Anti-aggregation; protein synthesis inhibition; induction of autophagy	Neuropathy, Cancer, Ischemia
HSPB9	CT51	17.5	Testis	Cancer/testis antigen	Cancer
HSPB10	ODF1	28.4	Testis	Cytoskeleton stabilization	

Table adapted from Boncoraglio et al. 2012 & Garrido et al. 2012

1.3.3 Structure & Function of small Heat Shock Proteins

The sHSP family of molecular chaperones are of low monomeric molecular weight, ranging between 16 and 30 kDa (Table 1.1). They are characterised by a highly conserved α-crystallin domain at the C-terminal region which consists of a β-sandwich and 2 anti-parallel β-sheets (Figure 1.5). The α-crystallin domain mediates many intra- and inter-molecular interactions that lead to the formation of dimers which have been proposed to be the active chaperoning unit of sHSPs (Benesch, Ayoub et al. 2008). The N-terminal region is more variable and can contain α-helical elements (Kappe, Franck et al. 2003). The sHSP family can readily assemble into higher molecular weight homo- or hetero-meric complexes. These high molecular weight complexes are dynamic and can readily exchange subunits (van Montfort, Basha et al. 2001; Haslbeck 2002; Narberhaus 2002; Horwitz 2003; Kappe, Franck et al. 2003). Hsp20 exists as a dimer of 43kDa or a large homo-meric 470kDa multimer, depending on its concentration. Another noteworthy feature about Hsp20 is that it has a shorter, less polar C-terminal extension relative to the majority of sHSPs (van de Klundert, Smulders et al. 1998).

The most important mechanism for regulating complex formation and client substrate specificity of the sHSPs is post-translation modification. The majority of sHSPs contain phosphorylatable serine residues. Hsp27 is phosphorylated at serine 15 (S15), S78 and S82 by the MAPKAP Kinase 2/3, downstream of the p38 pathway (Rogalla, Ehrnsperger et al. 1999). αB-crystallin is phosphorylated at S45 by p44/p42 MAPK, at S59 by MAPKAPK-2 and at S19 by an unknown kinase (Kato, Goto et al. 1994). Hsp20 is phosphorylated at S16 by cyclic nucleotide dependent kinases; protein kinase A (PKA) and protein kinase G (PKG) (Beall, Bagwell et al. 1999). Hsp22 is also phosphorylated by PKA at residues S24 and S57 (Shemetov, Seit-Nebi et al. 2008) and HspB10 is phosphorylated at S193 by Cyclin-dependent kinase 5 and its activator p35 (Rosales, Sarker et al. 2007). Phosphorylation of sHSPs can occur in response to a variety of stress signals and can alter protein conformation from one that favours large multimeric complexes towards low-n conformations such as monomers and dimers (Figure 4). Conformation can be crucial for chaperone function as phospho-mimetic substitutions of Hsp27 and Hsp22 result in decreased oligomer formation and attenuated chaperone activity (Rogalla, Ehrnsperger et al. 1999; van Montfort, Basha et al. 2001; Shemetov, Seit-Nebi et al. 2008). Hsp20 is found predominately in its dimeric form and has been shown to be a relatively poor chaperone in comparison to αB-crystallin (van de Klundert, Smulders et al. 1998).

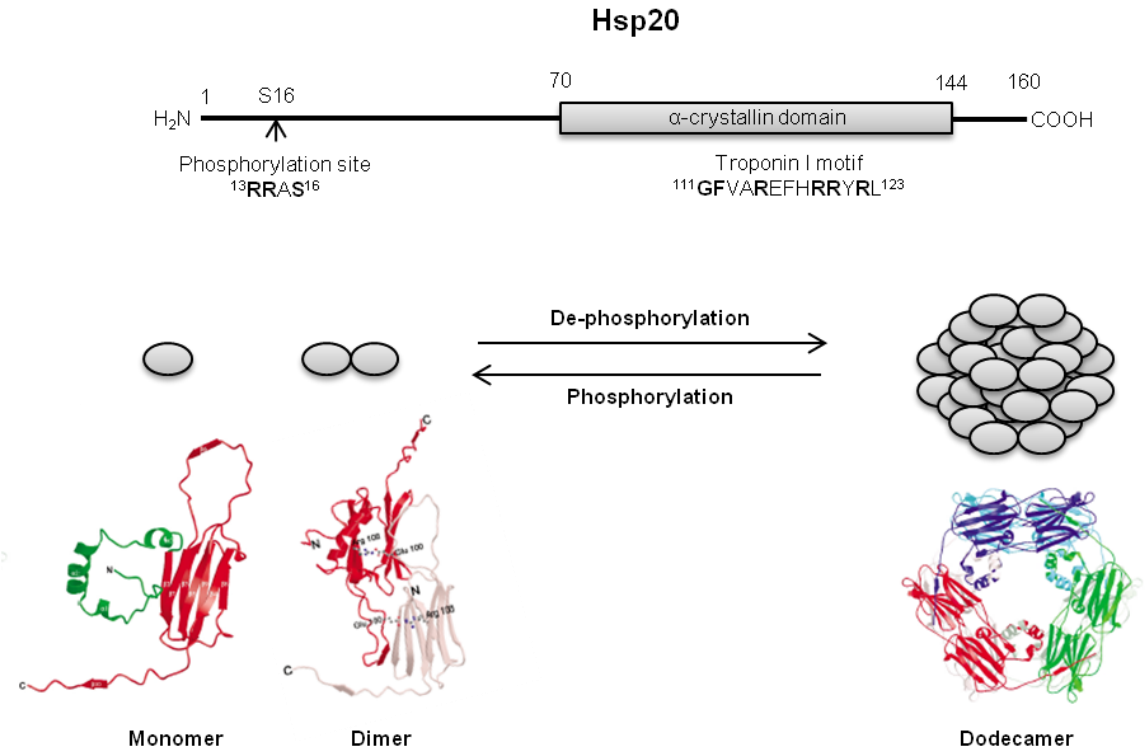

Figure 1.5 – Structure of Hsp20.
The Hsp20 protein contains an α-crystallin domain at the C-terminal end which is highly conserved among small heat shock proteins. Hsp20 is unique in that it contains a troponin I motif within the α-crystallin domain which regulates cardiomyocytes contractility. Hsp20 is phosphorylated at a consensus protein kinase site which results in its release from high molecular weight oligomers into monomeric and dimeric species which are the physiologically active subunits of Hsp20. The structures of an Hsp20 homolog from wheat, Hsp16.9 are shown in colour. The equilibrium between low molecular weight subunits and higher molecular weight oligomers is dependent on temperature and post translational modifications such as phosphorylation (van Montfort, Basha et al. 2001; Garrido, Paul et al. 2012).

The family of sHSPs perform a number of physiological functions within cells. These include; chaperone-like activities (discussed previously), cytoskeletal stabilisation, anti-apoptotic functions and regulation of protein quality control pathways. The ability of Hsp27, αA-crystallin, αB-crystallin and Hsp20 to modulate the structure of the cytoskeleton at the microfilament and intermediate filament level has been thoroughly investigated (Boncoraglio, Minoia et al. 2012). All of these sHSPs are known to interact with cytoskeletal elements and influence their stability. Hsp27 can directly stabilise actin filaments (Lavoie, Gingras-Breton et al. 1993). αA-crystallin and αB-crystallin have been shown to play important role in regulating actin dynamics and localise to lamellipodia in migrating lens epithelial cells (Maddala and Rao 2005). Reduced αB-crystallin expression has been shown to modify cell morphology, destabilise the microfilament network and a reduce cell adhesion (Iwaki, Iwaki et al. 1994). Hsp20 can bind to filamentous F-actin or globular actin depending on its phosphorylation status. The actin binding region of hsp20 is homologous with the actin association motif in myofilament protein troponin I (figure 1.5), which is important for cardiac contractility and relaxation (Rembold, Foster et al.

2000). Hsp20 also interacts with the scaffolding protein 14-3-3 which prevents the association of cofilin, an actin depolymerising protein (Dreiza, Brophy et al. 2005).

Several sHSPs have potent cytoprotective properties and can protect against apoptosis induced via hyperthermia, oxidative stress or several cytotoxic compounds (Boncoraglio, Minoia et al. 2012). αB-crystallin protects against the actions of a range of apoptosis-inducing agents and can sequester pro-apoptotic proteins such as p53 and the Bcl-2 family proteins, Bax and Bcl-Xs, preventing their translocation to the mitochondria (Mao, Liu et al. 2004; Liu, Li et al. 2007). Hsp20 regulates apoptosis in cardiomyocytes via an interaction with Bax, resulting in reduced caspase-3 activity following ischemic/reperfusion injury (Fan, Ren et al. 2005). Hsp20 can also inhibit apoptosis and cardiac remodelling, induced via chronic β-adrenergic stimulation, through regulation of apoptosis signal-regulating kinase 1 (ASK1) (Fan, Yuan et al. 2006).

Another important cellular function ascribed to sHSPs is protein quality control via the partitioning of proteins towards either renaturation or proteosomal degradation. Referred to as protein triage, the process involves the ubiquitin-proteasome system which is an error-checking pathway that directs incorrectly folded proteins towards degradation (Figure 1.3). The coordinated interaction between sHSP induced renaturation and proteasome degradation is not fully understood but several sHSPs have been shown to regulate several aspects of protein triage (Garrido, Paul et al. 2012). Hsp27 enhances the catalytic activity of the 26S proteasome, promoting increased degradation of ubiquitinated proteins. αB-crystallin can interact with C8 subunit of the 20S proteasome and also the ubiquitin ligase FBX4, which drives the ubiquitination and subsequent degradation of protein substrates including cyclin D1 (Lanneau, Wettstein et al. 2010). Hsp22 is directly involved in regulating autophagy, a process of non-selective cellular recycling that sequesters the cytoplasm, cellular organelles and aggregated proteins into double membrane bound vesicles that are subsequently delivered to lysosomes for degradation (Carra, Brunsting et al. 2009). A non-phosphorylatable mutant of Hsp20 has also been shown to suppress autophagy leading to increased necrosis, suggesting that Hsp20 is also intrinsically involved in autophagy (Qian, Ren et al. 2009).

The family of sHSPs perform a number of cellular functions that are vital for maintaining protein homeostasis in order to positively regulate the balance between life and death of a cell. Their ability to form homo- and hetero-meric complexes results in a vast interactome and this in turn, accounts for their involvement in diverse processes such as proteolysis,

apoptosis, proliferation, autophagy and smooth muscle relaxation. sHSPs are becoming attractive therapeutic targets for a number of human diseases, particularly disorders of aggregated protein deposition such as Alzheimer's disease (Sun and MacRae 2005).

1.3.4 sHSPs & Amyloids

Several neurological diseases are characterised by accumulation of aggregation-prone proteins. This class of diseases include Aβ peptide in Alzheimer's, huntingtin in Huntington's and α-synuclein in Parkinson's. The deposits associated with these diseases share a common feature in that they all contain amyloid fibrillar forms of the respective causative protein. Amyloid fibril formation can occur to any protein under certain physiological conditions (Chiti and Dobson 2006). sHSPs have been found to be up-regulated in response to conditions associated with amyloid fibril formation and several sHSPs have been shown to co-localise with amyloid deposits (see below). sHSPs are thought to play key roles in the protective response against these diseases, as cells evoke the anti-aggregation and cytoprotective properties of sHSPs as an early defence mechanism against proteotoxic stress (Ecroyd and Carver 2009).

One well studied example of a disease protein associated with amyloid fibril formation is α-synuclein protein in Parkinson's. The protein α-synuclein forms intracellular fibrillar inclusions known as Lewy bodies and the aggregation of α-synuclein into these deposits plays a key role in the pathogenesis of this disease (Spillantini, Crowther et al. 1998). In brain tissue from Parkinson's disease patients, Hsp27 and αB-crystallin co-localise with α-synuclein in Lewy body deposits (Poutney 2005; Mclean 2002). Hsp27 can attenuate the aggregation potential of α-synuclein and subsequently inhibit its cytotoxic effects (Zourlidou, Payne Smith et al. 2004). The reduction in toxicity can be highly significant. In one study, Hsp27 was found to reduce toxicity of α-synuclein in a cell model by around 80% compared to a 20% reduction induced by αB-crystallin (Outeiro, Klucken et al. 2006).

Huntington disease is an inherited neurodegenerative disease that is caused by the triplet expansion CAG in the huntingtin gene. The resultant protein contains extended glutamine repeats of more than 40 residues (polyQ). The disease is characterised by protein misfolding and aggregation with a concurrent increase in proteotoxic stress (Orr 2012). sHSPs have been shown to differentially affect the aggregation propensity of mutant Huntington exon 1 (Htt). Hsp20, cvHsp, Hsp22 and HspB9 all strongly inhibit aggregation of Htt carrying 43 CAG repeats (HttQ43) whereas HspB2, HspB3, αB-crystallin and

HspB10 have no effect (Vos, Zijlstra et al. 2010). In a separate study both Hsp20 and Hsp22 where shown to interact with the co-chaperone Bag3, a regulator of autophagy, to prevent accumulation of aggregated HttQ43 by targeting the protein for degradation (Fuchs, Poirier et al. 2010).

Alzheimer's disease associated amyloid plaques are known to contain several other proteins in addition to the Aβ peptide. αB-crystallin and Hsp27 were the first sHSPs to be studied immunohistochemically in the cerebral cortex of human AD patients. αB-crystallin levels where found to be elevated in the temporal and frontal lobes and localised in astrocytes and oligodendrocytes. Hsp27, on the other hand, was elevated in the temporal, frontal and parietal lobes and presented in degenerating neurons in the cerebral cortex (Shinohara, Inaguma et al. 1993). Another study found that Hsp27, αB-crystallin, HspB2 and Hsp20 were all detected extracellularly in classic senile plaques. Both Hsp27 and αB-crystallin were also observed in astrocytes associated with senile plaques and cerebral amyloid angiopathy. Additionally, Hsp20 was also detected in diffuse senile plaques, suggesting that Hsp20 has certain affinity for non-fibrillar Aβ. Furthermore, Hsp20 levels in classic senile plaques in the hippocampus and neocortex correlated with age. As sHSPs are typically found intracellularly, their extracellular deposition is thought to result from necrotic cell-death associated with Aβ accumulation (Wilhelmus, Otte-Holler et al. 2006).

1.3.5 sHSPs and Aβ

The most widely studied target for sHSP chaperone activity associated with disease related fibrils is the Aβ peptide. There have been several conflicting reports regarding the effect sHSPs can have on amyloidogenesis particularly with respect to αB-crystallin. An initial study by (Kudva, Hiddinga et al. 1997), showed that Hsp27 dose-dependently inhibited the rate of $A\beta_{1-42}$ amyloidogenesis measured through thioflavine T (ThT), a compound which selectively binds to aggregated Aβ resulting in a shift in its fluorescence spectrum (LeVine 1993), while αB-crystallin had no effect on the rate of aggregation. Treatment of pre-formed aggregates with Hsp27 also resulted in reduction in ThT fluorescence but to a far lesser extent, therefore it was deduced that the dominant effect of Hsp27 on aggregation was through inhibition of amyloid formation (Kudva, Hiddinga et al. 1997). Another study utilising ThT to characterise the effect of αB-crystallin on Aβ aggregation found that αB-crystallin inhibited fibril formation of $A\beta_{1-40}$ but in doing so created a non-fibrillar Aβ/αB-crystallin complex that was highly toxic to cells. It was suggested that αB-crystallin was stabilising oligomers in a neurotoxic protofibrilar form and could therefore be

inadvertently exacerbating Aβ induced neuronal damage (Stege, Renkawek et al. 1999). αB-crystallin has also been shown to promote fibril formation of $A\beta_{1-40}$ through the exchange of subunits of αB-crystallin and Aβ fibril intermediates. The dynamic interaction between αB-crystallin and Aβ was investigated using fluorescence resonance energy transfer (FRET) between pyrene-labelled $A\beta_{1-40}$ and the tryptophan residues on un-labelled αB-crystallin (Liang 2000).

Inhibition of fibril elongation by αB-crystallin was described by Raman et al. 2005. This group reported that αB-crystallin does not form a stable complex with $A\beta_{1-40}$ and they went on to identify distinct mechanisms that distinguish amorphous aggregation and fibril growth. Notably, αB-crystallin preferentially interacts with the fibril nucleus and inhibits polymerisation of amyloid fibrils (Raman, Ban et al. 2005). Several mutations, and complete removal of the flexible C-terminal extension on αB-crystallin have also been shown drastically modulate chaperone activity towards either amorphous amyloid aggregates or fibrils (Treweek, Ecroyd et al. 2007).

One study looking at αA-crystallin found that a domain within the α-crystallin domain shares homology with a site within Aβ which plays a key role in amyloidogenesis. This motif is known as the KLVFF domain. Utilising a "mini-αA-crystallin", this 19 amino acid peptide was sufficient to block amyloidogenesis and attenuate subsequent cytotoxicity. However it did not work as well as full length αA-crystallin (Santhoshkumar and Sharma 2004).

Several sHSPs species have also been shown to inhibit *in vitro* amyloidogenesis (Wilhelmus, Boelens et al. 2006). The Verbeek group characterised the ability of five different sHSPs to affect fibril formation of $A\beta_{1-42}$ and $A\beta_{1-40}$ carrying the Dutch mutation (Q22G). The latter forms fibrils more readily than the WT $A\beta_{1-40}$. αB-crystallin had the highest affinity for $A\beta_{1-42}$ and Dutch Aβ followed by Hsp20 then Hsp27. The co-oligomer HspB2/B3 which was found to co-localise with CAA had no detectable affinity for either Aβ peptide tested. The affinity of the sHSPs for Aβ was higher for $A\beta_{1-42}$ than for Dutch $A\beta_{1-40}$ which could possibly account for the severe early-onset form of AD, HCHWA-D (discussed previously) due to perturbation of the endogenous anti-aggregation effect of sHSPs. Co-incubating the various sHSPs with Aβ peptides resulted in attenuation of subsequent Aβ induced cytotoxicity when overlaid on cultured human brain pericytes. Hsp20 and αB-crystallin dose-dependently reduced Aβ induced cytotoxicity and the level of protection afforded by co-incubating the Aβ peptides and the various sHSPs correlated

with affinity. Furthermore, Hsp20 was the only sHSP that prevented accumulation of $A\beta_{1-40}$ at the cell surface (Wilhelmus, Boelens et al. 2006).

The examples detailed above make a strong case to support the fact that sHSPs can inhibit amyloidogenesis of the Aβ peptide. The potential exploitation of this finding to create novel therapeutics is under way. One study has used a transgenic *Caenorhabditis elegans* strain expressing human $A\beta_{1-42}$ and found this lead to increased expression of the Hsp16 family of proteins, which are homologous to αB-crystallin. Hsp16 has been previously shown to co-localise intracellularly with human $A\beta_{1-42}$ peptide (Fonte, Kapulkin et al. 2002). In a follow-up study, the transgenic model of *C. elegans* was transfected with Hsp16.2 and this attenuated $A\beta_{1-42}$ induced toxicity. Hsp16.2 reduced amyloid fibril formation but did not affect accumulation of Aβ suggesting that sHSPs reduce Aβ toxicity directly by modulating the oligomerisation pathways in order to reduce the formation of toxic intermediates in the amyloidogenic pathway (Fonte, Kipp et al. 2008).

In light of the data described above, there appears to be two therapeutic avenues down which sHSP-related technology could be developed in order to protect against diseases such as AD. First would be to positively manipulate expression of sHSPs in order to prevent the formation of toxic Aβ species early in the disease process. This would mimic natural processes seen when sHSPs are upregulated in cells surrounding senile plaques and Aβ deposits. Additionally, sHSPs are found to co-localise with Aβ deposits in AD brain tissue suggesting a possible protective mechanism that becomes overwhelmed as the disease progresses. This is particularly evident in the study conducted by Wilhelmus et al. (2006c) where Hsp20 was protective against $A\beta_{1-40}$ induced cell death at 1:1 molar ratios but not at 25:1 ($A\beta_{1-40}$:Hsp20) (Wilhelmus, Boelens et al. 2006). The second strategy would be to mimic stress responses within the cell by altering sHSP function via conformational changes triggered by post-translational modifications such as phosphorylation. The effect of phosphorylation on the activity of various sHSPs in relation to Aβ aggregation has not previously been investigated, however, it is crucial in mediating cardio-protective effects (Edwards, Scott et al. 2012). If effective, this concept could serve as a more convenient and controllable way to amplify the neuro-protective functions of the sHSPs.

1.4 Second Messenger Signal transduction in Cognition & Disease

Cell surface, 7-span, transmembrane (7TM) receptors recognise various extracellular ligands, known as 'first messengers', and transform them into intracellular signals. This allows cells to alter specific aspects of their homeostasis in response to physical or chemical challenges. As such, cellular signals propagated in this way must be highly regulated so that their amplitude and timing produce measured and appropriate responses. The signal must be strong enough to produce the desired effect but also be transient so that the cell can easily prepare for other potential inputs. Additionally, the signal must be targeted to the correct functional "machinery", which often resides in discrete intra-cellular locations. To achieve all of these goals, cells have developed signalling molecules known as 'second messengers' to convey complex information from receptors, temporally and in three dimensions, into the cell to signalling nodes where functional decisions are made (Beavo and Brunton 2002).

One of the prototypical, ubiquitous second messenger signalling systems uses the cyclic nucleotides cAMP and cGMP. Cyclic nucleotides undertake many important roles including the regulation of synaptic function. A super-family of enzymes called phosphodiesterases (PDEs) provide the sole means of hydrolysing cyclic nucleotides and thereby dictate the spatial and temporal aspects of cyclic nucleotide signalling processes. As a consequence PDEs have been targeted to treat a variety of neurological disorders including; AD, depression, schizophrenia and are seen as an amenable way to improve cognition and reverse synaptic dysfunction resulting from disease. Development of PDE inhibitors has seen significant scientific effort over the last few decades and several compounds have been discovered that have shown encouraging results in animal models of AD (Bales K. R. 2010).

1.4.1 Cyclic Adenosine Monophosphate (cAMP)

The second messenger 3'-5'-cyclic adenosine monophosphate (cAMP) was discovered by Sutherland et al. in 1958, during an investigation into how the hormone adrenaline activated glycogen phosphorylase to induce glycogenolysis in the liver. They found that a heat-stable factor containing adenine, ribose and phosphate at a ratio of 1:1:1, was stable to boiling in hydrochloric acid but could be inactivated enzymatically to 5'-AMP. Soon after this, it was discovered that cAMP was synthesised at the membrane by adenylyl cyclase (AC) in response to hormones and degraded to 5'-AMP by the action of cyclic nucleotide

phosphodiesterases (PDEs) in the cytoplasm. Discovery of cAMP second messenger system was deemed important enough for Sutherland and colleagues to win the Nobel prize some years later (Beavo and Brunton 2002).

Even when the ubiquitous nature of cAMP signalling system had been established, it was still unclear how extracellular ligands could lead to increased intracellular cAMP. Several studies carried out by Birnbaumer and Rodbell found that hormone-sensitive cAMP synthesis required GTP. This discovery led to the hypothesis that a 'transducer' must link receptors with AC. Birnbaumer and Rodbell also demonstrated that non-hydrolysable analogues of GTP could stimulate AC activity in the absence of an extracellular ligand. The transducer was later found to be the stimulatory G-protein $G_s\alpha$. It is now dogma that ligands which target 7TM receptors, signal through cAMP using G-proteins that activate or inhibit AC. The consequences of increased synthesis of cAMP by AC are mediated through a variety of 'effector' proteins that become activated in response to increases in cAMP concentrations. One of the most important effector proteins for cAMP signalling is the cAMP-dependent protein kinase A (PKA), which once activated via cAMP can phosphorylate a large number of intracellular targets that are essential for regulating essential physiological functions (Figure 1.6A) (Beavo and Brunton 2002). Other molecular targets of cyclic nucleotides include, cGMP-dependent protein kinase G (PKG), exchange protein activated by cAMP (EPAC), cyclic nucleotide-gated ion channels (CNGs) and several PDEs through the binding to N-terminal GAF domains (Lugnier 2006).

The role of cAMP in learning and memory was pioneered in two separate invertebrate model organisms, *Aplysia californica* and *Drosophila melanogaster*. Synaptic connections between sensory neurons in *Aplysia* undergo a variety of plastic changes that are related to associative and non-associative forms of learning and memory storage, and this bolsters its attractiveness as a model system. Studies involving *Aplysia* synapses provided the first evidence that the cAMP second messenger pathway could regulate the strength of synaptic transmission via ion channel modulation and enhancement of neurotransmitter release. cAMP was implicated unequivocally in presynaptic facilitation following the observation that injection of cAMP or active PKA into presynaptic sensory neurons simulated the synaptic response to a level similar to that induced by serotonin. A similar response was also observed following the treatment of *Aplysia* sensory neurons with the adenylyl cyclase activator, forskolin. In addition, it was found that tail stimuli or shock of peripheral nerves produced an increase in cAMP levels in sensory neurons (Byrne and Kandel 1996).

Genetic screens in *Drosophila* that looked for mutants, which could affect learning and memory processes, further highlighted the involvement of cAMP second messenger pathway in memory formation. *Drosophila* exhibit strong olfactory learning and memory phenotypes and after exposure to two odours, one paired with an electric shock, the flies learn to avoid the odour which is paired with the negative response (Pavlovian conditioning) (Dudai, Jan et al. 1976). Two *Drosophila* mutants were isolated via this screening process. One of the mutant phenotypes resulted from disruption of a gene encoding *Drosophila* adenylyl cyclase (Rutabaga), while the other encoded a cAMP-dependent phosphodiesterase (Dunce) (Silva, Kogan et al. 1998). Taken together these mutants highlighted the fundamental importance of cAMP metabolism in this invertebrate model of learning and memory.

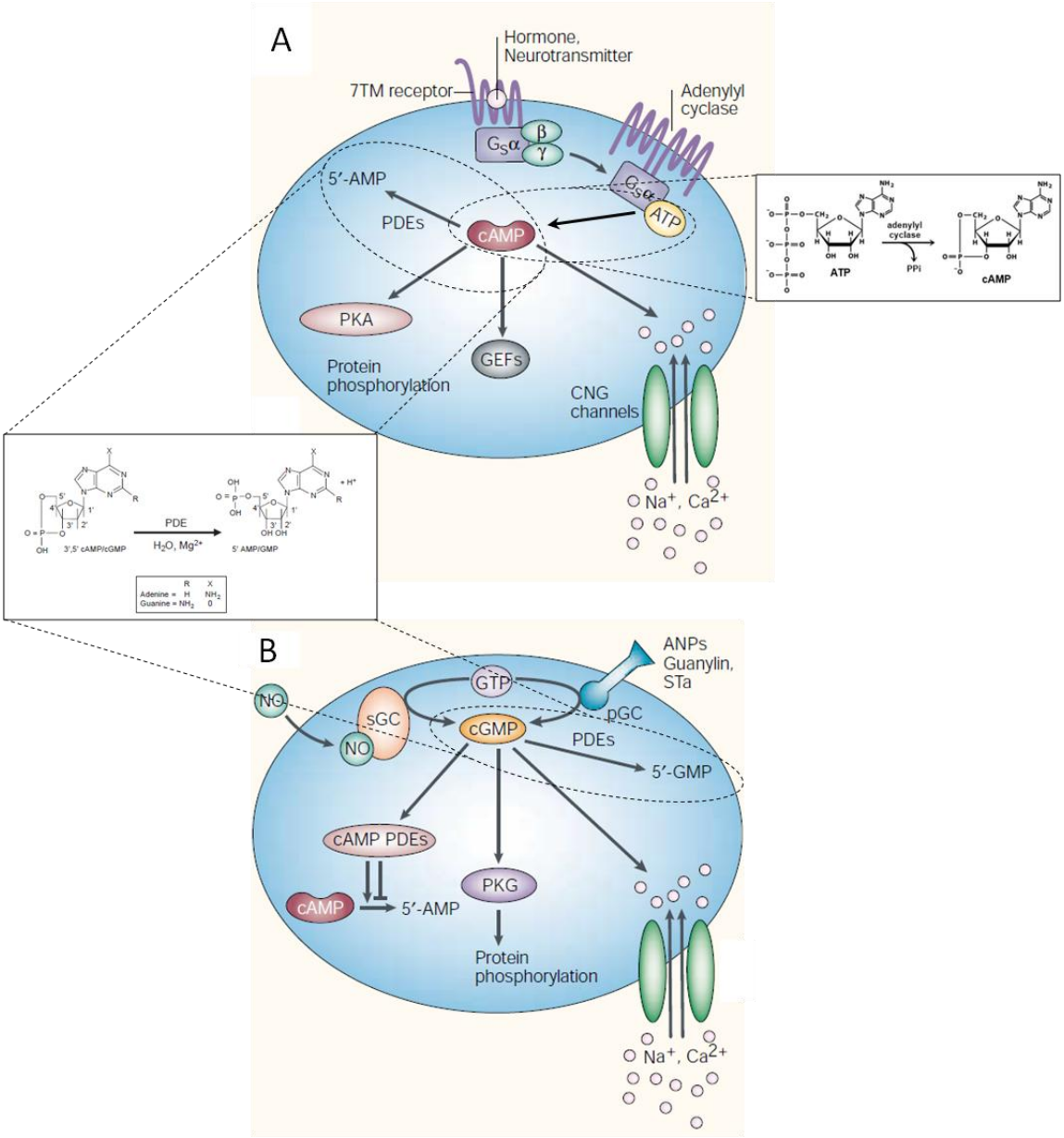

Figure 1.6 – Cyclic nucleotide second messenger signalling cascade.

Diagram illustrates the basic synthetic and regulatory pathways of cAMP (A) and cGMP (B) metabolism. A - The cAMP signalling pathway is activated following the binding of extracellular ligands which include hormones and neurotransmitters to 7TM receptors. The signal is transduced via the G-protein (Gsα) which stimulates adenylyl cyclase to convert ATP to cAMP (inset). Increases in intracellular concentration of cAMP leads to activation of Protein kinase A (PKA), the guanine-nucleotide exchange factor (GEF) EPAC and cyclic nucleotide gated (CNG) ion channels. cAMP specific phosphodiesterases hydrolyse cAMP into AMP (inset) in order to attenuate the second messenger signal. B – cGMP signalling pathway can commence via two inputs; either through atrial natriuretic peptides (ANPs) activating particulate guanylyl cyclase (pGC) or through the membrane permeable gas nitric oxide (NO) binding to soluble guanylyl cyclase (sGC) to induce cGMP synthesis. Both pGC and sGC convert GTP to cGMP in a process analogous to cAMP synthesis. Increased cGMP concentrations activate protein kinase G (PKG) and CNG channels as well as differentially regulating the activity of PDEs containing GAF domains. cGMP-dependent PDEs degrade cGMP into GMP in order reduce cGMP concentrations (Adapted from Beavo & Brunton 2002).

1.4.2 Cyclic Guanosine Monophosphate (cGMP)

Distinct from cAMP, the cyclic guanosine 3', 5' –monophosphate (cGMP) is also an important second messenger that regulates processes such as heart contractility and smooth muscle relaxation. cGMP is synthesised by particulate bound guanylyl cyclases (pGCs) and cytosolic soluble guanylyl cyclases (sGC) in response to natriuretic peptides and nitric oxide (NO), respectively. NO binds to a haem group on the β-subunit of sGC and induces up to a 200-fold increase in activity. Activation of sGC leads to the conversion of GTP to cGMP in a process analogous to cAMP synthesis (Figure 1.6A). The resultant elevation of cGMP leads to the activation of cGMP effector proteins such as; cGMP-dependent protein kinase (PKG), Cyclic nucleotide gated ion (CNG) channels and cGMP-regulated PDEs (Figure 1.6B) (Francis, Busch et al. 2010).

The canonical NO/sGC/cGMP/PKG signalling cascade also plays a fundamental role in synaptic plasticity and learning. NO is generated by Ca^{2+}/calmodulin-regulated neuronal NO synthase (nNOS) in the brain where it can be produced either in the postsynapses and diffuse into presynaptic terminals, (retrograde signalling) or vice versa (anterograde signalling). Functionally, NO stimulates sGC to synthesise cGMP. Increasing concentrations of cGMP activate PKG which can modulate the cytoskeleton and synaptic vesicle transport in neuronal cells (Kleppisch and Feil 2009).

The past few years has seen renewed interest in cGMP signalling because of the therapeutic successes that have been achieved by targeting cGMP-dependent signalling pathway to treat erectile dysfunction and cardiovascular disorders. Furthermore, neuronal cGMP signalling has been targeted to treat neurodegenerative and psychiatric diseases with cognitive impairments including AD and schizophrenia (Kleppisch and Feil 2009).

1.4.3 PKA & PKG

One of the most important discoveries surrounding second messenger signalling was the identification of cyclic nucleotide-dependent protein kinases. The first kinase to be discovered in this regard was cAMP-dependent protein kinase A (PKA), a heterotetrameric holoenzyme consisting of two regulatory subunits (R) and two catalytic subunits (C). The regulatory units of PKA are encoded by four genes; RIα, RIβ, RIIα and RIIβ, while the catalytic units are encoded by three genes; Cα, Cβ and Cγ. The various subunits are differentially expressed in cells and tissue and can form homo- and heterodimers. The R & C subunits are bound non-covalently and two cAMP molecules bind cooperatively to each R subunit. The binding of four cAMP molecules to the R subunits results in the release of two C subunit monomers which become catalytically active and phosphorylate serine and threonine residues on specific protein substrates (Tasken and Aandahl 2004).

The cGMP-dependent protein kinase (PKG) is the main effector component of the NO/cGMP signalling pathway and regulates a number of cellular functions including; cardiac protection, smooth muscle relaxation, neuronal plasticity, endothelial permeability and gene transcription (Francis, Busch et al. 2010). PKG is a homodimer and all mammalian isoforms, PKGIα, PKGIβ and PKGII, have similar domain configurations. Coiled coils at the N-terminal promote homo-dimerisation of PKG with a parallel configuration, this is upstream an autoinhibitory domain and two tandem cyclic nucleotide binding sites which act cooperatively to regulate the catalytic activity of the C-terminal domain. The biggest structural distinction between PKA and PKG is that PKG has both its regulatory and catalytic domains together in a single polypeptide. The model of PKG Iα activation relies heavily on the auto-inhibitory domain at the N-terminal. This region acts as a pseudo substrate sequence that can inhibit the catalytic C-terminal when the enzyme is in an inactive state. Autophosphorylation at N-terminal residues weakens the inhibitory effect and only cGMP binding to both the A- and B- domains promotes the conformational change required for full kinase activity (Osborne, Wu et al. 2011).

Both PKA and PKG are members of a subclass of serine/threonine specific protein kinases and share significant structural and functional similarities (Figure 1.7). An early study of substrate specificity showed that PKA and PKG can phosphorylate the same substrates *in vitro* (Lincoln and Corbin 1977). PKA is known to phosphorylate the general sequence RRXS/T with the arginine residues acting as essential components of substrate specificity (Kemp, Graves et al. 1977). PKG can recognise both RRXS and RKXS with a stronger

preference for the latter sequence as demonstrated using *in vitro* peptide libraries (Tegge, Frank et al. 1995; Dostmann, Nickl et al. 1999).

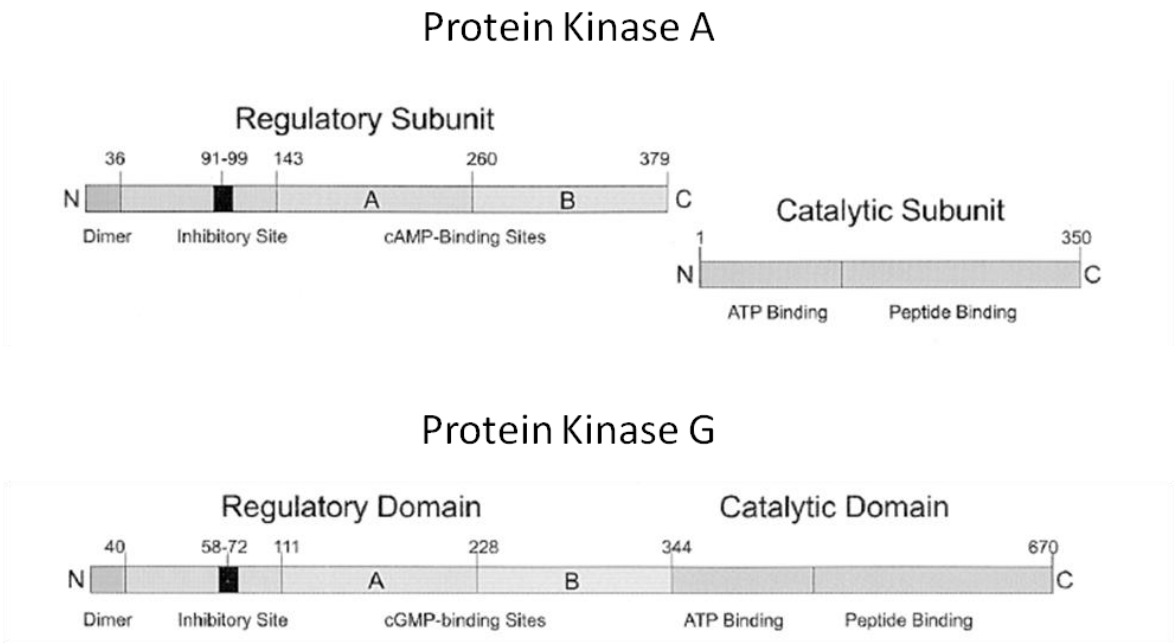

Figure 1.7 – Domain structures of PKA and PKG
Cyclic nucleotide-dependent protein kinases show a high degree of structural and functional similarities. Numbering taken from RIα and Cα subunits of PKA and PKG Iα (Taken from Dostmann, Nickl et al. 1999).

A common substrate of both PKA and PKG, which plays a key role in the regulation of cognitive processes, is the cAMP responsive element binding protein (CREB). CREB is a transcription factor that is activated via phosphorylation and regulates gene expression required for long-term memory storage. The cAMP/PKA/CREB pathway is involved in a model of synaptic plasticity known as long-term potentiation (LTP). LTP is the most comprehensively studied mechanism of learning and memory and is characterised by long-lasting enhancement of synaptic transmission in hippocampal neurons (Silva, Kogan et al. 1998). LTP occurs in two phases; short-term LTP, which lasts less than three hours and is unaffected by inhibitors of protein synthesis, and long-lasting LTP which requires both gene transcription and protein synthesis (Nguyen 1994). Early studies found that analogues of cAMP can induce LTP while inhibitors of PKA attenuated this phenomenon (Frey, Huang et al. 1993). The requirement for CREB for controlling gene expression associated with LTP was demonstrated when mice carrying mutations in the CREB gene had deficient long-term memory capacity when measured using a Pavlovian fear conditioning tasks (Bourtchuladze, Frenguelli et al. 1994). Subsequent biochemical analysis of synaptic plasticity has uncovered components of cAMP/PKA/CREB pathway that may be targeted

therapeutically to treat diseases associated with memory decline such as AD (Tully, Bourtchouladze et al. 2003).

The Aβ peptide has been shown to negatively regulate activity of this signalling cascade. Impairment of LTP was demonstrated using electrophysiological studies in mice overexpressing Aβ. However this impairment did not correlate with synaptic loss, amyloid deposition or cell-death, instead it led to a sustained decrease in PKA activity in cultured hippocampal neurons and also inhibited CREB phosphorylation in response to glutamate stimulation. The inhibition of PKA mediated CREB phosphorylation was reversible with the use of agents that can increase intracellular cAMP levels, namely the AC activator forskolin, and the PDE4 inhibitor rolipram. Rescue of LTP was also blocked using the PKA inhibitor H89 (Vitolo, Sant'Angelo et al. 2002). Although the direct mechanism by which Aβ attenuates PKA activity was not established by Vitolo et al. , the study was valuable as it provided direct evidence that targeting cAMP signalling pathways in the brain may improve memory and alleviate mild cognitive impairments associated with early stage AD.

The NO/cGMP/PKG signalling cascade has been shown to work in parallel with cAMP/PKA pathway in order to maintain hippocampal and cortical LTP through convergent CREB activation (Lu, Kandel et al. 1999). This mechanism was investigated for its role in Aβ induced suppression of LTP (Puzzo, Vitolo et al. 2005). NO levels rescued impairment of LTP in hippocampal slices perfused with Aβ and this was consistent with previous studies of neuroprotective effects mediated by pharmacological NO donors. The neuroprotective effects of NO were blocked with an inhibitor of sGC, while activation of sGC rescued Aβ-induced impairment of LTP. Additionally, analogues of cGMP also reversed Aβ-induced LTP inhibition. Several agents were able to re-establish normal levels of phospho-CREB following treatment with $A\beta_{1-42}$ and this was mediated through PKG as treatment with the PKA inhibitor KT5720 did not attenuate the beneficial effect whereas the PKG inhibitor KT5823 abrogated the effects of cGMP analogues (Puzzo, Vitolo et al. 2005).

Another substrate of both PKA and PKG that is involved in a number of key physiological processes is Hsp20. Hsp20 can be phosphorylated by either PKA or PKG at serine 16 at the consensus phosphorylation site ^{13}RRAS^{16}. Phosphorylation of Hsp20 by PKA has been studied extensively in cardiac tissue and is known to be protective in a number of pathophysiological cardiac processes. Transgenic mice with cardiac specific

overexpression of Hsp20 are protected against ischemia/reperfusion (I/R) induced myocardial infarctions and have improved contractile performance in the reperfusion phase which is often associated with apoptosis and necrosis of heart tissue. Phospho-mimetic substitutions at serine 16 confer protection against chronic β-adrenergic-induced apoptosis whereas non-phosphorylatable S16A substitutions fail to protect. Phosphorylation of Hsp20 also prevents cardiac remodelling events such as hypertrophy which can ultimately lead to heart failure (Edwards, Cameron et al. 2011).

Hsp20 is also an important regulator of smooth muscle relaxation. Relaxation of various types of smooth muscle can be induced by forskolin and the NO donor sodium nitroprusside through the activation of either PKA or PKG, respectively (Beall, Kato et al. 1997). Phosphorylation of Hsp20 is essential for effective cyclic nucleotide mediated relaxation in human umbilical artery smooth muscle (HUASM) (Flynn, Brophy et al. 2005). Hsp20 induced relaxation of arterial smooth muscle (ASM) has also been studied extensively. ASM contraction involves increased phosphorylation of myosin regulatory light chain (MRLC) at serine 19 by MRLC kinase following increased intracellular calcium. This process can be modulated via the NO/cGMP/PKG pathway and has been targeted therapeutically to treat erectile dysfunction by inhibiting of the cGMP specific phosphodiesterase 5 (PDE5) to increase cGMP levels and activate PKG (Beavo and Brunton 2002). However, a novel form of smooth muscle relaxation exists independently of MRLC phosphorylation and intracellular calcium changes. This phenomenon is known as force suppression and it directly correlates with levels of phosphorylated Hsp20. It is thought that Hsp20 mediates the relaxation process through a consensus sequence homologous to that seen in the thin filament protein troponin I. This motif interacts with the actin cytoskeleton in response to calcium changes and modulates structural changes within smooth muscle cells (Edwards, Cameron et al. 2011).

The physiological functions of Hsp20 in the brain are only beginning to be investigated, however, several studies have revealed protective functions similar to that seen in the heart, and these may also be regulated via phosphorylation by PKA or PKG (Edwards 2011). Given the multiple protective mechanisms employed by Hsp20, increasing its activity via the cyclic nucleotide second messenger cascade may be of therapeutic relevance in treating diseases such as AD. One existing mechanism to promote increased phosphorylation of PKA/PKG substrates such as CREB and Hsp20 is through inhibition of phosphodiesterases the sole mediators of cyclic nucleotide degradation (Tully, Bourtchouladze et al. 2003; Sin, Edwards et al. 2011).

1.4.4 Phosphodiesterases and Cognition

Cyclic nucleotide phosphodiesterases (PDEs) were discovered soon after the discovery of cAMP and cGMP (Beavo and Brunton 2002). Early studies of cyclic nucleotides concentrated on their hydrolysis, as enzymatic processes were amenable to researchers via radio-labelled cyclic nucleotide substrates. The scale of the PDE superfamily of enzymes was fully recognised following the onset of new biochemical and molecular techniques (Bender and Beavo 2006).

1.4.4.1 PDE Structure & Function

All the different mammalian PDEs share common structural characteristics: a catalytic domain of about 270 residues that is conserved within each family; a regulatory domain between the N-terminus and the catalytic domain; and a domain between the catalytic domain and the C-terminus with, as yet, undefined function. The catalytic domain is the most highly conserved domain across all isoforms of PDEs, sharing between 20-45% sequence identity, and includes consensus metal binding motifs for Zn^{2+} and Mg^{2+} which are essential for the hydrolysis of cyclic nucleotides (Fig. 1.6). PDEs are also characterised by their substrate specificity; PDE4, PDE7 and PDE8 are cAMP specific, PDE5, PDE6 and PDE9 are cGMP specific while the remaining ones have dual specificity and can hydrolyse both cAMP and cGMP (Lugnier 2006). The specificity for cyclic nucleotides is governed by the "Glutamine switch", a residue which is known to stabilise the binding of the purine ring within the catalytic pocket. For dual specificity PDEs this glutamine residue must be able to rotate freely so it can form hydrogen bonds with both cAMP and cGMP. For PDEs specific to one cyclic nucleotide, this glutamine residue is constrained by surrounding residues so that it adopts a highly selective orientation for either cAMP or cGMP (Bender and Beavo 2006).

Each cell type can express several different PDEs and the enzymes' sub-cellular localisation dictates local cyclic nucleotide concentrations within the cell. In addition to genetic regulation of PDE activity via expression level, PDE activity is also modulated via biochemical mechanisms such as phosphorylation, allosteric binding of cGMP or cAMP, binding of Ca^{2+}/calmodulin, and through a vast array of protein-protein interactions. The role of PDEs is to shape the three-dimensional cAMP "cloud" formed after cell surface receptor activation. Fine control of the amplitude and duration of the cyclic-nucleotide second messenger response underpins the specificity of receptor function by modulating downstream signalling events (Bender and Beavo 2006). The complexity of cyclic

nucleotide signalling is exemplified by the diversity of the PDE superfamily of enzymes. There are 11 gene families of PDEs, PDE1-11, in humans and each family can be encoded by up to 4 distinct genes. Further diversity results from the fact that each gene produces multiple splice variants, resulting in more than 100 different PDE isoforms (Lugnier 2006). A summary of the human PDE superfamily is given in table 1.2.

Table 1.2 - The Phosphodiesterase (PDE) Superfamily

Protein Name	Isoforms	Substrate	Property	Inhibitors	Tissue Expression Profile
PDE1	A, B & C	cAMP, cGMP	Ca-calmodulin-activated	Vinpocetine, ICC224, IBMX	Brain, smooth muscle, heart, lung, sperm
PDE2	A	cAMP, cGMP	cGMP-activated	EHNA, BAY60-7550, IBMX	Brain, adrenal medulla, heart, macrophages
PDE3	A & B	cAMP, cGMP	cGMP-inhibited	Cilostamide, Milrinone, IBMX	Heart, vascular smooth muscle, platelets, oocyte kidneys
PDE4	A, B, C & D	cAMP	cGMP-insensitive	Rolipram, Rofumilast, Cilomilast, IBMX	Ubiquitous
PDE5	A	cGMP	PKA/PKG-phosphorylated	Sildenafil, Zaprinast, Tadalafil, IBMX, Dipyridamole	Platelets, vascular smooth muscle, brain, lung, heart, kidney, skeletal muscle
PDE6	A, B & C	cGMP	Transducin-activated	Dipyridamole, Sildenafil	Retina
PDE7	A & B	cAMP	Rolipram-insensitive	IBMX	Brain, immune cells, heart, liver skeletal muscle
PDE8	A & B	cAMP	Rolipram-insensitive IBMX-insensitive	Dipyridamole, PF-04957325	Brain, testis, immune cells
PDE9	A	cGMP	IBMX-insensitive	BAY 73-6691, PF-04447943	Brain, spleen, gastrointensital, prostate
PDE10	A	cAMP, cGMP	cAMP-activated	Papaverine, Dipyridamole, PF-2545920	Brain, testis, Striatum
PDE11	A	cAMP, cGMP	Unknown	Dipyridamole, Tadalafil, BC11-38	Brain, skeletal muscle, prostate, testis

Table adapted from Bender & Beavo 2006, Lugnier 2006.

1.4.4.2 PDE Expression in the Brain

The characterisation of PDE isoform expression profiles has been a crucial step for the targeting of PDE inhibitors to different pathophysiological processes. A comprehensive study of PDE mRNA distribution in the brain was carried out (Lakics, Karran et al. 2010) and it showed that PDEs are broadly distributed in brain regions, which control higher cognitive functions, such as learning and memory. However, some isoforms are more restricted in their distribution and are far more abundant in specific brain regions (Lakics, Karran et al. 2010).

PDE1 is found in several brain regions. PDE1B mRNA is found at high levels in caudate and nucleus accumbens, while PDE1C is found at high levels in the substantia nigra and is thought to play an important role in signal transduction in these regions (Lakics, Karran et al. 2010). PDE1B knockout mice have increased locomotor activity and in certain contexts decreased learning and memory. A role for PDE1B in dopaminergic signalling has also been suggested. PDE1C is highly expressed in olfactory sensory cilia and is thought to modulate signalling pathways involving odorant stimulation (Bender and Beavo 2006).

The most prevalent PDE mRNA in the hippocampus is PDE2A. Studies using cultured rodent neurons have shown that PDE2A plays an important role in regulating cGMP levels in the hippocampal region, and inhibition of PDE2A leads to improved memory performance (Lakics, Karran et al. 2010). PDE2A expression in neuronal dendrites and axons, suggests that compartmentalisation of this isoform at the input/output regions of neurons and its localisation at synapses is thought to directly affect synaptic activation. PDE2A expression is also concentrated in the mossy fibres from hippocampal dentate granule cells and at the entorhinal cortex, one of the first regions to show morphological changes in AD (Bales, Plath et al. 2010).

Ubiquitous distribution of PDE4A, B and D is found throughout the human brain, while low levels of PDE4C mRNA are detectable in cortex and cerebellar granule cells. Human genomic association analyses have identified fundamental roles of PDE4B and D in depression, schizophrenia and memory (Lakics, Karran et al. 2010). Several PDE4 knockout mice have been created to facilitate characterisation of the physiological functions of different PDE4 isoforms. PDE4B knockout, for example, results in increased antidepressant and reduced anxiolytic behavioural phenotypes. PDE4D knockout mice display an increase in long-term memory and an increase in anti-depressant behavioural

phenotypes, and also a reduction in a behavioural correlate of emesis (Houslay, Schafer et al. 2005).

PDE5A mRNA is detected at relatively low levels in all brain regions. High levels of expression have been detected in cerebellar Purkinje neurons but most of PDE5A mRNA is located in the vasculature (Lakics, Karran et al. 2010). A study using in situ hybridisation in aged human brains did not detect any PDE5A mRNA (Reyes-Irisarri, Markerink-Van Ittersum et al. 2007). Despite this, PDE5 inhibition has been shown to be neuroprotective in rodent models of AD and can modulate certain aspects of neurological processing in humans (Reneerkens, Rutten et al. 2009).

The mRNA levels for PDE7A are lower in the brain than for other tissues such as spleen, skeletal muscle and heart. PDE7B expression is more prevalent in the CNS than PDE7A, and is most highly detected in nucleus accumbens, cortex and hippocampus (Lakics, Karran et al. 2010). The other high affinity cAMP-specific PDE, PDE8, is also detectable in the human brain. PDE8A mRNA levels are similar to PDE8B in cerebellum, dorsal root ganglion, spinal cord, thalamus and substantia nigra. PDE8B is strongly expressed in caudate, nucleus accumbens, cortex, hippocampus, thalamus and hypothalamus (Lakics, Karran et al. 2010). PDE7 and 8 have been shown to be upregulated in respect to AD progression, as classified through Braak and Braak staging (Braak and Braak 1991). PDE7A is upregulated in early stages of AD, whereas PDE8B transcripts increased significantly in more advanced stages of AD (Perez-Torres, Cortes et al. 2003).

Significant levels of PDE9A mRNA are detectable in all regions within the CNS. This points to the importance of PDE9A in the regulation of basal cGMP levels within the brain (Lakics, Karran et al. 2010). PDE9A expression is readily detectable in the olfactory bulb, hippocampus and cortical layer V. PDE9A mRNA has also been detected in astrocytes and Scwann cells. In human post-mortem brain tissue, PDE9A mRNA was detected in the cortex, hippocampus and cerebellum, an expression profile similar to that in rodents. There were also no apparent differences in PDE9A expression profile in AD patients compared to healthy elderly controls. In PDE9A knockout mice, LTP was enhanced in hippocampal slices and this effect was repeated in rats using a highly selective PDE9A inhibitor (Bales, Plath et al. 2010).

PDE10 has a more distinctive expression pattern, with high expression in caudate nucleus, nucleus accumbens, basal ganglia, cerebellum and cerebral cortex. Papaverine and more

selective inhibitors of PDE10 have shown efficacy in behavioural assays relevant to antipsychotic activity in wild-type but not PDE10 knockout mice. As a result of these findings, PDE10 has now become a major target for the treatment of schizophrenia (Lakics, Karran et al. 2010).

1.4.4.3 PDE inhibition as a therapeutic strategy

Soon after the original discovery of PDEs, caffeine was found to be an effective inhibitor of PDE activity and a number of related xanthines, such as theophylline, have been used therapeutically for many years (Bender and Beavo 2006). Sadly, most of the early PDE inhibitors had a narrow therapeutic window as they would be non-selective and inhibit a broad range of PDE types. Despite these early problems with non-selectivity, the principle of PDE inhibition became a widely accepted avenue for therapeutic intervention (Bender and Beavo 2006).

There are a number of reasons that make PDEs such good therapeutic targets; firstly, the pharmacological premise that modulation of degradation of any signalling molecule often results in a more rapid and pronounced change in concentration compared to modulation of synthesis. It has been known for many years that most tissues contain at least an order of magnitude higher maximal cyclic nucleotide phosphodiesterase activity than for cyclic nucleotide cyclase activity. Secondly, the large numbers of different PDE isoforms expressed in mammalian cells are closely connected with various physiological processes in the body and presumably to various pathological conditions. It is widely believed that the development of isoform specific inhibitors can target specific pathophysiological conditions with a reduced chance of causing non-specific side-effects. The therapeutic and commercial success of the PDE5 inhibitor sildenafil (Viagra®) has been the proof of principle in this field. Thirdly, PDEs are good targets due to their substrate concentrations within cells. Cyclic nucleotide levels within cells typically range between 1 and 10µM. This means that a competitive inhibitor doesn't have to compete with high concentrations of endogenous substrates to be effective. Evidence from the pharmacological landscape suggests that it is relatively straightforward to develop small molecules that are highly selective for different members of the PDE families (Bender and Beavo 2006).

The prototypical PDE4 inhibitor rolipram has the longest established neuro-modulatory effects and has been shown to promote cognitive enhancement and neuroprotection. PDE4s have unique architecture consisting of a sub-family specific C-terminal domain, dual

regulatory domains called upstream conserved region 1 (UCR1) and upstream conserved region 2 (UCR2) together with an isoform specific N-terminal region which determines sub-cellular localisation (Houslay, Schafer et al. 2005). With over 25 different isoforms, PDE4 is the most common cAMP hydrolysing enzyme in the body. Selective inhibition of PDE4 with rolipram can produce behavioural and neuroprotective effects through the cAMP/PKA/CREB signalling cascade. Rolipram has been tested as a monotherapy for depression since its discovery, and rolipram's effects have been suggested to be through its activity towards PDE4D in particular, as knockout mouse models have decreased immobility in tail suspension and forced-swim tests, which are predictive of depressive-like behaviour. Furthermore, rolipram did not affect isoproterenol induced potentiation of cAMP signalling in PDE4D knockout mice. PDE4 predominately hydrolyses cAMP formed by the stimulation of β-adrenergic receptors, which are thought to mediate the effects of several anti-depressant drugs and may be indicative of a common mechanism of efficacy (Halene and Siegel 2007).

Interestingly, Hsp20 directly interacts with the catalytic domain of PDE4D5 and disruption of this complex promotes phosphorylation of Hsp20 and promotes its protective effects in cardiomyocytes (Sin, Edwards et al. 2011). This interaction was discovered following experimentation on the ability of rolipram to induce Hsp20 phosphorylation in the absence of agents that increased synthesis of cAMP (such as forskolin or isoproterenol). Disruptor peptides targeting this interaction have been shown to protect against hypertrophic response induced via chronic β-adrenergic stimulation (Sin, Edwards et al. 2011). The functional consequences of targeting PDE4D5-Hsp20 interaction in the brain are discussed in subsequent chapters.

In schizophrenia models, the disruption of cAMP signalling mimics many of the phenotypic markers for schizophrenia and treatment using receptor-independent mechanisms to potentiate cAMP signalling pathways has been predicted to have anti-psychotic effects. Indeed, rolipram can alter markers of psychosis such as pre-pulse inhibition (PPI) of startle, event-related potentials and learning and memory. Rolipram is thought to mediate its anti-psychotic effects through inhibition of PDE4B, as the ED50 of rolipram in conditioned avoidance response was shifted threefold in PDE4B knockout mice. PDE4B is known to associate with DISC1 (Disrupted in Schizophrenia 1) and cAMP concentration regulates this association. Furthermore two mutant DISC1 proteins in mice had reduced ability to bind PDE4B and gave rise to phenotypes typical of schizophrenia and depression (Halene and Siegel 2007).

Interest in rolipram and PDE4 inhibition in general has resulted in the cAMP signalling system being regarded as a potential target for treating AD. The accumulation of Aβ peptides in AD animal models leads to inhibition of CREB activation and impairs LTP in the hippocampus. Therefore enhancing cAMP signalling to overcome Aβ-mediated inhibition of this pathway may be a novel way to treat cognitive deficits associated with the disease (Vitolo, Sant'Angelo et al. 2002).

Unfortunately, the clinical efficacy of rolipram and other PDE4 inhibitors has been limited due to adverse side effects such as, nausea, emesis and diarrhoea. This is thought to be due to inhibition of PDE4 subtypes in the emetic centres of the brain (Houslay, Schafer et al. 2005). Therefore the creation of subtype specific inhibitors or compounds without an emetogenic profile is highly desirable.

More recently, PDE5 inhibition has emerged as a strategy to improve cognition via the cGMP/PKG/CREB pathway (Bales, Plath et al. 2010). Inhibition of PDE5 was successfully pursued as a treatment of erectile disorders and resulted in the creation of highly selective PDE5 inhibitors such as sildenafil (Viagra), vardenafil (Levitra) and tadalafil (Cialis). These compounds and in particular sildenafil, have recently been shown to be neuroprotective and enhance cognition in a variety of animal models. Sildenafil has been shown to improve memory consolidation and object recognition in mice, reverse NO synthase inhibitor effects in a complex learning paradigm, and affect active and passive avoidance learning in several animal models (Reneerkens, Rutten et al. 2009). Recently, in a study using an AD mouse model, sildenafil was shown to rescue synaptic and memory deficits associated with amyloid deposition. Sildenafil increased the phosphorylation of CREB and caused both an acute and long-lasting reduction in Aβ levels (Puzzo, Staniszewski et al. 2009).

In the corpus cavernosum and vascular smooth muscle, sildenafil induces dose-dependent relaxation and has been associated with increases in Hsp20 phosphorylation. Phosphorylation of Hsp20 at serine 16 is necessary for smooth muscle relaxation, therefore Hsp20 is likely to be a major substrate of the NO/cGMP/PKG signalling cascade in this tissue (Tessier, Komalavilas et al. 2004). Whether sildenafil induced Hsp20 phosphorylation plays any physiological role in the brain has not previously been investigated.

Finally, the highly specific cGMP-phosphodiesterase that has received attention from the pharmaceutical industry in recent years is PDE9. PDE9A has one of the lowest Km values of any cGMP hydrolysing phosphodiesterase (70-170nM). Its localisation to brain regions that also express sGC and NO synthase suggests that PDE regulates cGMP levels in the brain (Bender 2006). The first reported PDE9A selective inhibitor was BAY 73-6691 with an *in vitro* IC_{50} of 55nM. BAY 73-6691 has been shown to enhance early LTP in hippocampal slices from rats and enhanced acquisition, consolidation, and retention of long-term memory in preclinical behavioural paradigms such as; social recognition, scopolamine-disrupted passive avoidance, and MK-801-induced short-term memory deficits through mechanisms associated with cGMP/PKG/CREB signalling. PDE9 inhibitors are currently undergoing clinical investigation by several companies and may provide therapeutic benefit for patients with AD (Bales, Plath et al. 2010).

Inhibitors of these three PDE families (4, 5 and 9) are being actively pursued as cognitive enhancers and are regarded as putative treatments for AD. The key effector protein appears to be CREB, on which both the cAMP and cGMP signalling cascades converge to modulate synaptic plasticity. However, other substrate proteins of both PKA and PKG cannot be ruled out as mediating the neuroprotective and cognitive enhancing effects mediated by PDE inhibition. The heat-shock protein Hsp20 is a substrate that can be targeted by both PKA and PKG and plays a key role in several physiological systems including smooth muscle relaxation and contractility of the heart; however its role as a neuroprotective agent is only beginning to emerge.

1.5 Thesis Aims & Hypothesis

Alzheimer's disease is a neurodegenerative disorder with high socioeconomic burden and unmet clinical need (Prince 2011). There are several endogenous pathways that can regulate the accumulation of toxic Aβ peptides; one of these includes the chaperone-like small heat-shock proteins. Heat-shock proteins can also regulate several key aspects of cellular homeostasis and attenuate cytotoxicity associated with aberrant protein folding, typical of Aβ amyloidogenesis. This makes sHSPs an attractive target as they orchestrate more than one protective pathway.

The small heat-shock protein, Hsp20 was of particular interest to our group (Baillie) due to it being a small heat-shock protein with a consensus PKA and PKG phosphorylation site. Phosphorylation of Hsp20 evokes a number of physiological functions that have been well

characterised in heart and smooth muscle (Fan and Kranias 2011). Recent evidence suggested that Hsp20 could associate with Aβ in the brain of AD patient brain tissue and may possibly represent an endogenous protection mechanism in this tissue. Furthermore, previous studies have shown that Hsp20 can associate with Aβ and alter its aggregation dynamics and reduce subsequent cytotoxicity.

Our hypothesis proposes that Hsp20 interacts with Aβ initially intracellularly were it acts primarily as an amateur chaperone to prevent Aβ misfolding. Through targeted phosphorylation of Hsp20, via activation of the second messenger signalling pathways; will further enhance Hsp20's chaperone functions resulting in improved capacity to bind Aβ. This in turn should lead to improved inhibition of Aβ aggregation, a reduction in Aβ induced toxicity and attenuation of neuronal cell-death (Fig. 1.8). We believe that the modulation of the Hsp20/Aβ interaction may represent a novel neuroprotective mechanism that could be targeted to potentially treat AD.

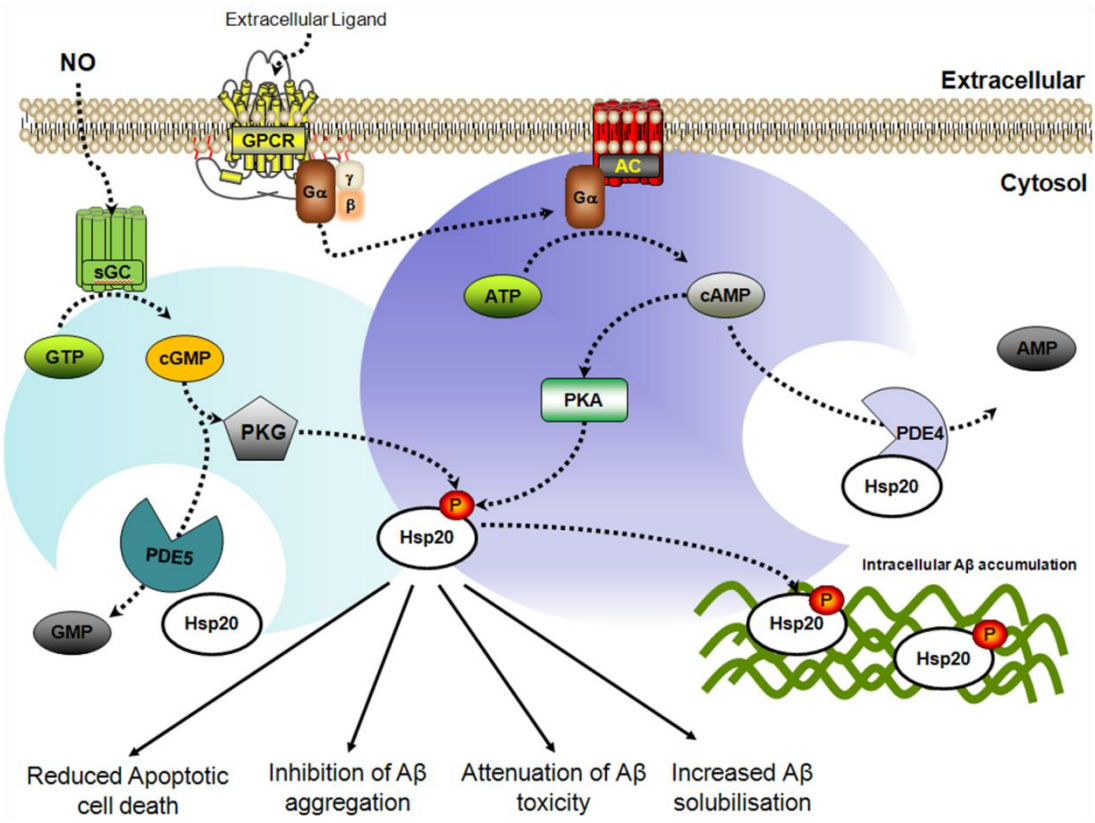

Figure 1.8 – Hypothesis – Phosphorylation of Hsp20 improves its ability to inhibit Aβ aggregation and attenuates Aβ toxicity.
Hsp20 has been shown previously to inhibit Aβ aggregation and reduce Aβ toxicity when co-incubated prior to overlaying cells. Furthermore, Hsp20 was shown to solubilise and clear Aβ that had accumulated and the cell membrane (Wilhelmus, Boelens et al. 2006). It has however been shown that Aβ intraneuronal accumulation occurs early in the aetiology of AD resulting in deficits in neurotransmission and precedes appearance of extracellular Aβ deposition (Oddo, Caccamo et al. 2003). By targeting Hsp20 phosphorylation either through activation of the cAMP or cGMP second messenger signalling pathways we can promote Hsp20's ability to interact with intraneuronal Aβ resulting in inhibition of Aβ aggregation, attenuation of Aβ induced toxicity and reduction in neuronal cell death.

In order to test this hypothesis we wanted to characterise the effect of Hsp20 phosphorylation on the binding of Aβ and whether phosphorylation of Hsp20 can alter the aggregation dynamics of the Aβ peptide, a key process in the aetiology of AD. In order to do this we utilised peptide array technology to map the binding domains on both Hsp20 and Aβ. We then developed several mutant of Hsp20, including a phosphomimetic where the serine at position 16 was mutated to an aspartic acid in order to mimic the charge of a phosphate group. Using these mutants we studied any differences in Hsp20's characteristics relative to the wild-type Hsp20 in a number of Aβ binding and aggregation assays.

Secondly, we wanted to develop a human-based cell model for characterising Aβ cytotoxicity. To do this we employed a novel real-time cell monitoring system to measure Aβ toxicity thereby providing a platform for testing agents with anti-AD potential. Using this platform we initially wanted to examine whether increasing intracellular expression of Hsp20 can attenuate Aβ-induced cytotoxicity and also whether activating the cAMP and cGMP second messenger pathways, promotes endogenous Hsp20 phosphorylation in human neuronal-like cells and promotes Hsp20's protective effects which have already been established in the heart. This would represent a novel neuroprotective mechanism (distinct from CREB activation) that may be induced using readily available PDE inhibitors.

As an aside we also wanted to develop novel inhibitors of PDE4 which lack the emetogenic profile typical of PDE4 selective inhibitors such as rolipram, which can promote Hsp20 phosphorylation and may also have repositioning potential for treating neurological conditions associated with pathophysiological changes in cAMP signalling pathways.

2 Materials & Methods

2.1 Materials

All chemicals used to conduct this research were of analytical grade and were supplied by Sigma-Aldrich, UK, unless otherwise stated. Compounds were typically dissolved in dimethyl sulfoxide (DMSO) and added to cells at a concentration no greater than 0.1% (v/v). For *in vitro* assays higher concentrations of DMSO were permissible alongside suitable controls. All aqueous solutions were prepared with deionised water (dH_2O) (Millipore, USA).

2.2 Preparation of Aβ

For cell-based assays synthetic Aβ peptides were purchased from rPeptide® (Georgia, USA). $A\beta_{1-42}$ (A-1002) peptides are the recombinant form of the human Aβ peptide. $A\beta_{1-42}$ scrambled peptide (Aβscr) (A-1004) which is a rearranged version of the peptide that carries the overall weight and charge of $A\beta_{1-42,}$ was used as a control. Peptides were dissolved in DMSO at a concentration of 5mg/ml and sonicated in a water bath for 15 minutes. Samples were aliquoted and stored at -20°C until required. To create neurotoxic $A\beta_{1-42}$ derivatives a method similar to that described by Lambert et al. (1998) was used, where $A\beta_{1-42}$ (or scrambled) peptides were brought to 100uM in cold PBS and incubated at 4-8°C for 24 hours. The resulting aggregated peptides were added directly to cell culture medium typically at 1:10 dilution (Aβ: media). Samples from each 100µM stock added were taken for SDS-PAGE and western blotting analysis.

For NMR assays ^{15}N uniformly labelled $A\beta_{1-40}$ (A-1101-2) was also purchased from rPeptide® (Georgia, USA). In order to fully monomerise the peptide it was resuspended in 1% NH_4OH and sonicated in a water bath for 15 minutes. The peptide concentration was brought to 400µM with cold NMR buffer (50mM NaPi (Na_2HPO_4) pH 7.5). The peptide was then dialysed in 4 litres of cold NaPi for 2 hours to remove NH_4OH and then added directly to Hsp20 containing NaPi buffer for immediate analysis. $A\beta_{1-40}$ was maintained below 4^oC in order to reduce aggregation.

For real-time $A\beta_{1-42}$ aggregation assays Synthetic $A\beta_{1-42}$ peptides were purchased from Anaspec Inc. (USA), suspended in 100% 1,1,1,3,3,3 hexafluoro-2-propanol (HFIP) at 5 mg/mL and incubated for complete solubilisation at room temperature for 1.5 h. HFIP was subsequently removed by evaporation under vacuum for 4 h and stored at -20^oC.

2.3 Plasmid DNA

For mammalian expression of wild-type human Hsp20 (NM_144617.1), pcDNA3.1-Hsp20-V5-His-TOPO was kindly provided by Dr Helen Edwards. For recombinant protein expression of human Hsp20, pET28c-His-Hsp20 was kindly provided by Dr Lucien Gibson. All plasmid work was carried out in sterile conditions and all buffers made in-house were autoclaved prior to use.

2.3.1 Site directed mutagenesis

Site-directed mutagenesis of both Hsp20 plasmids was carried out in accordance with QuikChange II Site-Directed Mutagenesis Kit (Agilent Technologies) using the following primers:

Hsp20-S16D –	Forward	5'-ttggctgcgccgcgccgatgccccgttgcccggac-3'
	Reverse	5'- aaccgacgcggcgcggctacggggcaacgggcctg-3'
Hsp20-S16A -	Forward	5'-ttggctgcgccgcgccgcggccccgttgcccgg-3'
	Reverse	5'-aaccgacgcggcgcggcgccggggcaacgggcc-3'
Hsp20-R13,14A	Forward	5'-cagccgtcttggctggccgccgcctcggccccgtt-3'
	Reverse	5'-gtcggcagaaccgaccggcggcggagccggggcaa-3'
Hsp20-P20L	Forward	5'-cctcggccccgttgctcggactttcggcgcc-3
	Reverse	5'-ggagccggggcaacgagcctgaaagccgcgg-3'

In brief, Hsp20-WT constructs were used as the template DNA and standard Polymerase Chain Reaction (PCR) was conducted using the mutagenic primers noted above. Following PCR the methylated template strand was digested using Dpn I for a minimum of 4 hours prior to transformation into appropriate *E. coli* strains.

2.3.2 Transformation

For mammalian transfection purposes One Shot® TOP10 (Invitrogen, UK) chemically competent *E. coli* cells were used for plasmid production. For recombinant protein expression One Shot® BL21 (DE3) chemically competent cells were used as these strains are specifically constructed for high level protein production.

Chemically competent cells were stored at -80°C and thawed on ice immediately prior to use. Approximately 10ng of appropriate plasmid DNA was added per aliquot of cells and mixed gently. Cells were then incubated on ice for 20 minutes then heat-shocked for 30 seconds at 42°C then returned to ice for 2 minutes before the addition of 500ul of SOC media (Invitrogen, UK) to the cells. Cells were then incubated at 37°C for 1 hour at 300rpm to allow for recovery of the cells. 50-500ul of transformation mix was then added to pre-warmed agar plates made with sterile Luria-Bertani medium (LB) (1% tryptone (w/v), 0.5% yeast extract (w/v), 170mM NaCl) supplemented with appropriate antibiotic, typically kanamycin (50ug/ml) or ampicillin (100ug/ml). Plates were incubated upside down at 37°C overnight and colony growth indicated successful transformation.

2.3.3 Amplification & Purification

In order to amplify plasmid DNA, single colonies were picked from the agar plates using sterile pipette tips and grown overnight at 37°C in LB with appropriate antibiotic in an orbital shaker (220rpm). For colonies containing plasmid subjected to site-directed mutagenesis colonies were grown in 25ml of LB overnight. The culture was pelleted and plasmid DNA was purified in accordance with QIAprep Spin Miniprep Kit (Qiagen), in accordance with manufacturer's protocol. The resulting plasmid DNA was performed by the University of Dundee DNA Sequencing and Services (www.dnaseq.co.uk) in order to verify that site-directed mutagenesis was successful. DNA was supplied as per website instructions and sequences were analysed using Sequence Scanner v1.0 (Applied Biosystems).

For mammalian expression purposes where high concentration of high quality plasmid DNA is required, 500ml of LB supplemented with appropriate antibiotic was inoculated from either single colonies from agar plates or from frozen glycerol stocks (see 2.3.4) and grown overnight at 37°C, 220rpm. DNA was isolated using QIAprep Maxiprep kit (Qiagen) in accordance with manufacturer's instructions. Purified DNA was then eluted using sterile dH_2O and stored at -20°C.

2.3.4 Quantification

Purified plasmid DNA concentration was determined using a Nanodrop 3300 spectrophotometer (Thermo-Scientific). The ratio of absorbance at 260nm and 280nm determines the purity of the DNA. The concentration is calculated using Beer-Lambert

law, where an optical density of 1 at 260nm is the equivalent of 50ug/ml of double-stranded DNA; this is done automatically by the Nanodrop software.

2.3.5 Plasmid Storage

For long-term plasmid storage, 800ul of overnight culture was added to 800ul of glycerol in a sterile cryovial, snap-frozen on dry ice then stored at -80°C until required.

For amplification of glycerol stocks, cryovials were placed on dry-ice to prevent thawing and frozen stocks were scraped using a sterile pipette tip and transferred to LB containing appropriate antibiotic.

2.4 Expression and Purification of Recombinant Proteins

2.4.1 Histidine purification

The human Hsp20 sequence was cloned into the pET-28c in order to introduce an N-terminal poly-histidine sequence and transformed into One Shot® BL21 chemically competent *E. coli* cells (Invitrogen, UK) for efficient expression of recombinant proteins. 25ml of LB medium supplemented with 50ug/ml of kanamycin were inoculated with BL21 cells containing the pET-28c plasmid and incubated overnight at 37°C at ~200rpm. Overnight cultures were then added to 500 ml of LB medium and grown until the optical density (OD_{600}) reached between 0.6 and 1.0 which indicates that the bacterial cells are in the exponential growth phase. At this point 1mM of isopropyl-β-D-thiogalactopyranoside (IPTG) was added to induce recombinant protein expression. Cultures were then grown until the following morning at 25°C to help prevent aggregation of Hsp20. Cultures were centrifuged at 6000rpm for 10 minutes at 4°C in order to pellet the cells. Cell pellets were then resuspended in His purification Lysis Buffer - PBS, 360mM NaCl, 5mM imidazole, pH 8.0, and then snap frozen on dry ice. Cells were then thawed at room temperature and cell slurry was supplemented with 1mM dithiothreitol (DTT), mini-complete protease inhibitor tablet (Roche) and DNase with added 1mM Mg^{2+}. Cells were then sonicated on ice at 40-60 kHz (Jencons, England) for 3 x 3 minute intervals to ensure sufficient lysis of cells. The slurry was then centrifuged at 50000xg for 30 minutes at 4°C to remove insoluble cell debris. The supernatant was then incubated with pre-equilibriated nickel-nitrilotriacetic acid (Ni-NTA) beads (Qiagen) overnight at 4°C under gentle agitation to allow binding of his-tagged protein. The solution was then transferred to a gravity flow column (Biorad) to allow for collection of Ni-NTA beads with bound protein. Several

washes with buffer A was carried out to ensure all of the beads were transferred into the gravity flow column. After several washes 46ml of Lysis Buffer was combined with 4ml of Elution Buffer - PBS, 360mM NaCl, 250mM imidazole, pH 8.0, for two more stringent washes. Protein was then eluted with Elution buffer in 1ml fractions and samples were analysed using SDS-PAGE with one gel being used for Coomassie staining to check for purity and another gel used for western blot analysis.

2.4.2 Protein concentration

The concentrations of purified recombinant proteins and cell lysates were determined in accordance with the Bradford dye-binding method (Bradford 1976). The Bradford assay is a colourimetric assay based on the colour change of Coomassie Blue G-250 when it binds to various concentrations of protein. In brief, Bradford reagent was prepared using 1 part Bradford dye (Bio-Rad) and 4 parts dH_2O. To generate a standard protein concentration curve bovine serum albumin (BSA) was used at concentrations ranging from 0 to 5 mg/ml. Protein samples were prepared at various dilutions, typically 1:10, 1:50 & 1:100, in a 96-well microtitre plate. Following addition of Bradford reagent, 96-well plates were read at 595nm on an MRX microplate reader (Dynex Technologies, UK). The standard curve of absorbance against protein concentration was plotted using least squares regression analysis to give linear regression and provide relative protein concentration. Dilution factors were then applied to the resulting protein concentration.

2.5 Protein-Protein Interaction Studies

2.5.1 Peptide Arrays

Peptide arrays were developed in-house using the SPOT™-synthesis technique described by (Frank 2002) using the AutoSpot-Robot ASS 222 (Intavis Bioanalytical Instruments). Solid phase peptide synthesis is based on standard Fmoc (9-fluorenylmethoxycarbonyl) chemistry (Fields 1990) and peptides are synthesised directly onto Whatman 50 cellulose membranes. Peptide arrays are able to bind recombinant proteins of interest and allow for rapid identification of interaction domains and biologically active motifs. Typically, a library of overlapping 25mer peptides, shifted sequentially by 5 amino acids in an N- to C-terminal direction are synthesised in order to identify interaction domains.

Following identification of possible binding sites, mutations can be introduced in order to ascertain the importance of a residue in mediating an interaction. In this case sequential

alanine scanning arrays were created to determine whether a residue is an essential mediator of an interaction. In the event of alanine being the native residue it is substituted for aspartic acid. However, any non-native amino acid can be readily introduced to a given peptide sequence in order to ascertain its effect on binding. Within this body of work I was able to introduce aspartic acid in place of serine as this can mimic the effect of introducing a negative charge to the peptide in a similar way as phosphorylation does *in vivo,* also referred to as a phospho-mimetic substitution.

Prior to probing arrays, they were first activated by bathing in 100% ethanol for several minutes followed by a 5 minute wash in TBST (20mM Tris-HCl, 150mM NaCl, 0.1% Tween20, pH 7.6) this removes preservative material from the arrays. Arrays were then blocked in 5% milk/TBST (w/v) solution for 1 hour at room temperature under agitating conditions. 10ug/ml of recombinant protein diluted in a 1% milk/TBST (w/v) solution was then incubated with arrays overnight at 4^{o}C with agitation. The following day arrays are washed 3 times for 10 minute intervals with TBST before being probed with the specific primary antibody raised against the recombinant protein or the fusion tag. Primary antibodies were diluted in 1% milk/TBST and left overnight at 4^{o}C. After incubation arrays were washed 3 times for 10 minutes before incubating arrays with secondary antibodies conjugated with horse-radish peroxidise (HRP) diluted in 1% milk/TBST for 1 hour. Arrays were then subjected to a further 3 x 10 minute washes before being analysed using Western Blotting techniques (see 2.6.3).

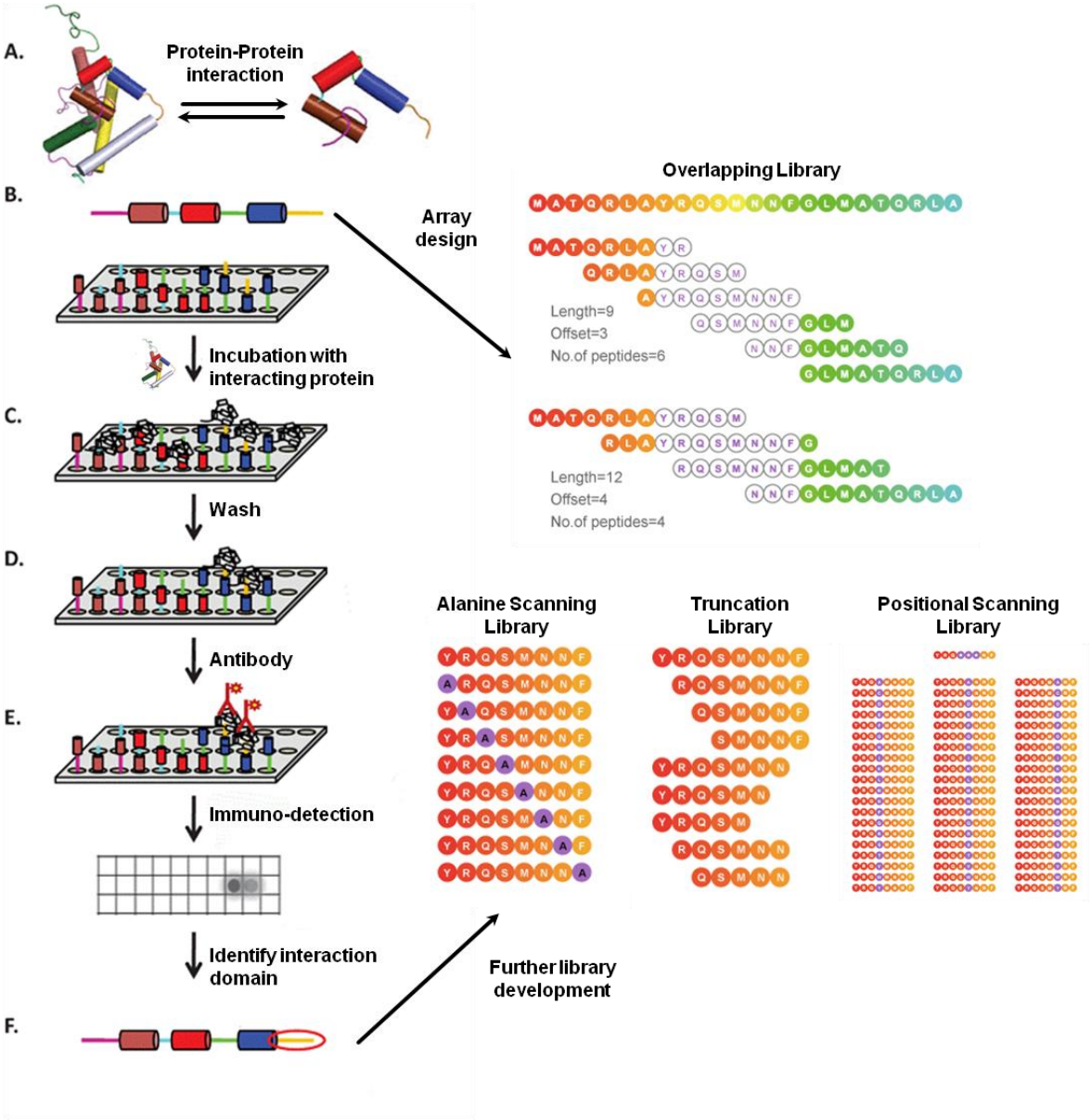

Figure 2.1 – Schematic representation of peptide array methodology
A general representation of peptide array design and screening. A protein-protein interaction is identified for analysis and one of the protein sequences are chosen to develop a peptide library (A). Initial array design is typically based on overlapping peptide sequences (≤ 25mers) that encompass the whole protein sequence (B). The scanning array requires incubation of the binding protein with the peptide array followed by several wash steps (C & D). Detection of the binding protein is done using an appropriate antibody which can subsequently be detected using enhanced chemi-luminescent techniques. Each dark spot on a developed array illustrates binding of the protein to a specific peptide (E). Analysis of spots allow for the identification of domains responsible for mediating the interaction. Positively interacting sequences can then be tested in further arrays such as an alanine scanning arrays to determine key residues within a binding domain, a truncation library to determine the minimum interacting domain, and a positional scanning Library which allows for peptide sequence optimisation (F). Modified from (Katz, Levy-Beladev et al. 2011).

2.5.2 *In vitro* pull-down assay

In vitro pull-down assays were carried out in order to validate interactions resulting from the peptide array data. This would ensure that discrete changes within 25mer peptides would have an effect on the full-length protein. Using equimolar concentrations, various His-purified Hsp20 proteins and monomeric $A\beta_{1-42}$ were co-incubated in PBS for more than 16 hours under agitating conditions. After incubation period insoluble aggregates were removed through centrifugation at 13000rpm. Hsp20 was then immunoprecipitated using His-agarose conjugated beads. Any complex between Hsp20 and $A\beta_{1-42}$ are captured by the beads which were then sedimented by centrifugation at 6000rpm for 3 minutes, followed by several washes in PBS. Proteins were eluted from beads by boiling in 2x SDS sample buffer for 5 minutes. Any interacting $A\beta_{1-42}$ was assessed using SDS-PAGE and Western Blotting techniques.

2.6 Protein Analysis

2.6.1 SDS-PAGE

The Sodium dodecylsulphate – polyacrylamide gel electrophoresis (SDS-PAGE) method was used to resolve proteins by their molecular weight and charge. SDS-PAGE analysis was carried out on 4-12% NuPage® pre-cast gels using Invitrogen X-cell apparatus and NuPage® Novex gel system. Proteins samples were prepared for SDS-PAGE by boiling for 5 minutes in 2x Laemmli sample buffer or 5x SDS sample buffer (assay volume dependent) supplemented with reducing agent (5% β-mercaptoethanol (v/v)). Samples were loaded into gels immersed in either NuPage 1 x MES buffer to resolve proteins smaller than 50kDa, or 1 x MOPS for proteins larger than 50kDa. Precision Plus All Blue Standards (BIO-RAD, USA) was used as a molecular weight marker. Gels were subjected to electrophoresis at 180V for between 40 minutes and 1 hour to allow for adequate separation.

2.6.2 Coomassie Staining

Coomassie staining was carried out in order to visualise protein levels following SDS-PAGE. Gels were removed from pre-cast NuPage cassettes and incubated in Coomassie staining solution (1.25g Coomassie Brilliant Blue R250, 444ml Methanol, 56ml acetic acid to a final volume of 1L with dH_2O) at room temperature for 1-2hours under gentle agitating conditions. Gels were then incubated with a de-stain solution (444ml Methanol,

56ml acetic acid to a final volume of 1L with dH_2O) for up to 16 hours at room temperature to remove the Coomassie stain. Coomassie Brilliant Blue R250 remains bound to all protein present in the gel and allows for identification of various proteins of interest. Gels were then scanned and saved as Jpeg or TIFF files for subsequent analysis.

2.6.3 Western blotting

SDS-PAGE gels were transferred to nitrocellulose membranes using an Invitrogen X-Cell apparatus (Invitrogen, Paisley) using Nupage® X-cell Blotting Module and 20x NuPage® transfer buffer containing 20% methanol (v/v) in 200ml of dH_2O. Proteins were transferred at 28V for 1.5 hours and transfer efficacy was established through visualisation of molecular weight markers or Ponceau staining. Following transfer membranes were incubated in 5% milk solution (w/v) in 1x TBST (20mM Tris-Cl pH7.6, 150mM NaCl, 0.1% Tween 20) for 1 hour at room temperature under agitating conditions to block non-specific antibodies binding to the membrane. Membranes were then incubated in 1% milk solution with the appropriate primary antibody added and incubated overnight at 4°C with agitation. The membrane was then washed for 3 x 10mins with 1x TBST, and incubated in fresh 1% milk solution containing appropriate horse-radish peroxidise (HRP)-conjugated secondary antibody for 1-2 hours at room temperature (details of antibodies and dilutions given in Table 2.1). After incubation membranes were washed for 3 x 10mins before adding Pierce enhanced chemi-luminescence (ECL) Western Blotting Substrate (Thermo Scientific, USA). Membranes were incubated in ECL substrate for 1 minute before transferring to a light-sensitive cassette. Autoradiographic film was used to detect any signals from membranes and films were developed on a Kodak X-omat Model 2000 processer. Resulting images were quantified using Quantity One (BioRad, USA).

2.6.4 Ponceau Staining

Ponceau staining is a reversible way of visualising proteins on a nitrocellulose membrane following transfer. Membranes were incubated in Ponceau Staining solution (1g Ponceau S, 50ml acetic acid made up to 1L dH_2O) for 30 minutes with gentle agitation. Blots were either scanned or washed in dH_2O until staining was removed then used for Western blotting.

Table 2.1 – List of Antibodies

Antibody	Host	Supplier	Catalogue Number	Dilution	Application
α-Hsp20	Rabbit	Upstate	07-490	1:2500	WB
α-pS16-Hsp20	Rabbit	Abcam	ab58522	1:2000 1:500	WB ICC
α-Amyloid β	Mouse	Sigma-Aldrich	A8354	1:5000 1:500	WB ICC
Pan-PDE4A, B & D	Sheep	Scottish Antibody Production Unit (SAPU)	Custom made	1:5000	WB
α-polyHistidine-HRP	Rabbit	Abcam	ab1187	1:10000	WB
α-alpha-tubulin-HRP	Mouse	Abcam	ab40742	1:10000	WB
α-Mouse-HRP	Sheep	GE Healthcare	NXA931	1:5000	WB
α-Rabbit-HRP	Goat	Sigma-Aldrich	A6154	1:5000	WB
α-Sheep-HRP	Donkey	Sigma-Aldrich	A3415	1:5000	WB
α-PolyHistidine-Agarose	Mouse	Sigma-Aldrich	A5713	1:25	IP
α-Mouse-Alexa Fluor® 488	Goat	Invitrogen	A-11001	1:500	ICC
α-Rabbit- Alexa Fluor® 594	Goat	Invitrogen	A-11012	1:500	ICC

2.7 Amyloid Aggregation Analysis

2.7.1 NMR

^{15}N-labelled Aβ_{1-40} samples were combined with 1mg/ml of various His-Hsp20 constructs to give a final concentration of 200µM of Aβ_{1-40} and 25µM of Hsp20 (4:1 molar ratio) in 50mM NaPi buffer, 200µM Aβ_{1-40} only was used as a control.

NMR spectra were recorded on Bruker AVANCE 600MHz spectrometer at 4°C to assess pre-aggregation spectra prior to incubating all samples at 37°C for 4 days under agitating conditions (300rpm). Samples were then reanalysed at 4°C to ascertain how much Aβ_{1-40} peptide remained in solution. Following NMR analysis samples were centrifuged at 13000rpm in order to remove insoluble aggregates that had formed during the aggregation process and supernatant was analysed using SDS-PAGE and western blotting to ensure any loss of signal was not due to proteolytic degradation of the ^{15}N-labelled Aβ_{1-40} peptide.

Supernatants from each sample were then used to undertake co-immunopurification using anti-polyhistidine-agarose conjugated beads (Sigma-Aldrich, UK). 20ul of His-agarose beads were added to 500ul of the Aβ1-40:Hsp20 solutions and incubated at 4°C overnight on a rotating wheel. Each sample was then spun at 6000rpm to isolate the beads. Following removal of supernatant beads were subjected to a further 3 washes in PBS prior to addition of 2 x SDS sample buffer. Samples were then run on an SDS-PAGE gel to verify the interaction between Aβ and Hsp20.

2.7.2 Fluorescence quenching Aggregation Protocols

To obtain HFIP-induced aggregates, pre-treated Aβ_{1-42} monomers were resuspended in dimethylsulfoxide (DMSO) to a concentration of 2.5 mg/mL. Aβ_{1-42} peptides were subsequently diluted in Tris-HCl buffer solution (50 mM, pH 7.9) to the final desired concentration and ≤ 4 % HFIP was added to induce aggregation (Nichols, Moss et al. 2005). Incubation of the peptides for 1 hour at 4^{o}C with vigorous agitation by continued vortexing results in the progressive formation of Aβ_{1-42} globular structures.

For oligomeric and fibril-like aggregates formed at pH 7.9, HFIP-pre-treated Aβ_{1-42} monomers were resuspended in DMSO to a concentration of 2.5 mg/mL and subsequently diluted to 7 µM in 50 mM Tris-HCl buffer solution containing 150 mM NaCl and incubated at 37^{o}C for 24 hours as reported previously (Jan, Hartley et al. 2010). Final Aβ

concentrations were determined by absorbance spectroscopy using extinction coefficients of 150000 $cm^{-1}M^{-1}$ at 560 nm for $A\beta_{555}$ and 250000 $cm^{-1}M^{-1}$ at 653 nm for $A\beta_{647}$. Final concentrations of ThT were determined using an extinction coefficient of 36000 $cm^{-1}M^{-1}$ at 412 nm (Qin, Vastl et al. 2010).

2.7.2.1 Fluorescence Spectroscopy of $A\beta_{1-42}$ Aggregates

Fluorescence emission spectra from N-terminally labelled $A\beta_{1-42}$ aggregates were obtained using a peltier-cooled Varian Eclipse fluorescence spectrophotometer during incubation. Cuvettes with 1 cm path length were used and agitation was achieved with the insertion of magnetic stirring bars. Spectra from $A\beta_{555}$ were recorded using excitation wavelengths of 547 nm. Fluorescence spectra of ThT in the presence of unlabelled Aβ were recorded using an excitation wavelength of 440 nm.

2.7.2.2 Fluorescence Lifetime Measurements

Fluorescence lifetime measurements were performed with a Hamamatsu C6860 Synchroscan streak camera. The 80 MHz, 100 fs (full width half maximum) 800 nm output of a Ti:Sapphire oscillator was frequency doubled with a beta barium borate crystal, giving 400 nm excitation pulses. The 400 nm light, with an average power of less than 1 mW, was subsequently focussed through the optical path length (1 cm) of the solution cuvette. The photoluminescence from the sample was then collected and collimated with a lens before being focussed onto the entrance slit of a Chromex 250is imaging spectrograph. Excitation light was removed with a yellow schott glass filter that cuts all light below 420 nm. Spectral windows of 540-680 nm (single-colour quenching assay) and 540-590 nm (dual-colour FRET assay) were selected with the spectrograph before the light was directed into the streak camera. Time resolved photoluminescence dynamics were then recorded over a number of time ranges, giving an ultimate resolution with deconvolution with the instrument response function of ~2 ps.

2.7.2.3 Transmission Electron Microscopy

The structures of $A\beta_{1-42}$ amyloid aggregates were analysed by negative staining for transmission electron microscopy. Pioloform and carbon-coated 100-mesh copper grids (Agar Scientific, UK) were placed face down on droplets containing Aβ aggregates and incubated for 2 min at room temperature to allow binding of the protein structures to the grids. The grids were subsequently washed and stained twice on droplets of 3% aqueous

uranyl acetate for 2 min each followed by removal of excess staining solution by gently blotting the side of the grid with filter paper. The grids were then air dried and analysed in the electron microscope. Aβ amyloid structures were sampled by taking 5 micrographs per sample with a JEOL 1200 transmission electron microscope on Ditabis imaging plates (DITABIS Digital Biomedical Imaging Systems AG, Germany). Micrographs were selected to represent the average distribution, density and size of the Aβ aggregates (Goldsbury, Baxa et al. 2011).

2.8 Mammalian Cell Culture

All cell culture was carried out in Class II hoods using standard aseptic techniques and sterile equipment. Cell media was typically supplied by Sigma-Aldrich while culture flasks, plates, pipettes etc. were generally supplied by Corning. Cell cultures were examined using a phase contrast inverted microscope (Leitz Diavert, Germany) in order to analyse the condition of the cells and to monitor for contamination. SH-SY5Y cells were grown in Dulbecco's Modified Eagle's Medium (DMEM) and F12-Ham's at a 1:1 ratio, media was supplemented with 10% (v/v) foetal bovine serum (FBS), 1% (v/v) L-Glutamine, 1% (v/v) Minimum Essential Medium – With Non-essential Amino Acids (MEM-NAA) and 1% (v/v) Penicillin-Streptomycin. HEK293 cells were cultured in DMEM with the same supplements as SH-SY5Y media. Cells were cultured in a humidified, 5% (v/v) CO_2, 37°C incubator.

Culture media was routinely replaced every 3-4 days and upon reaching >80% confluency cells were passaged. To passage, cells were washed gently in warm, sterile PBS in order to remove culture media, cells were then treated with 1ml of trypsin-EDTA solution and incubated for more than 3 minutes to allow cells to disassociate from the culture flask. 5ml of culture media was then added to the flask to de-activate the trypsin and the cell/media solution was transferred to a 15ml falcon tube and cells were collected by centrifugation at 1000rpm for 3 minutes at room temperature. The supernatant was then discarded and cell pellets were resuspended in fresh media and added to fresh culture flasks at the required dilution (typically 1:5, v/v). For long term storage of cells, cell pellets were resuspended in 800ul of fresh media along with 800ul of cell freezing solution (20% DMSO in FBS) and stored at -80°C for a minimum of 24 hours before being transferred to liquid nitrogen.

2.8.1 Transfection of plasmid DNA

For PDE assays HEK293 cells were transfected with various PDE isoforms using Fugene HD (Promega, UK) in accordance with manufacturer's instructions. For the more difficult to transfect SH-SY5Y cells I used an electroporation method using Amaxa® Cell Line Nucleofector® Kit V (Lonza) in order to attain higher transfection efficiency.

2.8.2 Stable cell-lines

To create stably expressing SH-SY5Y cell lines the less efficient Fugene HD reagent was used to transfect cells. Cells were plated onto 100mm dishes and at confluency of 50% transfected with relevant plasmid containing a neomycin cassette. After 24 hours G418 solution was added to culture media at a final concentration of 500ug/ml. After 10 days remaining single colonies were isolated using Cloning rings (Sigma-Aldrich) through trypsinisation and expanded into to further culture vessels. Once adequate quantities of cells could be harvested cell lysates were created and expression levels of each respective protein were analysed. G418 levels were maintained at 500ug/ml throughout all stable cell culture work in order to ensure appropriate selection of plasmid DNA.

2.9 Preparation of Whole Cell Lysates

Whole cell lysates were prepared using 3T3 cell lysis buffer (50mM NaCl, 50mM NaF, 25mM HEPES, 5mM EDTA, 30mM sodium pyrophosphate, 10% glycerol (v/v), 1% Triton X-100 (v/v); pH 7.5) supplemented with protease inhibitor cocktail tablet (mini-complete, Roche) and phosphatase inhibitor cocktail tablet (PhosSTOP, Roche). Cell culture media was removed and cells were washed 3 times with ice cold sterile PBS. All remaining PBS was removed before the addition of 3T3 buffer and cells were incubated for a minimum of 1 hour before cells collected using a sterile scraper into 1.5ml eppendorfs. Cell lysate solution was then centrifuges at 13000rpm for 10 minutes in order to remove insoluble cellular components. Supernatants were then added to appropriate loading buffer and analysed using SDS-PAGE and Western Blotting techniques.

For PDE activity experiments KHEM buffer (50mM KCl, 50mM HEPES pH7.2, 10mM EGTA, 1.9mM MgCl2) supplemented with protease inhibitor cocktail tablet (mini-complete, Roche). Samples were then frozen on solid CO2, thawed and then manually homogenised, followed by passage through a 26-gauge needle several times to ensure

complete cell lysis. Cells were centrifuged at 13,000rpm for 10 min to remove insoluble membrane fraction. The resulting supernatant was frozen in solid CO_2 and stored at −80ºC.

2.10 Cell-Based Experiments

2.10.1 Cell Viability Assays

Cell viability assays were carried out using a standard colorimetric MTT-based assay, which measures viable cells through their ability to reduce MTT to insoluble formazan. This only occurs if the cell's mitochondria are active and producing the specific enzymes to carry out this reaction.

SH-SY5Y cells transfected with various Hsp20 plasmids were seeded at a density of $5x10^3$/well into 96-well plates and left overnight to allow for cell attachment. The following day cells were incubated with 20µM $A\beta_{1-42}$ or Aβscr control and incubated for a further 48 hours. After incubation period CellTiter 96® Non-Radioactive Cell Proliferation Assay (G4000, Promega, UK) was used to measure viability. MTT dye solution was incubated with cells for 4 hours prior to the addition of the Stop Solution. Plates were kept in a humidified container in the dark overnight to allow for complete solubilisation of the coloured formazan. Plates were then read at 595nm on an MRX microplate reader (Dynex Technologies, UK).

2.10.2 Real-Time Cell Monitoring (xCELLigence)

The xCELLigence system Real-Time Cell Analyzer RTCA-SP (ACEA Biosciences, USA) is an electrical impedance-based real-time cell monitoring system for detection of cellular viability (Fig. 2.2). The recording of cell index values (CI), normalisations and the monitoring of $A\beta_{1-42}$ mediated cytotoxicity was performed using RTCA Software 1.2. The RTCA-SP device was calibrated using RTCA Resistor Plate 96 prior to each experiment and impedance measurements were carried out in 96-well E-plates (ACEA). The impedance readout is expressed as arbitrary cell index values. The normalisation of cell index arbitrarily sets cell index to 1 at a desired time point, which is typically the time of adding compounds. The background impedance caused by the media is measured using 100ul in each well prior to seeding of cells and is automatically subtracted by the RTCA software using the following equation: $CI - (Z_i - Z_o)/15$ with Z_i as the impedance at any given time point and Z_o being the background signal (Diemert 2012).

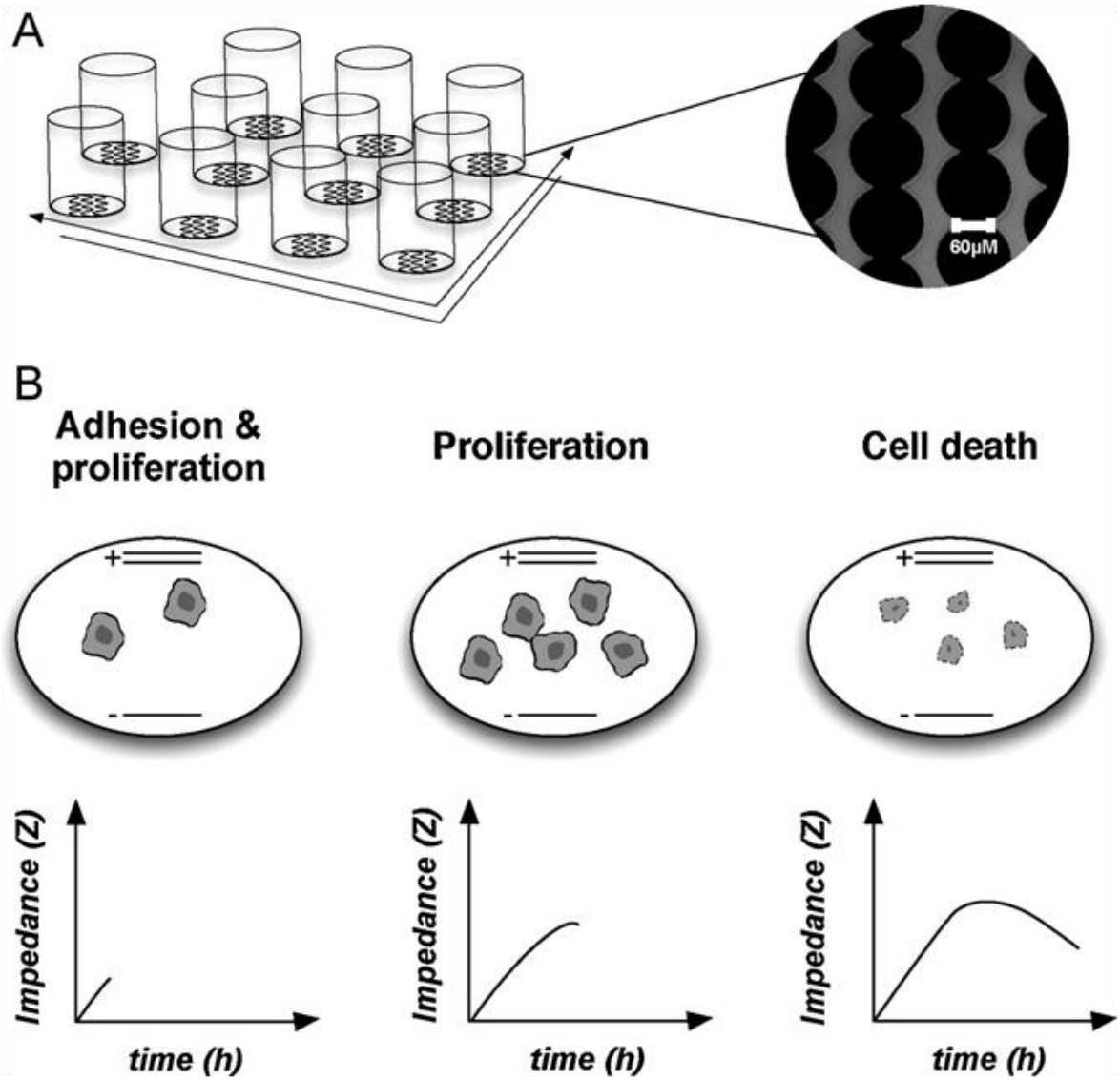

Figure 2.2 – Schematic representation of xCELLigence Real-Time Cell Monitoring
This schematic illustrates the principle of cellular impedance as a non-invasive method for measuring cell growth characteristics. A – Each well of a 96 well culture plate (E-plate) has gold electrodes embedded at the bottom. Each electrode array has a minimal distance of 30µM between adjacent electrodes. The right image is how electrodes appear at 10x magnification. B – Cells are seeded on top of the electrode-covered surface and upon adherence to the bottom of the well; the cells partially insulate the electrodes resulting in a rise in electrical impedance (Z). With increasing cell number cells have a greater insulating capability which correlates with an increase in impedance. Cell death causes changes in cellular morphology, cell shrinkage and detachment which results in a decrease in cellular impedance. Therefore the xCELLigence system is a highly sensitive system for measuring the effects of cytotoxic agents such $A\beta_{1-42}$. Figure from Diemert 2012.

Prior to commencing experiments using SH-SY5Y cells, the cell density had to be optimised to ensure linear growth throughout the time-course of each assay. To do this I seeded SH-SY5Y cells at various densities and observed their growth characteristics, without any interventions such as changing media (Fig 2.3A). It was found that the density that gave the most linear growth over 72 hours was $5x10^3$ cells/well whereas all other densities tested resulted in peak Cell Index after 48 hours followed by growth inhibition or

a reduction in cell index as the wells became over-confluent. Therefore $5x10^3$ cells/well was used for all subsequent assays. Images of the cells were taken at the 48 hour time-point in order to compare Cell Index with the confluency of each well (Fig 2.3B)

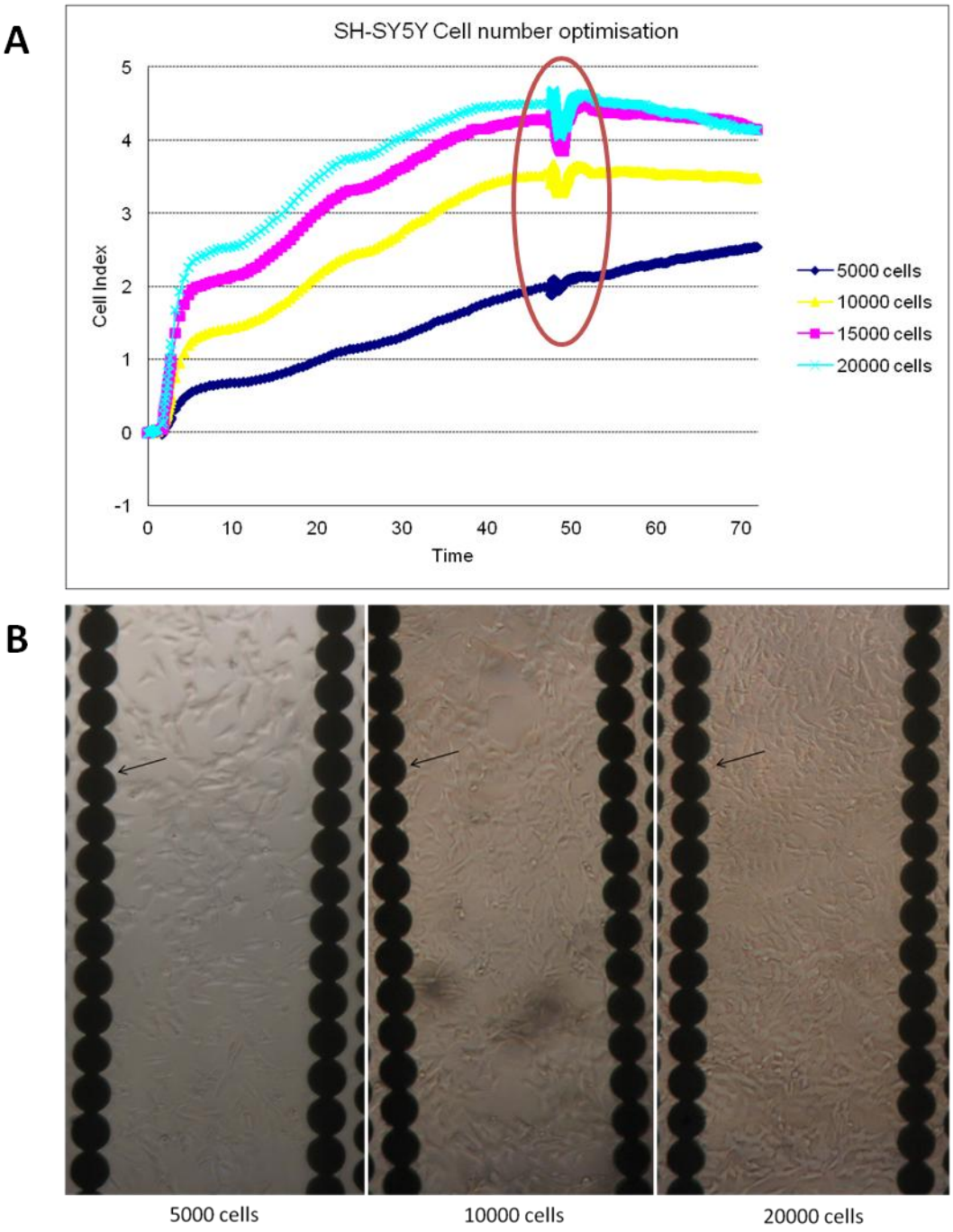

Figure 2.3 – Cell number optimisation on xCELLigence system.
A - SH-SY5Y cells were seeded into 96 well E-plates at several densities in order to determine which cell density would give linear growth throughout the time-course of a typical cytotoxicity assay. After 48 hours the plate was removed briefly from incubation and several images were taken in order to compare cell density with Cell Index. This resulted in transient changes in Cell Index due to the changes in temperature of the E-plate (red circle). B - The images validated that cell number correlated with Cell Index. The 20000 cell wells were 100% confluent and no further growth was detected in these wells whereas 5000 cells continued to expand linearly when placed back in incubation. Arrows indicate gold electrodes integrated at the bottom of the E-plate. SH-SY5Y cells observed under brightfield microscopy at 10x magnification.

SH-SY5Y cells transfected with various Hsp20 plasmids were seeded at a density of $5x10^3$/well into 96-well E-plates and left overnight to allow for cell attachment and left until cell index of reached a value of 1 prior to addition of Aβ peptides and vehicle controls to ensure consistency of cell number and effect of Aβ peptides. Remaining cells were seeded into 6 well plates and harvested after 48 hours to confirm expression of the various Hsp20 proteins. The xCELLigence SP system (ACEA Biosciences, USA) was used for real-time monitoring of cell growth. For PDE inhibition assays non-transfected SH-SY5Y cell were seeded at the same density and treated with Aβ peptides, again once the average cell index reached a value of 1. PDE inhibitors were then added 6 hours post Aβ addition and monitored until the 48 hour time-point. The resulting data was exported to Microsoft excel using the RTCA software for further manipulation.

2.10.3 Hsp20 phosphorylation assays

SH-SY5Y cells were seeded at a density of $1x10^6$ cell per well onto 6 well plates for at least 16 hours prior to treatment with various PDE inhibitors. Compounds were diluted in media and added to cells for 0.5, 1, 2, 4 & 6 hours for time course assays or incubated for 15 minutes for dose-response assays prior to harvesting using 3T3 lysis buffer supplemented with protease inhibitor Mini-Complete and phosphatase inhibitor phosSTOP (Roche, UK). Phospho-Hsp20 levels were analysed using standard SDS-PAGE and Western Blotting techniques described previously.

2.11 Phosphodiesterase Activity Assay

PDE activity was determined using a two-step radio-assay procedure as described previously by (Marchmont and Houslay 1980). The first step, samples are incubated with 8-[3H]-labelled cAMP substrate, and PDEs in the sample hydrolyse this to [3H]-5'-AMP. The second step, uses snake venom (*Crotalus Atrox*) to hydrolyse the 5'AMP to [3H]-adenosine, and subsequent incubation with anion exchange resin binds negatively charged, unhydrolysed cAMP, separating it from the adenosine. The amount of [3H]-adenosine is then calculated by scintillation counting, to determine the rate of cAMP hydrolysis.

Various PDE isoforms were transiently over-expressed in HEK293 cells prior to lysis with KHEM buffer. For experimentation, the protein concentration of whole-cell lysate from transfected cells was equalized (typically to 1 μg/μl). Pilot assays were also carried out to

prior to inhibition to verify PDE activity and ensure activity fell within the linear range of 6000-16000 counts.

For inhibition assays various PDE cell lysates were incubated for 10 min at 30 °C in 20 mM Tris, pH 7.4, 5 mM $MgCl_2$, 0.1 μCi tritiated cyclic nucleotide, 0.1 or 1 μM unlabelled cyclic nucleotide the various inhibitors discussed in Chapter 5. The concentrations of PDE inhibitors used in experiments ranged from 1 nM to 200 μM. After incubation samples were boiled at 100°C for 1 min to terminate protein activity. Assays were cooled on ice for 15 minutes then 25 μl of *Crotalus Atrox* venom (1 mg/ml) was added to each assay and incubated at 30 °C for 10 min. Then 400 μl of a 1:1:1 (v/v/v) slurry of Dowex 1X8 200–400 MESH CI resin, ethanol and water were added, samples were vortexed and incubated on ice for 15 minutes. Samples were again vortexed then centrifuged at 13000rpm for 3 minutes. 150 μl of supernatant was mixed with 1ml Opti Flow SAFE 1 scintillant and counted on a Wallac 1409 Liquid Scintillation Counter. The cyclic nucleotide concentration in each assay was typically 1/3 of the Km value for the substrate for each particular PDE family. Dose-response curves and IC50's were calculated using GraphPad Prism software.

2.12 Microscopic Analysis

2.12.1 FRET Imaging

FRET imaging experiments were performed 24-48 h after SH-SY5Y cells stably expressing Epac1-camps FRET probe (REF) were seeded onto glass cover slips. Cells were maintained at room temperature in DPBS (supplier), with added CaCl2 and MgCl2, and imaged on an inverted microscope (Olympus IX71) with a PlanApoN, 60X, NA 1.42 oil, 0.17/FN 26.5, objective (Japan). The microscope was equipped with a CCD camera (cool SNAP HQ monochrome, Photometrics), and a beam-splitter optical device (Dual-channel simultaneous-imaging system, DV^2 mag biosystem (ET-04-EM)). Imaging acquisition and analysis software used was Meta imaging series 7.1, Metafluor, and processed using ImageJ (http://rsb.info.nih.gov/ij/). FRET changes were measured as changes in the background-subtracted 480/545-nm fluorescence emission intensity on excitation at 430 nm and expressed as either R/R0, where R is the ratio at time t and R0 is the ratio at time = 0 sec, or ΔR/R0, where ΔR = R – R0. Values are expressed as the mean ± SEM.

2.12.2 Immunocytochemical staining of SH-SY5Y cells

SH-SY5Y cells (2 x 10^5/well) were grown overnight in 6 well plates containing sterile coverslips. Coverslips were sterilised using an ethanol: ether solution (1:1, v/v) and air dried for a minimum 30 minutes in a cell culture hood. The following day cells were fixed on glass coverslips using -20°C methanol solution for 5 minutes, then washed twice for 5 minutes in cold PBS with gentle agitation. Cells were permeabilised for 20 minutes at room temperature with PBST (0.1% Triton-X100 in PBS), then washed for 5 minutes in PBS alone. Nonspecific antibody binding sites were blocked by incubating with blocking buffer (0.5% BSA (w/v) in PBS) for either 30 minutes at room temperature, or overnight at 4°C, coverslips were then washed twice in PBS for 5 minutes. One or two primary antibodies were diluted to the desired concentrations in blocking buffer, and coverslips were incubated with primary antibodies overnight at 4°C. Coverslips were then washed three times for 10 minutes in PBS, and incubated with 1:500 dilutions of appropriate fluorescently labelled secondary antibodies in a final volume of 500µl per coverslip and protected from light. This step took place for either 1 hour at room temperature, or overnight at 4°C. Following secondary antibody incubation, coverslips were washed once in PBS and mounted onto glass slides using ProLong Gold antifade reagent with DAPI (4',6-diamidino-2-phenylindole) nuclear stain (Molecular Probes) and air dried for a minimum 48 hours prior to use. Coverslips were stored at 4°C, protected from light for up to 1 month.

2.13 Statistical Analysis

In this thesis all values are presented here as mean value ± standard error of the mean (SEM) from at least 3 independent experiments. Statistical significances between two groups of data were determined using paired, two-tailed Student's *t*-test. Statistical analysis of several groups was carried out using one way analysis of variance (ANOVA) with Dunnett's post test comparison against control experiments. A *p*-value greater than 0.05 was not considered significant (NS), *p*-value < 0.05 was considered significant (*), *p*-value < 0.01 was considered highly significant (**), and *p*-value < 0.001 was considered extremely significant (***).

3 Hsp20 phosphorylation modulates its binding to Aβ and promotes neuroprotection

3.1 Introduction

One of the pathological hallmarks of Alzheimer's disease (AD) is the extracellular disposition of amyloid-like filaments that form neuritic plaques in the brain. The principle component of amyloid plaques is a small peptide known as amyloid–β (Aβ), which is derived from sequential proteolytic cleavage of the amyloid precursor protein (APP) (Hardy and Selkoe 2002). Increases in Aβ levels following an imbalance between the rates of production and clearance of the peptide, promote Aβ oligomerisation and lead to the formation of both insoluble fibrillar deposits and soluble Aβ oligomers. Various types of Aβ oligomers promote neuronal dysfunction and cell death leading to neurodegeneration (Harrison, Sharpe et al. 2007). This series of events is described as the "amyloid cascade hypothesis" and is supported by a wealth of biochemical and genetic data, though recent failures of a number of anti- Aβ aggregation drugs has recently cast some doubt on the hypothesis (Reitz 2012). The most abundant peptide fragment found in AD is $A\beta_{1\text{-}40}$, which accounts for approximately 90% of amyloid plaques, whereas the remaining 10% is made up by the more amyloidogenic fragment $A\beta_{1\text{-}42}$. These short peptides are unstable and readily aggregate to form fibrils and a variety of other aggregated species that have been shown to be highly cytotoxic (Morgan, Colombres et al. 2004).

Small Heat Shock Proteins (sHSPs) are a group of ATP-independent chaperones that can prevent the aggregation of mis-folded proteins or peptides and as such, are protective against a number of protein aggregation diseases (Eyles and Gierasch 2010). This is particularly evident in the field of neurological disease where sHSPs have been shown to have a protective role against Alzheimer's, Parkinson's and Huntington's disease (Brownell, Becker et al. 2012). One of the ten known sHSPs, Hsp20, has been specifically linked with AD as it associates with pathological lesions in diseased brains (Wilhelmus, Otte-Holler et al. 2006). These included senile plaques (SP) and cerebral amyloid angiopathies (CAA) both of which consist mainly of aggregated Aβ (Wilhelmus, Boelens et al. 2009). Expression of Hsp20 has also been observed in reactive astrocytes and microglia found surrounding both SP and CAA (Wilhelmus, Otte-Holler et al. 2006). The co-localisation of Hsp20 with Aβ aggregates within AD brain tissue suggests that Hsp20 may represent an endogenous neuronal protection mechanism to combat or prevent Aβ oligomerisation. Indeed, the physical interaction between Hsp20 and Aβ has been reported

to prevent Aβ oligomerisation and protect neuronal-type cell lines from Aβ mediated toxicity (Wilhelmus, Boelens et al. 2006), however, the molecular nature of the interaction is unknown.

3.1.1 Experimental Aims

Although an interaction between Hsp20 and Aβ has previously been reported (Wilhelmus, Otte-Holler et al. 2006) & (Wilhelmus, Boelens et al. 2006) the molecular nature of this interaction has yet to be established. The primary aim of experimental work carried out in this chapter was to map the protein-protein interaction between Hsp20 and the Aβ peptide to elucidate which domains within each respective protein are involved in binding. Upon identification of residues that facilitate binding, mutations were incorporated into full-length Hsp20 sequences in order to validate the identified residues on Hsp20's ability to bind Aβ. I investigated several mutants of Hsp20 in relation to; binding with Aβ, effect on Aβ aggregation, and protection against Aβ-induced cell-death.

3.1.2 Experimental Procedure

1 – Characterise the interaction between Hsp20 and Aβ using peptide array technology (Frank 2002). This *in vitro* method allows for rapid elucidation of key domains and residues responsible for protein-protein interaction using immobilised peptide libraries, pure proteins and detection methods analogous with Western Blotting.

2 – Create mutants based on peptide array data using site-directed mutagenesis of Hsp20 wild-type (WT) sequence and determine the impact on the protein's characteristics, specifically its ability to interact with Aβ through co-immunoprecipitation.

3 – The Hsp20 mutants described in 2 (above) were tested using two separate assays that were designed to monitor Aβ aggregation: (A) Nuclear Magnetic Resonance (NMR) spectroscopy with ^{15}N-labelled $A\beta_{1-40}$ peptide was used to assess what affect these mutations have on Hsp20's capacity to bind to Aβ and affect its aggregation into higher molecular weight species. (B) A novel Aβ aggregation assay based on fluorescence self-quenching of fluorophore-tagged $A\beta_{1-42}$ that can differentiate between two distinct, physiologically relevant Aβ aggregation pathways, oligomerisation and fibrillisation was also used.

4 – Using xCELLigence technology, I developed and utilised a novel cell-based assay for monitoring $A\beta_{1-42}$ induced cytotoxicity in real-time. This validated complementary experimentation using more traditional methods for measuring viability of the human neuroblastoma cell-line SH-SY5Y (MTT assay). Various constructs of Hsp20 were expressed in this cell-line and their ability to attenuate $A\beta_{1-42}$ induced cytotoxicity was established.

3.2 Results

3.2.1 Mapping the interaction between Hsp20 and $A\beta_{1-42}$ using Peptide Array

As the interaction between Hsp20 and $A\beta_{1-42}$ had previously been demonstrated through immuno-histochemical and co-incubation techniques (Wilhelmus, Otte-Holler et al. 2006) & (Wilhelmus, Boelens et al. 2006), I decided to use synthetic peptide array technology in order to map the interaction domains between Hsp20 and Aβ. This method has been used successfully to characterise the molecular interactions between Hsp20-PDE4D5 (Sin 2011). The entire Hsp20 sequence was divided into overlapping 25mer peptides that shift sequentially in amino- to carboxyl-terminal direction, in 5 amino acid increments and SPOT synthesised onto cellulose membranes (Figure 2.1) (Frank 2002). The arrays were then incubated with either $A\beta_{1-42}$ or a scrambled version of $A\beta_{1-42}$ ($A\beta_{scr}$) that has the same overall molecular weight and charge but does not possess the aggregation or cytotoxic properties of $A\beta_{1-42.}$ Following incubation, arrays were probed with an anti-Aβ antibody to see which Hsp20 domains had a positive interaction with $A\beta_{1-42}$ (Fig. 3.1B). The intensity of any resultant chemiluminescent signal directly correlates with the levels of protein bound to each 25mer spot. There was non-specific antibody binding observed at the α-crystallin domain of Hsp20 when the arrays were overlaid with both $A\beta_{1-42}$ and Aβscr, however, positive interactions were detected between Hsp20 peptides 1, 2 and 3 and Aβ1-42 (Fig. 3.1B) that were not apparent on arrays overlaid with $A\beta_{scr}$. Peptides 1, 2 and 3 span the amino acid sequence M^1-E^{35} within the N-terminal domain of Hsp20 (Fig. 3.1A), which contains the PKA/PKG consensus site at serine 16 (Fan, Chu et al. 2004).

To gain further insight into which amino acids within the N-terminal domain of Hsp20 might be critical in binding to $A\beta_{1-42}$, I focussed on the W^{11}-E^{35} region and produced an alanine scanning array, where each residue was sequentially substituted for an alanine. In the event that alanine was the endogenous residue, it was substituted with aspartic acid.

This library of peptides was again incubated with $A\beta_{1-42}$ (Fig. 3.1C: upper panel) or $A\beta_{scr}$ (Fig. 3.1C:lower panel) and subsequent western blotting undertaken. This procedure identified a region of Hsp20 likely to be important for association with $A\beta_{1-42}$, namely the double arginine (R^{13}, R^{14}) that forms part of the PKA/PKG consensus (RRAS). As the original array (Fig. 3.1B) suggested that the PKA/PKG site may be involved in facilitating the binding of $A\beta_{1-42}$ I included either a phospho-serine (pS16) residue or a phospho-mimic substitution (S16D) in position 16 of the $Hsp20^{11-35}$ peptide (Fig. 3.1C, lower panels). Significantly more $A\beta_{1-42}$ bound to the 25mers that included pS16 or S16D when compared to the native sequence. This result suggests that PKA/PKG phosphorylation of serine 16 may regulate the association of Hsp20 with $A\beta_{1-42}$.

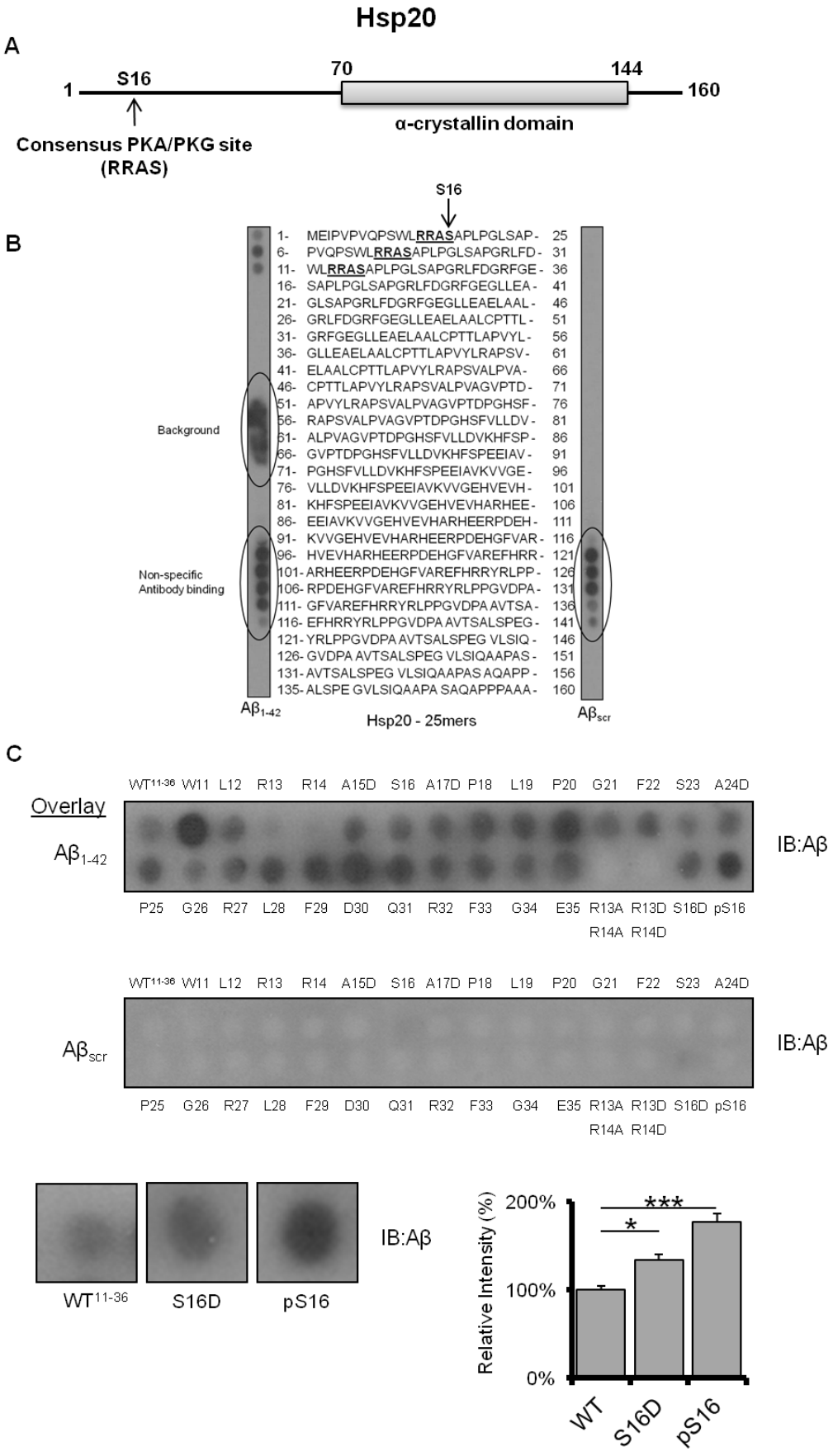

Figure 3.1 – Mapping the interaction between Hsp20 and $A\beta_{1-42}$.
Peptide array was used to map the domains responsible for Hsp20/$A\beta_{1-42}$ interaction. A – Structure of Hsp20 highlighting the PKA/PKG site located in the N-terminal domain of Hsp20 and the conserved α-crystallin domain is located between residues 70 and 144. B - The entire sequence of Hsp20 was fragmented into overlapping 25mer peptides and the probed with either $A\beta_{1-42}$ or $A\beta_{scr}$

the domains found to have a positive interaction with $A\beta_{1-42}$ all included the consensus PKA/PKG phosphorylation site (RRAS) proximal to serine 16. C - Subsequent alanine scanning arrays demonstrated that the arginine residues are essential for facilitating $A\beta_{1-42}$ binding. Furthermore, substitution of serine 16 with a phospho-serine or phospho-mimetic substitution (serine changed to aspartic acid) significantly increased the association of $A\beta_{1-42}$ suggesting a mechanism by which this interaction may be regulated *in vivo*.

We then undertook reciprocal peptide array analysis to determine which sites on $A\beta_{1-42}$ are required for Hsp20 interaction. The $A\beta_{1-42}$ arrays were incubated with His-tagged purified Hsp20 (His-Hsp20) or as a control, His-tagged purified RACK1 (His-RACK1) (Fig. 3.2B). We observed strong association of Hsp20 (but not RACK1) to the first 3 spots of the $A\beta_{1-42}$ array (representing amino acids 1-35). Alanine scanning analysis of the first 25 amino acids of $A\beta_{1-42}$ (Fig. 3.2C) showed that the tri-peptide spanning H^{14}, Q^{15} and K^{16} was important for Hsp20 binding, with the latter lysine residue being essential (Fig. 3.2C). Interestingly, this region abridges the $K^{16}LVFF^{20}$ oligomerisation domain of $A\beta_{1-42}$. This region is known as the pathogenic aggregation site of the peptide and is essential for beta-sheet formation and subsequent amyloidogenesis (Hilbich, Kisters-Woike et al. 1992), (Tjernberg, Naslund et al. 1996). Taken together (Fig. 3.1 and 3.2), our peptide array data suggests a mechanism where phospho-Hsp20 binds more avidly to $A\beta_{1-42}$ in order to prevent the self-association of the peptide.

3.2.2 *In vitro* pull-down of $A\beta_{1-42}$ with His-Hsp20

The peptide array data highlighted that the introduction of a phospho-mimetic substitution (S16D) may increase the avidity of the full-length Hsp20 protein towards $A\beta_{1-42}$. Identification of the Hsp20 binding site on $A\beta_{1-42}$ also suggested that mutating both arginine residues at position 13 & 14 should ablate Hsp20's ability to bind $A\beta_{1-42}$ (Fig. 3.1C). In order to validate the peptide array data, we initially cloned the wild-type Hsp20 construct into the pET28c vector and expressed it in BL21 cells. The purified His-Hsp20-WT plasmid was then subjected to site directed mutagenesis in order to create the His-Hsp20-S16D and His-Hsp20-R13A,R14A (arginine double mutant, ADM). Purified His-Hsp20 was predominately found in its monomeric form, pre- and post- incubation, but stable dimers and tetramers are also apparent across all the Hsp20 variants (Fig. 3.3: lower panel), demonstrating that the S16D or the R13A,R14A mutations have no apparent effect on the proteins ability to form stable quaternary structures.

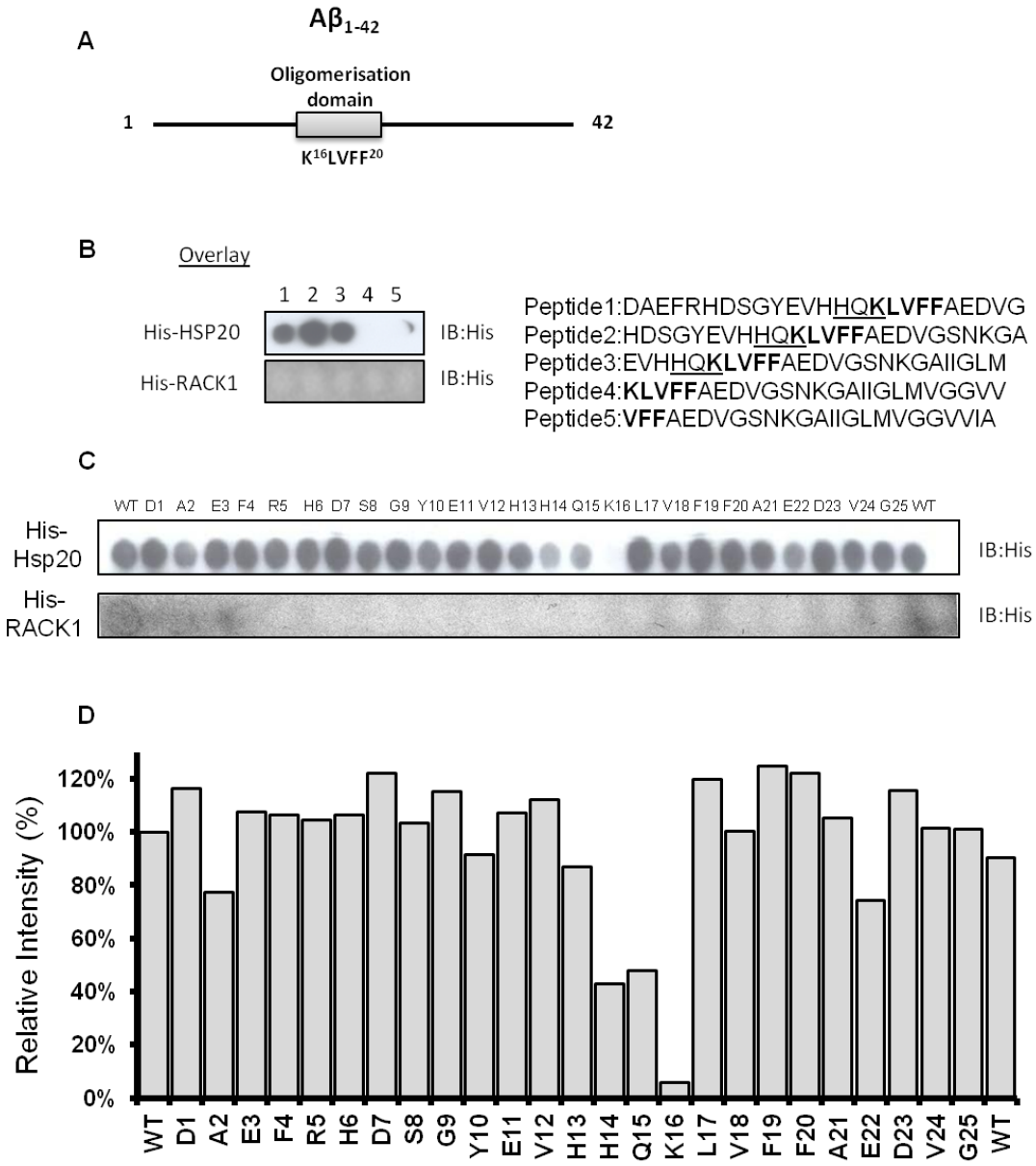

Figure 3.2 – Mapping the interaction between Aβ$_{1-42}$ and Hsp20.
A – Structure of Aβ$_{1-42}$ peptide with oligomerisation domain highlighted. B - The Aβ$_{1-42}$ sequence was fragmented into overlapping 25mer peptides and the probed with either His-Hsp20 or His-RACK1. Strong association of His-Hsp20 was detected in spots 1-3 while no signal was detected with arrays overlain with His-RACK1. C – Alanine scanning array shows that only the lysine residue at position 16 is essential for mediating binding of His-Hsp20. However, densitometry analysis suggests that histidine at position 14 and glutamine at position 15 also play a role in mediating binding of His-Hsp20.

Primary data in Figure 3.2 B & C was generated by Ruth MacLeod

To characterise any changes in avidity for Aβ$_{1-42}$, I conducted *in vitro* pull-down assays with the various His-tagged Hsp20 proteins by co-incubating either Hsp20-WT, Hsp20-S16D or Hsp20-ADM with Aβ$_{1-42}$ at 1:1 molar ratio in PBS. Samples of Aβ$_{1-42}$ were incubated overnight at 37°C under agitating conditions which typically promotes the aggregation of Aβ$_{1-42}$ into insoluble fibril-like structures prior to immunopurification with

α-His-agarose conjugated beads. Hsp20 successfully bound to $A\beta_{1-42}$ at a variety of molecular weights reflecting the various SDS-stable species of $A\beta_{1-42}$ formed during aggregation. All Hsp20 variants bound monomeric $A\beta_{1-42,}$ demonstrating that the Hsp20 variants were able to bind to low molecular weight species of $A\beta_{1-42}$. The phospho-mimetic variant Hsp20-S16D showed the greatest avidity for higher molecular weight oligomers of $A\beta_{1-42}$ (Fig. 3.3).

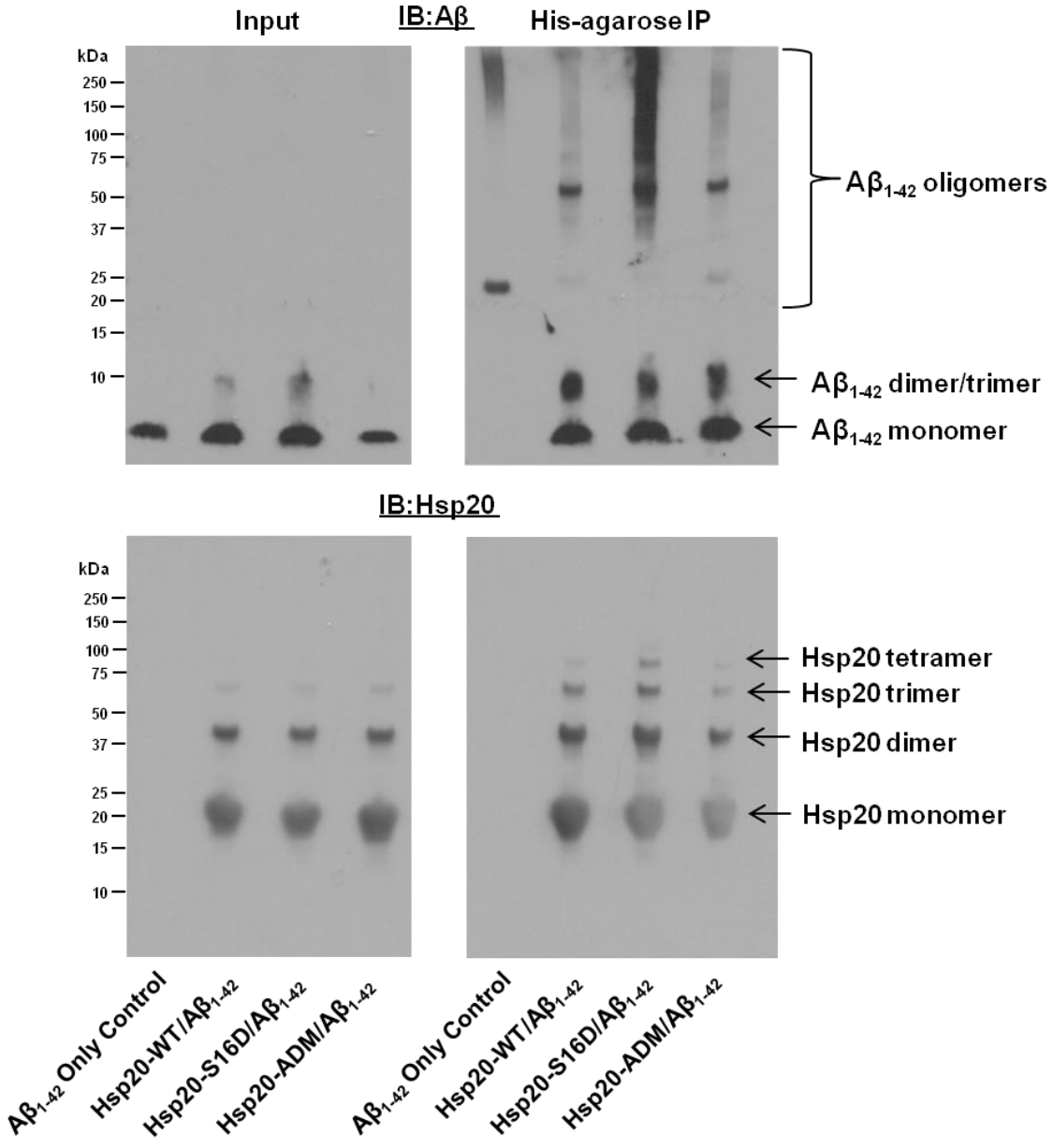

Figure 3.3 – Co-immunoprecipitation of $A\beta_{1-42}$ with His-Hsp20
Pure protein co-immunoprecipitation experiment using purified His-Hsp20 and $A\beta_{1-42}$ peptides. Peptides were incubated at 37°C under agitation for > 16 hours prior to immunopurification with His-agarose conjugated beads. All Hsp20 variants effectively pulled-down low molecular weight $A\beta_{1-42}$ however, Hsp20-S16D was most effective at pulling down $A\beta_{1-42}$ oligomers. Data is representative of three separate experiments.

3.2.3 Hsp20 phosphorylation alters Aβ aggregation dynamics

3.2.3.1 Nuclear Magnetic Resonance Spectroscopy to monitor $A\beta_{1-40}$ aggregation

Nuclear magnetic resonance (NMR) spectroscopy is a tool that has been used for more than 20 years to examine the structure of proteins in solution. NMR works on the principle that stable isotopes, such as ^{1}H, ^{13}C and ^{15}N, carry magnetic dipoles. These dipoles take up different orientations in a magnetic field, and each orientation has a different energy. By applying pulses of electromagnetic radiation at precise frequencies, the transitions between the energy states can be observed, thus giving rise to the NMR signal. Nuclei in different environments, such as different ^{1}H nuclei in a protein, resonate at different frequencies and the intensity of each proton is plotted against resonance frequency. The most useful NMR spectra are the 1D ^{1}H-NMR spectra, which show the signals for each hydrogen atom (proton) in a protein, and the 2D-^{15}N-HSQC (heteronuclear single-quantum coherence) spectra, which give a signal for each covalently bonded ^{1}H-^{15}N group. Typically a 2D-^{15}N-HSQC spectrum is displayed topographically and contains one peak for each residue in the protein, therefore providing a high-resolution 'fingerprint' of a protein. The process of assigning a particular peak to a specific residue is essential for elucidating any structural or functional information about the protein (Kwan, Mobli et al. 2011).

NMR has been used extensively to characterise synthetic Aβ peptides. In solution, the Aβ peptide can fold into either α-helical, random chain or soluble β-sheet structures. The abundance of each structure depends on the solution conditions; hydrophobic lipid-like environments promote the α-helical structure, which is the principal role of the Aβ sequence as part of the transmembrane domain of APP, whereas high ionic strength and pH ranging from 4-7 favours formation of β-sheets. The α-helical and random extended chain structures are monomeric while β-sheet structures in solution are oligomeric and eventually precipitate as amyloid. Due to the β-sheet structure being neurotoxic, therapeutically useful inhibitors of amyloidogenesis should bind to and stabilise the α-helical, random extended chain or early formed, non-toxic β-sheets (Hilbich, Kisters-Woike et al. 1991), (Zagorski and Barrow 1992), (Zeng, Zhang et al. 2001). Several natural exogenous compounds have been identified as being inhibitors of amyloidogenesis including; nicotine from tobacco (Salomon, Marcinowski et al. 1996), curcumin from the spice turmeric (Reinke and Gestwicki 2007), and resveratrol a polyphenol found in red wine (Ge, Qiao et al. 2012). NMR studies have shown that these compounds interact directly with Aβ peptides preventing oligomerisation into fibril structures, and as

consequence these compounds are now being pursued as potential therapeutics for treating AD.

I have used NMR spectroscopic analysis to examine the effect of Hsp20 on the oligomerisation of synthetic ^{15}N-labelled Aβ_{1-40} peptide. I had originally tried ^{15}N-Aβ_{1-42} but found the aggregation kinetics too fast, even when maintained at low temperatures, and I was not able to detect any signal. However insoluble Aβ_{1-42} aggregates were visible in each sample immediately after peptide preparation. Initial analysis of the ^{15}N-Aβ_{1-40} was carried out at 4°C to prevent oligomerisation of the peptide and to quantify uniformity of the starting product prior to commencing aggregation. Each assay contained 200µM of ^{15}N -Aβ_{1-40} peptide incubated with 50µM of either, Hsp20-WT, Hsp20-S16D, Hsp20-ADM (molar ratio 4:1, Aβ: Hsp20), while the ^{15}N-Aβ_{1-40} peptide on its own served as a control. As planned, the starting concentrations of ^{15}N-Aβ_{1-40} were identical across all samples (Fig. 3.4). Small changes in chemical shifts were detectable across all residues compared to ^{15}N-Aβ_{1-40} only control, but the largest changes are seen at the region proximal to the oligomerisation domain (Fig 3.5), spanning the sequence H^{13}HQKL^{17}, which includes the same region identified in the peptide array experiments (Fig. 3.2B). Hsp20-ADM induced the largest changes in chemical shift for residues within this region, while Hsp20-S16D increased the shift distance across 80% of the assigned residues relative Hsp20-WT.

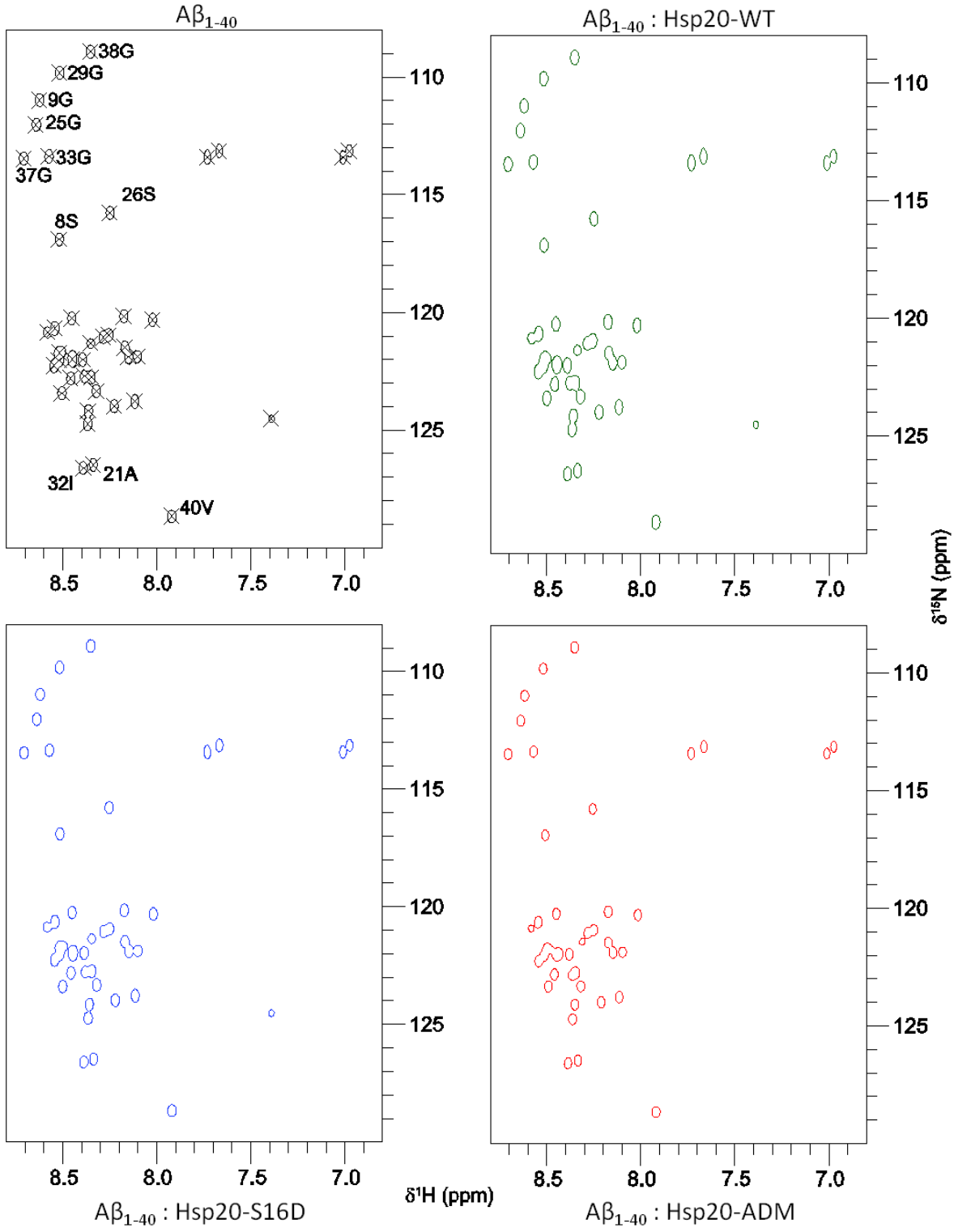

Figure 3.4 – NMR Analysis of ^{15}N-Aβ$_{1-40}$ co-incubated with Hsp20 pre-aggregation
Partial [^{1}H,^{15}N]-HSQC spectra of recombinant ^{15}N-Aβ$_{1-40}$ peptide (200µM) in 50mM sodium phosphate buffer (NaPi) at pH 7.5 and 4°C and 14.1 T. ^{15}N-Aβ$_{1-40}$ only peptide (black), ^{15}N-Aβ$_{1-40}$ and 50µM His-Hsp20-WT (green), ^{15}N-Aβ$_{1-40}$ and 50µM His-Hsp20-S16D (blue) & ^{15}N-Aβ$_{1-40}$ and 50µM His-Hsp20-ADM (red). All samples show similar pattern of peaks that are similar to previous reported assignments of ^{15}N-Aβ$_{1-40}$ (Hou, Shao et al. 2004). NMR spectra recorded on a Bruker AVANCE 600 MHz spectrometer.

Following initial 1D ^{1}H-NMR and 2D ^{15}N-HSQC spectral analysis each sample was incubated at 37°C for 4 days under agitating conditions (300rpm) to promote oligomerisation of ^{15}N-Aβ$_{1-40}$. Samples were then re-analysed in order to determine how

much ^{15}N-Aβ_{1-40} peptide would still be visible in solution given that aggregated species larger than 50kDa are not detected using NMR spectroscopy (Kwan, Mobli et al. 2011)(Fig. 3.6). As expected the ^{15}N-Aβ_{1-40} only control had significantly reduced peak intensities suggesting reduced concentration of monomeric Aβ peptide. The same was also true for the ^{15}N-Aβ_{1-40} peptide co-incubated with Hsp20-ADM although to a lesser extent. However, both the Hsp20-WT and the Hsp20-S16D co-incubations maintained significantly more ^{15}N-Aβ_{1-40} in its monomeric form when compared to both ^{15}N-Aβ_{1-40} control and Hsp20-ADM (Fig. 3.6).

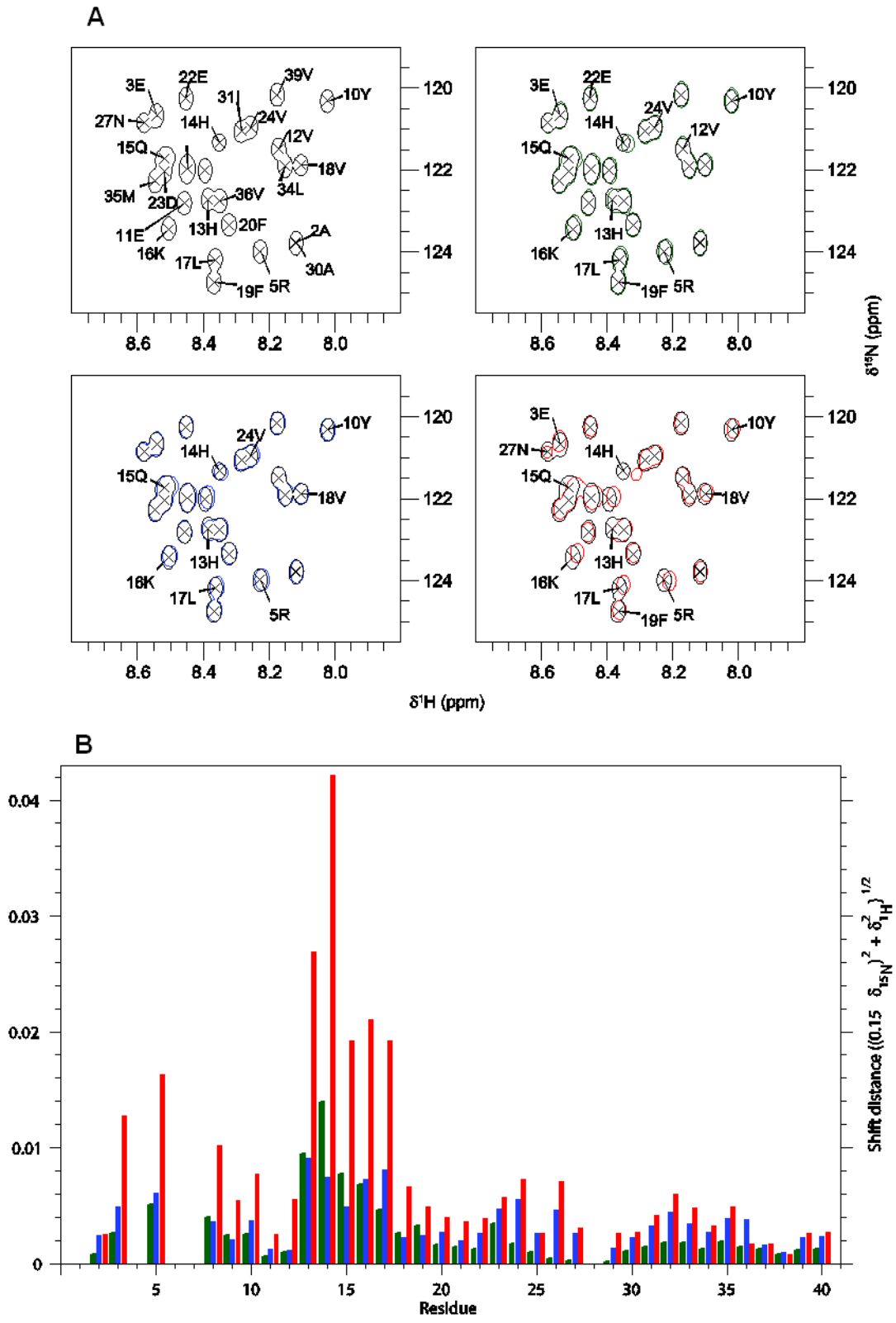

Figure 3.5 – Chemical Shift Difference Analysis of ^{15}N-Aβ$_{1-40}$ co-incubated with Hsp20
Top panels - 2D HSQC experiments showing ^{15}N-Aβ$_{1-40}$ (black); co-incubated with either Hsp20-WT (green), Hsp20-S16D (blue) or Hsp20-ADM (red) at 4°C prior to aggregation. B – Chemical shift perturbation plot from the same experiment, relative to ^{15}N-Aβ$_{1-40}$ only control.

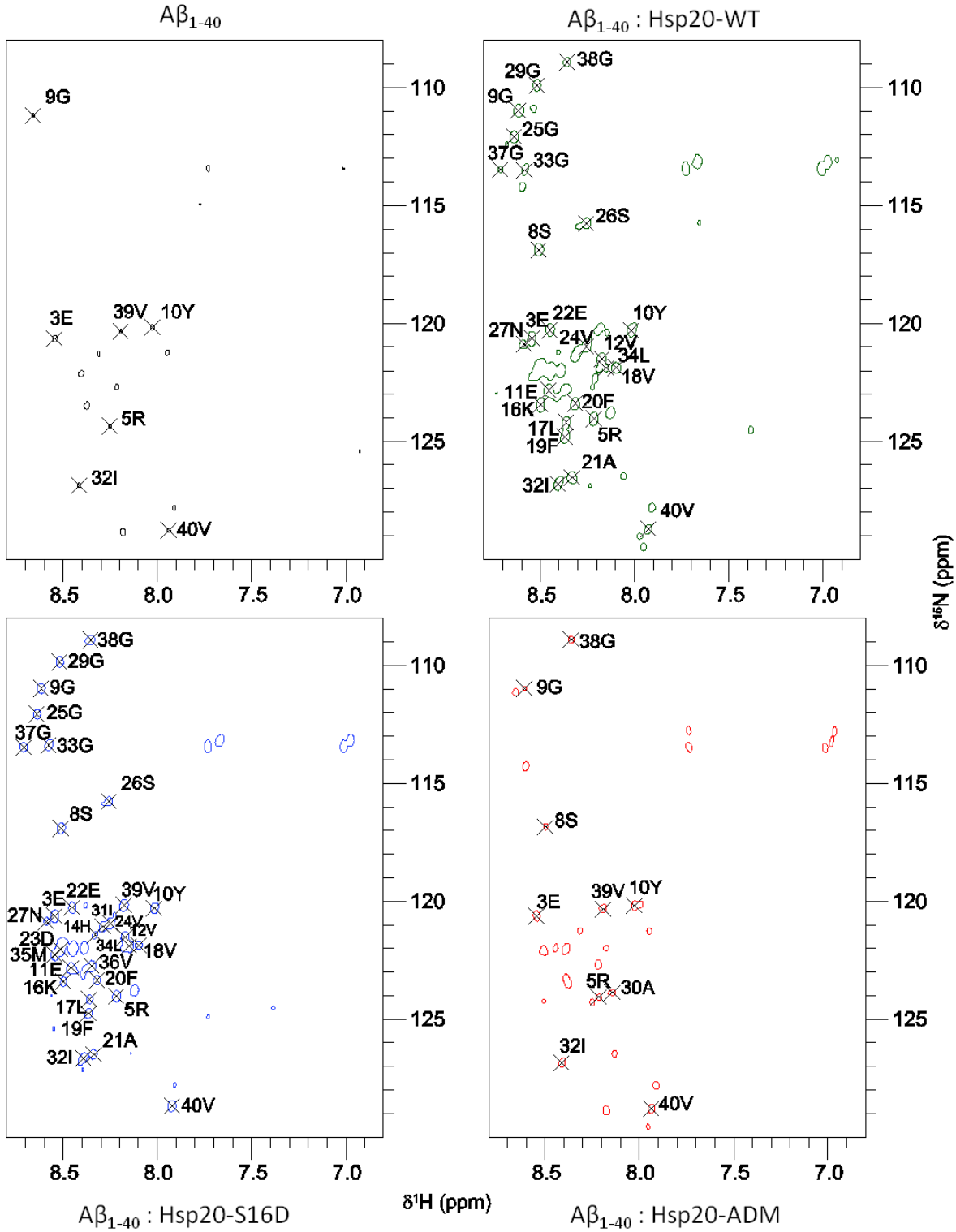

Figure 3.6 – NMR Analysis of ^{15}N-Aβ$_{1-40}$ co-incubated with Hsp20 post-aggregation
Partial [^{1}H,^{15}N]-HSQC spectra of recombinant ^{15}N-Aβ$_{1-40}$ peptide (200µM) in 50mM sodium phosphate buffer (NaPi) at pH 7.5 and 4°C and 14.1 T. ^{15}N-Aβ$_{1-40}$ only peptide (black), ^{15}N-Aβ$_{1-40}$ and 50µM His-Hsp20-WT (green), ^{15}N-Aβ$_{1-40}$ and 50µM His-Hsp20-S16D (blue) & ^{15}N-Aβ$_{1-40}$ and 50µM His-Hsp20-ADM (red). Samples were re-analysed at 4°C following 4 days incubating under aggregating conditions (37°C at 300rpm). There is a marked reduction in signal intensity in both ^{15}N-Aβ$_{1-40}$ only peptide (black) and ^{15}N-Aβ$_{1-40}$ and 50µM His-Hsp20-ADM (red) suggesting a lack of aggregation inhibition. NMR spectra recorded on a Bruker AVANCE 600 MHz spectrometer.

In order to confirm that any loss in signal was the result of Aβ$_{1-40}$ aggregation and not proteolytic degradation, the samples were subjected to western blotting analysis (Fig 3.7). Samples were initially spun at 13,000rpm to remove the insoluble amyloid fibrils that had

formed during the aggregation process. Samples were then taken from each supernatant for western blotting analysis. From this, I found that in the ^{15}N-Aβ_{1-40} only control sample, the levels of monomeric Aβ_{1-40} had virtually disappeared. Co-incubation with His-Hsp20-S16D resulted in the highest levels of monomeric and low molecular weight species remaining in solution, followed by His-Hsp20-WT. The Aβ binding mutant His-Hsp20-ADM maintained no detectable levels of monomeric Aβ_{1-40} in solution; however various low molecular weight species were detectable between 10-25 kDa (Fig. 3.7:top left panel).

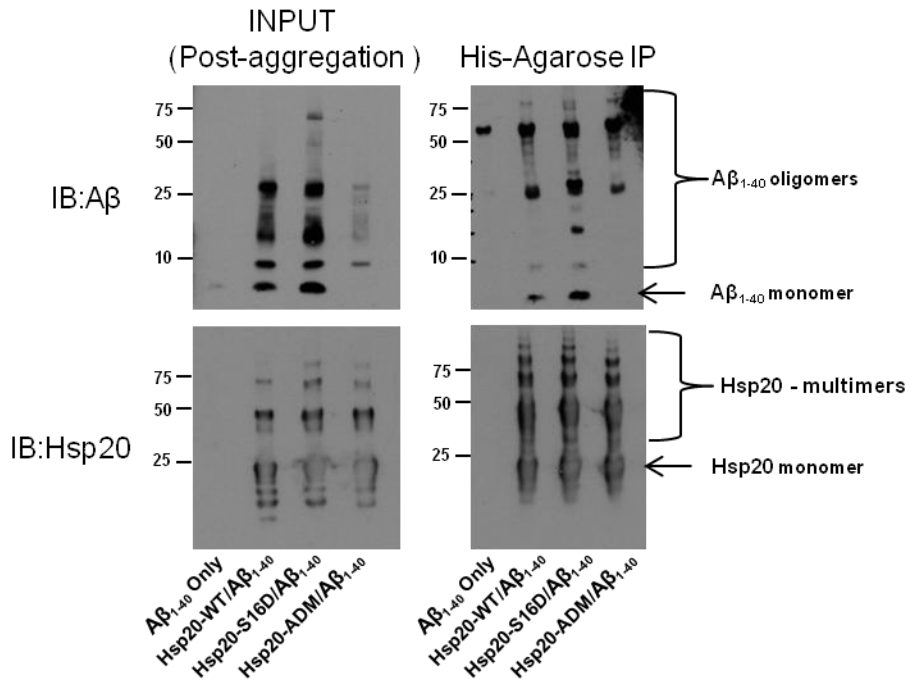

Figure 3.7 – Co-immunoprecipitation of NMR ^{15}N-Aβ_{1-40}/Hsp20 co-incubations.
Following NMR spectral analysis samples were spun down to remove insoluble Aβ_{1-40} aggregates and then analysed using SDS-PAGE to ensure that loss of signal was due to aggregation and not degradation. Very little signal was detected in Aβ_{1-40} only input due to its aggregation into insoluble aggregates. Hsp20-S16D maintained more monomeric Aβ_{1-40} in solution followed by Hsp20-WT, while monomeric Aβ_{1-40} levels in Hsp20-ADM co-incubation were undetectable. This was in agreement with previous NMR analysis. Samples were then incubated with His-Agarose beads for 16 hours at 4°C in order to test if the various Hsp20 proteins could pull-down A$\beta_{1-40.}$ Again Hsp20-S16D was the most effective at pulling down both low and high molecular weight species of A$\beta_{1-40.}$

The NMR samples were then subjected to co-immunoprecipitation studies analogous to experiments carried out in figure 3.3. This confirmed that Hsp20-S16D was able to pull-down more monomeric Aβ_{1-40} than the WT variant. Interestingly, Hsp20-S16D was also able to coIP an Aβ_{1-40} species around the size expected for Aβ tetramers (16kDa) (Fig 3.7:upper right). This Aβ species was not detected in the Hsp20-WT IP despite there being species of this size in solution with Hsp20-WT post aggregation (Fig 3.7:upper left). Despite similar levels of Hsp20-ADM precipitating with the His-agarose beads (Fig 3.7:lower right), there were no low molecular weight species of Aβ_{1-40} detected in this coIP (Fig 3.7:upper right).

Taken together, the NMR data and subsequent *in vitro* pull-down analysis shows that Hsp20 interacts with $A\beta_{1-40}$ and prevents it from aggregating into higher molecular weight oligomers, even at a molar ratios of 1:4 (Hsp20:Aβ). Both Hsp20-WT and –S16D maintained significantly more LMW species of $A\beta_{1-40}$ in solution than the $A\beta_{1-40}$ only control. The interaction between all Hsp20 variants and $A\beta_{1-40}$ was strongest at domains important for beta-sheet formation and oligomerisation of Aβ. Finally, the introduction of the phospho-mimetic S16D increased the chemical shifts at a number of residues and maintained the $A\beta_{1-40}$ peptide in its non-toxic, random coil conformation more so than Hsp20-WT. This data backs up findings from the array data to suggest that the phosphorylation of Hsp20 enhances its interaction with Aβ to inhibit amyloidogenesis.

3.2.3.2 A morphology-sensitive assay for $A\beta_{1-42}$ aggregation based on fluorescence self-quenching

A variety of techniques such as NMR (discussed previously), atomic force microscopy (Mastrangelo, Ahmed et al. 2006) and x-ray diffraction (Sunde, Serpell et al. 1997), have allowed for the molecular analysis of Aβ related polymorphisms. Optical based techniques such as green birefringence of the Congo red dye (Howie and Brewer 2009) and the fluorescent enhancement of Thioflavin T (ThT) upon binding to Aβ aggregates (LeVine 1993) have been the most widely employed methods to monitor the real-time kinetics of Aβ aggregation. However, neither of these optical based assays can differentiate between the various amyloid morphologies that can exist. In addition, the mechanisms by which these optical probes interact with Aβ are not yet fully understood. These limitations have hampered both the understanding of Aβ aggregation and the elucidation of the pathophysiologically relevant Aβ species.

Here we have utilised a novel morphology-sensitive assay, developed by Quinn et al. (2013) that exploits the phenomenon of fluorescence quenching of fluorophore labelled $A\beta_{1-42}$. Aggregation of HiLyte Fluor 555 conjugated to the N-terminal of $A\beta_{1-42}$ ($A\beta_{555}$) organizes the covalently attached fluorophores in to close enough proximity that it triggers a self-quenching process (Fig. 3.8A). This allows for real-time monitoring of the $A\beta_{1-42}$ aggregation process and is unique in that it can distinguish between two physiologically relevant amyloid morphologies. It has previously been shown that addition of dilute hexafluoroisopropanol (HFIP) (1-4% v/v) rapidly promotes the formation of soluble ring-like and globular structures of Aβ (Nichols, Moss et al. 2005) via a mechanism involving the formation of HFIP micro-droplets that act as interfaces to promote $A\beta_{1-42}$ aggregation

(Quinn 2013). Whereas insoluble fibril-like morphologies can be promoted by incubating Aβ at 37°C in the presence of physiological NaCl concentrations (150mM) (Fig 3.8E).

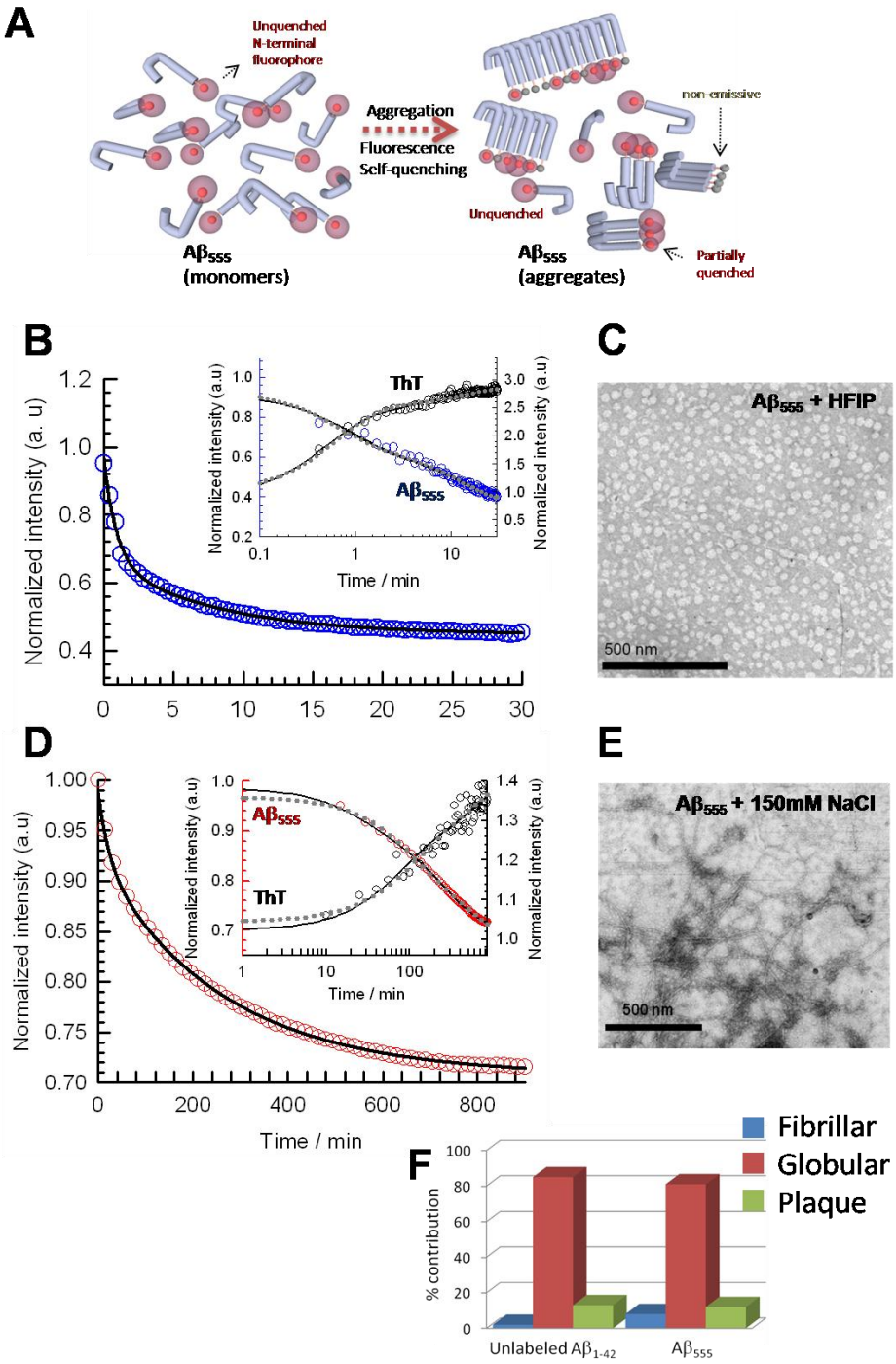

Figure 3.8 – Fluorescence quenching for real-time analysis of two distinct $A\beta_{1-42}$ aggregation pathways.
A – Schematic illustrating the principles of the fluorescence self-quenching assay. N-terminally attached HiLyte Fluor 555-$A\beta_{1-42}$ ($A\beta_{555}$) peptides are progressively quenched as monomers aggregate, resulting in combinations of partially quenched and fully quenched (non-emissive) fluorophores. The range and form of the morphologies are illustrative only, and not to scale. B- Normalised variation in fluorescence intensity of 7µM freshly prepared non-aggregated sample of $A\beta_{555}$ as a function of time at 4°C following injection of 1.5% HFIP to promote oligomerisation. The sold line fits a biexponetial decay function. *Inset:* Normalised fluorescence enhancement of Thioflavin T (ThT) obtained with identical experimental conditions. Dotted grey lines represent the results from a global fit of both ThT and $A\beta_{555}$ assays. C – Transmission electron micrograph (TEM) of $A\beta_{555}$ aggregates obtained following addition of 1.5% HFIP (v/v). D – Normalised variation in

steady-state fluorescence emission as a function of time obtained during the aggregation of a 7μM sample of $A\beta_{555}$ at 37°C (pH 7.9, 150mM NaCl) to promote fibrillisation. *Inset:* Normalised fluorescence enhancement of ThT obtained with identical experimental conditions. E – TEM of aggregated $A\beta_{555}$ obtained at pH 7.9 and 150mM NaCl. The kinetics of the fluorescence self-quenching method and the more common ThT binding assays were identical under both conditions. F - Unlabeled $A\beta_{1-42}$ and $A\beta_{555}$ show almost identical distribution of amyloid morphologies. Amyloid aggregates generated by injection of 1.5 % (v/v) HFIP were imaged and quantified using TEM (Quinn, Dalgarno et al. 2014).

This work was published by Quinn, Dalgarno et al. 2014.

The self-quenching and kinetic properties of the two aggregation pathways vary considerably. For example, the addition of 1.5% (v/v) of HFIP to a fresh non-aggregated solution of $A\beta_{555}$ in aqueous buffer (pH 7.9) induced a 62 (±4) % decrease in the fluorescence intensity over a 30 min time window (Fig. 3.8B). However, conditions that promote fibril-like morphologies only induced a 25 (±3) % decrease in fluorescence intensity and the kinetics of fibril growth is much slower and measured over 800 minutes (Fig. 3.8D). Both aggregation pathways were validated by testing the aggregation of $A\beta_{555}$ in parallel with the commonly used ThT binding assay. The kinetics of aggregation measured by either fluorescence self-quenching or ThT were found to be almost identical (Fig. 3.8B&D inset). The morphologies resulting from these two independent aggregation pathways were evaluated using transmission electron microscopy. TEM images of freshly prepared HFIP-induced aggregates of $A\beta_{555}$ (Fig 3.8C) and fibril-like structures (Fig 3.8E) allowed visualisation of the different aggregate morphologies. Furthermore, these morphologies are identical to those produced by $A\beta_{1-42}$ aggregated under the same conditions, and in agreement with previous studies (Nichols, Moss et al. 2005). This confirmed that the conjugation of HiLyte Fluor 555 at the N-terminal has negligible effects on the aggregation behaviour of $A\beta_{1-42}$.

This novel assay was used to investigate the inhibitory properties of Hsp20 against $A\beta_{1-42}$ aggregation. When we incubated $A\beta_{555}$ in the presence of Hsp20-WT, we observed a significant inhibition of amyloid growth under fibril-like conditions when using a molar excess of Hsp20-WT (i.e., 1:2 molar ratio Aβ:Hsp20), the efficiency of the self-quenching process decreasing by 5-fold from 25 ± 3 to 5 ± 1 % (Fig. 3.9B). In contrast, no significant inhibition was detected under HFIP-induced aggregation or at any experimental conditions when using a 4:1 molar excess of Aβ over Hsp20-WT (Fig. 3.9A & B). We then tested several variants of Hsp20 to gain further insights into the mechanistic details of Hsp20 modulating Aβ aggregation. The Hsp20 variants tested in the fluorescence quenching

assays included Hsp20-WT, -S16D, -ADM and a polymorph of Hsp20 which changes a highly conserved proline to leucine at position 20 (P20L) (Nicolaou, Knoll et al. 2008).

The Hsp20-P20L mutant has been shown to induce secondary structure alterations that lead to a reduced capacity to be phosphorylated by PKA at serine 16. The P20L mutation has also been shown to perturb the ability of Hsp20 to attenuate apoptosis in cardiomyocytes following simulated ischemia/reperfusion injury. This rare substitution is found heterozygously in the general population and has been hypothesised to adversely affect carrier's ability to deal with cellular stress (Nicolaou, Knoll et al. 2008). Because of this we decided to characterise whether this missense mutation, which is in close proximity to the Aβ binding site, would alter Hsp20's ability to inhibit Aβ aggregation and possibly represent a novel biomarker for detecting the risk of developing AD.

The phospho-mimetic variant Hsp20-S16D exhibited higher inhibition efficiency (~50%) of globular- (Fig. 3.9A) and fibril-like (Fig. 3.9B) structures than Hsp20-WT, even at molar ratios of 4:1 (Aβ:S16D), whereas Hsp20-WT showed no significant inhibitory effect. The inhibition of fibrils was also strongly increased as reflected by the relative decrease in fluorescence quenching from 13 ± 5 % for 4:1 molar ratio (Aβ:S16D) to a practically undetectable level (4 ± 1%) when using a 1:2 molar ratio (Aβ:S16D) (Fig 3.9A & B). In agreement with the peptide array and NMR data, these results also demonstrate that replacing serine 16 by aspartic acid promotes the Hsp20/Aβ interaction and decreases the effective concentration of Hsp20 required to disrupt the formation of amyloid aggregates. However, the effect was more pronounced under fibril forming conditions.

For Hsp20-ADM and Hsp20-P20L variants the deviation in fluorescence self-quenching also showed a remarkable dependence on type of aggregate and the molar ratio. P20L failed to inhibit the formation of globular structures at both molar ratios investigated (Fig. 3.9A). Actually, we observed a significant increase in fluorescence quenching from 62 ± 4 % in the absence of P20L to values of 85 ± 3 % and 75 ± 3 % at 4:1 and 1:2 molar ratios (Aβ:P20L), respectively. In contrast, P20L was able to inhibit the formation of fibrillar structures (Fig. 3.9B), although even at the highest molar ratio the self-quenching efficiency was only 9 ± 5 % as opposed to 5 ± 1 % for –WT, and 4 % for the ADM and S16D variants. The ADM behaviour under fibril forming conditions was similar to that observed for S16D (Fig. 3.9B), whilst its ability to disrupt the formation of globules was slightly lower than for S16D at the 1:2 molar ratios (Aβ: ADM) (Fig. 3.9A). However at

the 4:1 molar ratio (Aβ: ADM) behaved in a similar manner to the P20L mutant in that it appeared to promote the aggregation of $A\beta_{555}$.

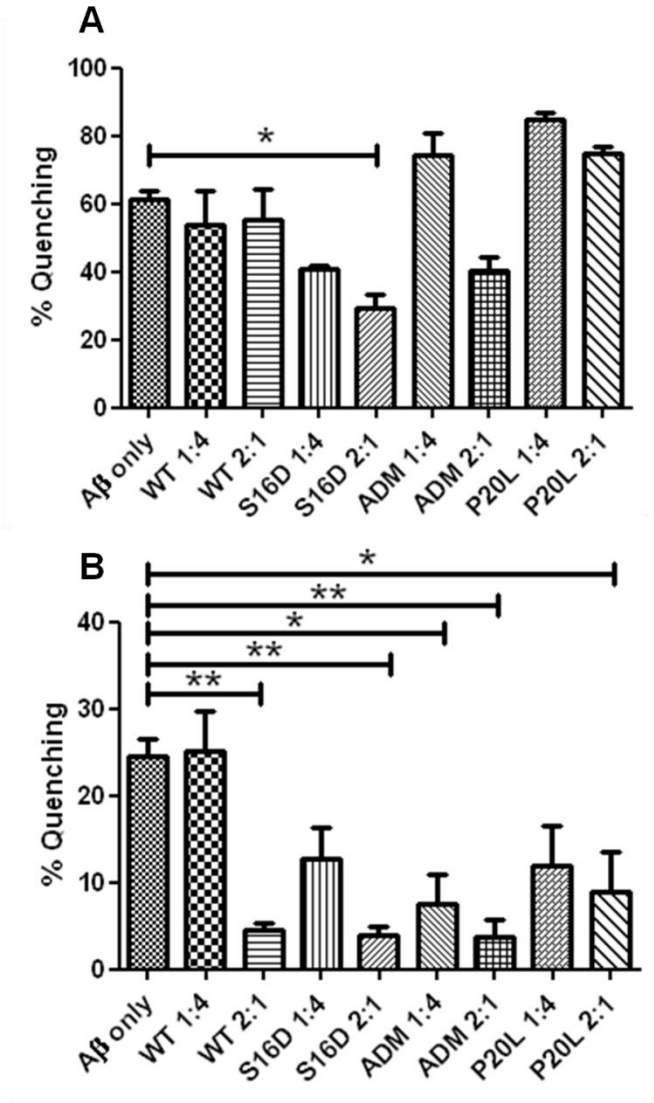

Figure 3.9 – Morphology specific inhibition of $A\beta_{1\text{-}42}$ aggregation by Hsp20 using fluorescence self-quenching
The interaction between Hsp20 variants and $A\beta_{1\text{-}42}$ labelled at the N-terminus with HiLyte Fluor 555 ($A\beta_{555}$) was monitored using fluorescence self-quenching under globular (A) and fibrillar (B) growing conditions. No variation in self-quenching efficiency (~60%) was observed upon incubation of Hsp20-WT with $A\beta_{555}$ at 4:1 and 1:2 (Aβ:Hsp20) molar ratios, suggesting that Hsp20-WT does not inhibit the formation of globular structures induced by 1.5% (v/v) HFIP. Under fibril growing conditions (37°C, pH 7.9, 150 mM NaCl), Hsp20-WT had no effect on the aggregation of $A\beta_{555}$ at 4:1 molar ratios (Aβ:Hsp20) but induced a significant decrease at 1:2 molar ratios. Hsp20-S16D was the most potent at inhibiting aggregation of globular $A\beta_{555}$ while Hsp20-ADM and Hsp20-P20L appear to promote aggregation at 4:1 molar ratios. All Hsp20 variants were able to inhibit fibril growth of $A\beta_{555}$. Mean values ±SEM, p-values - * < 0.05, ** <0.01; ANOVA, n = 3.

These aggregation assays were conducted by Steven Quinn, analysis, interpretation and figure created by myself.

We then repeated experiments using 25-mer peptide analogues of Hsp20 sequences. We used the N-terminal domains of Hsp20-WT, S16D and ADM that incorporate the

Hsp20/Aβ interaction motifs identified from peptide array studies (Fig. 3.1 peptide 2). The most significant differences between experiments using full length proteins and peptide analogues were that the 25-mer S16D variant is approximately 2-fold less efficient in disrupting the formation of fibrils and globular structures than the full-length form (Fig. 3.10A and B). In the globular aggregation assay, the 25mer peptides derived from the Hsp20-WT sequence performs better than the full length protein (Fig. 3.10A). Both the S16D and ADM 25mers displayed partial inhibition of globular aggregation when the molar ratios were 1:2 (Aβ:Hsp20). With regard to performance in fibrillar assays, the S16D 25mer inhibited aggregation more efficiently than the WT 25mer at 1:2 molar ratios (Aβ: Hsp20), 8 ± 4 % vs. 22 ± 7 %, respectively. However, this represented a ~50% reduction in inhibition efficiency compared to their respective full-length proteins. Interestingly, whilst the full-length Hsp20-ADM mutant protein was capable of efficiently inhibiting the formation of fibrillar structures, the 25-mer version of the ADM variant was unable to do so at both molar ratios. In fact, we observed a pronounced increase in fluorescence self-quenching (64 ± 15 %) with the 25-mer ADM at 4:1 molar ratio compared to 25 ± 2 % with the $A\beta_{555}$-only control experiment, which was indicative of higher levels of aggregation. When a 1:2 molar ratio of Aβ:ADM was used, the fluorescence self-quenching returned to values similar to those obtained in the Aβ-only controls (Fig. 3.10B).

This novel, morphology sensitive assay for monitoring $A\beta_{1-42}$ aggregation has allowed us to observe the differential effects of various Hsp20 constructs, including a polymorphism that could potentially involved in AD susceptibility. Consistent with previous results, we have shown that introduction of a phospho-mimetic substitution increases the ability of Hsp20 to effect Aβ aggregation. This assay has also allowed us to establish the efficacy of Hsp20 inhibition of Aβ aggregation in two distinct pathways and has demonstrated selectivity for Hsp20 in modulating the growth of insoluble fibril-like species of Aβ. This is in general agreement with the finding that Hsp20 co-localises with insoluble amyloid fibrils in post-mortem brain tissue (Wilhelmus 2006).

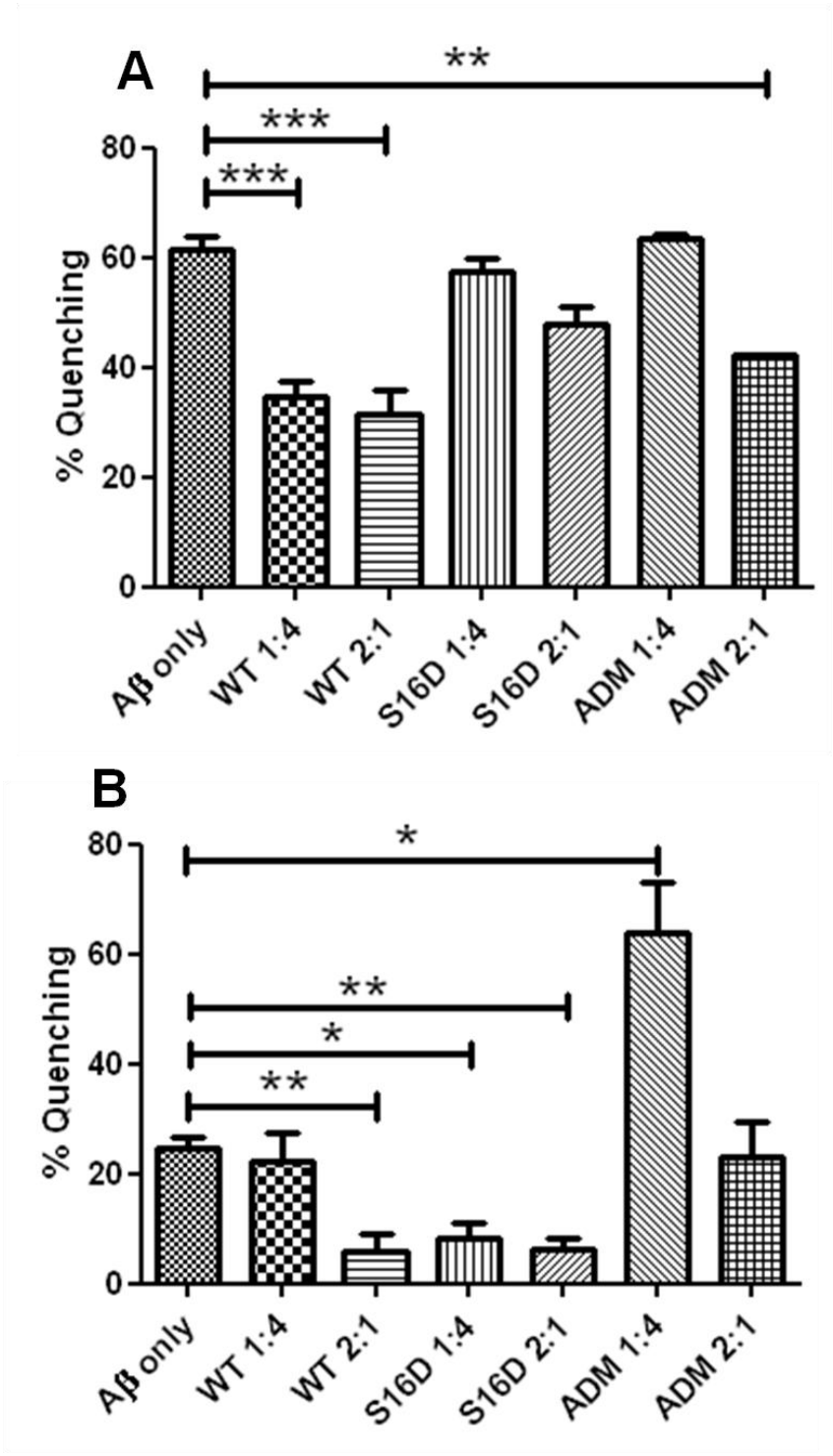

Figure 3.10 - Morphology specific inhibition of $A\beta_{1-42}$ aggregation by 25-mer peptides based on Hsp20 N-terminal domain.

The interaction between Hsp20 N-terminal 25mers and $A\beta_{1-42}$ labelled at the N-terminus with HiLyte Fluor 555 ($A\beta_{555}$) was monitored using fluorescence self-quenching under globular (A) and fibrillar (B) growing conditions. Significant reduction in self-quenching efficiency (~60%) was observed upon incubation of WT-25mer with $A\beta_{555}$ at 4:1 and 1:2 (Aβ:Hsp20) molar ratios. The S16D and ADM 25mers performed similarly in globular assay and did not inhibit the formation of globular structures induced by 1.5% (v/v) HFIP at 4:1 molar ratios but did attenuate aggregation at molar ratios of 1:2 (Aβ:Hsp20). Under fibril growing conditions (37°C, pH 7.9, 150 mM NaCl), S16D 25mers preformed significantly better than the WT 25mer at molar ratios of 4:1 but inhibition efficiency was similar at 1:2 molar ratios. The ADM 25mer was able to enhance the aggregation of $A\beta_{555}$ at 4:1 molar ratios but this returned to control levels when 1:2 molar ratio was used. Mean values ±SEM, p-values - * < 0.05, ** <0.01, *** <0.001; ANOVA, n = 3

These aggregation assays were conducted by Steven Quinn, analysis, interpretation and figure created by myself.

3.2.4 Hsp20 overexpression attenuates $A\beta_{1-42}$ induced cytotoxicity

Previous studies looking at Hsp20 protection against $A\beta_{1-42}$ induced cytotoxicity have concentrated on co-incubation of Hsp20 with $A\beta_{1-42}$ prior to overlay onto various neuronal-like cells (Wilhelmus, Boelens et al. 2006; Wilhelmus, Boelens et al. 2006; Wilhelmus, Otte-Holler et al. 2006) (Lee, Carson et al. 2006). I wanted to assess whether over-expression of Hsp20 would confer protection against $A\beta_{1-42}$ induced cytotoxicity given that $A\beta_{1-42}$ intraneuronal accumulation has been shown to be an early event in the aetiology of AD that leads to synaptic dysfunction and LTP deficits well in advance of extracellular deposition (Oddo, Caccamo et al. 2003). Furthermore, previous studies have shown that soluble Aβ peptides can diffuse across the cell membrane and accumulate intracellularly (Lambert, Barlow et al. 1998). Soluble Aβ is readily taken up by SH-SY5Y and accumulates in lysotracker positive acidic vesicles within 4 hours. Furthermore, SH-SY5Y cells incubated with $A\beta_{1-42}$ for several days, display time-dependent increases in intracellular HMW Aβ aggregates (Hu, Crick et al. 2009). Fibril accumulation results in cell-death and amyloid structures being released into the extracellular space (Friedrich, Tepper et al. 2010).

By increasing the concentration of Hsp20 within neuronal-like SH-SY5Y cells I hypothesised that the accumulation of cytotoxic species of Aβ would be reduced due to the molecular interaction between Hsp20 and Aβ described earlier in this chapter.

To determine whether the ability of Hsp20 to protect neuronal cells from Aβ is enhanced following phosphorylation at serine 16, I set up a MTT reduction based viability assay using SH-SY5Y neuroblastoma cells (Fig. 3.11A). Addition of 20 μM $A\beta_{1-42}$ but not $A\beta_{scr}$, resulted in a significant (# = $p < 0.001$) reduction in cell viability (69 ± 2% Vs 92 ± 3%, respectively) when compared with vehicle only control (Fig. 3.11A). $A\beta_{1-42}$-mediated reduction in cell viability was less pronounced in cells transfected with Hsp20-WT (88 ± 8%) or the phospho-mimic Hsp20-S16D (80% ± 6%). A phospho-null Hsp20 mutant where the serine at position 16 is mutated to alanine (S16A) did not confer any protection against $A\beta_{1-42}$ (68 ± 7%) suggesting that phosphorylation enhances Hsp20-mediated protection (*=$p<0.05$: comparing $A\beta_{1-42}$ treated, transfected cells with $A\beta_{1-42}$ treated, empty vector transfected cells). Although the MTT assay is the most common means of assessing

$A\beta_{1-42}$ cytotoxicity in neuronal cells (Datki, Juhasz et al. 2003; Lee, Carson et al. 2006), the assay is limited by its sensitivity (Mozes, Hunya et al. 2012) and lack of ability to detect neuroprotective effects (Lobner 2000). Also, the fact that it is an endpoint assay supplies limited information about the temporal nature of the cytotoxic effect of $A\beta_{1-42}$.

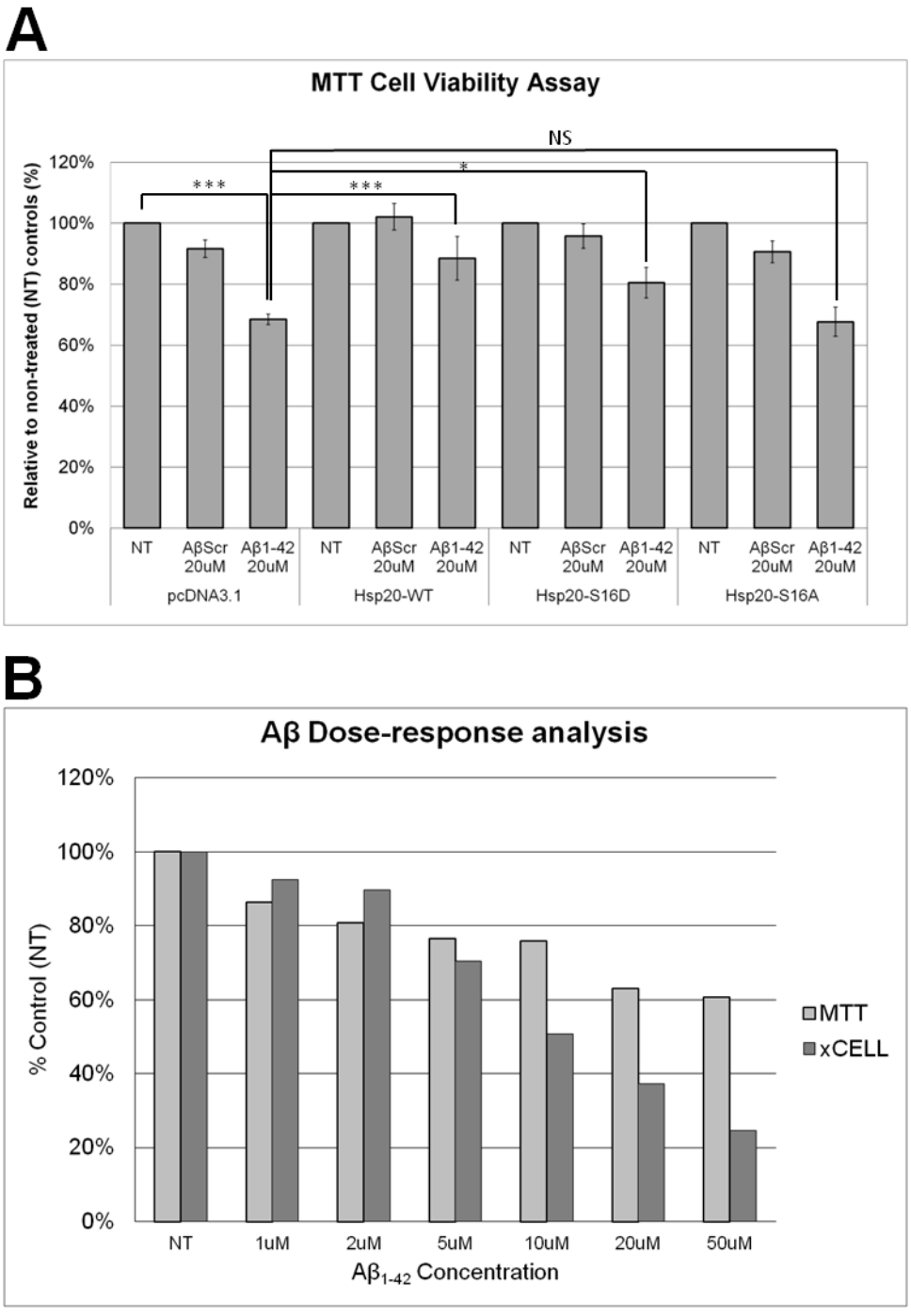

Figure 3.11 – Cell viability assays to monitor $A\beta_{1-42}$ mediated cytotoxicity.
A - Initial studies using MTT cell viability assays showed that addition of $A\beta_{1-42}$ but not $A\beta_{scr}$ resulted in significant reduction in cell viability. This reduction in viability was significantly attenuated by overexpressing either Hsp20-WT or the phospho-mimic Hsp20-S16D, but not by a phospho-null mutant Hsp20-S16A, Mean values ±SEM, p-values - * < 0.05, *** <0.001, NS – not significant; ANOVA, n = 3. B – Direct comparison of dose-dependent reduction in cell viability as measured with MTT or a reduction in cell index using the xCELLigence real-time monitoring system following treatment with $A\beta_{1-42}$ and normalised to non-treated (NT) control. SH-SY5Y cells were treated in with Aβ peptides for 48 hours in triplicate, n=1.

To gain further insights into the temporal nature of Aβ-mediated cytotoxicity I have utilised the xCELLigence system (ACEA Biosciences) a novel, real-time, non-invasive cell monitoring tool which tracks cellular responses and growth through the measurement of electrical impedance. Gold electrodes integrated at the bottom of 96-well tissue culture plates (E-Plates) exquisitely measure changes in resistance induced by changes in cell size and shape. The signal produced by the cell impedance measurements is extrapolated as 'Cell Index', which is used to measure cell growth and monitor cytotoxicity (Fig. 2.2). This technique has been shown to be an accurate and reliable method by which to decipher the kinetics of cell death in neuronal cultures (Mosse, Laudenslager et al. 2008; Diemert, Dolga et al. 2012), something that cannot be achieved using discontinuous methods such as MTT. By comparing the cytotoxicity dose-response of $A\beta_{1-42}$ in SH-SY5Y neuroblastoma cells (Figure 3.11B) it was apparent that impedance was a more sensitive readout of Aβ-induced cytotoxicity than MTT, especially at $A\beta_{1-42}$ concentrations of 5μM and above (Fig. 3.11B).

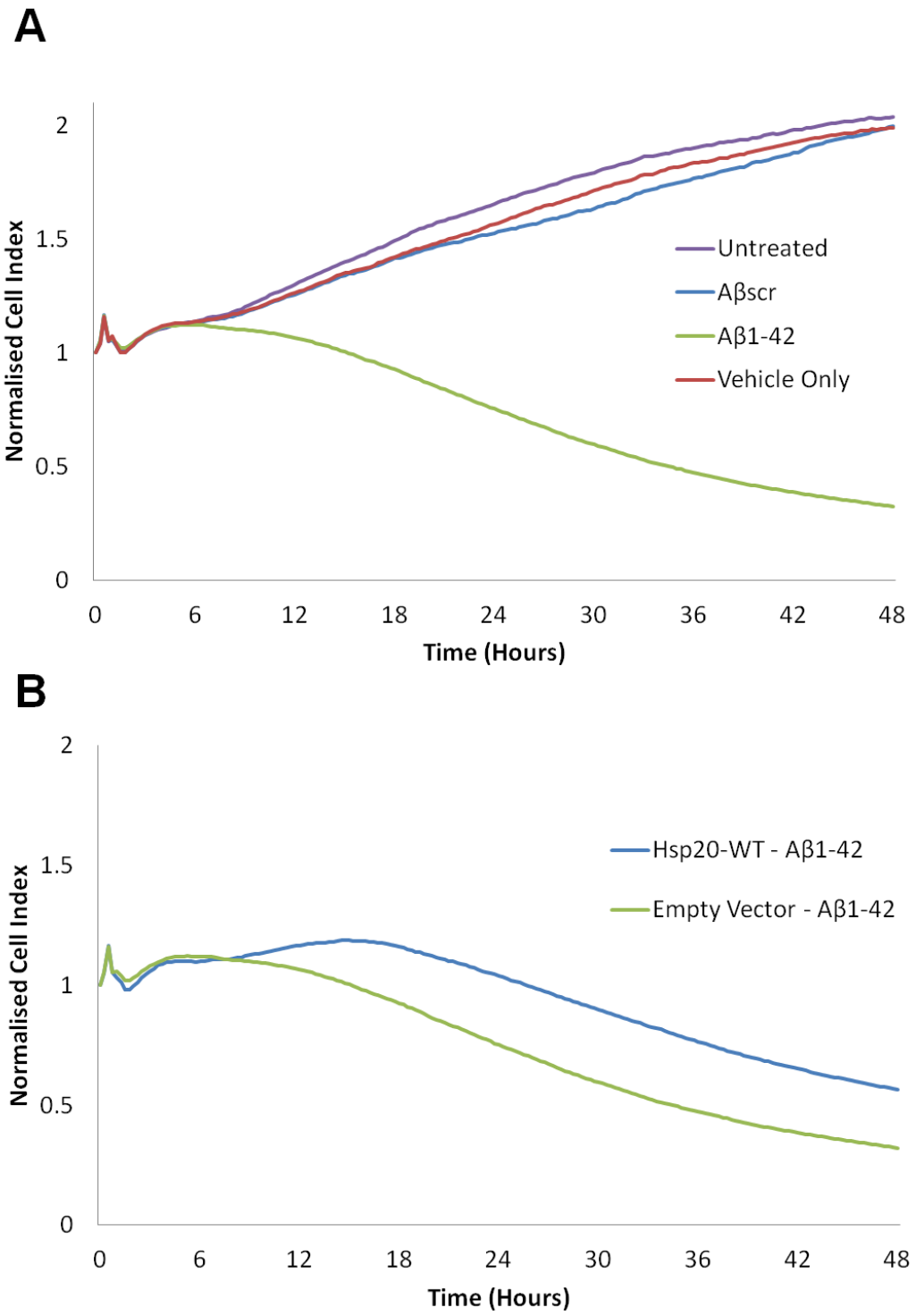

Figure 3.12 – Real-time cell monitoring of $A\beta_{1-42}$ mediated cytotoxicity.
A – Average growth curves of cells treated with either $A\beta_{1-42}$ or $A\beta_{scr}$ control. $A\beta_{scr}$ had no effect on the growth characteristics of SH-SY5Y cells whereas $A\beta_{1-42}$ treatment resulted in a significant reduction in cell index. B – Comparison of average growth curves following treatment of cells overexpressing Hsp20-WT or transfected with the empty vector (pcDNA3.1). Hsp20 overexpression delays the cytotoxic effects of $A\beta_{1-42}$ and attenuates the overall reduction in cell index (n=3).

Given that the data using the xCELLigence platform appeared to be more robust in comparison to well established cell viability assays, I decided to establish our own *in vitro* assay for monitoring $A\beta_{1-42}$ induced cytotoxicity. This was an assay derived for using human SH-SY5Y cells, human derived synthetic $A\beta_{1-42}$ and human Hsp20 constructs. For

all cell-based $A\beta_{1-42}$ cytotoxicity assays I have used the protocol developed by Lambert et al. 1998 ,where they established that diffusible, non-fibrillar ligands, referred to as Aβ-derived diffusible ligands (ADDLs), are potent neurotoxins. ADDLs can be formed by incubating monomeric $A\beta_{1-42}$ at low temperatures (4-8°C) for 24 hours. The toxicity of $A\beta_{1-42}$ prepared in this manner is demonstrated in our xCELLigence assay, where 10µM of $A\beta_{1-42}$ induced approximately 50% reduction in Cell Index after 48 hours (Fig. 3.11B). Analysis of SH-SY5Y cell growth in real-time following the treatment with either $A\beta_{1-42}$ or $A\beta_{scr}$,revealed that addition of the $A\beta_{1-42}$ peptide had no effect on cell growth for the first 6 hours, but was then followed by a constant reduction in Cell Index (Fig. 3.12A) that is characteristic of cell-death (Diemert, Dolga et al. 2012). Treatment with $A\beta_{scr}$ had no effect on cell growth when compared to either non-treated wells or cells treated with PBS (vehicle) (Fig 3.12A). As expected, transfection of Hsp20-WT into SH-SY5Y cells delayed the cytotoxic effect of $A\beta_{1-42}$ and slowed the decrease in Cell Index (Fig 3.12B).

To further assess any attenuation in $A\beta_{1-42}$ cytotoxicity induced by Hsp20 over-expression, SH-SY5Y cells were transfected with either pcDNA3.1 vector (control), Hsp20-WT, -S16D, or -S16A. Following transfection, cells were seeded into a 96 well E-plate and incubated for 24 hours prior to allow for cell adhesion and expression of the Hsp20 constructs, prior to addition of 10 µM $A\beta_{1-42,}$ $A\beta_{scr}$ control peptide (10µM) or PBS vehicle control (Fig. 3.12). Cell growth was monitored at 15 minute intervals for 48 hours post addition of the Aβ peptides (Fig 3.13). All SH-SY5Y cells, no matter what they were transfected with, displayed no significant differences in cell growth when treated with $A\beta_{scr}$. (Fig 3.13, upper graph). However, following addition of $A\beta_{1-42}$ the Cell Index of control transfected cells displayed the most pronounced decrease in Cell Index at 48 hours, reducing to 0.27 ± 0.02. Compared with control, SH-SY5Y cells expressing Hsp20-WT exhibited more than a 2-fold increase in Cell Index (0.56 ± 0.14, p-value < 0.03) following $A\beta_{1-42}$ treatment. Furthermore, both Hsp20-S16D and –S16A expressing cells prevented the extent of reduction of Cell Index to 0.37 ± 0.06, p-value < 0.05, and 0.49 ± 0.1, p-value < 0.03, respectively, after addition of $A\beta_{1-42}$. The average expression level of Hsp20 also found Hsp20-S16D expression to be the lowest of the three variants.

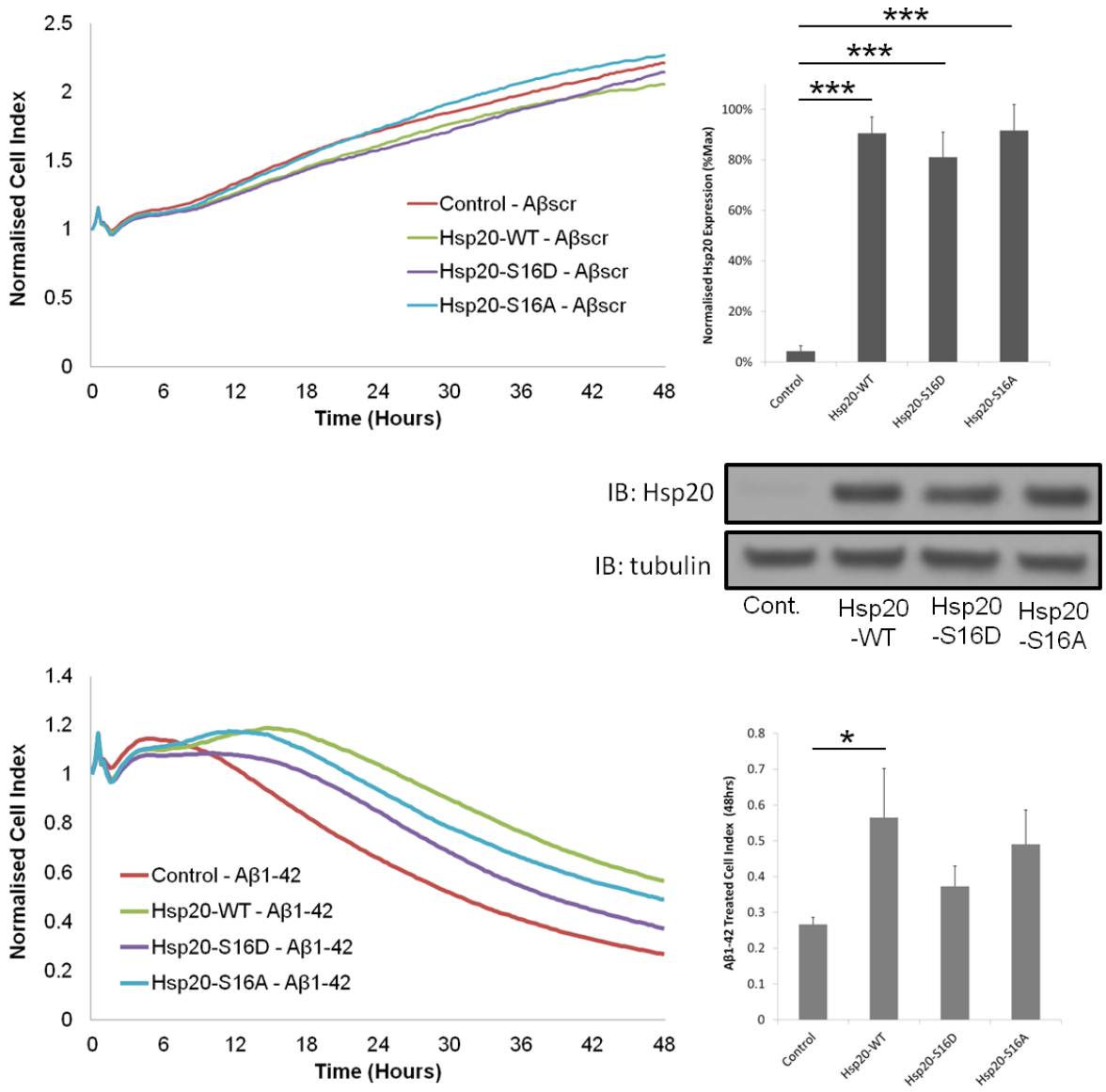

Figure 3.13 – Hsp20 overexpression attenuates $A\beta_{1-42}$ mediated cytotoxicity.
SH-SY5Y cell growth monitored using xCELLigence real-time cell monitoring system. Cells were transfected with either pcDNA3.1 vector (control) or Hsp20 constructs 24 hours prior to treatment with 10μM of $A\beta_{scr}$ (A) or $A\beta_{1-42}$ (B). Expression levels of Hsp20 were assessed from a parallel culture of cells from the same transfection and harvested at the start of each experiment. The average Cell Index at 48 hour time-point highlighted that only Hsp20-WT transfection significantly attenuates $A\beta_{1-42}$ induced cytotoxicity, Mean values ±SEM, p-values - * < 0.05, *** <0.001; ANOVA, n = 3.

The cytotoxicity of $A\beta_{1-42}$ is known to be highly variable and dependent on concentration and methods of preparation. The various multimeric conformations that $A\beta_{1-42}$ can generate, such as oligomers, fibrils and Aβ-derived diffusible ligands (ADDLs) also produce differing levels of toxicity (Datki, Juhasz et al. 2003; Klein, Stine et al. 2004) . I have defined the cytotoxicity of low molecular weight soluble $A\beta_{1-42}$ known as ADDLs (Lambert et al. 1998), by analysing the inhibitory affect of non-fibrillar $A\beta_{1-42}$ on cellular growth. Initial studies treated cells with insoluble fibrillar aggregates but I found no detectable changes in cell viability, via MTT or inhibition of cell growth using

xCELLigence (data not shown). I utilised the xCELLigence system to assess the IC_{50} value of $A\beta_{1-42}$ prepared in accordance with Lambert et al. 1998 (24 hour incubation at 4-8°C) on SH-SY5Y cells stably expressing either pcDNA3.1 construct as a control or Hsp20-WT. Several different concentrations of soluble $A\beta_{1-42}$ (500nM – 50µM) were incubated with cells for 48 hours. For controls $A\beta_{scr}$ was used and had little effect on cell growth. As expected there was a dose-dependent reduction in Cell Index which correlated with $A\beta_{1-42}$ induced cytotoxicity. The calculated IC_{50} values for $A\beta_{1-42}$ treatment were 5.97µM (± 1.1) for pcDNA3.1 expressing SH-SY5Y cells compared with 9.61 (± 0.29) for cells stably expressing Hsp20-WT. The increase in IC_{50} value in the Hsp20-WT expressing cells was statistically significant, *p-value* = 0.0086. A significant right-shift in dose-response curve in Hsp20 expressing cells was also apparent at certain concentrations (Fig. 3.14A). When I examined the differences in Hsp20 protein levels by western blotting analysis (Fig. 3.14B), Hsp20 was readily detectable in the SH-SY5Y stables. This also resulted in higher basal levels of phospho-Hsp20 without the need for exogenous induction by artificially raising cAMP.

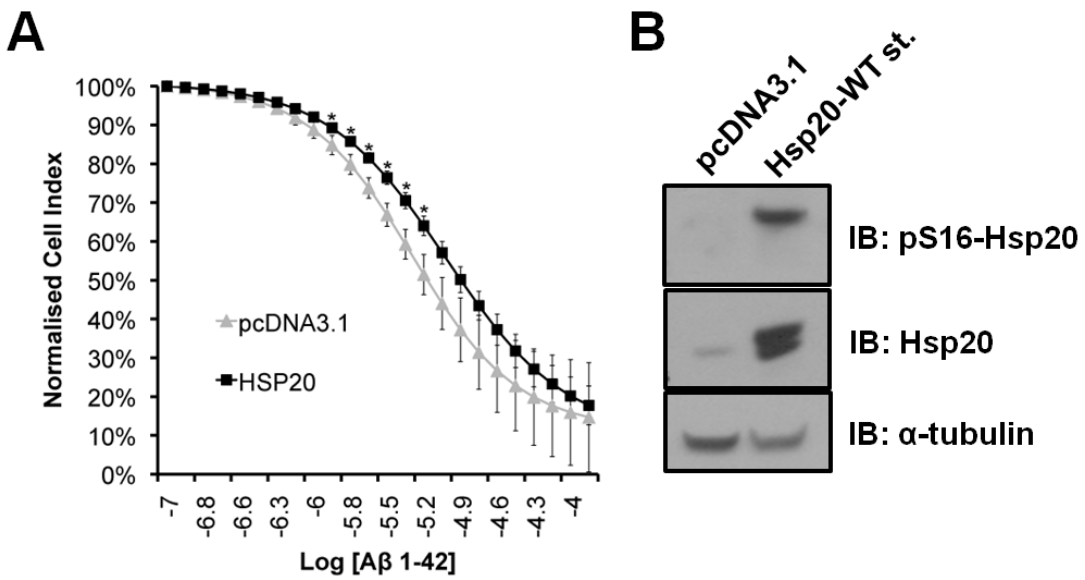

Figure 3.14 – $A\beta_{1-42}$ Dose-Response Analysis
A – SH-SY5Y cells stably expressing either Hsp20-WT (Hsp20-WT st.) or pcDNA3.1 incubated with various concentrations (0.25 – 50µM) of $A\beta_{1-42}$ for 48 hours. The average IC50 value for $A\beta_{1-42}$ on pcDNA3.1 stables was 5.97µM (± 1.1µM) compared to 9.61µM (± 0.29µM) for Hsp20-WT stables (P-value = 0.0086, n = 3). IC50 values were calculated using Real-Time Cell Analyzer (RTCA) software (ACEA). Mean values ±SEM, * = p-value < 0.05, Student-T-test. B – Western blotting analysis of endogenous Hsp20 and phospho-Hsp20 (pS16-Hsp20) expression in respective SH-SY5Y stable cell-line.

3.3 Discussion

Small heat-shock proteins have been shown for some time to have the capacity to bind Aβ peptides and inhibit aggregation and subsequent cytotoxicity *in vitro* (Kudva, Hiddinga et al. 1997) (Lee, Carson et al. 2006) (Wilhelmus, Otte-Holler et al. 2006). In particular, Hsp20 has been shown to interact with soluble Aβ and inhibit its aggregation and optimisation of the interaction between sHSPs and Aβ has been identified as a potential therapeutic target (Wilhelmus, Boelens et al. 2006). Here I have shown for the first time a mechanism of how the interaction between Aβ and Hsp20 may be regulated *in vivo*. Importantly, the phosphorylation of Hsp20 at serine 16 by PKA/G has established effects in a number of physiological processes (Edwards, Cameron et al. 2011). The data presented here also uncovers a novel neuroprotective role for Hsp20 that functions specifically to attenuate the cytotoxic effects associated with the Aβ peptide.

3.3.1 The interaction of Hsp20 with $A\beta_{1-42}$ is modulated via PKA/G phosphorylation

By utilising peptide array technology, I accurately characterised the interaction domains of Hsp20 and $A\beta_{1-42}$ and showed that the binding avidity of Hsp20 towards $A\beta_{1-42}$ is mediated by the N-terminal region of Hsp20, at a domain which includes a consensus PKA/G site. Peptide array technology also allowed us to introduce either a phospho-serine or phospho-mimic residue at the serine site of the PKA/G consensus. Both modifications significantly increased the binding of the $A\beta_{1-42}$ peptide, suggesting that this interaction may be regulated *in vivo* (Fig. 3.1). Reciprocal arrays showed the binding domain on $A\beta_{1-42}$ to which Hsp20 binds, is proximal to the oligomerisation domain (KLVFF), which is necessary for the assembly of toxic aggregates (Beyreuther, Dyrks et al. 1992) (Fig. 3.2). A number of peptide based molecules which inhibit Aβ aggregation have been developed that are based on sequence homology with the KLVFF region (Tjernberg, Naslund et al. 1996; Soto, Sigurdsson et al. 1998). Also, several aggregation inhibitors have been designed to have the 'recognition' sequence KLVFF and a 'disruptor' group at the N- or C- terminals (Carter, Simms et al. 2010). The fact that Hsp20 binds proximally to this domain suggests that the chaperone is acting to inhibit aggregation directly at the site of oligomerisation.

The sequential alanine scanning array of $A\beta_{1-42}$ demonstrated that the lysine residue in position 16 was the only residue in the sequence essential for mediating binding of Hsp20. This demonstrates that charge interaction is an important regulator of binding, as the

introduction of a negatively charged phosphate group at serine 16 on Hsp20 would increase avidity towards $A\beta_{1-42}$ via the positively charged lysine reside. This lysine residue plays an important role in the non-amyloidogenic processing of APP, as α-secretase cleavage at this site does not generate the Aβ peptide (Zheng and Koo 2006). The scanning array also highlighted that H14 and Q15 are also important residues that mediate the binding of Hsp20. H14 has been shown to play an important role in co-ordinating metal ion binding, such as zinc, copper. These metal ions can have significant effect on aggregation propensity of Aβ (Diaz, Linnehan et al. 2006; Olofsson, Lindhagen-Persson et al. 2009). Interestingly, I also saw a reduction in binding when a glutamic acid residue was substituted for alanine. Mutations at this residue cause severe early onset familial AD. This is particularly true of the 'Dutch' mutation (E22Q) and the 'Arctic' mutation (E693G). Given the role that sHSPs play as chaperones in protein surveillance, mutations that effect the interaction of Aβ peptides with sHSPs, such as Hsp20 may perturb Aβ clearance resulting in further amyloid deposition.

3.3.2 Hsp20 interacts with Aβ to maintain it in a non-toxic conformation

After identifying that phosphorylation of Hsp20 at a consensus PKA/G site may modulate Aβ aggregation, I conducted *in vitro* pull-down assays (Fig. 3.3). All His-tagged Hsp20 variants bound to monomeric and dimeric $A\beta_{1-42}$; therefore it is possible that Hsp20 binds to these smaller assemblies, preventing them from forming into higher molecular weight species. Unexpectedly, the Hsp20-ADM binding mutant could still bind to, and pull-down significant quantities of $A\beta_{1-42}$ suggesting that there may be more than one domain which can interact with Aβ. Indeed the α-crystallin domain of sHSPs has been proposed to be the active chaperoning unit (Benesch, Ayoub et al. 2008). Also, the fact that that several members of the sHSP family interact with Aβ but do not contain a consensus PKA is also suggestive of other binding sites. The biological relevance of Hsp20-S16D binding to higher molecular weight species of $A\beta_{1-42}$ may be related to a second mechanism by which some sHSPs are able to reduce the cytotoxic effects of $A\beta_{1-42}$. In a study looking at a different sHSP, also named Hsp20 from the bovine parasite *Babesia bovis*, it was established that as well as binding to Aβ and preventing aggregation, this particular sHSP was able to form a complex surrounding Aβ at lower concentrations, leading to solubilisation of Aβ oligomers and attenuation of subsequent cytotoxicity (Lee, Carson et al. 2006).

Further insights into the effect of Hsp20 phosphorylation on the aggregation dynamics of Aβ were gleaned using NMR spectroscopy. Due to the aggregation kinetics being so quick for $A\beta_{1-42}$, it was not possible to visualise soluble, low molecular weight species of $A\beta_{1-42}$ using NMR. Instead, I used the slower aggregating $A\beta_{1-40}$ peptide. Early structural characterisation of $A\beta_{1-40}$ in solution using NMR spectroscopy have shown that when in solution $A\beta_{1-40}$ contains two helical regions spanning Q^{15} - D^{23} and I^{31} – M^{35}, with the rest of the peptide adopting a random coil formation (Sticht, Bayer et al. 1995). Initial analysis of the chemical shift perturbations for all Hsp20 variants were most pronounced in these two helical regions and also in agreement with the peptide array data as the biggest shift differences occurred in region spanning the oligomerisation domain, residues H^{13} – L^{17}(Fig. 3.5). It was also shown that the introduction of the phospho-mimetic substitution (S16D) increased the shift difference in the large majority of residues relative to Hsp20-WT, demonstrating that the introduction of a negative charge at serine 16 increases the interaction of Hsp20 with $A\beta_{1-40}$. The docking is likely mediated through the lysine residue at position 16 which was shown to be essential in the peptide array experiment. Greater shift differences between Hsp20-WT and –S16D were also detected in the region spanning residues G^{29} – V^{36} which spans the second helical region and suggests that phosphorylation of Hsp20 enhances its interaction with the both helical regions within $A\beta_{1-40}$ in order to maintain it in its soluble conformation. Crucially, both of these regions interact with each other upon structural conversion into insoluble fibrils and current models show that the two regions fold into a β-strand-turn-β-strand conversion. This step is the primary nucleation event of β-sheet secondary structure which is essential for fibrillar growth (Ahmed, Davis et al. 2010).

Rather unexpectedly, we found that the ADM 'binding mutant' induced the most pronounced changes in shift distance across all residues within $A\beta_{1-40}$. This was most pronounced at the oligomerisation domain, particularly at residues H^{13} and H^{14} and is likely due to the removal of the two adjacent, positively charged arginine residues, removing the charge repulsion that would normally occur at the two histidine residues. Interestingly, two adjacent histidine residues, followed by a hydrophobic region also play a key role in the molecular docking of Hsp20 with PDE4D5 (Sin, Edwards et al. 2011). Despite the Hsp20-ADM mutant inducing the biggest change in chemical shifts, this did not translate into increased aggregation inhibition, relative to Hsp20-WT and –S16D. Both Hsp20-WT and S16D maintained significant amounts of $A\beta_{1-40}$ in solution in its monomeric conformation despite 4 days of aggregation at 37°C. The conformational

transition of Aβ from random coil to α-helix to β-sheet structures is a key step in promoting neurotoxicity of the peptide (Simmons, May et al. 1994), therefore it appears that chaperone activity of Hsp20 functions to stabilise Aβ in a non-toxic conformation. We did not see significant differences in the $A\beta_{1-40}$ NMR spectra between the respective Hsp20-WT and –S16D co-incubations post-aggregation. However, following removal of insoluble aggregates by centrifugation, western blotting analysis demonstrated clearly that the levels of monomeric $A\beta_{1-40}$ in solution were higher with Hsp20-S16D relative to -WT. Levels of $A\beta_{1-40}$ in solution, in the absence of Hsp20, was barely detectable, and in the Hsp20-ADM co-incubation there was no monomeric $A\beta_{1-40}$ detected at all, suggesting it had aggregated into insoluble fibrils and removed in the centrifugation step.

Closer analysis of the *in vitro* pull-down assay with Hsp20-S16D and $A\beta_{1-40}$ following aggregation, revealed distinct low molecular weight species at 17kDa and 27kDa that have previously been described by Lambert et al. (1998) as being neurotoxic. This suggests that Hsp20-S16D has a higher propensity to bind soluble toxic species relative to –WT. This would also explain the lack of difference between $A\beta_{1-40}$ levels in solution between the two incubations, as any complex between low molecular weight, oligomeric species of $A\beta_{1-40}$ and Hsp20-S16D would become invisible to NMR spectroscopy once the combined complex size increased beyond 50kDa (Kwan, Mobli et al. 2011).

Taken together, the experimental data outlined in this chapter suggests that Hsp20 interacts with domains involved in the structural conversion from soluble, non-toxic monomers into toxic conformations that are involved in the nucleation of amyloid fibrils (Ahmed, Davis et al. 2010). Furthermore, the introduction of a phosphate group at serine 16 of Hsp20 enhances its interaction with Aβ and increases the levels of Aβ peptide maintained in solution thereby inhibiting growth of insoluble fibrils. This presents a mechanism by which the inhibitory effects of Hsp20 can be further enhanced through phosphorylation and may provide a means of targeting this post-translational modification to prevent aggregation of Aβ, a key step the amyloid cascade hypothesis (Hardy and Selkoe 2002).

3.3.3 Hsp20 attenuates two morphologically distinct Aβ aggregation pathways

The development of the novel Aβ aggregation assay by Quinn et al. (2014) allowed us to test the efficacy of Hsp20 to inhibit aggregation via two distinct mechanisms. Our previous evidence suggested that Hsp20 could inhibit fibrillar growth and our phospho-mimetic

Hsp20 had enhanced ability to interact with oligomeric species of Aβ. Our NMR and *in vitro* pull-down assays have shown an affinity for low molecular weight Aβ species and in agreement with our earlier studies, the fluorescence quenching assay demonstrated that Hsp20 is more effective at inhibiting fibrillar growth of the Aβ peptide. Nonetheless Hsp20-S16D was able to significantly inhibit HFIP induced oligomerisation of $A\beta_{1-42}$ relative to $A\beta_{1-42}$ only control. In AD patient brain tissue, Hsp20 was shown to associate predominately with non-fibrillar Aβ in the form of diffuse senile plaques (Wilhelmus, Otte-Holler et al. 2006). However, the phosphorylation state of this Hsp20 pool was not determined in the study. In the globular forming assay, the P20L mutant was actually shown to promote aggregation, which was interesting given that this mutation is known to affect its secondary structure and reduce its capacity to be phosphorylated at serine 16 (Nicolaou, Knoll et al. 2008). Whether this single nucleotide polymorphism (SNPs) is associated with AD may warrant further investigation, as several SNPs within sHSP family are also associated with a number of protein folding diseases (Boncoraglio, Minoia et al. 2012).

Under fibril growing conditions (Fig. 3.9B); we again found that Hsp20-ADM significantly inhibited aggregation, further confirming that it does bind to Aβ and has inhibitory properties despite the mutations. This suggests that there is another binding domain within Hsp20 that can function to inhibit fibril growth. In early peptide array studies, we found binding within the α-crystallin domain, but this was also apparent in $A\beta_{scr}$ control incubated arrays and was assumed to be non-specific binding (Fig 3.1B). However the immunoglobulin-like α-crystallin domain also contains β-sheet structures (Chen, Feige et al. 2010) and may explain the non-specific interaction at this domain thereby may mask the secondary binding domain. Given that I had evidence that there may be another Aβ binding site within Hsp20, I wanted to determine the efficacy of short 25mer peptides based on the N-terminal sequence of Hsp20. In the HFIP induced oligomerisation assay, the S16D mutant was 2-fold less inhibitory than full-length Hsp20-S16D, while the WT 25mer was more effective than its respective full-length protein. Similar results were seen with the 25mer peptides as was observed with the full length Hsp20 constructs. For example, 25mers corresponding to Hsp20-WT and –S16D, under fibril growing conditions, were still effective inhibitors of aggregation in this pathway, with Hsp20-S16D the most efficacious at the lower concentration tested. Intriguingly, the ADM 25mer resulted in a pronounced change in self-quenching; promoting it to levels seen with HFIP induced aggregation at the 4:1 molar ratio (Aβ:25mer). The ADM 25mer is substantially more hydrophobic than the WT or S16D peptides and a hydrophobic

environment is important for promoting spherical oligomeric conformations (Kayed, Head et al. 2003). Therefore it is possible the ADM 25mer is seeding oligomerisation of $A\beta_{1-42}$ into more globular like structures, this characteristic would have to be tested against another hydrophobic peptide or TEM imaging of this particular assay would be required to confirm if this is the case. It also important to note that the HFIP induced "globularisation" of Aβ is not a natural aggregation pathway (1% HFIP and 4°C incubation) therefore the activity of Hsp20 in this assay might have no relevance physiologically. However, the fibril growing conditions are more representative of what is happening *in vivo* as we use physiological salt concentrations and an incubation temperature of 37°C. It would have also been advantageous to use a non-Aβ interacting His-tagged protein as a control against non-specific protein effects. Nonetheless, full-length Hsp20-S16D consistently outperformed Hsp20-WT across all experiments, as expected.

Taken together, the self-quenching assay has shown that Hsp20 can differentially effect the aggregation of $A\beta_{1-42}$ and has particular selectivity for inhibiting Aβ fibrillar growth. The introduction of the phospho-mimetic substitution increases the efficacy of full-length Hsp20 to inhibit globular aggregation of Aβ, while also increasing the efficacy of Hsp20 to inhibit fibril aggregation at lower protein concentrations, relative to Hsp20-WT. The S16D 25mer peptide was still effective at reducing fibril growth but given that the efficacy was reduced by 2-fold, it would appear that the N-terminal domain itself is not sufficient for the full inhibitory effect of Hsp20. The fact that the S16D 25mer still significantly inhibited fibril growth is interesting as transducible phospho-mimetics based on the N-terminal sequence of Hsp20 have been developed previously, to combat a number of disease-related conditions including, reducing keloid scarring, subarachnoid haemorrhage, and platelet aggregation (Edwards, Cameron et al. 2011). Whether such peptides would have physiological efficacy in reducing fibril formation may be worthy of further investigation.

3.3.4 Increased intracellular expression of Hsp20 is protective against $A\beta_{1-42}$ induced cytotoxicity

Hsp20 has been shown previously to neutralise the toxic effects of Aβ when co-incubated at various molar ratios, prior to overlay onto neuronal-type cells (Lee, Carson et al. 2006) (Wilhelmus, Boelens et al. 2006). Given that low molecular weight soluble species of Aβ readily accumulate intracellularly leading to fibril outgrowth (Friedrich, Tepper et al. 2010), I wanted to establish if neuronal-like cells would be protected from $A\beta_{1-42}$ induced cytotoxicity if the expression levels of Hsp20 were increased intracellularly. Levels of

soluble Aβ species correlate more strongly with synaptic loss and severity of cognitive impairment than the number of insoluble fibrillar plaques in the brain (McLean, Cherny et al. 1999; Wang, Dickson et al. 1999). $A\beta_{1-42}$ intracellular accumulation is also known to occur at the early stages of the disease process and precedes hallmarks such as NFTs and Aβ amyloid deposition (Gouras, Tsai et al. 2000; Mori, Spooner et al. 2002). A triple transgenic mouse model demonstrated that deficits in LTP and synaptic dysfunction correlated with intracellular Aβ accumulation and became apparent before plaque and tangle pathology (Oddo, Caccamo et al. 2003). This suggests that the neurotoxic effect of Aβ is an early event in the aetiology of the disease and I believe Hsp20 phosphorylation represents and endogenous neuroprotective mechanism.

I utilised a protocol that promotes soluble, highly toxic diffusible $A\beta_{1-42}$ species to induce cell death (Lambert, Barlow et al. 1998) in neuronal-like SH-SY5Y cells overexpressing several variants of Hsp20, the WT variant, a phospho-mimic (S16D), and a phospho-null (S16A). Our cell viability assays were originally based on MTT reduction which has been used extensively to characterise Aβ neurotoxicity (Datki, Juhasz et al. 2003). Overexpression of Hsp20-WT or –S16D significantly increased cell viability in cells treated with $A\beta_{1-42}$ but the phospho-null Hsp20-S16A did not, suggesting that phosphorylation at serine 16 differentially modulates the protective properties of Hsp20 (Fig. 3.11A).

I adapted our cell viability assay for use with the xCELLigence system so that I could monitor the effect of $A\beta_{1-42}$ cytotoxicity in real-time to see if I could glean any temporal information concerning $A\beta_{1-42}$ mediated cytotoxicity. The xCELLigence system was far more sensitive to $A\beta_{1-42}$ cytotoxicity than MTT as demonstrated through a dose-dependent reduction in Cell Index that was more pronounced than the reduction in cell viability measured by MTT (Fig. 3.11B). The real-time monitoring of $A\beta_{1-42}$ mediated cytotoxicity showed that there were no differences in cell growth for the first 6 hours (Fig. 3.12A), relative to our control peptide $A\beta_{scr}$ which does not aggregate or form cytotoxic species. After 6 hours I began to see a divergence of both growth curves (control vs. $A\beta_{1-42}$ treated), which is characteristic of cell-death (Diemert, Dolga et al. 2012). Soluble Aβ oligomers have been shown to induce significant cell-death in primary rat hippocampal cultures from 8 hours onwards (Reifert, Hartung-Cranston et al. 2011). Following transfection of Hsp20-WT, I saw a delay in cell-death induction and an increase in Cell Index relative to $A\beta_{1-42}$ treated control transfection (Fig. 3.12B). When I transfected in both the phospho-mimic (S16D) and the phospho-null (S16A), SH-SY5Y cells were also significantly protected

against $A\beta_{1-42}$ induced cytotoxicity, however the phospho-null mutant was actually more protective than S16D. When I compare the binding of $A\beta_{1-42}$ in the alanine scan of $Hsp20^{11-36}$ there is no significant difference between binding of $A\beta_{1-42}$ for S16D and S16A with relative intensities of 134% vs. 128%, respectively. Therefore the difference in protective effects is more likely due to differences in expression levels (Fig. 3.13). The lack of difference between the protective effects of Hsp20-S16D and –S16A are also suggestive of a mechanism distinct from Hsp20's ability to directly inhibit cell-death, as both of these variants have significantly different effects when expressed in cardiomyocytes. Hsp20-S16D can directly inhibit apoptosis whereas non-phosphorylatable S16A mutant cannot (Fan and Kranias 2010). In agreement with the MTT reduction assay, Hsp20-WT evoked the greatest protective effect; further signifying that phosphorylation at serine 16 is required for the full inhibitory effect.

The variability of $A\beta_{1-42}$ toxicity between studies in the literature has traditionally been due to significant differences in actual concentration, preparation, source and secondary conformation of $A\beta_{1-42}$. I prepared the synthetic $A\beta_{1-42}$ in such a way as to maximise the levels of soluble low molecular weight species that are potently neurotoxic (Lambert 1998). I then utilised the novel xCELLigence system to monitor effects on the neuronal-like SH-SY5Y cell line. Consistent with previous studies, higher concentrations of $A\beta_{1-42}$ are more cytotoxic. The real-time cell analysis (RTCA) software allowed direct comparison of $A\beta_{1-42}$ IC_{50} values in SH-SY5Y cells stably expressing either a control vector (pcDNA3.1) or Hsp20-WT. The Hsp20-WT expressing cells had much higher levels of phospho-HSP20 without the need for induction of phosphorylation; this resulted in a significant right-shifted dose-response curve and further demonstrated increased levels of protection against $A\beta_{1-42}$ cytotoxicity. One reason for the protective effects of Hsp20 expression not being more pronounced is that SH-SY5Y cells readily express Hsp20 therefore these cells would have level of protection against $A\beta_{1-42}$ resulting less significant difference relative to controls. Ideally, the experiments should have been done in Hsp20 knockout cells, however, siRNA against Hsp20 did not work.

The data presented here is consistent with previous studies, which show that Hsp20 is modified post-translationally *in vivo* and that phosphorylation at serine 16 evokes its protective functions (Fan and Kranias 2010). So for the very first time, I have demonstrated that this modulation represents a novel means for attenuating $A\beta_{1-42}$ cytotoxicity. Our data highlights how phosphorylation of Hsp20 may increase its ability to inhibit two morphology distinct Aβ aggregation pathways relevant to physiological

amyloidogenesis and early nucleation events. Hsp20 binds directly to domains involved in the structural conversion to neurotoxic Aβ species and functions as an amateur chaperone to maintain Aβ in a soluble non-toxic conformation. Phospho-mimetic Hsp20 also binds to higher order structures which may represent a mechanism of solubilising hydrophobic $A\beta_{1-42}$ conformations to neutralise toxicity or increase Aβ peptide clearance. Finally using a novel label-free cell monitoring system I was able to confirm that increased intracellular levels of phospho-Hsp20 protects against cytotoxicity associated with diffusible Aβ and that this protection is likely mediated through a direct interaction as opposed to the anti-apoptotic properties of Hsp20. Therefore I believe that targeting PKA/G induced phosphorylation of Hsp20 represents a novel endogenous protection mechanism that may be targeted therapeutically for the treatment of AD.

4 PDE Inhibition Promotes Neuroprotection Via Hsp20 Phosphorylation

4.1 Introduction

Alzheimer's disease is the most common of the degenerative brain diseases and is characterised by impairment of cognitive function. Patients with this disorder lose the ability to encode new memories. Eventually, both declarative and non-declarative memory is significantly impaired, resulting in the capacity for reasoning, abstraction and language becoming progressively reduced. The early, subtle signs of cognitive impairment occur in the absence of clinical signs of brain injury, suggesting that something discrete is interrupting synaptic function and inhibiting the encoding of new declarative memories. An abundance of evidence has pointed towards the highly hydrophobic 42 amino acid Aβ peptide as being a causative factor in AD. Aβ can assemble into highly stable oligomeric and fibrillar species that become deposited as amyloid plaques in the brain, one of the pathological hallmarks of the disease (Selkoe 2002).

Many studies have shown the Aβ peptide to be a key toxic component in AD. However, the underlying toxic mechanism and target of toxicity have not been fully elucidated. Several compelling arguments have been made with regard to the Aβ peptide and the involvement of either soluble or higher order species, aggregation in various intra- or extra-cellular compartments, and its neurotoxicity. Another important finding was that AD is a disease of synaptic failure and a hallmark of the latter stages of diseased brains is major loss of neurons (Selkoe 1991). As such, considerable focus has been put on developing therapeutic agents that can prevent neuronal death. Furthermore, it has been recognised that synaptic dysfunction is a more proximal pathological event and synaptic pathology is responsible for the mild cognitive impairment (MCI) associated with the earliest phase of the disease. Attenuating synaptic dysfunction in AD has been predicted to have beneficial effects on cognition and may possibly slow progression of the disease (Bales, Plath et al. 2010).

One pathway that has been targeted therapeutically to improve synaptic function is the cyclic nucleotide second messenger system. cAMP and cGMP are intrinsically involved in the regulation of synaptic plasticity, a complex process whereby neuronal architecture and signalling pathways are adjusted in response to recent brain activity, in preparation for future activity. Repeated activity increases synaptic strength, and can be measured in a

model of synaptic plasticity known as long-term potentiation (LTP), which is widely accepted as an *in vitro* model of learning and memory (Bales, Plath et al. 2010). The second messenger signalling cascade regulates learning and memory processes primarily through PKA or PKG phosphorylation of CREB. Upon phosphorylation CREB becomes activated, translocates to the nucleus where it regulates gene expression required for long-term memory storage (Silva, Kogan et al. 1998). Studies looking at the effect of Aβ on synaptic plasticity found that extracellular perfusion of $A\beta_{1-40}$ and $A\beta_{1-42}$ can inhibit LTP at sub-lethal concentrations (Cullen, Suh et al. 1997; Itoh, Akaike et al. 1999). Furthermore, the intracellular injection of $A\beta_{1-40}$ or $A\beta_{1-42}$ can completely block LTP. Notably, the concentration of $A\beta_{1-40}$ required was 1000-fold greater than $A\beta_{1-42}$ to induce the same effect (Nomura, Takechi et al. 2012).

The superfamily of phosphodiesterases (PDEs) are an attractive target for modulating synaptic plasticity via second messenger signalling as they provide the sole means of cyclic nucleotide degradation. There are 21 different genes that encode PDEs and these are separated functionally into 11 families depending on characteristics such as, cyclic nucleotide specificity and modular structure (Lugnier 2006). Further diversity is generated through multiple splice variants existing for a number of PDE families resulting in more than 60 different isoforms of PDEs (Lugnier 2006). A number of PDEs have been associated with signalling pathways involved in neuropsychiatric disorders including AD. Of particular note are PDE4, PDE5 and PDE9, the latter two more recently emerging as novel therapeutic targets for AD (Xu, Zhang et al. 2011).

PDE4 is the most complex of all the PDE families and is encoded by four genes, PDE4A, B, C & D. It represents the major cAMP-regulating enzyme in the body and isoforms A,B and D are readily expressed in the brain (Perez-Torres, Miro et al. 2000). PDE4 has been a therapeutic target for a number of years following the discovery that the prototypical PDE4 inhibitor rolipram, exhibited antidepressant activity in a clinical setting. More recently PDE4 has been targeted therapeutically to treat inflammatory disorders and one inhibitor, Roflumilast, has been approved to treat condition such as chronic obstructive pulmonary disease (COPD) (Fabbri, Beghe et al. 2010). However, targeted PDE4 inhibition has re-emerged as a therapeutic target for cognitive disorders following the discovery that rolipram could potentiate and extend LTP. Such an observation demonstrated that PDE4 is a key regulator of long-term memory formation in the hippocampus (Barad, Bourtchouladze et al. 1998).

The Aβ peptide has been shown to directly inhibit LTP in cultured hippocampal neurons. Aβ treatment leads to the inhibition of PKA activity resulting in decreased CREB phosphorylation. However, this was reversible through agents that could increase intracellular cAMP, namely rolipram, but blocked using the PKA inhibitor H89. This finding suggested for the first time that induction of the cAMP/PKA/CREB signalling cascade using a PDE inhibitor may be able to alleviate cognitive deficits associated with AD (Vitolo, Sant'Angelo et al. 2002). Several studies have also examined the effects of rolipram in rodent models of AD. Firstly (Gong, Vitolo et al. 2004) demonstrated that rolipram could ameliorate deficits in LTP and contextual learning in the human APP Swedish (KM670/671NL) and presenilin-1 (M146V) expressing transgenic mouse (APP/PS1). An important aspect of this study was that the effects of rolipram were long lasting and extended beyond the treatment duration. Rolipram administration improved LTP and synaptic transmission, and improved memory deficits for up to 2 months after completion of treatment. It was hypothesised that expression of CREB regulated genes may make synapses more resistant to the neurotoxic effects associated with Aβ accumulation (Gong, Vitolo et al. 2004).

A study examining environmental enrichment, which is associated with reduced risk of AD onset, highlighted that APP/PS1 mice raised in a stimulating environment were protected against cognitive impairments. These mice had significantly improved performance in several behavioural tasks compared to transgenic mice raised in standard housing. Furthermore, treatment with rolipram for 2 weeks mimicked the effect of environmental enrichment and could restore normal cognitive functions to severely impaired AD mice (Costa, Cracchiolo et al. 2007). As well as improving cognitive functions, activation of the cAMP/PKA/CREB signalling pathway via rolipram protected against the oligomeric Aβ triggered acute decrease in dendritic spine density and alterations of spine morphology in non-transgenic hippocampal slices. More importantly, rolipram treatment was shown to reverse the chronic loss of dendritic spine density in the hippocampus of aged APP/PS1 transgenic mice, suggesting that the adverse effects on synaptic architecture induced by Aβ may be reversible, even in aged animals (Smith, Pozueta et al. 2009). Similar studies have been carried out in rats treated with synthetic $A\beta_{1-40}$ and a shorter peptide known to have toxic effects, $A\beta_{25-35}$. Perfusion with these peptides produced memory impairments that could be reversed dose-dependently with rolipram (Cheng, Wang et al. 2010). Furthermore, treatment with $A\beta_{25-35}$ or $A\beta_{1-42}$ in rats was associated with increase expression of the pro-apoptotic protein Bax in the hippocampus (Wang, Yang et al. 2012).

The effects of rolipram can be mimicked by selective knockout of PDE4D in mice. PDE4D deficient mice displayed memory enhancement in several hippocampal related tests including, water maze and object recognition. PDE4D5 deficient mice also demonstrate increased CREB phosphorylation and hippocampal neurogenesis (Li, Cheng et al. 2011). Furthermore, microRNAs mediated knockdown of long forms PDE4D4 and PDE4D5, also had the same effect. This is of particular relevance as the Baillie group recently discovered that Hsp20 interacts directly with PDE4D5. Disruption of this interaction leads to sustained Hsp20 phosphorylation and promotes several protective functions of Hsp20 in cardiomyocytes, including anti-apoptotic and anti-hypertrophic effects (Sin, Edwards et al. 2011; Edwards, Scott et al. 2012).

The PDE5 inhibitor sildenafil (Viagra®) was the first commercially successful drug developed to target a PDE isoform. This success has generated significant interest in cGMP-specific PDE5 as a therapeutic target for other disorders, particularly related to cognition given the role of NO/cGMP/CREB signalling in synaptic transmission (Bales 2010). An initial study looking at the effects of sildenafil on cognition found that it improved long-term retention in a passive avoidance task. This one-trial learning paradigm uses an aversive stimulus, such as electric shock, that has to be remembered. The effect of sildenafil was long lasting with performance after 1 week and 1 month comparable to 48 hour post training retention performance (Baratti and Boccia 1999). Sildenafil was also shown to improve memory performance in an object recognition task which was associated with increased cGMP levels in neuronal fibres in the hippocampus (Prickaerts, van Staveren et al. 2002). Despite elevated cGMP levels in the hippocampus being required to improve memory performance in object recognition and passive avoidance, it does not seem to improve spatial learning. Furthermore, timings of treatment were crucial to the modulatory effects of sildenafil on memory performance, suggesting a role for cGMP in early stage memory formation (Prickaerts, Sik et al. 2004).

PDE5 inhibition has also been shown to rescue synaptic function and memory deficits in the human APP/PS1 transgenic mouse model of AD. Sildenafil treatment was able to re-establish CREB phosphorylation and attenuate the effect of high Aβ levels on synaptic function for a period beyond treatment. Sildenafil was also able to induce long-lasting reduction in $A\beta_{1-40}$ and $A\beta_{1-42}$ levels in the cortex of APP/PS1 mice (Puzzo, Staniszewski et al. 2009). In a recent study, the effect of sildenafil in APP/PS1 transgenic mice was also shown to reverse the neuroinflammatory response induced by Aβ and reduce the levels of soluble $A\beta_{1-40}$ and $A\beta_{1-42}$ in the hippocampus. The effects of sildenafil were inhibited

following intra-hippocampal infusion with a PKG inhibitor, further pointing to the fact that targeting the cGMP/PKG/CREB signalling pathway may represent a novel AD therapy (Zhang, Guo et al. 2013).

The cognitive enhancing effects of sildenafil are very similar to that of rolipram, in that they both activate CREB via their respective protein kinases, leading to increased LTP. Both inhibitors can reverse decreases LTP induced via Aβ perfusion or overexpression and both inhibitors appear to have long-lasting effects that are sustained beyond the treatment regime. The difference between the two inhibitors is the effect on spatial working memory. Rolipram has no effect in these test paradigms, whereas sildenafil can immediately enhance spatial working memory. Another major difference between the two compounds is that sildenafil can significantly reduce Aβ levels in the brain while rolipram improves cognitive impairment without affecting Aβ burden (Puzzo, Staniszewski et al. 2009).

The latest phosphodiesterase to emerge as a target for ameliorating cognitive impairments associated with AD is PDE9. PDE9 has the highest affinity for cGMP out of all known cGMP hydrolysing PDEs (Fisher, Smith et al. 1998). PDE9A is the only known gene, however, there are 20 different splice variants that result in a complex differential tissue expression profile. PDE9 is expressed throughout the brain at low levels and is thought to play a key role in regulating basal levels of cGMP signalling in the CNS (Andreeva, Dikkes et al. 2001; Rentero, Monfort et al. 2003; Van Staveren, Steinbusch et al. 2003). PDE9 mRNA is detectable in the human cortex, hippocampus, and cerebellum in a pattern comparable to rodents. However, there were no differences in PDE9 expression patterns in AD patient brains relative to controls (Reyes-Irisarri, Markerink-Van Ittersum et al. 2007).

Following development of the first potent PDE9 inhibitor, BAY 73-6691 (Wunder, Tersteegen et al. 2005), it was subsequently shown that inhibition of PDE9 enhanced early LTP in hippocampal slices from rats. BAY 73-6691 was shown to enhance acquisition, consolidation, and retention of long-term memory in several behavioural paradigms, such as social recognition, scopolamine-disrupted passive avoidance, and MK-801-induced short-term memory deficits (van der Staay, Rutten et al. 2008). LTP was also enhanced in hippocampal slices from PDE9A knock-out mice. These mice had significantly increased levels of cGMP throughout the brain, resulting in improved performance in a spatial recognition task. These effects could be mimicked pharmacologically with a novel selective PDE9 inhibitor, PF-04447943 (Menniti 2008; Schmidt 2009). PF-04447943 was also shown to significantly increase cGMP levels in the cerebrospinal fluid in healthy

human volunteers (Nicholas 2009). These findings underscore the importance of cGMP regulation in the CNS and also underpin the importance of PDE9 in modulating cognitive functions. So it seems that PDE9 appears to be an effective target for ameliorating symptoms associated with AD (Bales, Plath et al. 2010).

Despite strong evidence supporting a role for PDE inhibitors as cognitive enhancers, the underlying mechanisms of how they strengthen synapses or make synapses more resistant to neurotoxic insults has not been elucidated. Indeed, the effects of PDE inhibitors in modulating the effects of acute Aβ-induced neurotoxicity have yet to be examined. Given the correlation between synaptic loss and cognitive impairments in AD, agents with neuroprotective functions are seen as potential therapies for AD.

4.1.1 Experimental Aims

I have recently demonstrated that the phosphorylation of the small heat-shock protein, Hsp20 at a consensus PKA/PKG site (RRAS) increases the avidity of Hsp20 for the Aβ peptide. Hsp20 can maintain Aβ in a non-toxic conformation and prevent it from aggregating into higher molecular weight amyloid species that are the pathological hallmarks of AD. Furthermore, I have demonstrated that increased levels of intracellular phospho-Hsp20 can attenuate the acute toxicity associated with soluble oligomeric forms of Aβ.

As a result of discovering this novel neuroprotective mechanism, we were approached by a Danish pharmaceutical company, Lundbeck, who had developed a number of selective PDE9 inhibitors and we were asked by them to help establish whether the protective mechanism elicited by PDE9 inhibition is driven by increased levels of Hsp20 phosphorylation. Lundbeck had created a transgenic AD mouse model that over-expressed the human form of APP, resulting in a 5-fold increase in $A\beta_{1-42}$ levels relative to normal mice. These mice display significant cognitive dysfunction at 7 months, which can be reversed through selective PDE9 inhibition (Personal communication from A. Parachikova, Lundbeck). We wanted to test whether PDE9 inhibition could activate the protective properties of Hsp20 in our cell model of Aβ toxicity. I decided to examine the effects alongside the PDE4 inhibitor rolipram and the PDE5 inhibitor sildenafil as all three PDE inhibitors have been shown to significantly enhance cognitive functions and have been proposed as potential AD therapies.

4.1.2 Experimental Procedure

This chapter was put together with data from 3 main experimental procedures as follows:

1 – Determination of the expression levels of PDE9 in neuronal-like SH-SY5Y cells.

2 – Characterisation of the effects of PDE4, 5 & 9 inhibition has on endogenous Hsp20 phosphorylation in SH-SY5Y cells. These cells readily express Hsp20 and are an ideal cell model for testing PDE inhibitor induced phosphorylation.

3 – Using our xCELLigence based real-time cell monitoring platform for measuring Aβ cytotoxicity I investigated whether selective PDE inhibition could attenuate Aβ-induced cell death in SH-SY5Y cells by increasing levels of intracellular phospho-Hsp20.

4.2 Results

4.2.1 PDE9 is expressed in human neuronal-like SH-SY5Y cells

First of all we had to verify that PDE9 was expressed in SH-SY5Y cells to ensure it was a suitable cell model for testing the effects of the PDE9 inhibitors. This was initially carried out using reverse transcriptase PCR (Fig. 4.1A). SH-SY5Y cells were harvested for RNA in order to check PDE9A transcript mRNA levels, which are generally a good indication of expression. Amplification of the resultant cDNA was carried out using RT-PCR primer pairs targeted to three distinct intron spanning regions of the PDE9A1 gene. All three PDE9A targeted primers amplified PDE9A cDNA from SH-SY5Y cells. Secondly, I tested a number of cell lysates for PDE9A expression using a commercially available PDE9A antibody (Scottish Biomedical, UK). Cell lysates were resolved using SDS-PAGE followed by western blot analysis to probe for protein expression. All cell types tested positive for PDE9A expression and a number of different molecular weight isoforms were detected (Fig. 4.1B). With regard to PDE4 expression in SH-SY5Y cells, I have recently reported that PDE4B and PDE4D isoforms are readily expressed in these neuronal-like cells (Cameron, Coleman et al. 2013). PDE5 is also readily expressed in SH-SY5Y cells as has been reported previously (Hsu, Liu et al. 2010).

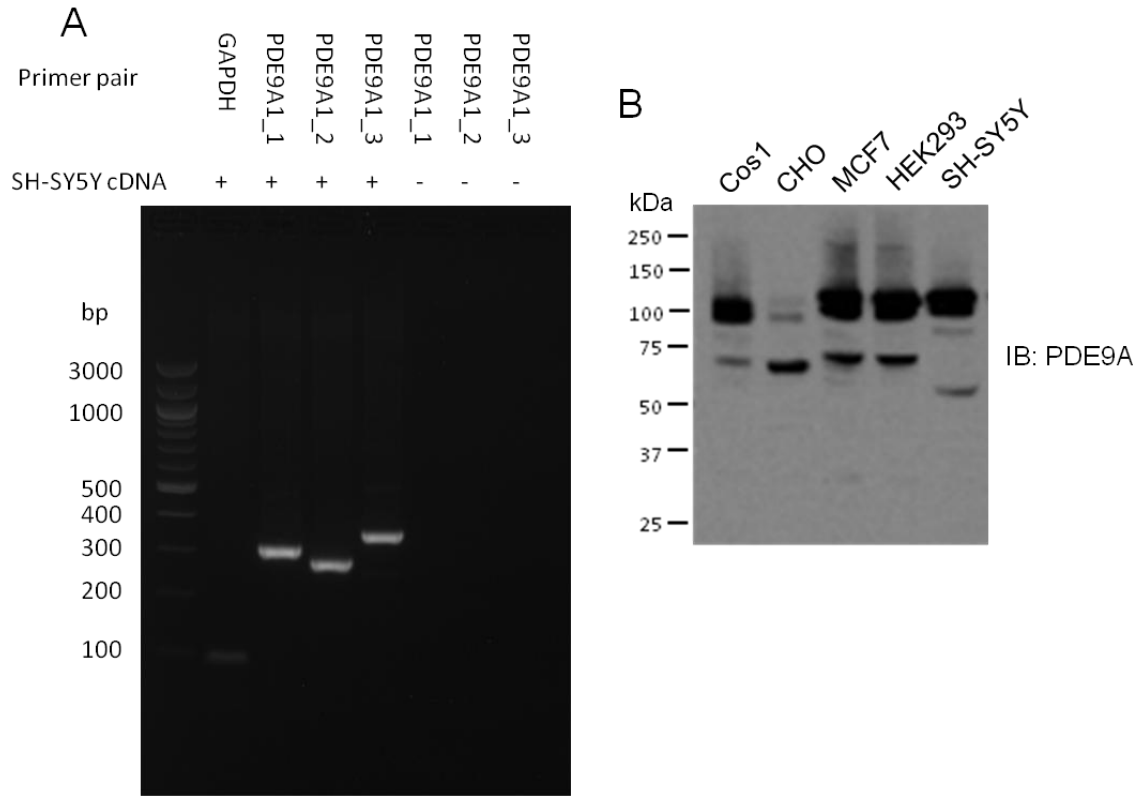

Figure 4.1 – PDE9 expression analysis.
A – RT-PCR of SH-SY5Y RNA using PDE9A1 intron-spanning RT-PCR primer pairs designed to three separate regions of the gene sequence (PDE9A1_1, PDE9A1_2, PDE9A1_3). No template control reactions lacking cDNA were included to ensure primer contamination had not occurred. The resultant PCR product was resolved on a 1.8%, 0.5x TBE agarose gel. Bands corresponding to the predicted molecular weight were obtained for each PCR reaction strongly suggesting that PDE9A1 mRNA is expressed in SH-SY5Y cells. B – Western blot analysis of a variety of different cell lines using a PDE9 selective anti-body (Scottish Biomedicals). Lysates were resolved on a 4-12% SDS-PAGE gel and several bands corresponding with various isoforms of PDE9A were detected.

Figure 4.1A was carried out by Dr. Jon Day

4.2.2 PDE9 inhibition promotes Hsp20 Phosphorylation

As Hsp20 becomes phosphorylated upon activation of PKG (Beall, Kato et al. 1997) I decided to characterise the effects of two different PDE9 inhibitors (provided by Lundbeck) on changes in endogenous phospho-Hsp20 levels in SH-SY5Y cells. Initially no biochemical information was provided for the two PDE9A inhibitors; named F13 and F14. Therefore they were initially tested at 25µM, a relatively high concentration for selective PDE inhibition. Utilising Western blotting techniques, I examined changes in phospho-Hsp20 levels over a 6 hour time-course (Fig. 4.2). Both inhibitors induced significant increases in phospho-Hsp20 levels relative to controls (t=0). Phosphorylation of Hsp20 peaked for both treatments after 1 hour, F13 treatment induced a significant 4-fold increase (± 0.5, *p-value* < 0.01) after 1 hour (Fig. 4.2 A) compared to a 9-fold increase (± 4, *p-value* < 0.05) following F14 addition (Fig. 4.2 B). Similarly, the PDE5 inhibitor

sildenafil (Fig. 4.2 D) induced significant increases in phospho-Hsp20, which peaked at 1 hour after addition. However, rolipram only produced a 2-fold increase (± 0.17) in Hsp20 phosphorylation relative to control, while sildenafil induced a 2.7-fold increase (± 0.64, *p-value* < 0.01).

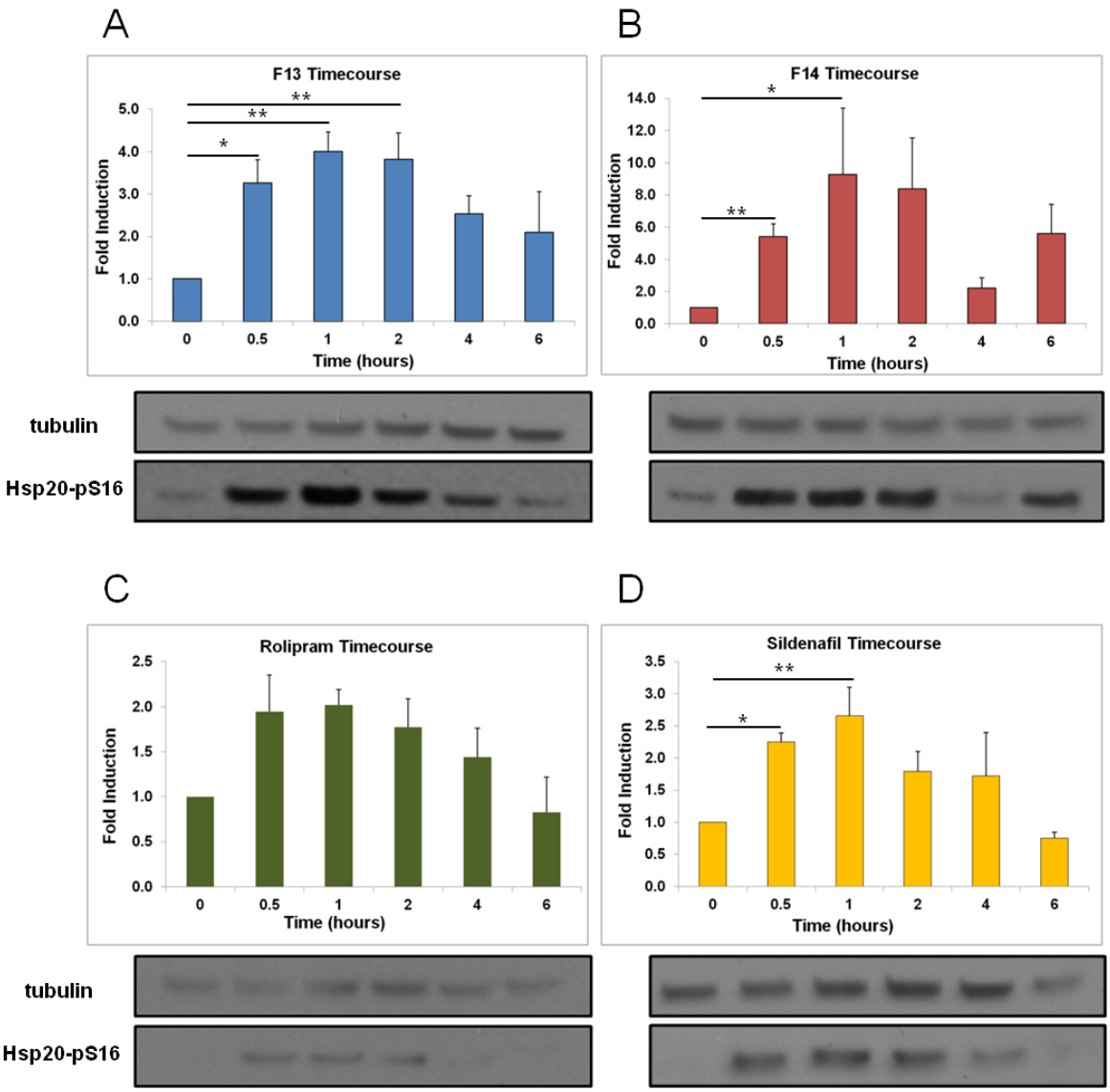

Figure 4.2 - PDE9, 4 & 5 inhibitors increase phospho-Hsp20 levels in a time-dependent manner.
SH-SY5Y cells were incubated with either PDE9 inhibitor F13 (A), F14 (B) at relatively high concentrations for selective PDE inhibition (25µM). SH-SY5Y Cells were also incubated with 10µM Rolipram (C) or 1µM of Sildenafil (D), which is approximately 10 times higher than published IC_{50} values for both inhibitors. All inhibitors were administered over a time course of 6 hours. Western blot analysis demonstrates that all compounds induce an increase in phospho-Hsp20 which peaked at the 1 hour time-point. This demonstrates that selective inhibition of PDE9 can induce pronounced and sustained phosphorylation of Hsp20 in neuronal-like SH-SY5Y cells. Mean values ±SEM, p-values - * < 0.05, ** < 0.01; repeated measures ANOVA, n = 3.

After establishing that PDE9 inhibition could lead to robust and long-lasting phosphorylation of Hsp20, I then examined if each inhibitor could induce Hsp20 phosphorylation in a dose-dependent manner. SH-SY5Y cells were treated with various concentrations of inhibitors and incubated for 15 minutes (Fig. 4.3). All of the inhibitors

tested, promoted dose-dependent increases in Hsp20 phosphorylation, with the 25µM-treated cells being statistically significant for PDE9 inhibitor F14 and PDE5 inhibitor sildenafil.

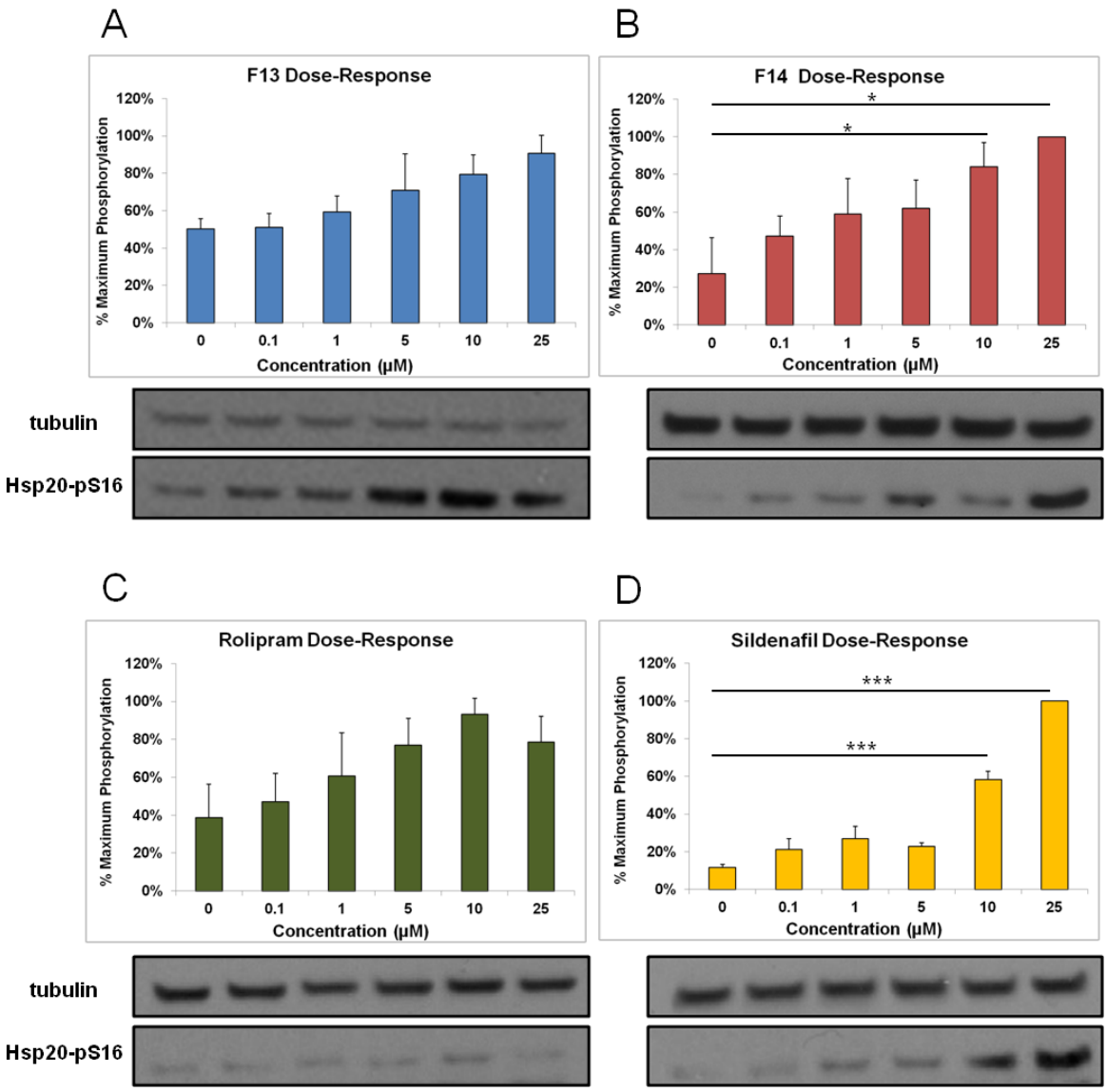

Figure 4.3 - PDE9, 4 & 5 inhibitors modulate phospho-Hsp20 levels dose-dependently. SH-SY5Y cells were incubated with various concentrations of PDE9 inhibitors F13 (A), F14 (B), PDE4 inhibitor rolipram (C) or PDE5 inhibitor sildenafil (D) for 15 minutes. Western blot analysis demonstrates that all compounds induce a dose-dependent increase in HSP20-pS16 levels relative to tubulin controls. Mean values ±SEM, p-values - * < 0.05, *** <0.001; ANOVA, n = 3.

4.2.3 PDE inhibition attenuates $A\beta_{1-42}$ induced cytotoxicity

In chapter 3, I utilised the xCELLigence system for label-free, real-time monitoring of Aβ-induced cytotoxicity. Using this platform, I demonstrated that increasing intracellular levels of Hsp20 could attenuate $A\beta_{1-42}$ mediated cell-death. This technique can also be used to screen compounds for potential neuroprotective properties that may be relevant for treating AD. As the cognitive enhancing properties of PDE4, 5 and 9 inhibitors have been

well characterised, I wanted to establish if PDE inhibition could also protect neuronal-like cells from acute Aβ cytotoxicity via PKA/PKG mediated phosphorylation of Hsp20.

First of all, I had to determine at which time-point the PDE inhibitors should be added to elicit the greatest level of protection against $A\beta_{1-42}$ toxicity. I initially treated cells with PDE9 inhibitors F13 and F14 or vehicle (DMSO) control, 2 hours after the addition of $A\beta_{1-42}$ or Aβscr, before any apparent onset of cell death (Fig. 4.4A & B). I saw no difference in Cell Index for either F13 or F14 treated wells relative to DMSO/$A\beta_{1-42}$ treated control when using this protocol. I also identified a possible problem with the F14 compound (Fig 4.4 B), which triggered a sharp decrease in Cell Index on initial addition. This may have been due to an error in the DMSO concentration of the stock solution which was above the 0.1% permissible in cell based assays. This problem was remedied in future experiments.

As it was possible that cell death responses had already been initiated at 2 hours post Aβ treatment, I carried out a 1 hour pre-treatment of PDE9 inhibition in order to increase intracellular levels of Hsp20 prior to addition of $A\beta_{1-42}$. However, as before I found no discernible differences between F13 or F14 treated cells and DMSO/$A\beta_{1-42}$ treated control (Fig. 4.4 C & D).

A

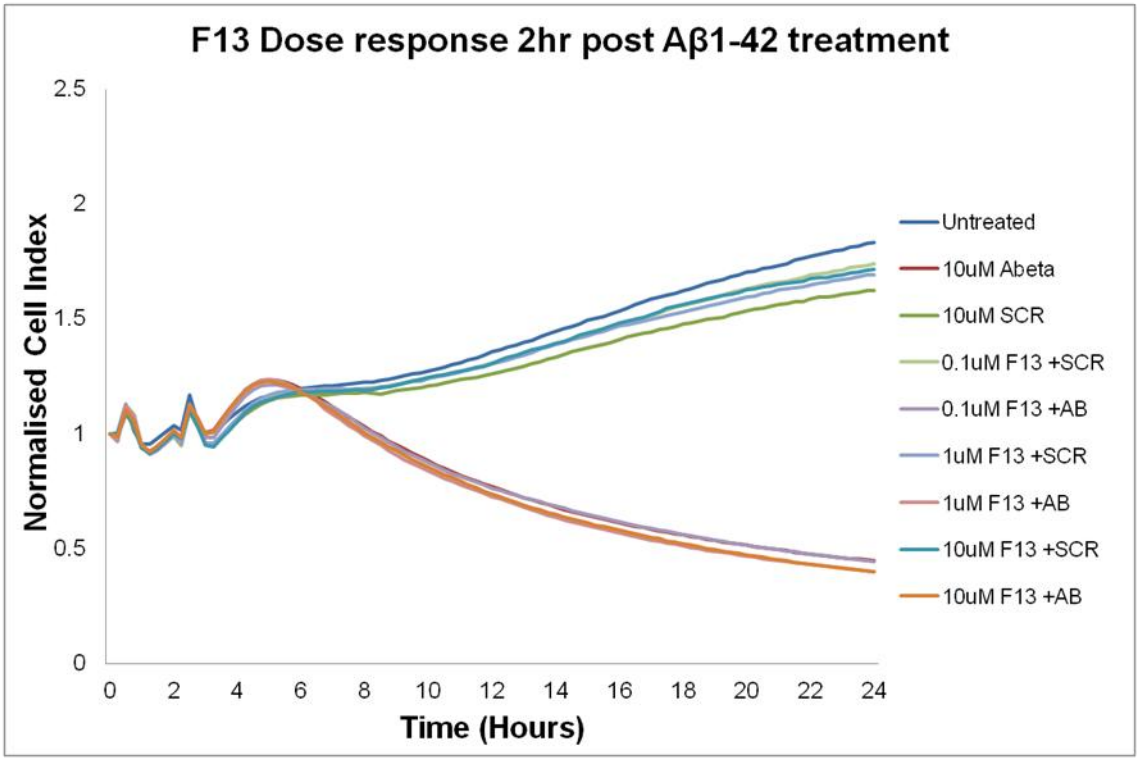
F13 Dose response 2hr post Aβ1-42 treatment
Normalised Cell Index
Time (Hours)
Untreated
10uM Abeta
10uM SCR
0.1uM F13 +SCR
0.1uM F13 +AB
1uM F13 +SCR
1uM F13 +AB
10uM F13 +SCR
10uM F13 +AB

B

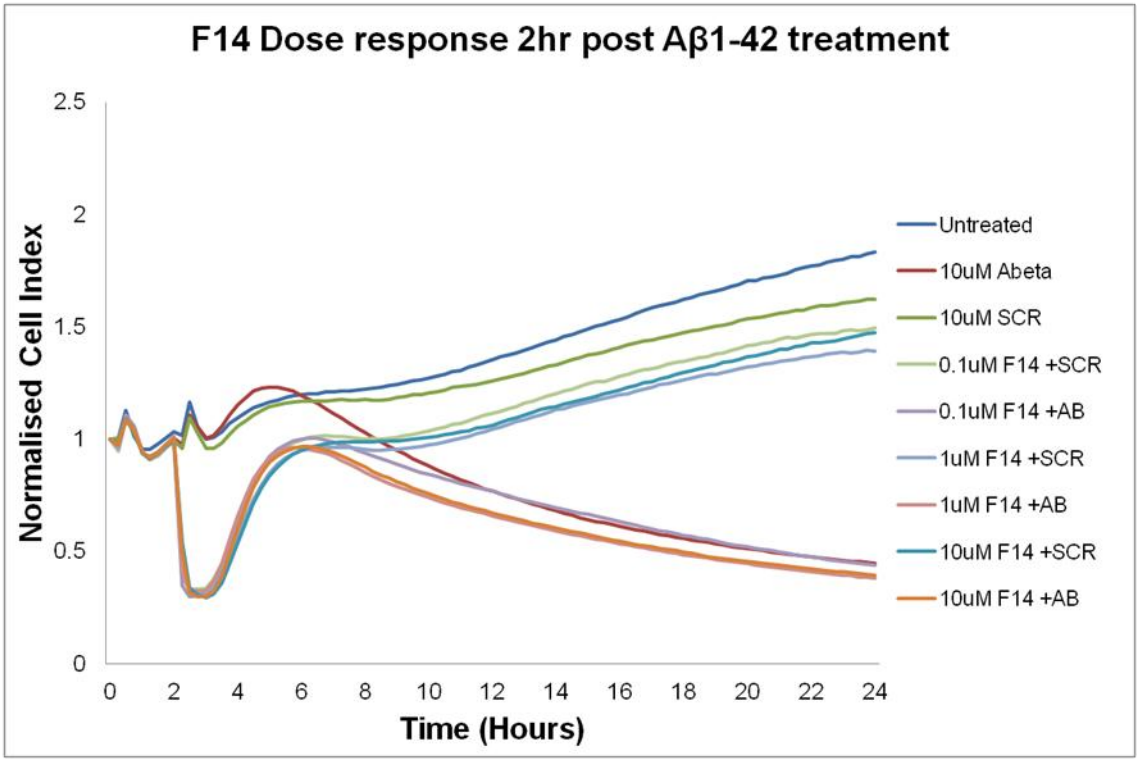
F14 Dose response 2hr post Aβ1-42 treatment
Normalised Cell Index
Time (Hours)
Untreated
10uM Abeta
10uM SCR
0.1uM F14 +SCR
0.1uM F14 +AB
1uM F14 +SCR
1uM F14 +AB
10uM F14 +SCR
10uM F14 +AB

C

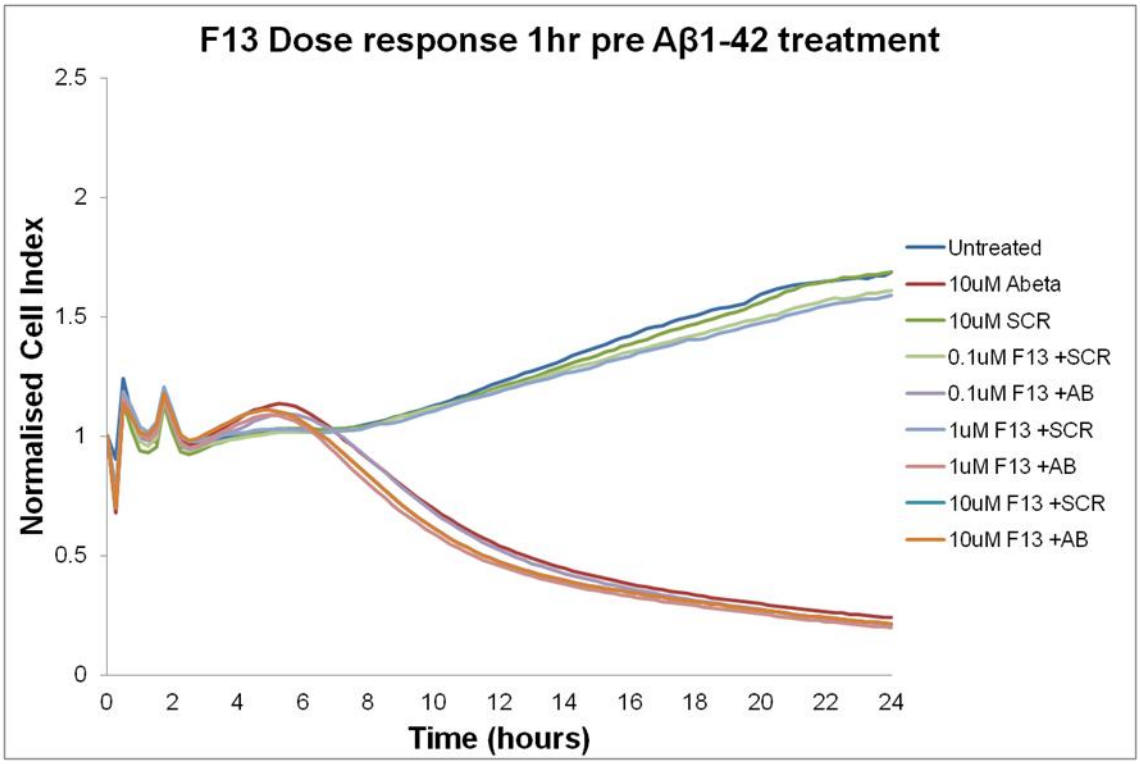
F13 Dose response 1hr pre Aβ1-42 treatment
Normalised Cell Index
Time (hours)
Untreated
10uM Abeta
10uM SCR
0.1uM F13 +SCR
0.1uM F13 +AB
1uM F13 +SCR
1uM F13 +AB
10uM F13 +SCR
10uM F13 +AB

D

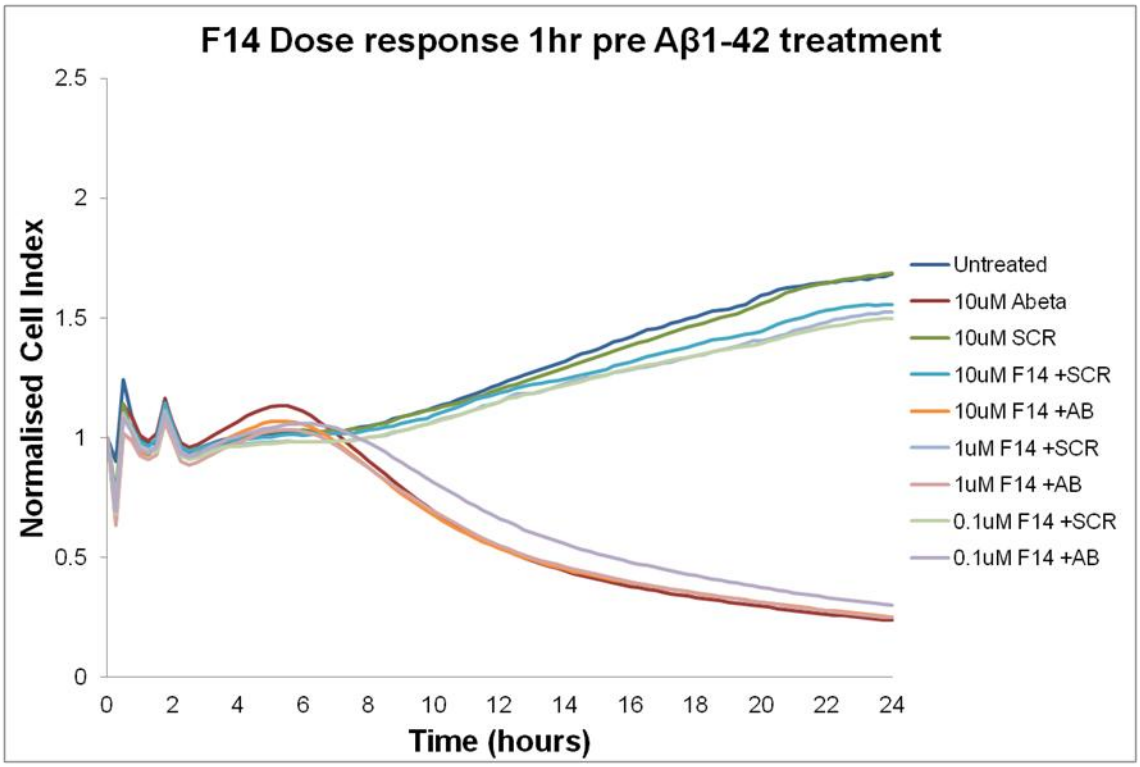
F14 Dose response 1hr pre Aβ1-42 treatment
Normalised Cell Index
Time (hours)
Untreated
10uM Abeta
10uM SCR
10uM F14 +SCR
10uM F14 +AB
1uM F14 +SCR
1uM F14 +AB
0.1uM F14 +SCR
0.1uM F14 +AB

E

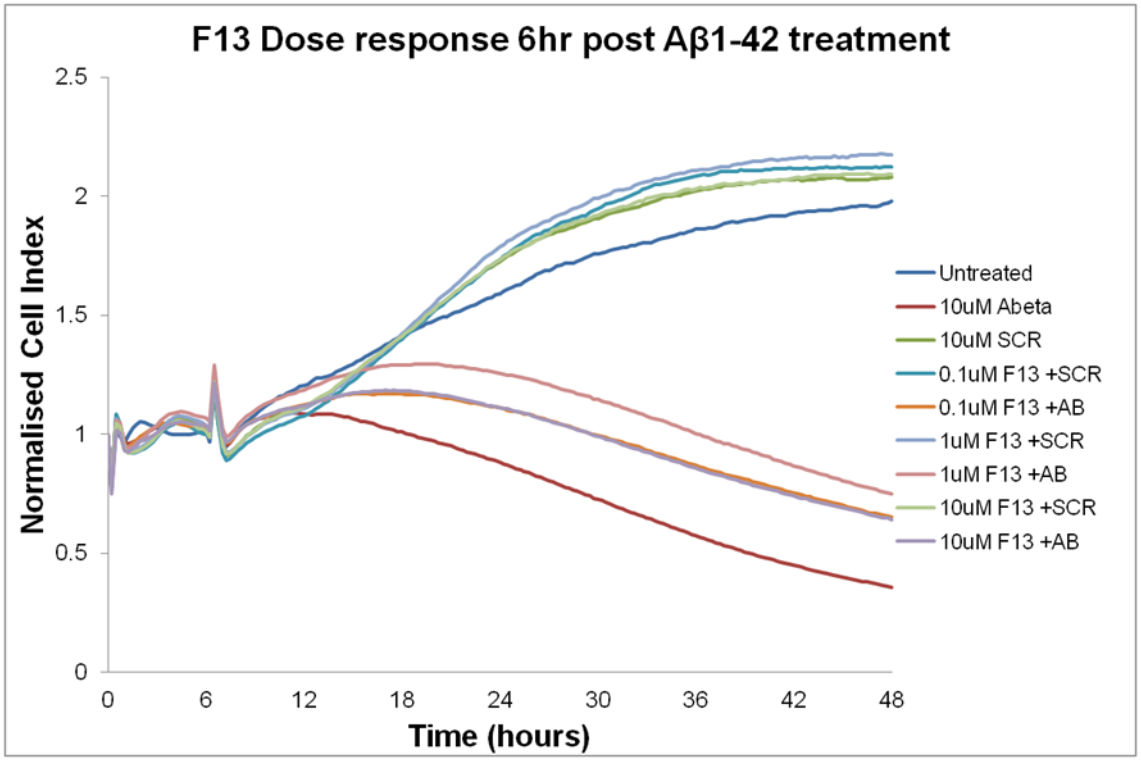
F13 Dose response 6hr post Aβ1-42 treatment
Normalised Cell Index
Time (hours)
0
0.5
1
1.5
2
2.5
0
6
12
18
24
30
36
42
48
Untreated
10uM Abeta
10uM SCR
0.1uM F13 +SCR
0.1uM F13 +AB
1uM F13 +SCR
1uM F13 +AB
10uM F13 +SCR
10uM F13 +AB

F

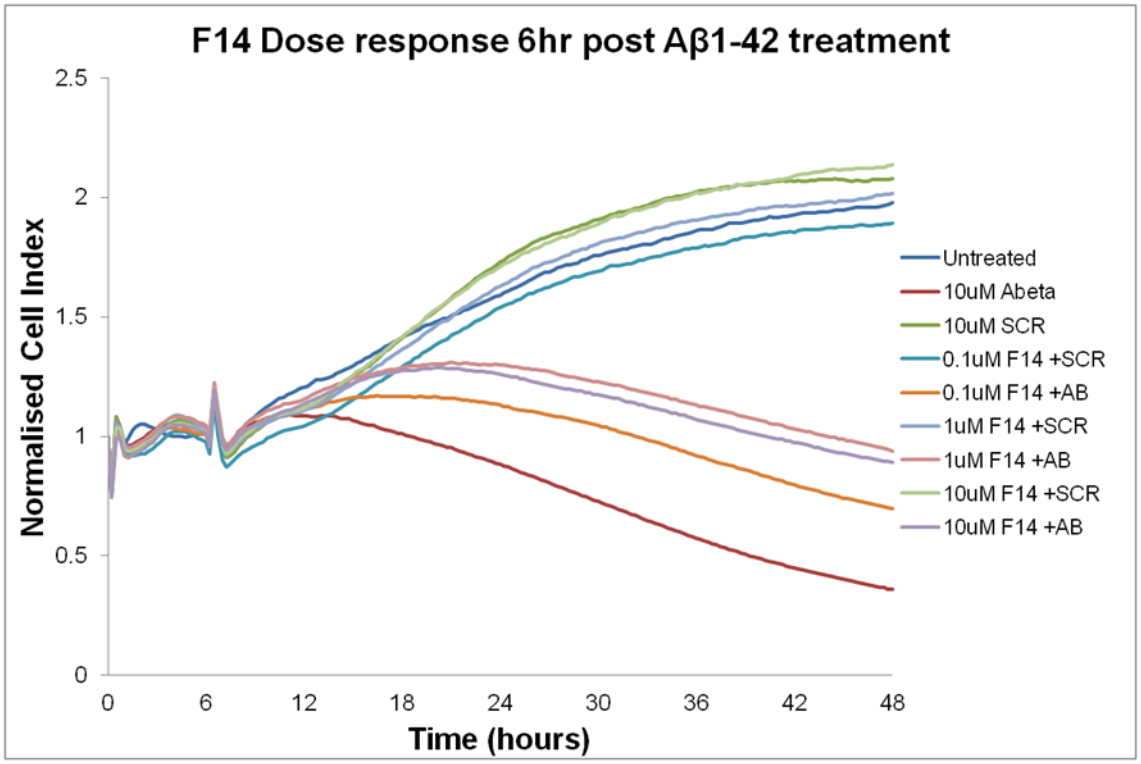
F14 Dose response 6hr post Aβ1-42 treatment
Normalised Cell Index
Time (hours)
0
0.5
1
1.5
2
2.5
0
6
12
18
24
30
36
42
48
Untreated
10uM Abeta
10uM SCR
0.1uM F14 +SCR
0.1uM F14 +AB
1uM F14 +SCR
1uM F14 +AB
10uM F14 +SCR
10uM F14 +AB

G

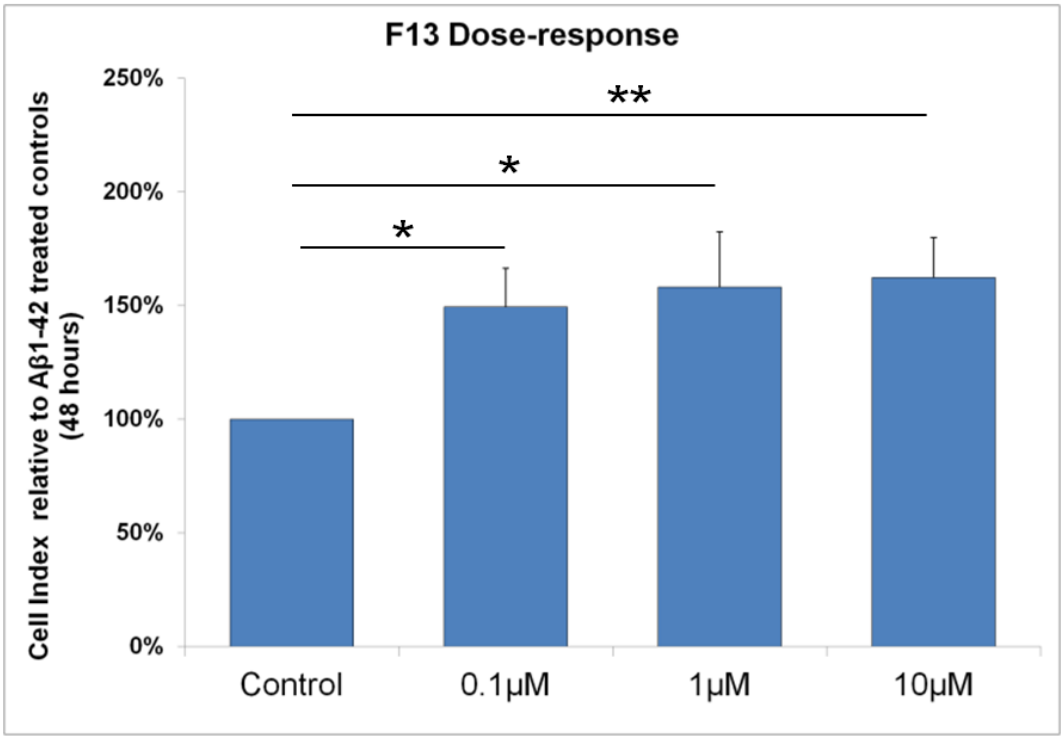

H

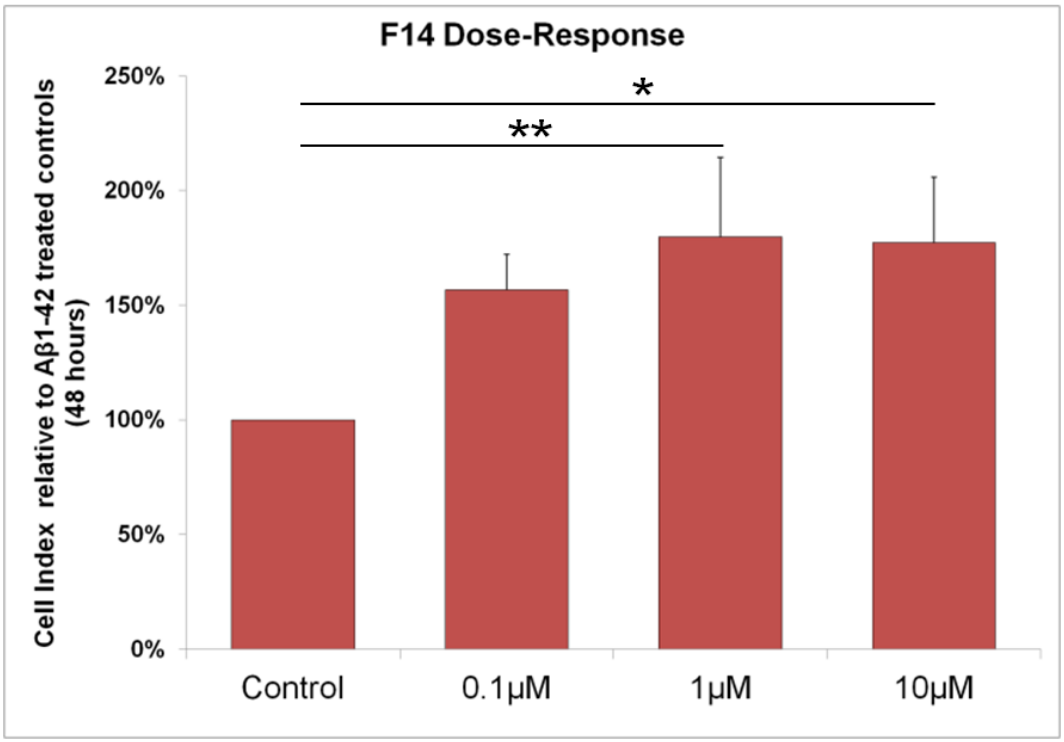

Figure 4.4 - PDE9 inhibition Pre & Post Aβ treatment.
SH-SY5Y cells were seeded into 96-well E-plate (ACEA) at a density of 5 x10^4 cells per well. Cells were left overnight to allow for adherence and for the Cell Index reached a value of at least 1. A & B – Cells were treated with 10μM Aβ1-42 or Aβscr for 2 hours prior to addition of F13, F14 or DMSO control. C & D – Cells were treated with F13, F14 or DMSO 1 hour prior to addition of 10μM Aβ1-42 or Aβscr. E & F - Cells were treated with 10μM Aβ1-42 or Aβscr for 6 hours prior to addition of F13, F14 or DMSO control. All treatments carried out in triplicate, n=1, average curves shown normalised to point of first treatment. G & H – Average cell index for each inhibitor concentration (Added 6 hours post Aβ1-42 treatment) at the 48 hour time-point normalised to Aβ1-42 treated controls. Mean values ±SEM, p-values - * < 0.05, ** < 0.01; ANOVA, n = 4.

It is noteworthy that throughout all of our $A\beta_{1-42}$ toxicity experiments, I have consistently observed an obvious divergence between the $A\beta_{1-42}$ and Aβscr growth curves after approximately 6 hours of incubation (Fig. 4.5 A. I have considered two possible explanations for this. Firstly, it is at this time-point that apoptotic pathways become fully established, leading to the significant morphological changes associated with programmed cell-death. Secondly, it is possible that it takes 6 hours for significant quantities of soluble $A\beta_{1-42}$ oligomers to accumulate intracellularly before the cytotoxic effects become apparent. Phospho-Hsp20 has well characterised anti-apoptotic functions in the heart (Fan, Zhou et al. 2008), and I have discovered that Hsp20 phosphorylation enhances its ability to interact with Aβ and attenuate its cytotoxic effects. Therefore I decided to add the PDE9 inhibitors at exactly this time point. Treatment with either F13 or F14, 6 hours post $A\beta_{1-42}$ addition induced a pronounced effect on the growth curves across all of the concentrations tested (Fig. 4.4 E & F). PDE inhibitors where then added at this time point for all subsequent assays.

After several repeats of this experiment, I found a slight dose-dependent effect against $A\beta_{1-42}$ induced cytotoxicity, particularly with regard to F13 (Fig. 4.4). However, both inhibitors promoted significant increases in Cell Index when normalised to DMSO/$A\beta_{1-42}$ treated controls (Fig.4.4G & H). Even at 0.1μM F13 increased normalised Cell Index by 149% (± 17%). The maximum increase for F13 treated cells was 162% (± 17%) at 10μM, whereas the maximum effect of F14 was 180% (± 35%) at 1μM.

When I compared the average curves of the PDE9 inhibitors for the 1μM concentration I found that F14 produced the most pronounced protective effect against $A\beta_{1-42}$ induced cytotoxicity (Fig. 4.5A). The reduction in slope for $A\beta_{1-42}$ control treated cells was also steeper, resulting in time-dependent increase in the relative protective effects of F13 and F14 (Fig. 4.5B). After 12 hours of $A\beta_{1-42}$ incubation (6 hours post inhibitor/DMSO addition) the significant effects of PDE9 inhibition became apparent until it reached a maximum of 158% (± 24%) for F13 and 180% (± 35%) for F14, after 48 hours.

A

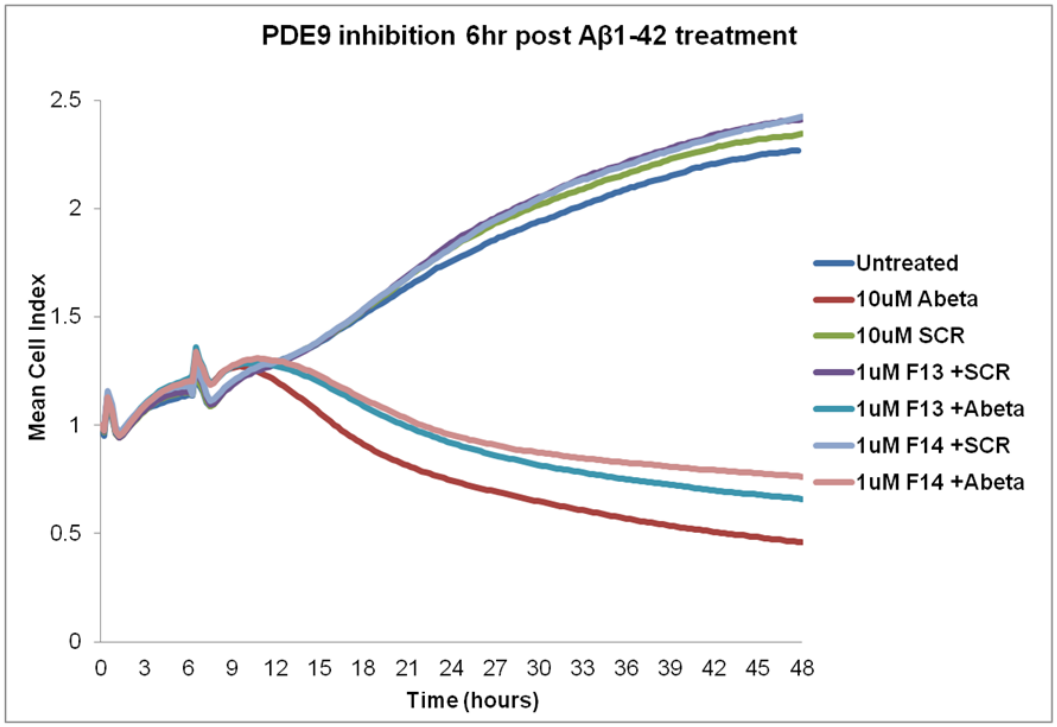

B

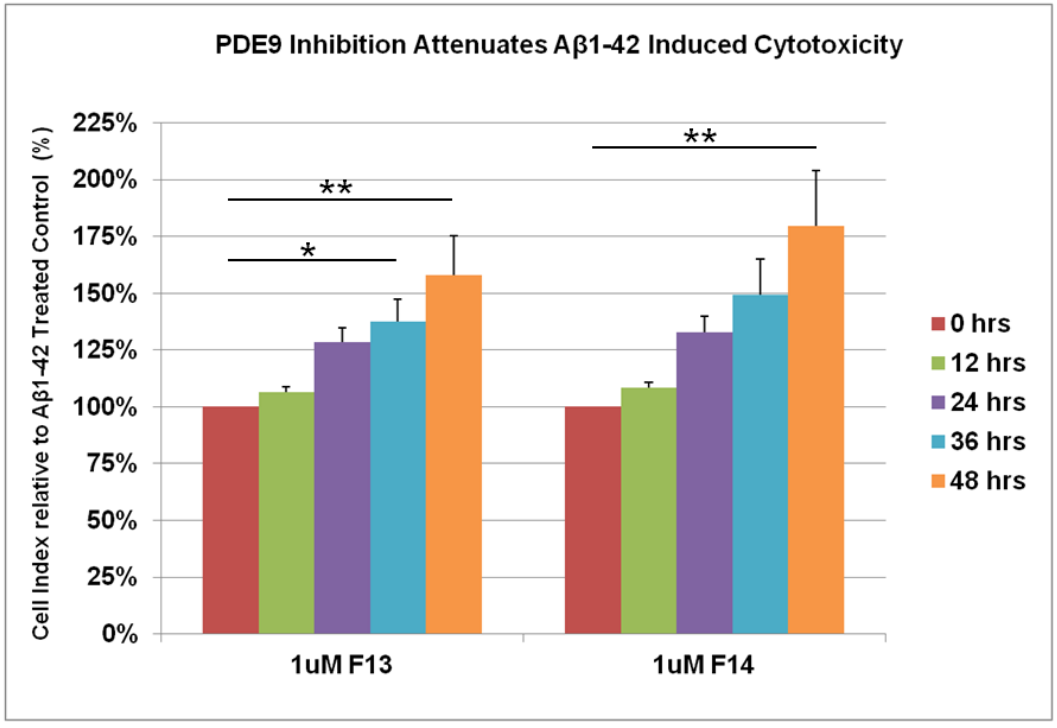

Figure 4.5 - PDE9 inhibition attenuates $A\beta_{1-42}$ induced cytotoxicity.
SH-SY5Y cells treated with 10μM $A\beta_{1-42}$ or $A\beta_{scr}$ control. After 6 hours cells were further treated with either 1μM F13 or F14. A - Average growth curves of treated cells. $A\beta_{scr}$ peptide has no significant effect on cell growth when compared to untreated controls. $A\beta_{1-42}$ induces significant reduction in Cell Index which can be attenuated by both F13 and F14. B - Cell Index at given time-points relative to cells treated with 10μM $A\beta_{1-42}$. Mean values ±SEM, *p-values* - * < 0.05, ** < 0.01; ANOVA, n = 4.

The PDE4 inhibitor rolipram and PDE5 inhibitor sildenafil were tested at approximately 10-fold higher concentration than their reported IC_{50} values (10μM for rolipram, and 1μM

for sildenafil). The effect on attenuation of $A\beta_{1-42}$ cytotoxicity was less pronounced than PDE9 inhibition (Fig. 4.6A). However, the increase in Cell Index relative to $A\beta_{1-42}$ control was significant at the 36 hour and 48 hour time-point for both inhibitors (Fig 4.6B). The normalised cell index value for rolipram treated cells highlighted maximum increase of 145% (± 18%) at the 48 hour time-point. Values for sildenafil were similar, with a maximum increase of 144% (± 24%) at 48 hours (Fig. 4.6B).

Given that all the PDE inhibitors significantly protected neuronal-like SH-SY5Y cells against $A\beta_{1-42}$ induced cell death, it was important for us to establish if this protective mechanism was mediated directly through Hsp20. Unfortunately attempts at using RNAi to knock-down Hsp20 were unsuccessful. Several attempts were made using siRNA targeting the Hsp20 gene (HSPB6) and various transfection reagents were tried. However, I was unable to reduce Hsp20 expression levels. Failure of the siRNA could be a result of the fact that Hsp20 exists in large pools of high molecular weight SDS-stable multimers in SH-SY5Y cells (Appendix 1B). A previous study looking at the effects of Hsp20 in rat cardiomyocytes managed to reduce Hsp20 levels by around 40% but this required an adenovirus containing anti-sense Hsp20 cDNA (Wang, Zingarelli et al. 2009). Interestingly, that study found that Hsp20 could inhibit NF-κB activity and reduce cytokine production. NF-κB is also activated by Aβ, promoting neuroinflammatory responses that play an important role in the progression of AD. Rolipram has recently been shown to reverse Aβ mediated increases in NF-κB expression in the rat hippocampus (Wang, Yang et al. 2012). Regrettably, due to time constraints, I was unable to pursue viral based vectors as a means stably to knock-down Hsp20.

A

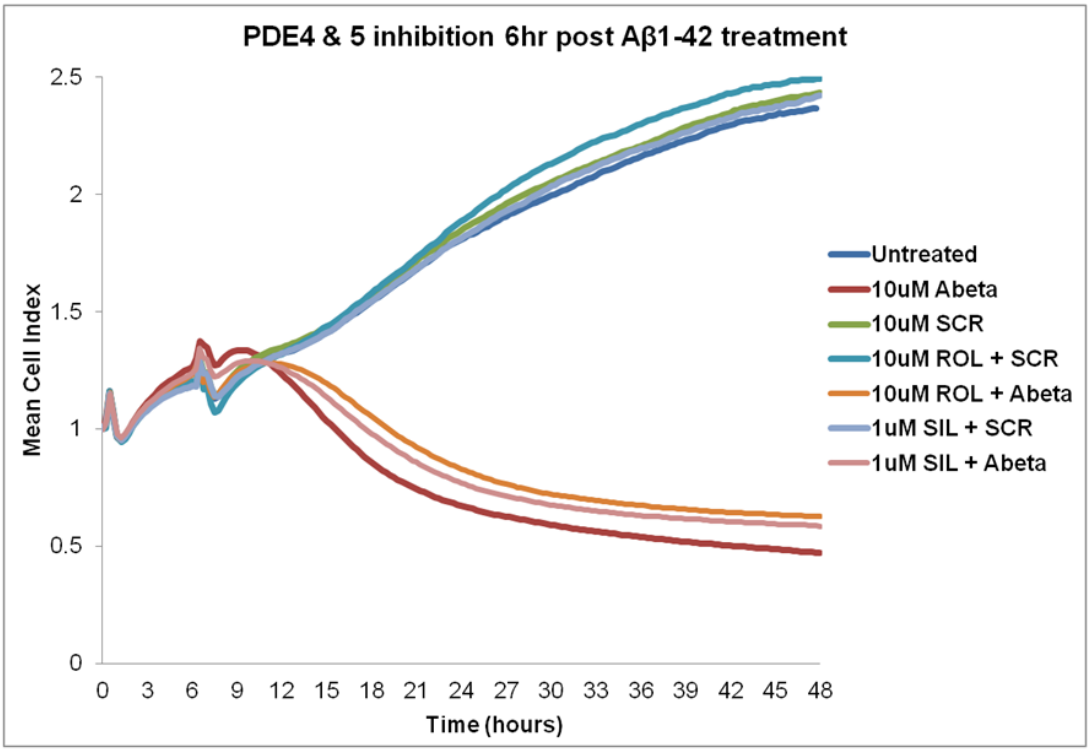

B

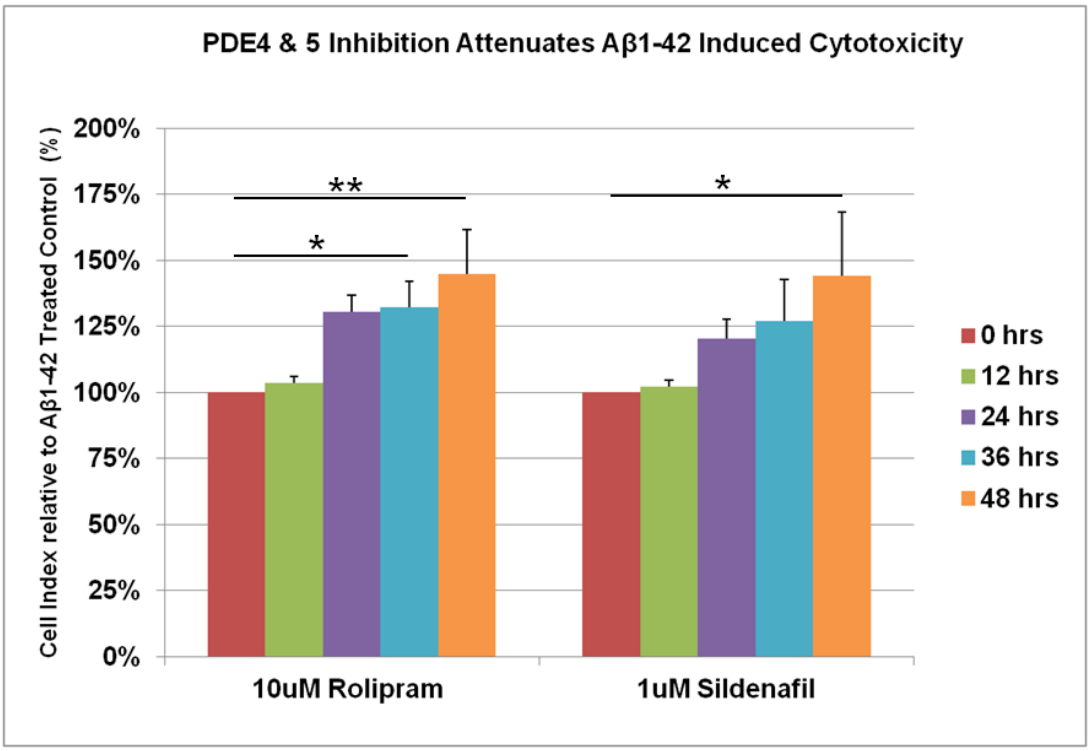

Figure 4.6 – PDE4 & PDE5 inhibition attenuates $A\beta_{1-42}$ induced cytotoxicity.
SH-SY5Y cells treated with 10μM $A\beta_{1-42}$ or $A\beta_{scr}$ control. After 6 hours cells were further treated with either 10μM rolipram or 1μM sildenafil. A - Average growth curves of treated cells. $A\beta_{scr}$ peptide had no significant effect on cell growth when compared to untreated controls. $A\beta_{1-42}$ induces significant reduction in Cell Index which can be attenuated by both rolipram and sildenafil. B - Cell Index at given time-points relative to cells treated with only 10μM $A\beta_{1-42}$. Mean values ±SEM, *p-values* - * < 0.05, ** <0.01; ANOVA, n = 3.

4.3 Discussion

The Aβ peptide is widely accepted as a major toxic agent in the pathogenesis of AD. Through the evaluation of cell death and synaptic plasticity, researchers have identified several oligomeric intermediates (both brain-derived and synthetic) as being neurotoxic. However, although much research effort has been expended in this area, the exact nature of toxic Aβ species has yet to be defined. In this regard recent research has pointed to the fact that toxic Aβ oligomers are more relevant in early stages of AD (Gilbert 2013). Preventing the formation of toxic Aβ oligomers has, therefore, been proposed as an effective means of treating AD. For example, biologics, which can bind to and stabilise the Aβ monomer should prevent oligomerisation and allow for increased clearance through endogenous processes (Walsh and Selkoe 2007).

I have previously described (Chapter 3) an endogenous neuroprotective mechanism where the small heat shock protein Hsp20 can bind to and stabilise monomeric Aβ and prevent it from aggregating. Furthermore, the interaction between Hsp20 and Aβ can be enhanced through phosphorylation of a consensus PKA/PKG site leading to protection against Aβ induced cytotoxicity. Cyclic nucleotide-dependent second messenger signalling pathways also regulate cognitive functions (Halene and Siegel 2007), therefore targeting Hsp20 phosphorylation through mechanisms such as PDE inhibition may have neuroprotective effects that are distinct from the cognitive enhancing effects associated with PDE inhibition (Bales, Plath et al. 2010).

4.3.1 PDE9 inhibition promotes Hsp20 Phosphorylation

The phosphorylation of Hsp20 at serine 16 has been implicated in a number of physiological and pathophysiological processes such as smooth muscle relaxation, platelet aggregation, myocardial infarction and atherosclerosis (Fan and Kranias 2011). In the heart, Hsp20 has well established cardio-protective functions that are modulated via phosphorylation. The beneficial effects of Hsp20 in the heart can be enhanced using the phospho-mimetic S16D mutation, while the non-phosphorylatable mutant S16A confers no protection (Fan, Chu et al. 2004). Furthermore, hearts from Hsp20 transgenic mice display improved functional recovery and decreased cell-death following ischemia/reperfusion injury through a direct interaction with the pro-apoptotic protein Bax. Hsp20 phosphorylation also promotes cardioprotection via a range of diverse processes that include modulation of contractility to prevention of apoptosis (Fan and Kranias 2011).

The role of Hsp20 and its phosphorylation in the brain is only beginning to emerge, but protective effects against cellular stress are likely to be conserved in this tissue given that Hsp20 is readily expressed throughout the mammalian brain (Verschuure, Tatard et al. 2003; Kirbach and Golenhofen 2011). In a study looking at hypoxic stress in newborn mammals, Hsp20 was shown to be rapidly induced in the hippocampus of piglets, well before hypoxia-inducible factor HIF1α. It was proposed that the rapid induction of Hsp20 would afford the hippocampus the benefits of vascular relaxation and reduce the local severity of hypoxic stress in a brain region essential for the establishment of cognitive functions in young mammals (David, Boelens et al. 2006). Another study found that treatment with transducible phospho-mimetic peptide analogues of Hsp20 could effectively inhibit cerebral perfusion in a rat model of subarachnoid haemorrhage (Furnish, Brophy et al. 2010). More recently, Hsp20 phosphorylation has been shown to protect against in vitro ischemia/reperfusion injury of mouse neuroblastoma cells and could potentially be targeted therapeutically to treat ischemic stroke (Zeng, Tan et al. 2010; Zeng, Tan et al. 2013).

The human neuroblastoma cell line SH-SY5Y, is a well established cell model for a number of neurological diseases due to its neuronal-like properties (Agholme, Lindstrom et al. 2010)). It readily expresses Hsp20, making it is an ideal model for testing potential neuroprotective agents that can promote Hsp20 phosphorylation. The PDE4 inhibitor rolipram and the PDE5 inhibitor sildenafil have previously been shown to promote the phosphorylation of Hsp20 in different tissue (Tessier, Komalavilas et al. 2004; Sin, Edwards et al. 2011). I have shown here, that both of these inhibitors promote sustained and dose-dependent increases in phosphorylation of Hsp20 in SH-SY5Y cells, confirming that Hsp20 can be modulated by both PKA and PKG mediated phosphorylation in neuronal-like cells. After confirming that PDE9 is expressed in SH-SY5Y cells (Fig. 4.1) I found that PDE9 inhibitors F13 and F14 can also promote significant induction of Hsp20 phosphorylation (Fig. 4.2). However, in the initial time course experiments, I used high concentrations of inhibitor, 25μM. Typically selective PDE inhibitors have IC_{50} values in the nanomolar range (Bender and Beavo 2006). PDE9 is a key regulator of cGMP levels in cells and has the highest affinity for cGMP out of all the known cGMP-specific PDEs. As such, it is thought to regulate basal levels of cGMP (Fisher, Smith et al. 1998), (Soderling, Bayuga et al. 1998). With this in mind, I hypothesised that PDE9 inhibition should have a more pronounced effect on intracellular cGMP levels than PDE5 inhibition. Indeed, I observed a more robust and sustained phosphorylation of Hsp20 following treatment with PDE9 inhibitors. I also found that all the PDE inhibitors tested produced an acute (15 minutes) and dose-dependent increase in Hsp20 phosphorylation without the need for

agents that increase cyclic nucleotide levels (Fig 4.3). This was expected for rolipram as Hsp20 interacts directly with the catalytic domain of PDE4 (Sin, Edwards et al. 2011) and A-kinase-anchoring protein, AKAP-Lbc (Edwards, Scott et al. 2012), meaning that an increase in global cAMP concentration is not required for rolipram to induce Hsp20 phosphorylation. Whether Hsp20 interacts directly with the catalytic domains of PDE5 or PDE9 has yet to be investigated. However, the concentrations that induced significant levels of Hsp20 phosphorylation relative to controls were again relatively high for selective PDE inhibition. Nonetheless, PDE9 inhibition promoted significant and long lasting Hsp20 phosphorylation which would suggest that PDE9 inhibitors F13 and F14 could be used to promote the neuroprotective effects of Hsp20 and may also have therapeutic relevance for treating diseases other than AD, such as ischemic stroke.

4.3.2 PDE inhibition attenuates $A\beta_{1-42}$ induced cytotoxicity

PDE4, 5 and 9 inhibitors have well established cognitive enhancing effects, as previously discussed, however the neuroprotective properties of these PDE inhibitors are less well known. The PDE4 inhibitor rolipram has been shown to protect primary cortical neurons against several distinct cell models of injury including hypoxia and glutamate induced neurotoxicity (Chen, Williams et al. 2007). Rolipram can also promote axonal regeneration following spinal cord injury (Nikulina, Tidwell et al. 2004). However, the ability of rolipram to promote neuroprotection following CNS trauma to the spinal cord or the brain can also be attributed to cAMP-dependent regulation of inflammatory processes, which are also key mediators of neurodegenerative disorders (Schaal, Garg et al. 2012). The PDE5 inhibitor sildenafil has been shown to promote neurogenesis and reduce neurological deficits in a rodent model of stroke (Zhang, Wang et al. 2002). Sildenafil can also promote neuroprotection in pelvic ganglia neurones, which can be damaged following surgery for prostate, bladder and colorectal cancers (Hlaing, Garcia et al. 2012). The neuroprotective role of PDE9 inhibition is only now being investigated but is expected have strong neuroprotective functions given the importance of the NO/cGMP/PKG pathway plays in neuroprotection (Calabrese, Mancuso et al. 2007).

I have shown for the first time, the neuroprotective effects of PDE4, 5 & 9 inhibition in our cell model of Aβ toxicity. PDE inhibition which has been associated with improving cognition in rodent models of AD can also significantly protect neuronal-like SH-SY5Y cells against the cytotoxic effects of $A\beta_{1-42}$. The PDE9 inhibitor F14 was the most effective at increasing cell index relative to $A\beta_{1-42}$ treated control cells. Interestingly F13, which was

less effective at inducing Hsp20 phosphorylation, was also less effective at attenuating the cytotoxic effects of $A\beta_{1-42}$ relative to F14. In this experimental setup, selection of the most apt time of compound addition was essential for inducing the neuroprotective effect of PDE inhibition. I only evoked cytoprotective effects when I added inhibitors 6 hours post $A\beta_{1-42}$ addition, as this was the time point where the $A\beta_{1-42}$ treated growth curves begin to diverge from controls. This could be due to phospho-Hsp20 neutralising $A\beta_{1-42}$ at the point where it has accumulated intracellularly to levels that become toxic to cells. $A\beta_{1-42}$ is readily taken up by SH-SY5Y cells leading to the accumulation of high molecular weight aggregates capable of seeding amyloid fibril growth (Hu, Crick et al. 2009). An alternative hypothesis is that increasing intracellular levels of phospho-Hsp20 inhibits apoptosis at the point of initiation of the morphological changes associated with programmed cell death. Unfortunately, without RNAi data ascribing the protective effects to Hsp20, any one of the vast array of PKA and PKG substrates that are phosphorylated following increases in intracellular cyclic nucleotide concentration could be involved in this process. A positive identification of Hsp20 as the causative factor of the attenuation of $A\beta_{1-42}$ mediated cytotoxicity could not be made.

Interestingly, despite rolipram and sildenafil having very similar protective effects against $A\beta_{1-42}$ mediated cytotoxicity, they both differ in their ability to reduce Aβ levels *in vivo*. Rolipram did not affect Aβ plaque load in the hippocampus of APP/PS1 mice (Gong, Vitolo et al. 2004), however, sildenafil treatment reduced Aβ levels which persisted several months after treatment finished (Puzzo, Vitolo et al. 2005). A recent study has confirmed that sildenafil treatment can reduce both $A\beta_{1-40}$ and $A\beta_{1-42}$ levels in APP/PS1 mice (Zhang, Guo et al. 2013). Confirmation of rolipram's inability to reduce Aβ levels is necessary as this suggests distinct mechanisms of action. Also, whether PDE9 inhibition would have a similar effect in reducing Aβ levels as PDE5 inhibition has not yet been reported but it would be beneficial to compare the efficacy of PDE9 inhibitors *in vivo* under the same experimental conditions as sildenafil.

The inability to effectively silence Hsp20 using RNAi prevented us from proving conclusively that the cytoprotective effects of PDE4, 5 or 9 inhibition are mediated through Hsp20. Hsp20 can exist within SH-SY5Y cells in large SDS-stable high molecular weight complexes (Appendix 1B). I have also previously carried out MG132 and cyclohexamide treatments of SH-SY5Y cells and found the level of monomeric Hsp20 within cells is highly stable (Appendix 2 & 3). It is likely that the quantities of the Hsp20 protein exists in these stable high molecular complexes is in excess and masking changes Hsp20 expression

levels with silencing or blocking of Hsp20 gene expression (HSPB6) having no apparent affect on monomeric levels.

PDE4, 5 & 9 inhibition has been proposed as a novel means for treating AD due to cognitive enhancing effects and the ability to reduce Aβ levels *in vivo*. I have demonstrated for the first time that these PDE inhibitors also protect neuronal-like SH-SY5Y cells against the acute cytotoxic effects associated with $A\beta_{1-42}$ treatment. I believe that one of the mechanisms for protecting cells against the toxicity associated with $A\beta_{1-42}$ is mediated through the activation of Hsp20 which has well established anti-apoptotic effects in other tissue. More recently I have established that Hsp20 phosphorylation also enhances its interaction with Aβ peptides in order to help maintain Aβ in a non-toxic monomeric conformation and prevents from aggregating into higher order toxic Aβ species. This makes Hsp20 a multi-faceted protein that can protect against two of the most important aspects of the 'amyloid hypothesis', namely Aβ associated neurotoxicity and subsequent neuronal cell death.

5 The Development of Novel PDE4 Inhibitors to Induce Hsp20 Phosphorylation

5.1 Introduction

The escalating costs and diminishing returns of drug development have fuelled a growing focus on drug repositioning in recent years (Ashburn and Thor 2004). As annual approvals of new molecular entities (NMEs) dwindle in the face of increasing economic and regulatory pressures (Paul, Mytelka et al. 2010), greater emphasis is being placed on the development of systematic approaches for identification of compounds with repositioning potential, including the application of *in silico* structure-based and chemoinformatic methodologies (Vasudevan, Moore et al.; Hert, Keiser et al. 2008; Keiser, Setola et al. 2009; Vasudevan, Moore et al. 2012). We have used such approaches to find novel inhibitors of the important cAMP hydrolyzing phosphodiesterase 4 (PDE4) enzyme family, which has been implicated in the pathophysiology underlying a range of diseases and conditions including cancer, rheumatoid arthritis, depression, schizophrenia, stroke and Alzheimer's disease (AD) (Houslay, Schafer et al. 2005).

PDE4 is one of eleven known phosphodiesterase families and plays a pivotal role in mediating hydrolytic degradation of the important cyclic nucleotide second messenger, cyclic AMP (cAMP) (Lugnier 2006). The PDE4 family acts to regulate downstream signalling events induced by cAMP, and does so *via* the action of approximately 25 different isoforms that manifest as multiple splice variants encoded by four distinct genes (*PDE4A*, *B*, *C* and *D*) (Conti and Beavo 2007). The fact that all PDE4 enzymes have been highly conserved through evolution suggests that they have non-redundant functional roles in regulating cAMP homeostasis linked to the compartmentalisation of cAMP signalling (Baillie 2009). As all PDE4 isoforms have similar K_m and V_{max} parameters for cAMP hydrolysis, their functional roles are determined largely by their cellular location and post-translational modification. Discrete intracellular targeting of individual PDE4 isoforms is most often directed by a "postcode" sequence within their unique N-terminal domains (Houslay, Baillie et al. 2007), which are responsible for promoting many of the protein-protein and (in one case) protein-lipid interactions that act to anchor PDE4s to signalling nodes in sub-cellular compartments (Houslay 2009).

It is well established that inhibitors, which target the catalytic pocket of PDE4s, show promise for the treatment of chronic obstructive pulmonary disease (COPD), asthma,

rheumatoid arthritis, inflammatory bowel disease and psoriasis (Houslay, Schafer et al. 2005; Page and Spina 2012). PDE4 inhibitors have also been shown to be effective in enhancing memory function and reversing the effects of Aβ-associated cognitive impairments in rodent models of AD (Barad, Bourtchouladze et al. 1998; Vitolo, Sant'Angelo et al. 2002; Gong, Vitolo et al. 2004; Costa, Cracchiolo et al. 2007) (Cheng, Wang et al. 2010; Wang, Yang et al. 2012). Thus, in principle, PDE4 inhibitors have considerable therapeutic potential. In practice, however, their clinical utility has been compromised by mechanism-associated side effects that limit maximally tolerated doses (Zhang, Ibrahim et al. 2005). Headache, nausea, emesis and diarrhoea are the most commonly reported side effects and these stem from the inhibition of PDE4 activity in non-target tissues. In particular, PDE4D expression is high in a region of the brain, the area postrema, where inhibitor action may trigger nausea (Zhang, Ibrahim et al. 2005). Despite the challenges to therapeutic deployment of PDE4 inhibitors, one such compound, roflumilast, has recently been approved by the European Commission and US Food and Drug Administration (FDA) for the treatment of severe COPD (Fabbri, Beghe et al. 2010), albeit that concern remains over side-effects such as diarrhoea, pancreatitis and weight loss associated with its administration (Gupta 2012).

With this in mind, one strategy to develop a novel, safer class of PDE4 inhibitor would be to survey existing approved drugs for PDE4-inhibitory activity. In collaboration with Shoichet Laboratory, University of California, who carried out a high-throughput computational approach to identify several FDA approved drugs with potential PDE4 inhibitory activity. Each drug was compared to the sets of ligands for each PDE4 subtype according to ChEMBL (Gaulton, Bellis et al. 2011) with the Similarity Ensemble Approach (SEA) (Keiser, Roth et al. 2007; Keiser, Setola et al. 2009).

The similarity ensemble approach (SEA) is one of a number of in silico methods now used to identify off-target activity of drugs. The technique measures the topological similarity between bait molecules and a set of ligands annotated to any given target in a library of target-ligand sets. The observed similarities between the bait molecule(s) and the ligand-sets are compared to what would be expected at random, and the expectation value of seeing the level of similarity observed is calculated (Hert, Keiser et al. 2008; Keiser, Setola et al. 2009). Because SEA compares molecules to annotated ligands as sets, collective similarity can be established even when the pair-wise similarity to any single ligand in the set may be modest. It has been applied successfully to predict activity of established drugs against previously unreported targets (Hert, Keiser et al. 2008; DeGraw, Keiser et al. 2010)

and also used to predict biological activity in natural products (Sa, de Menezes et al. 2011). Here SEA was applied to probe the MDL Drug Data Report (MDDR), a database currently comprising >180,000 biologically relevant compounds, with a focus on drugs that have been approved or under current development. In doing so, we identified several candidate PDE4 inhibitors, using ChEMBL to compare against known sets of PDE4 active compounds (Gaulton, Bellis et al. 2011).

5.1.1 Experimental Aims

Our strategy was to use a chemical informatics *in silico* approach to identify potential PDE4A,B,C and D inhibitors by SEA. Several "hits" were validated for inhibition of phosphodiesterase activity using PDE assays. Compounds with bona fide PDE4-inhibitory activity were then tested in several cell based assays to determine if they could induce increases in intracellular cAMP levels, thereby making them potential therapeutic agents.

5.1.2 Experimental Procedure

1 - *In silico* screening hits were validated using a two-step radio-assay to measure PDE activity (Marchmont and Houslay 1980). This allowed the determination of inhibitory activity against several PDE4 isozymes, the type of inhibition (competitive vs. allosteric), and also selectivity over other PDE isoforms (PDE5A & PDE8A).

2 – Temporal changes in intracellular cAMP concentration were evaluated using the genetically encoded fluorescence resonance energy transfer (FRET)-based sensor based around the cAMP binding domain of Epac1 (Epac1-camps) (Nikolaev, Bunemann et al. 2004). Potential PDE4 inhibitors were tested in SH-SY5Y cells stably expressing Epac1-camps. Their ability to alter cAMP concentrations through selective PDE4 inhibition were measured in real-time.

3 – To determine whether increases in cellular cAMP concentrations were physiological, I measured PKA activity indirectly by looking at the phosphorylation of Hsp20 at serine 16. This was apt because of the cytoprotective role for Hsp20 I have established in previous chapters.

4 – Finally we utilised an MTT-based cell viability assay to determine whether our novel PDE4 inhibitor could protect SH-SY5Y cells against $A\beta_{1\text{-}42}$ induced cytotoxicity. The neuroprotective effect was compared with the PDE4 inhibitor rolipram and the PDE5

inhibitor sildenafil, which I have established previously, can attenuate the cytotoxic effects of $A\beta_{1-42}$.

5.2 Results

5.2.1 Chemical informatics and docking studies identify moexipril as a candidate PDE4 inhibitor.

In total, six compounds were identified initially; moexipril, an angiotensin-converting enzyme (ACE) inhibitor (Chrysant and Chrysant 2003) was identified as a potential PDE4A,B,C and D inhibitor by SEA, with an E-value of 1.71^{-11} and a max Tanimoto coefficient in ECFP4 fingerprints of 0.35. Searching for analogs of moexipril was done with ZINC (Irwin, Sterling et al. 2012). Docking to PDB Code 1MKD (Lee, Markowitz et al. 2002) was performed with DOCK3.6 (Irwin, Shoichet et al. 2009), the best scoring pose that overlapped the known ligand was chosen. This helped to identify a further 5 compounds; tranilast, an anti-inflammatory drug with poorly understood mechanisms of action (Spiecker, Lorenz et al. 2002); devazepide, a cholecystokinin antagonist selective for the CCK_1 subtype (Weller 2006); verazide, a compound with anti-tuberculous activity (Rubbo and Cymerman-Craig 1955); methonalide, a tranquilizer (Perron 1959 - patent US2870146); itopride, a dopamine D2 antagonist with acetylcholinesterase effects (Holtmann, Talley et al. 2006) (Fig. 5.1A). From the identified ligands, moexipril produced the most significant reduction in PDE4B1 activity (20% activity relative to non-treated control) at the highest concentration tested (100µM), followed by verazide (56%), methonalide (60%), Devazepide (66%), Tranilast (73%). Itopride did not display any inhibitory activity against PDE4B1 (Fig. 5.1B). Moexipril also reduced PDE4 activity by 51% at 10µM and was selected for further analysis.

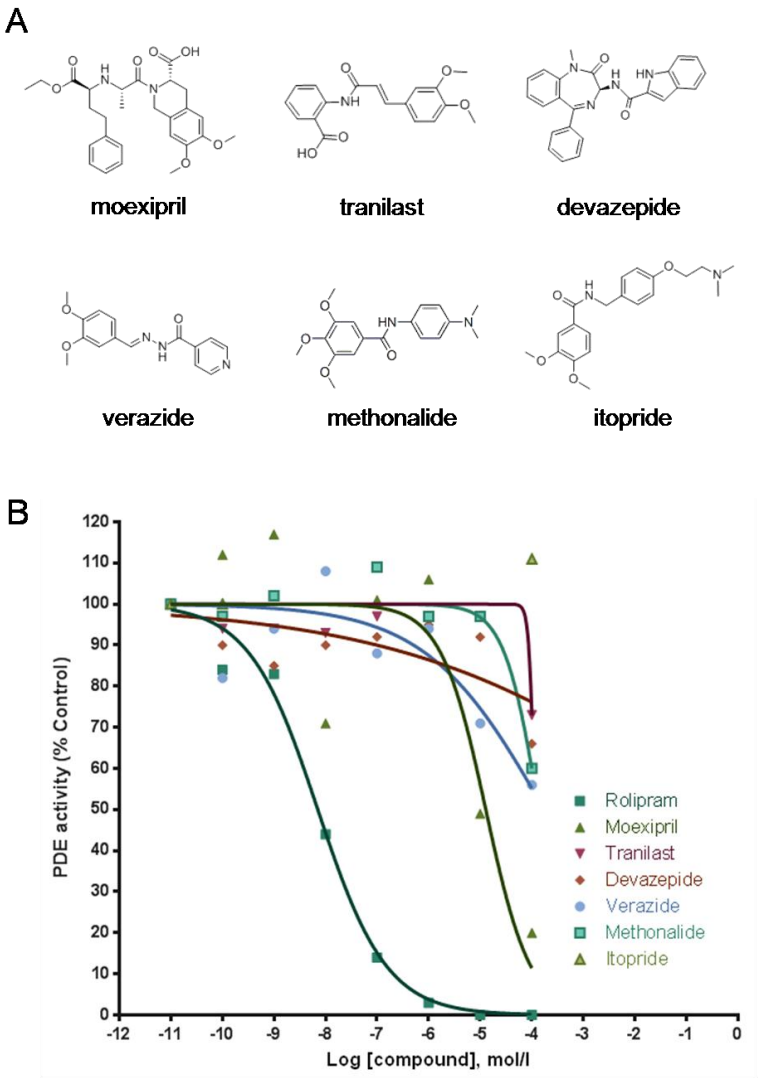

Figure 5.1 – FDA approved compounds identified through *in silico* screening.
A – 6 FDA approved compounds were identified using a chemical informatics approach. B – Compounds were screened for PDE4 inhibitory activity. The angiotensin converting enzyme (ACE) inhibitor moexipril reduced PDE4 activity by 80% at 100µM and was selected for further investigation. Rolipram was used as a positive control.

5.2.2 Model of moexipril and its analogues bound to catalytic domain of PDE4

As the structure of the PDE4 core catalytic domain is well defined by X-ray crystallography, with numerous co-crystal structures available for a range of inhibitors from different structural classes, we undertook the molecular docking of moexipril to consider its potential as a PDE4 inhibitor. Docking was carried out with DOCK3.6 (Irwin, Shoichet et al. 2009) against the co-crystal structure (PDB: 1MKD) of the PDE4D core catalytic domain with bound zardaverine (**2**, Fig. 5.2)(Lee, Markowitz et al. 2002). In the best scoring pose (Fig. 3A), the 6,7-dimethoxytetrahydroisoquinoline core of moexipril overlapped closely with the catechol ether subunit of zardaverine **(2)** to engage the purine-scanning glutamine, a residue that is conserved across the entire PDE superfamily and which ordinarily anchors the substrate nucleobase during enzymatic turnover. Catechol

ethers such as zardaverine (Schudt, Winder et al. 1991) constitute one of the main PDE4 inhibitor chemotypes and include rolipram **(3)** (Schwabe, Miyake et al. 1976), the archetypal PDE4-selective inhibitor, as well as the isoquinoline natural product, papaverine **(4)** (Triner, Vulliemoz et al. 1970). The recently approved first-in-class PDE4 inhibitor, roflumilast **(5)** (Rabe, Bateman et al. 2005), and other compounds such cilomilast **(6)** (Christensen, Guider et al. 1998) that have progressed to clinical trials also possess a catechol ether core structure. Numerous co-crystal structures are available for this class of PDE4 inhibitor (Lee, Markowitz et al. 2002; Card, England et al. 2004; Huai, Sun et al. 2006), and in all cases the catechol ether oxygen atoms straddle the Nε centre of the purine-scanning glutamine, forming convergent hydrogen bonds in the manner predicted for the docked moexipril model. The 3-carboxy group of the ligand in this pose would be orientated proximal to the bimetallic catalytic centre of the enzyme, whilst the side chain extension would be free to run across the hydrophobic rim of the catalytic pocket with little constraint.

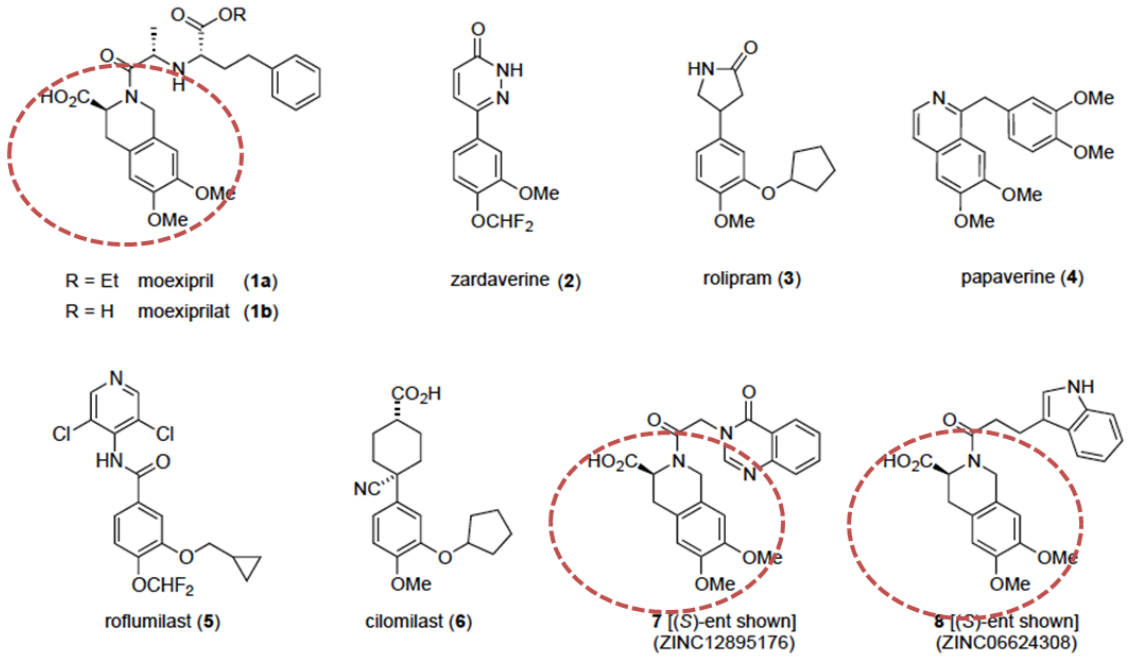

Figure 5.2 – Structural relationship of established PDE4 inhibitors.
Established PDE4 inhibitors (**2–6**) and newly identified PDE4 inhibitors 3-carboxy-6,7-dimethoxytetrahydroisoquinoline compounds (red dashed line) : moexipril (**1a**), **7** and **8**.

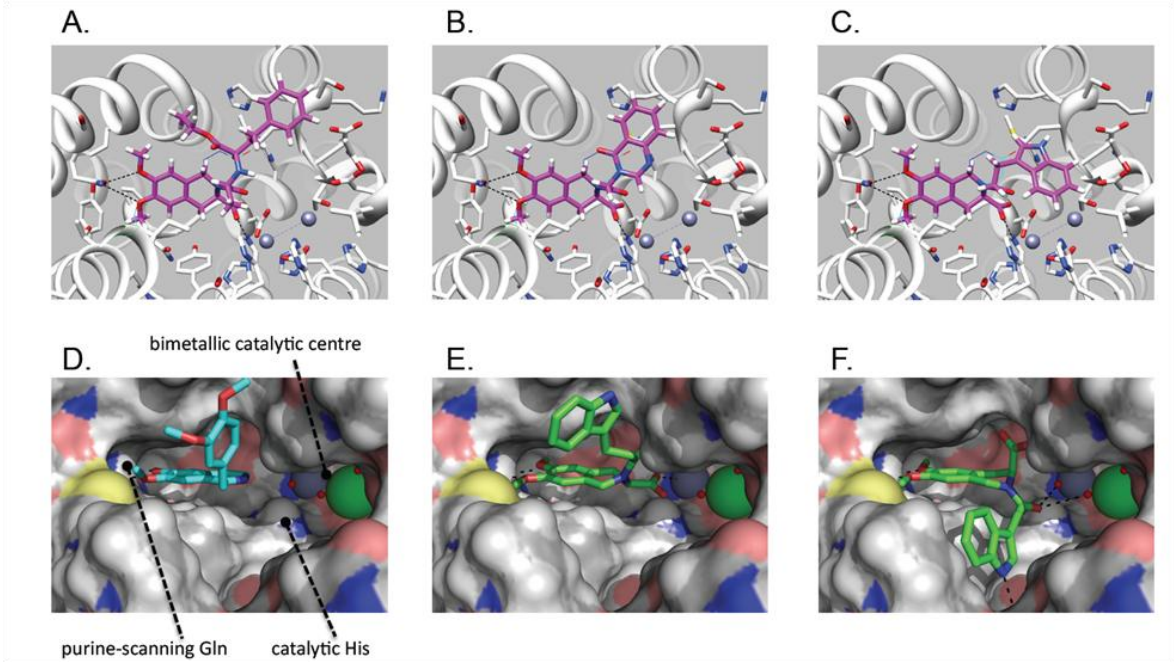

Figure 5.3 – Docking models of newly identified 3-carboxy-6,7-dimethoxytetrahydroisoquinoline inhibitors.
Moexipril (**1a**), compounds **7** and **8** fitted to the PDE4 catalytic pocket and comparison with papaverine (4). (A)–(C) best scoring poses for moexipril, 7 and 8 docked into the PDE4 zardaverine co-crystal structure (PDE4: 1MKD). (D) Structure of papaverine (cyan stick) bound to PDE4D core catalytic domain (PDB: 3IAK). (E)–(F) models of inhibitor 8 (green stick) fitted to the PDE4 papaverine co-crystal structure showing poses with alternative conformations for the tetrahydroisoquinoline core.

This work was carried out by Ryan G. Coleman & Dave Adams

5.2.3 Biochemical determination of moexipril potency as a PDE4 inhibitor

To further establish whether moexipril might exhibit PDE4-inhibitory activity, we assayed the compound for its ability to inhibit three widely expressed PDE4 isoforms PDE4A4, PDE4B2 and PDE4D5. Moexipril inhibited cAMP hydrolysis by all three isoforms in the micromolar range (Fig. 5.4A), but was most potent against the PDE4B2 isoform (IC_{50} 38 µM), with PDE4A4 and PDE4D5 showing respectively 4-fold and 6-fold lower sensitivity to inhibition. Having confirmed the prediction that moexipril should inhibit PDE4, we next undertook a search for other commercially available 3-carboxy-6,7-dimethoxytetrahydroisoquinolines using ZINC (Irwin, Shoichet et al. 2009). Our search identified two compounds (**7** and **8**) possessing the tetrahydroisoquinoline core of moexipril but with simplified N-acyl extensions. Both compounds were available in racemic form from Princeton BioMolecular Research (USA) and initial docking studies, undertaken with the (S)-configured structures, suggested that the PDE4 catalytic pocket should be able to accommodate these compounds, with the N-acyl side chains extending

across its rim (Fig. 5.3B and 5.3C). The (S)-enantiomers were selected for docking in order to match the absolute configuration at the tetrahydroisoquinoline 3-position of moexipril. The inhibitory activity of (*rac*)-**7** and (*rac*)-**8** was then assessed using PDE4B2, selected as the isoform that exhibited greatest sensitivity to inhibition by moexipril (Fig. 5.4B). The archetypal inhibitor, rolipram (**3**), was included in this comparative evaluation as a positive control. Consistent with the modelling, both of the moexipril analogues inhibited PDE4B2. Compound **8** showed the highest affinity for PDE4, having an IC_{50} of 6.9 µM, 7-fold better than moexipril, while compound 7 had an IC_{50} 89 µM. The inhibition curves suggest a binding mode that is competitive with cAMP for the catalytic site of the enzyme, consistent with the docked models (Fig. 5.3). By comparison, (*rac*)-rolipram, a drug optimized for this enzyme, had an IC_{50} 1 µM against it. Moexipril showed no activity against two other PDE family members, PDE8A and PDE5, suggesting that it could act as a PDE4 specific inhibitor (Fig. 5.4C).

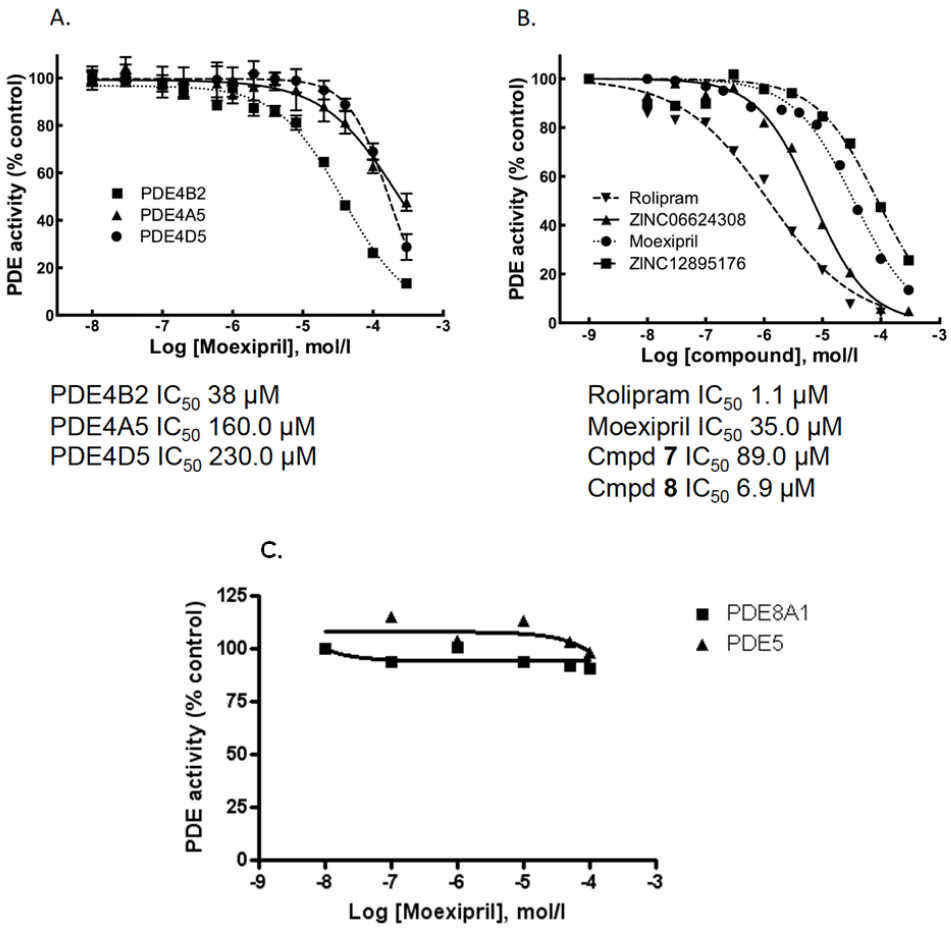

Figure 5.4 – Determination of the efficacy of established and novel PDE4 inhibitors.
Activities for each PDE4 subtype were related to a non-drug treated sample (100% control) over an increasing dose of the indicated compounds (n=3). IC50 values were calculated using Graphpad Prism 4.0. (A) Dose response curves of moexipril against 3 different PDE4 isoforms. (B) Dose response curves of four different PDE4 inhibitors against PDE4B2. (C) Dose-response curves of moexipril against PDE8A1 and PDE5.

5.2.4 Moexipril increases in intracellular cAMP

To determine whether the inhibition of PDE4 by moexipril and its analogues (**7** and **8**) could induce intracellular increases in cAMP, I employed a FRET-based biosensor constructed from the nucleotide binding domain of the type 1 exchange protein activated by cAMP, EPAC1 (Nikolaev, Bunemann et al. 2004) (see Figure 5A). This probe enables quantitative, real-time detection of rapid changes in global cAMP following cell treatment. Experiments were done using SH-SY5Y cells stably expressing the biosensor. This cell line endogenously expresses PDE4 isoforms from the PDE4B and PDE4D subfamilies (Fig. 6A and B) (Millar, Pickard et al. 2005). All compounds markedly increased intracellular cAMP levels over those induced by treatment with a sub-optimal dose of the adenylyl cyclase activator, forskolin alone (Fig. 4B-4E). No FRET changes were detected when the compounds were added alone (Data not shown). The FRET ratio changes I observe here (Fig. 4F), are in line with those previously published for rolipram potentiation of the forskolin-stimulated cAMP response (Nikolaev, Bunemann et al. 2004). Given that the magnitude of cAMP response produced by moexipril and its analogues evaluated here, is similar to that produced by rolipram, further supports the notion that the ACE inhibitor could, in principle, also act as a PDE4 inhibitor *in vivo*.

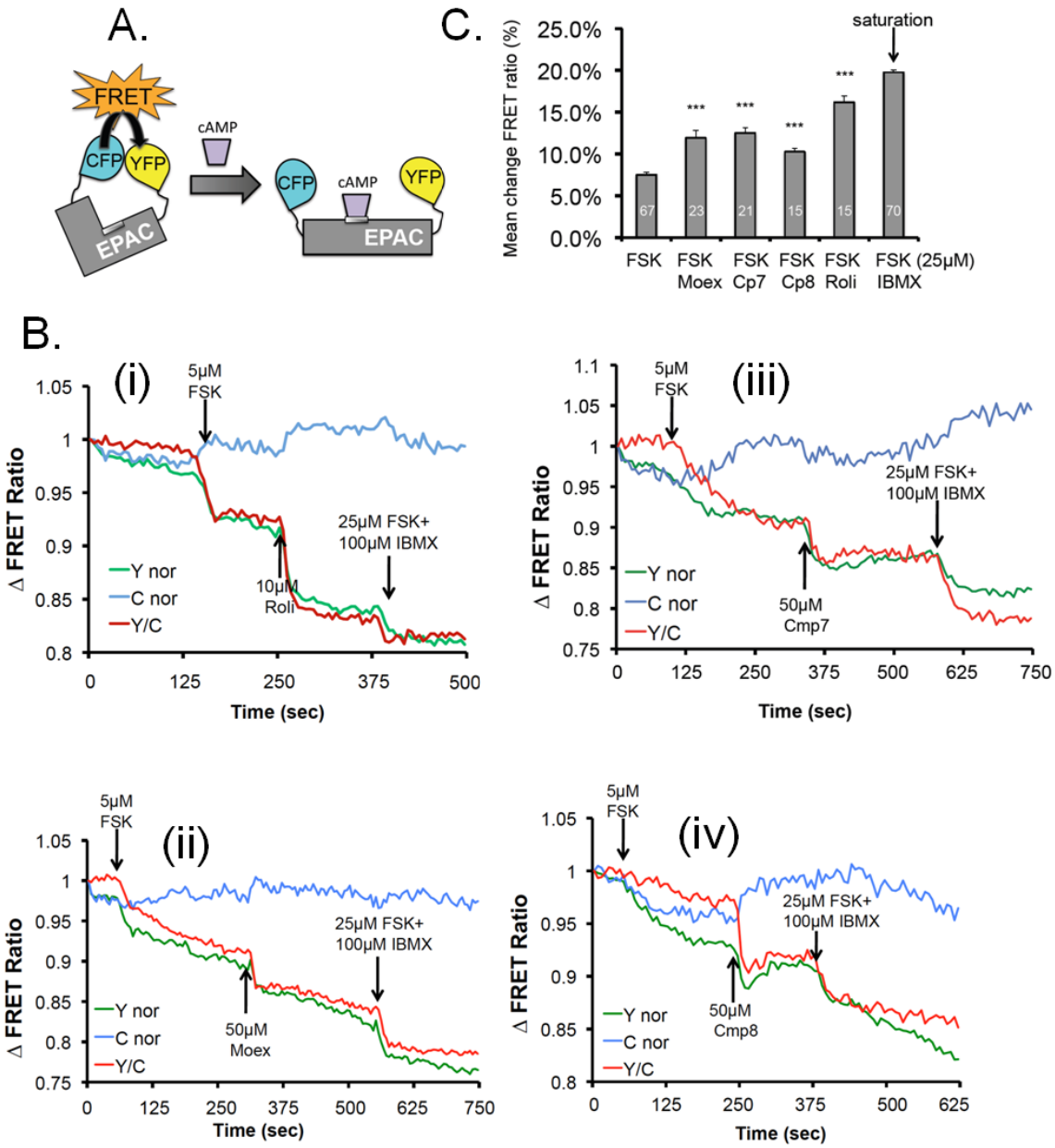

Figure 5.5 - Epac1-camps sensor for detecting intracellular cAMP changes.
A – Cartoon diagram of the Epac1-camps sensor depicting the conformational change that occurs upon binding of cAMP and the subsequent loss of fluorescence resonance energy transfer (FRET) between the two fluorophores. (B) Changes in FRET ratio triggered by a 5 μM application of forskolin (FSK), followed by treatment with PDE4 inhibitors (i) rolipram (Roli) (ii) moexipril (Moex) (iii) compound **7** (Cmp 7) and (iv) compound **8** (Cmp 8). Data is from single cell and is representative of experiments carried out at least n=15. (C) Quantification of mean change in FRET ratio for all of the treatments including in lane 6 a saturating dose of forskolin (25 μM) plus the general PDE inhibitor 3-isobutyl-1-methylxanthine (IBMX 100 μM). All other lanes forskolin (FSK) applied at 5μM. Significance evaluated using ANOVA, *** = p<0.001 when compared with FSK alone. White numbers within grey bars represents n number for each experiment.

5.2.5 Moexipril treatment promotes PKA-mediated phosphorylation of Hsp20

To evaluate whether, under the conditions of our *in vitro* studies, the elevation in global cAMP induced by moexipril and its analogues also resulted in downstream signaling events driven by the cAMP-effector protein, protein-kinase A (PKA), I studied a phosphorylation event I have recently demonstrated to be important for attenuating toxicity of Aβ peptides associated with Alzheimer's disease. The small heat shock protein Hsp20 is a chaperone protein, which combats a number of pathophysiological processes in the heart, vasculature and brain (Edwards, Cameron et al. 2011). The protective actions of Hsp20 require its phosphorylation by PKA on serine 16. Its association with PDE4 (Sin, Edwards et al. 2011), however, keeps cAMP levels surrounding Hsp20 low, maintaining Hsp20 in its basal, unphosphorylated state. Thus association with PDE4 prevents inappropriate phosphorylation and activation of Hsp20 by fluctuations in basal cAMP levels. A similar protective 'gating' effect through PKA sequestration has been observed for AKAP-anchored PKA in the centrosome (McCahill, McSorley et al. 2005; Edwards, Scott et al. 2012).

PKA phosphorylation of Hsp20 was chosen here as a readout for physiological PDE4 inhibition as it has been shown previously that PDE4 inhibition alone, via the action of rolipram, could trigger this phosphorylation event without the need for artificially raising cAMP with sub-optimal doses of forskolin to activate adenylyl cyclase (Sin, Edwards et al.). I thus monitored the transient phosphorylation status of Hsp20 in SH-SY5Y cells following treatment of cells with either rolipram, or moexipril, or moexipril analogues **7** and **8** (Figure 5.6C, D, E and F respectively). As previously observed with rolipram treatment (Sin, Edwards et al. 2011), challenge of cells with any of three 3-carboxy-6,7-dimethoxytetrahydroisoquinoline analogs significantly elevated Hsp20 phosphorylation. The temporal nature of Hsp20 phosphorylation induction differed somewhat between compounds. However, this is likely to reflect differences in their potency in elevating cAMP levels, where rolipram induces the largest increase in cAMP (Figure 5.4B) and triggers the most rapid Hsp20 phosphorylation (Fig. 5.6C). The transient nature of phosphorylation following treatment is likely to be attributed to compensatory mechanisms employed by the cell to combat cAMP increases, mechanisms that include activation of PDE4 enzymes by PKA (MacKenzie, Baillie et al. 2002) and dephosphorylation of Hsp20 by as yet unknown phosphatases. To prove that the observed phosphorylation events were PKA dependent, a PKA specific inhibitor (KT5720) was used to attenuate the

phosphorylation of Hsp20 induced by Moexipril and a sub-optimal dose of forskolin (Fig. 5.6G).

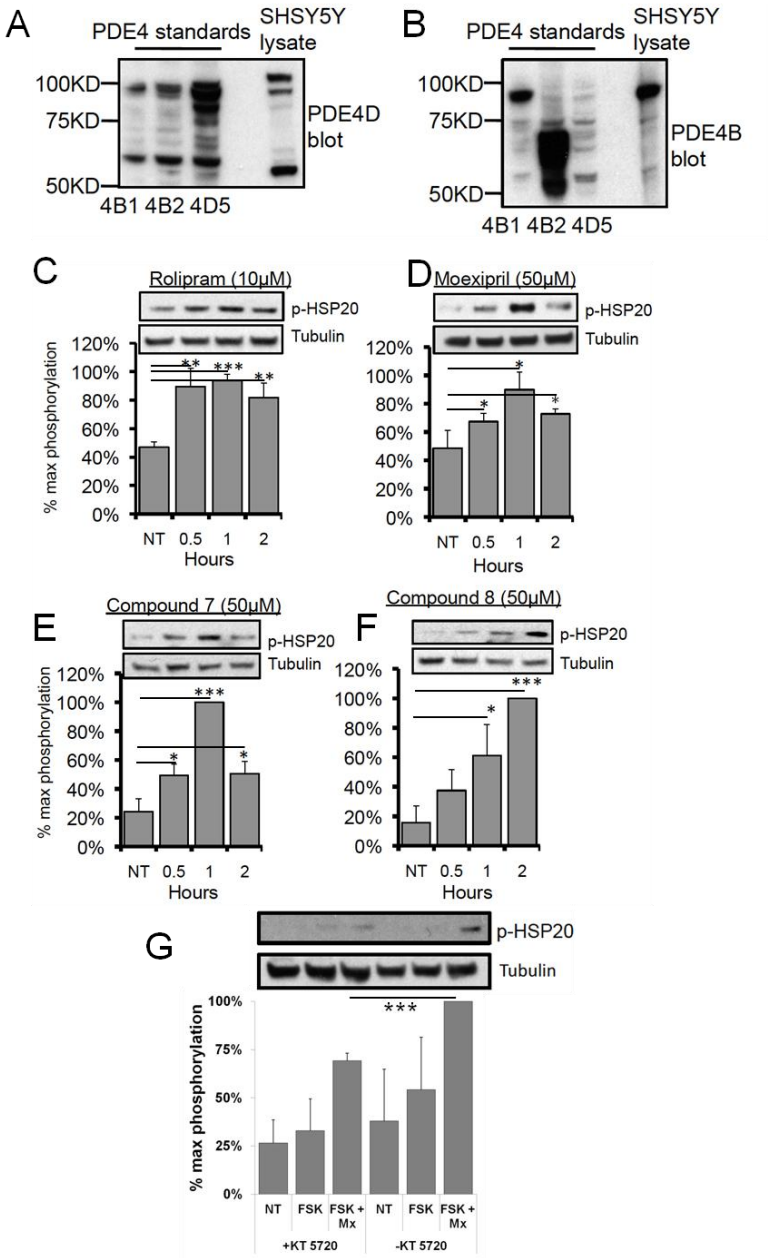

Figure 5.6 - PDE4 inhibitors induce PKA phosphorylation of the small heat-shock protein Hsp20.

Lysates from SH-SY5Y cells were blotted for the expression of endogenous (A) PDE4D (B) PDE4B enzymes. SH-SY5Y cells were treated with (C) rolipram (10 μM), (D) moexipril (50 μM) (E) Compound 7 (50 μM) and (F) Compound 8 (50 μM) for the indicated times. G – SH-SY5Y cells treated with PKA inhibitor KT5720 (4μM) 20 minutes prior to addition of forskolin (FSK, 10μM) or forskolin (FSK, 10μM) with moexipril (Mx, 50μM) for 5 minutes. Cell lysates subjected to SDS-PAGE and western blotting. Blots were probed for phospho-Hsp20 and a loading control (tubulin). Quantification of the relative amounts of phosphorylation on serine 16 vs. loading control were calculated following densitometry. Results are plotted as a percentage of the maximal phosphorylation over time. Mean values ±SEM, p-values - * < 0.05, ** <0.01, *** <0.001; ANOVA, n = 3

5.2.6 Moexipril attenuates $A\beta_{1-42}$ induced cytotoxicity

I have shown previously that PDE inhibition can protect against the acute cytotoxic effects associated with oligomeric $A\beta_{1-42}$ incubation. In order to examine if moexipril could exert the same protective effects, I compared its action alongside the PDE4 inhibitor rolipram and the PDE5 inhibitor sildenafil, both of which have been proposed as possible therapeutic agents for the treatment of AD (Puzzo, Staniszewski et al. 2009; Smith, Pozueta et al. 2009; Zhang, Guo et al. 2013).

The neuronal-like SH-SY5Y cells were treated with 10µM $A\beta_{1-42}$, which typically results in approximately 50% cell death after 48 hours incubation (discussed in chapter 3). SH-SY5Y cells were treated with either vehicle control (PBS), 10µM $A\beta_{1-42}$ or 10µM Aβscr followed by treatment with DMSO (control), rolipram, sildenafil or moexipril 6 hours post Aβ addition (as described in chapter 4). After 48 hours of incubation with Aβ peptides, cell viability was measured using the MTT reduction end-point assay which measures mitochondrial activity and hence cell viability.

All drug treatments significantly attenuated $A\beta_{1-42}$ induced reduction in cell viability, relative to control treated SH-SY5Y cells. Control cells treated with $A\beta_{1-42}$ were only 44% (± 3%) viable, compared to cells treated with rolipram, 67% (± 8%), sildenafil, 62% (± 5%), and moexipril 71%, (± 7%).

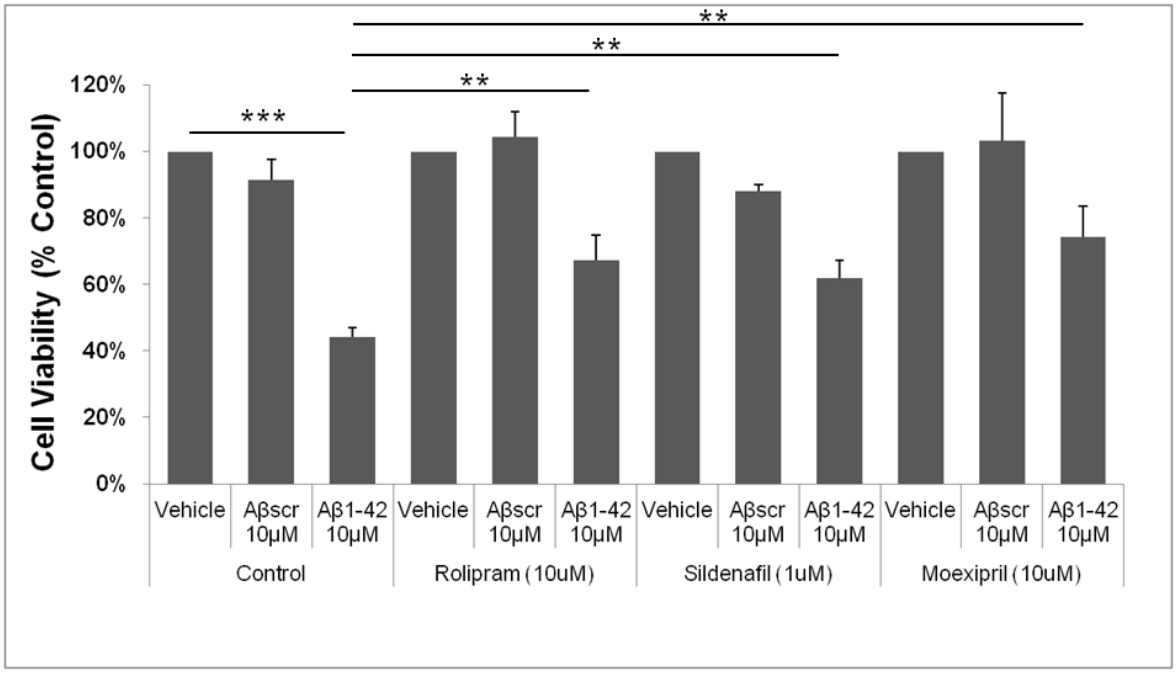

Figure 5.7 – Moexipril attenuates cytotoxicity associated with $A\beta_{1-42}$.
Cell viability assays showed that addition of $A\beta_{1-42}$ but not $A\beta_{scr}$ resulted in significant reduction in cell viability (# = p<0.001, relative to vehicle only control). This reduction in viability was significantly attenuated by treating cells with either rolipram (10μM), sildenafil (1μM) or moexipril (10μM) but not DMSO (control). The reduction in cell viability was measured with MTT and normalised to vehicle only controls. SH-SY5Y cells were incubated with Aβ peptides for 48 hours, PDE inhibitors were added 6 hours post Aβ peptide addition. Mean values ±SEM, *p-values* - ** < 0.01, ** < 0.001; ANOVA, n = 4.

This work was carried out by Masters Student Philippa Fowler under my supervision.

5.3 Discussion

Several FDA approved compounds were identified using chemical informatics approach to screen approved compounds for PDE4 inhibition. Four of the compounds identified contained a common dimethoxybenzene moiety (Fig. 5.1A) as would be expected using SEA. Several compounds exhibited PDE4 inhibitory activity in the initial screening process however this was only at very high concentrations. The compound, which showed the most significant inhibitory activity, even at the lower concentration of 10μM, was moexipril. This compound was chosen for further evaluation.

Moexipril (**1a**) was developed as a long-acting, nonsulfhydryl angiotensin-I converting enzyme (ACE) inhibitor suitable for once-daily administration (Klutchko, Blankley et al. 1986). The drug is used to treat hypertension and is well tolerated, apparently lacking emetogenic activity (Wyvratt and Patchett 1985; Gu and Strickley 1987). Although moexipril itself has ACE-inhibitory activity in its own right, it serves as a prodrug for the

more potent metabolite, moexiprilat (**1b**, Fig. 5.2), generated in vivo by hydrolysis of the side chain ester. PDE4-inhibitory activity has not previously been attributed to moexipril, but we identified the compound as a candidate PDE4 inhibitor by screening the MDDR drug database using the chemoinformatics SEA method. This prediction was further supported by molecular docking studies. These suggested that moexipril may feasibly bind to the PDE4 catalytic pocket with its methoxy groups engaging the purine-scanning glutamate in a manner similar to the binding mode adopted by the catechol ether class of PDE4 inhibitors. Indeed moexipril is structurally related to the 6, 7-dimethoxyisoquinoline natural product, papaverine (**4**), an established phosphodiesterase inhibitor of the catechol ether class for which a PDE4 co-crystal structure (PDB: 3IAK) has been determined (Fig. 5.3D).

To test the prediction that moexipril may inhibit PDE4, I evaluated its effect in assays using PDE4A4, PDE4B2 and PDE4D5, three ubiquitously expressed isoforms of the PDE4 family (Houslay 2009). Encouragingly, our initial assessment confirmed that moexipril possesses PDE4-inhibitory activity in these enzyme assays, but not against PDE8A or PDE5 (Fig. 5.4). Furthermore, the inhibition of endogenous PDE4 isoforms by moexipril was evaluated using a cytosolic Epac-based FRET probe and was shown to significantly enhance intracellular cAMP increases triggered by forskolin treatment. Epac-based FRET probes require association of only one cAMP molecule to alter FRET ratios by up to 30% and they also exhibit fast activation kinetics that allow "real-time" evaluation of cAMP dynamics (Ponsioen, Zhao et al. 2004) (Fig. 5.5). As the probes are not localized to any intracellular domains (Nikolaev, Bunemann et al. 2004), the readout reflects changes in "global" cAMP concentrations and this is appropriate as I show that moexipril has activity against multiple PDE4 isoforms (Fig. 5.4) that are known to target, via unique N-terminal sequences, to multiple and distinct cellular locations (Houslay, Baillie et al. 2007; Baillie 2009).

To demonstrate that cAMP increases initiated by the action of moexipril on PDE4s could result in downstream physiological consequences in cells, I monitored changes in the phosphorylation of a well-characterized PKA substrate, Hsp20 (Edwards, Cameron et al. 2011). Hsp20 is readily phosphorylated by PKA as it exists in a complex with the A-kinase anchoring protein (AKAP) AKAP-Lbc (Edwards, Scott et al. 2012). However, the activity of this Hsp20 anchored pool of PKA is tonically inhibited by sequestered PDE4 that also interact with Hsp20 (Sin, Edwards et al. 2011). These features make Hsp20 uniquely sensitive to PKA phosphorylation following PDE4 inhibition, even under basal cAMP

conditions. Both rolipram and moexipril significantly increased phospho-Hsp20 levels when compared with untreated cells, though the maximal effect was reached earlier with rolipram (Fig. 5.6). This is consistent with the other data I present, showing that rolipram challenge results in larger cellular increases in cAMP than does moexipril (Fig. 5.5C).

As a further functional test of PDE4 inhibition by moexipril we tested it along side known neuroprotective PDE inhibitors rolipram and sildenafil, in an $A\beta_{1-42}$ cytotoxicity assay. I have shown previously, that both the PDE4 inhibitor rolipram and the PDE5 inhibitor sildenafil can attenuate the cytotoxic effects of oligomeric $A\beta_{1-42}$ incubation, therefore I expected moexipril to also be protective albeit to a lesser extent than rolipram. However, to our surprise we found that moexipril was more effective than rolipram in protecting against $A\beta_{1-42}$-induced reduction in cell viability 71% vs. 67%, respectively. This may be due to the fact that moexipril shows more selectivity for PDE4B isoforms, whereas rolipram has very similar IC_{50} values for all PDE4 isoforms (Gibson, Hastings et al. 2006). Hsp20 is known to associate with all PDE4 isoforms via a binding site in the conserved catalytic domain of the PDE (Sin, Edwards et al. 2011), however a PDE4B-specific pool of Hsp20 may localise to the correct cellular area that confirms neuroprotection. Neuroprotective properties have been described previously for moexipril ,where it was shown to protect against glutamate, staurosporine or $Fe^{2+/3+}$ -induced cell death in primary chick embryonic neurons. Furthermore, pre-treatment with moexipril was shown to be neuroprotective in both mouse and rat models of focal cerebral ischemia, however, these effects were ascribed to radical scavenging properties (Ravati, Junker et al. 1999).

Moexiprilat (**1b**) was not readily available commercially and consequently we were unable to evaluate it for PDE4-inhibitory activity. Instead, we searched for other commercially available 3-carboxy-6, 7-dimethoxytetrahydroisoquinoline analogues in order to expand the study. Two compounds (**7** and **8**) were identified with no prior literature or patent associations and thus no previously reported biological or pharmacological activity. The compounds were sourced and tested in racemic form using PDE4B2. Indeed, both compounds showed activity, with analogue 8 exhibiting low micromolar potency against PDE4B2 (Fig. 5.4B). In keeping with their ability to inhibit PDE4, both compounds also significantly enhanced intracellular cAMP increases triggered by forskolin challenge (Fig. 5.5) and induced Hsp20 phosphorylation (Fig. 5.6).

Docking of the (S)-enantiomers of both **7** and **8** confirmed that the 3-carboxy-6, 7-dimethoxytetrahydroisoquinoline could fit the PDE4 catalytic pocket, whilst allowing the

N-acyl side chain to roam over the hydrophobic rim of the pocket. As compounds **7** and **8** were sourced in racemic form, we cannot say to what extent the activity resides with the (S)-configured 3-carboxytetrahydroisoquinoline ring. Our preliminary docking studies have suggested that both enantiomers of **7** and **8** might potentially be accommodated in the PDE4 catalytic pocket and further studies would, therefore, be required to evaluate the eudismic ratio for these compounds. This is potentially an important point because the absolute configuration at the C-3 stereocentre of the tetrahydroisoquinoline core could significantly affect any ACE-inhibitory activity displayed by these simplified by moexipril analogues. Thus, although there is currently no ACE•moexiprilat co-crystal structure available, inspection of co-crystal structures for closely related 'pril' family ACE inhibitors, such as enalaprilat (PDB: 1UZE) (Natesh, Schwager et al. 2004), suggests that ACE inhibition should show strong dependence on the absolute (S)-configuration for the moexipril(at) tetrahydroisoquinoline core. In particular, the carboxyl group of enalaprilat is directed into a pocket lined by Gln, Tyr and Lys residues that form tight hydrogen bonded and salt bridge interactions. Access to this pocket will be dependent on the absolute configuration of the stereocentre in the moexipril(at) tetrahydroisoquinoline subunit. The side chain carboxylate of moexiprilat is also expected to make a strong contribution to the compound's ACE-inhibitory activity, as (by analogy to enalaprilat) it should serve as a ligand to the zinc(II) catalytic centre of the enzyme. Thus, simplification of the N-acyl extension in compounds **7** and **8** is expected to substantially reduce any ACE-inhibitory behaviour. In short, the nature of the N-acyl side chain as well as the absolute configuration of the 3-carboxy-6, 7-dimethoxytetrahydroisoquinoline core is likely to have a profound influence on ACE inhibition, and these features might be exploited to develop related compounds as PDE4 inhibitors without ACE-inhibitory activity. However, it should be pointed out that we have not tested **7** and **8** for ACE inhibition in the present study.

The nature of the N-acyl side chain clearly also exerts a significant influence over the PDE4-inhibitory performance of the compounds that we have identified here. At present we cannot precisely rationalize this because the side chain extends from the opening of the catalytic pocket (Fig. 5.3 E and F) and there is some flexibility in the potential contact that it might make with the protein. The rim of the PDE4 catalytic pocket presents an extensive hydrophobic surface, and many inhibitors with extensions projecting from a core bound within the pocket fold across this sticky surface, as illustrated in Fig. 5.3D for papaverine, where the pendent dimethoxybenzyl side chain fulfils this role.

In addition to the ambiguity regarding the position adopted by the side chain in the PDE4-bound state, there may be more than one conformation possible for the N-acyl tetrahydroisoquinoline core. The best scored binding poses generated from the modelling software (DOCK) orientated the 3-carboxyl group proximal to the enzyme's catalytic metal ions (Fig. 5.3A-C). With this organization, the ionised carboxylate might directly act as a ligand on the more deeply sited (zinc) ion or potentially hydrogen bond to water ligands on the metal centres. The adoption of this bound pose, illustrated for compound **8** in Fig. 5.3E, introduces a degree of strain into the tetrahydroisoquinoline subunit. An alternative conformer, with less ring strain, would possess a pseudoaxial carboxyl group, as shown in Fig. 5.3F. In this case the N-acyl group is predicted to hydrogen bond to water ligands on the metal centres and also to the proximal His residue (labelled in Fig. 5.3D) that plays a role in PDE4 catalysis by protonating the nucleotide 3'-O during substrate turnover. We cannot definitively indicate which of these two possibilities will be favoured for the bound compounds. The binding pose presented in Fig. 5.3F positions the carboxyl group into a hydrophobic subpocket in the roof of the substrate binding site, but it offers a significantly more relaxed conformation to the tetrahydroisoquinoline. In principle, with this conformation, replacement of the polar carboxyl group by a small hydrophobic substituent might enhance the affinity and PDE4-inhibitory potency of the compound, and this design principle has been used previously in the development of another PDE4 inhibitor series (Allcock, Blakli et al. 2011).

Given the PDE4-inhibitory activity exhibited by moexipril, it is not entirely clear why the compound apparently lacks the typical side effects associated with PDE4 inhibitors. This could be due to its ADME properties, since neither moexipril nor moexiprilat is brain-penetrant. However, the dosing window may also play a role in the reported tolerance of moexipril. Thus, in one PK assessment, C_{max} for moexipril was determined at 25 µg/L (~50 nM) from an oral dose of 15 mg, clinical trials having focused on once-daily dosing regimens in the 7.5-30 mg range. The negative charge character of the ionised moexipril and moexiprilat structures may be a contributory factor underlying their poor uptake by the brain, as with the carboxyl-bearing second generation PDE4 inhibitor, cilomilast (**6**), for which brain penetration is also limited (Giembycz 2001). Thus, retention of the 3-carboxyl group may be a consideration if a non-emetogenic PDE4 inhibitor series is to be developed from moexipril.

A key underlying driver behind the work described here was to identify previously approved drugs that lack any emetogenic liability as PDE4 inhibitors. Such compounds

might either have direct potential for repositioning as PDE4 inhibitors or provide the starting point for development of novel PDE4 inhibitors with an improved therapeutic window. Given that the reported potency for inhibition of ACE by moexipril [IC50 40 nM vs. porcine serum ACE (Wyvratt and Patchett 1985; Gu and Strickley 1987)] is some three orders of magnitude greater than for the inhibition of PDE4 that we disclose here, direct repositioning of moexipril for indications that might respond to treatment by PDE4 inhibitors is therefore likely to be problematic. Not least because the profoundly higher concentrations needed to achieve PDE4 inhibition, compared to those required for ACE inhibition, may serve also to uncover an emetic response in moexipril. Nevertheless, moexipril might constitute a starting point for novel PDE4 inhibitor development, provided that derivatives can be made that lack an emetogenic profile.

6 Final Discussion

The aggregation of the Aβ peptide into amyloid fibrils is a central component in the onset and progression of AD (Hardy and Allsop 1991; Selkoe 1991). Several pieces of evidence support the role of Aβ as the causative agent in the development of AD, these include (i) the localisation of APP to chromosome 21 and 100% penetrance of AD in Down's syndrome patients (ii) synthetic Aβ peptides being toxic to neurons, in culture and *in vivo* and (iii) inherited mutations in APP either flanking or occurring within Aβ region leading to increases in production or aggregation propensity of Aβ, resulting in early-onset AD. As such, strategies that target toxic Aβ generation, either through perturbation of APP metabolism, inhibition of Aβ aggregation, attenuation of the neurotoxic effects of Aβ or promotion of Aβ clearance from the CNS, are seen as pathways that can be targeted therapeutically in order to prevent development and progression of the disease (Walsh and Selkoe 2007).

Within this body of work, I considered methods to promote the prevention of Aβ aggregating into toxic species and the attenuation of subsequent toxic effects on neuronal-like cells. In order to accomplish this, I investigated the actions of an endogenous multifunctional protective protein, Hsp20, which is found ubiquitously throughout the body and is readily expressed in the mammalian brain (Verschuure, Tatard et al. 2003). Hsp20 has well-established cardioprotective functions (Fan 2011), but more recently there is accumulating evidence that it has similar protective functions in the field of neuroscience, particularly with regard to protecting against hypoxic conditions (David, Boelens et al. 2006; Niwa, Hara et al. 2009; Zeng, Tan et al. 2013). The protective functions of Hsp20 are evoked via phosphorylation by cyclic nucleotide-dependent protein kinases, thereby permitting a mechanism for therapeutic intervention through the modulation of second messenger signalling pathways.

Several aims were identified with regard to establishing a neuroprotective role for Hsp20 in the context of AD. First of all, I wanted to examine what effect Hsp20 phosphorylation would have in regulating a previously identified interaction with Aβ. Secondly, I wished to establish what effect phosphorylation of Hsp20 would have on the aggregation dynamics of Aβ. Thirdly, I was interested to determine what effect increasing intracellular phospho-Hsp20 levels would have on Aβ-mediated cytotoxicity. The fourth and final aim was to develop novel therapeutic agents that could potentially be developed to treat AD via the induction of Hsp20 phosphorylation.

6.1 Hsp20 Inhibits Aβ Aggregation

The Aβ peptide is produced by regular metabolism of the APP and in its monomeric form is non-toxic (Morgan, Colombres et al. 2004). Early studies showed that the toxicity of Aβ is related to its aggregated state, as newly solubilised synthetic Aβ monomers were found to be neurotrophic, whereas aged synthetic Aβ peptides readily self-associated and were potently neurotoxic (Pike, Walencewicz et al. 1991). The aggregation of Aβ relies on a central hydrophobic domain of residues ^{17}LVFF^{20} (Hilbich, Kisters-Woike et al. 1992). A pentapeptide aggregation inhibitor was previously developed to target this domain. Based on sequence homology with ^{16}KLVFF^{20} it can bind full-length Aβ and prevent fibril formation (Tjernberg, Naslund et al. 1996). Using peptide array technology, I established that Hsp20 binds proximally to ^{16}KLVFF^{20}, and I also demonstrated that the lysine residue of this domain was essential for mediating the interaction between Aβ and Hsp20. This suggests that Hsp20 is interacting directly at the domain involved in Aβ self-association.

In order for Aβ peptides to self-associate, the monomer must convert from an α-helical/random coil conformation into a β hairpin. This structural conversion facilitates a nucleation-dependent polymerisation reaction and subsequent formation of soluble metastable oligomers. These oligomers then serve as a nucleus which can be extended through further monomer addition to create protofibrils, which bundle together to form the large cross β-sheet fibrils that are associated with amyloid plaques (Gilbert 2013). Our NMR study showed that Hsp20 only weakly interacted with monomeric Aβ, however, this interaction was enough to stabilise significant quantities of monomeric Aβ in its non-toxic α-helical/random coil conformation, reducing its propensity to aggregate into insoluble fibrils. Furthermore, the domains that showed the largest changes in chemical shifts corresponded with the two helical spanning regions, Q^{15} - D^{23} and I^{31} – M^{35} (Sticht, Bayer et al. 1995). These two largely hydrophobic regions interact with each other to form the β hairpin structure (Penke, Datki et al. 2003). Therefore Hsp20 is acting at the interface of these two regions to inhibit structural conversion and subsequent self-association. Gratifyingly, this was in agreement with the peptide array data, which also highlighted that the glutamine residue at position 15 was also important for mediating the interaction of Hsp20. This residue has also been shown to be involved in Aβ-Aβ interactions that drive its polymerisation into fibrils (Ahmed, Davis et al. 2010). Taken together, these data demonstrate that Hsp20 can inhibit the initial aggregation processes central to the generation of toxic Aβ species, one of the earliest events in the aetiology of AD.

There is a large variety of Aβ species in the aggregation cascade that are associated with neurotoxicity, however the identification of the exact species has proven problematic over the years (Hardy 2009). The Aβ peptide exists mainly in two states that are important in AD pathology, insoluble Aβ fibrils and soluble Aβ oligomers. Early studies initially pointed to insoluble fibrils as the cause of neurodegeneration due to their association with amyloid plaques in histopathological studies of AD (Gilbert 2013). However, the level of plaque abundance did not correlate well with the severity of symptoms in AD patients, and in transgenic mouse models of the disease, neuronal loss and cognitive impairments were shown to precede any plaque formation. This in turn led to Aβ oligomers being implicated as the main driver of neurotoxicity (Walsh and Selkoe 2007).

With this in mind, I established a collaboration with Carlos Penedo's group who have recently developed a novel assay that can differentiate between oligomerisation and fibrillisation of the Aβ peptide in real-time. Utilisation of this new technology allowed me to establish what effect Hsp20 would have on these two distinct aggregation pathways. Hsp20 was originally hypothesised to play a neuroprotective role in AD due to its co-localisation with diffuse plaques and to a lesser extent senile plaques (Wilhelmus, Otte-Holler et al. 2006). Interestingly, these plaques are observed in normal aged brains and are not associated with neuronal injury or reactive astrocytes and microglia (Selkoe and Schenk 2003). Given that this novel aggregation assay highlighted the fact that Hsp20 was more effective at inhibiting fibril growth when compared to oligomerisation of Aβ, the data suggests that Hsp20's association with diffuse plaques is preventing fibril elongation and may be having a neutralising effect on this type of amyloid. A similar mechanism has been hypothesised for a different heat-shock protein, also called Hsp20 from the bovine parasite *Babesia bovis*. This Hsp20 was shown to encapsulate Aβ fibrils when the molar concentration of Hsp20 was 1000-fold less than Aβ. This Hsp20/Aβ complex was found to be non-toxic when overlaid onto SH-SY5Y cells (Lee, Carson et al. 2006). Whether a similar mechanism exists with human Hsp20/Aβ interaction remains to be elucidated.

The main aim of the various Aβ aggregation assays that I conducted was to critically evaluate the effects of Hsp20 phosphorylation by comparing it to wild type Hsp20. To do this, I employed the phospho-mimetic mutant Hsp20-S16D, where the serine is substituted for aspartic acid in order to mimic the negative charge of a phosphate group. Understandably, this mutation is only a mimic and is unlikely to behave as effectively as phospho-serine; therefore it is possible that phospho-Hsp20 would have performed better than Hsp20-S16D in the various *in vitro* assays that I conducted. This was exemplified in

the initial peptide array experiment when I showed that the introduction of the phospho-serine induced increased binding of Aβ to far greater extent than aspartic acid substitution within the PKA/PKG consensus sequence. However, due to the recombinant protein constructs used in the *in vitro* assays, phospho-mimetics are a simpler approach to understanding the effect of introducing a negative charge at a specific phosphorylation sites, has on a protein's properties. Phospho-mimetic substitutions are also inherently more stable than phosphorylated serine residues.

Despite this caveat of the phospho-mimetic substituted mutant, I was still able to establish that Hsp20-S16D outperformed Hsp20-WT in all of the *in vitro* assays I conducted. Hsp20-S16D more readily pulled-down higher order Aβ aggregates, Hsp20-S16D was able to stabilise more monomeric Aβ and keep more Aβ in solution in our NMR experiments, and it was the only construct to significantly inhibit oligomeric aggregation in the novel real-time Aβ aggregation assay. Taken together, these data have established that Hsp20 is likely to be neuroprotective through direct inhibition of Aβ aggregation. Furthermore, this interaction is enhanced via phosphorylation, providing a mechanism that is amenable to modulation.

6.2 Hsp20 attenuates Aβ toxicity

Intraneuronal accumulation of Aβ is also an early event in aetiology of AD, which causes synaptic dysfunction and deficits in LTP, well in advance of any discernible extracellular deposition of amyloid (Oddo, Caccamo et al. 2003). Low molecular weight species of Aβ and soluble Aβ oligomers readily accumulate intracellularly where they become concentrated in low pH vesicles, promoting conditions that drive fibril formation (Hu, Crick et al. 2009). Furthermore, intracellular fibril out-growth from multivesicular bodies leads to the formation of amyloid plaques. Plaque formation induces cell death resulting in insoluble amyloid structures being released into the extracellular space (Friedrich, Tepper et al. 2010). In light of this, Aβ accumulation, aggregation and toxicity are primarily intracellular events and need to be targeted as such. All previous studies looking at the effect of sHSPs' ability to inhibit Aβ toxicity have utilised co-incubation of sHSPs with Aβ prior to overlaying the complexes onto neuronal-type cells. My aim was to establish that by increasing intracellular levels of Hsp20 I could attenuate toxicity given that the molecular interaction of the two proteins is likely to occur intracellularly.

Using two distinct toxicity assays, I was able to establish that the overexpression of Hsp20 significantly attenuated Aβ toxicity. My initial study utilised the standard MTT-based cell viability assay, where I showed that overexpression of either Hsp20-WT or Hsp20-S16D conferred significant levels of protection, whereas the non-phosphorylatable mutant, Hsp20-S16A did not protect cells from Aβ-mediated cytotoxicity. This was particularly interesting as the anti-apoptotic effects of Hsp20 in cardiomyocytes require phosphorylation at serine 16 (Fan, Chu et al. 2004). Furthermore, Hsp20 directly interacts with Bax to inhibit apoptosis (Fan, Ren et al. 2005). Given that the MTT assay is a measure of mitochondrial function it is possible that Hsp20 is attenuating Aβ-mediated toxicity through the modulation of apoptosis, in addition to a direct interaction with Aβ.

Our second Aβ toxicity assay, was based on real-time label-free measurement of cellular impedance, a technique capable of monitoring changes in cell morphology with a unique sensitivity to the effects Aβ toxicity. Surprisingly, increased expression of any of the Hsp20 constructs (including phospho-null) induced significant levels of protection against Aβ toxicity. To explain this, one must consider the peptide array where the introduction of alanine at serine 16 also increases the interaction of Aβ to levels similar to that of S16D. Therefore, increasing levels of Hsp20-S16A within cells would account for its significant levels of protection

The xCELLigence system also permitted dose-response analysis of Aβ's effects on cells. I therefore took advantage of this to compare stable cell-lines I had created that expressed either an empty pcDNA3.1 construct or our Hsp20-WT construct. This assay showed that stable expression of Hsp20-WT induced high levels of phospho-Hsp20 without the need for second messenger pathway activation and resulted in a significant right-shift in the dose-response curve of Aβ toxicity. Although significant increases in protection were observed, they were probably not as striking as anticipated due to SH-SY5Y cells expressing Hsp20 at relatively high levels, a feature that should act to negate any impact of Hsp20 overexpression. Again, the ability to knock-down Hsp20 would have been advantageous in this assay as Hsp20-null cells would be expected to offer less protection against Aβ-induced cytotoxicity, however I failed to find effective siRNA oligonucleotides directed at Hsp20 silencing.

My cell-based assays have allowed me to establish that increased expression of Hsp20 can attenuate the toxic effects of Aβ. This could be attributed to two distinct mechanisms of action, either via the well established anti-apoptotic effects of Hsp20, or through the direct

interaction with intracellular Aβ peptides and the inhibition of cell-death inducing fibrillar out-growth, as described by (Friedrich, Tepper et al. 2010) and (Hu, Crick et al. 2009). Consistently, the wild-type version of Hsp20 outperformed the phospho-mimetic mutant in cell-based assays, suggesting that phosphorylation of Hsp20 is required to fully activate Hsp20's Aβ toxicity attenuating properties.

6.3 Targeting Hsp20 phosphorylation as a therapeutic strategy for treating AD

In AD patients, early signs of mild cognitive impairment (MCI) occur in the absence of clinical signs of brain injury, suggesting some discrete molecule is interrupting synaptic function (Selkoe 2002). Soluble Aβ oligomers have been identified as the causative agent for inducing synaptic dysfunction, which is the early pathological event responsible for MCI (Walsh and Selkoe 2007). Attenuation of synaptic dysfunction has been predicted to have beneficial effects on cognition, and may also help slow progression of the disease (Bales, Plath et al. 2010). AD is a disease of synaptic failure and a hallmark for the latter stages of the disease is major neuronal loss and brain atrophy (Selkoe 1991). As such, considerable focus has been placed on developing therapeutic agents that prevent neuronal death.

The cyclic nucleotide second messenger system is intrinsically involved in synaptic function and has been targeted therapeutically through PDE inhibition in order to improve cognition. Learning and memory processes are thought to be mediated mainly through the phosphorylation of CREB by PKA or PKG, which in turn controls gene expression required to regulate synaptic plasticity (Bales, Plath et al. 2010). Given that PKA and PKG also mediate the phosphorylation of Hsp20, I wanted to ascertain if PDE inhibition could also induce neuroprotection in our cell model of Aβ toxicity. The effect of PDE inhibition on attenuating acute cytotoxicity associated with Aβ has not previously been examined and the underlying mechanisms of how cyclic nucleotide signalling systems can render synapses resistant to neurotoxic insults has yet to be elucidated. Therefore, I wanted to test the theory that Hsp20 phosphorylation is an endogenous mechanism that is up-regulated following PDE inhibition and results in protection against neuronal loss associated with Aβ toxicity.

First of all it was established that all PDE inhibitors could dose-dependently induce Hsp20 phosphorylation in SH-SY5Y cells. Rolipram and sildenafil inducing Hsp20

phosphorylation has previously been established (Beall, Kato et al. 1997). However, I have shown here for the first time that PDE9 inhibition also induces robust and sustained phosphorylation of Hsp20 in neuronal-like cells. I then demonstrated that all of the therapeutic agents that induced Hsp20 phosphorylation also attenuated subsequent Aβ-mediated cytotoxicity. I found good correlation between levels of Hsp20 activation, levels of cytoprotection and levels of induced co-localisation between Hsp20 and the Aβ epitope. However, without being able to measure the cytoprotective effects of PDE inhibition after Hsp20 knock-down I could not prove conclusively that these effects were mediated directly via Hsp20. Nonetheless, the data presented regarding PDE inhibition shows for the first time that these compounds can protect against the acute toxic effects associated with Aβ, making them potential clinical candidates for the treatment of AD.

Unfortunately, the PDE4 inhibitor rolipram has already failed in a clinical setting due to adverse side-effects. This compound has been shown to be effective at treating a number of conditions in animal models of disease, including AD, therefore we wanted to search for another FDA approved compound that could also function as a PDE4 inhibitor but was not associated with adverse side-effects. To do this we carried out an *in silico* screen and identified moexipril, an ACE inhibitor used to treat hypertension. Interestingly, hypertension is a major risk factor for the development of AD. Therefore it would be valuable to know what effect moexipril treatment has on the conversion to AD given that it modestly inhibits PDE4 and can attenuate Aβ-mediated cytotoxicity. Moexipril has also been shown to protect against ischemic brain injury in rodents, which could also be attributed to a protective effect induced via Hsp20 phosphorylation as opposed to a free radical scavenging property described by the authors (Ravati, Junker et al. 1999), given that Hsp20 is emerging as neuroprotective in ischemic/hypoxic conditions in the brain (David, Boelens et al. 2006; Zeng, Tan et al. 2013).

One of the biggest risks with using selective PDE inhibitors as therapeutic agents is that they target all PDE isoforms of that particular family. This is a result of a high degree of similarity of the catalytic unit between family members, a feature that can lead to unwanted side effects via perturbation of off-target pathways. A method for circumventing this issue involves perturbation of an individual PDE isoforms targeting within a cell rather than its activity *per se*. This novel approach has been pioneered by the Baillie group recently, and is described for Hsp20 in the paper by Sin et al. (2011). The report details a direct molecular interaction between Hsp20 and PDE4D5, which is required to mediate the hypertrophic response in cardiomyocytes. Short peptide sequences which act to disrupt the

Hsp20-PDE4D complex removes Hsp20 from the cAMP "sink" surrounding PDE4D5 and leads to more sustained phosphorylation of the chaperone. Due to time constraints, I did not examine the effects of these disruptor peptides in our Aβ toxicity assays and in any event, peptide based therapeutics would have trouble crossing the blood-brain barrier. Nonetheless, this approach provides an exquisite way for selectively targeting Hsp20 phosphorylation to induce its protective functions without the induction of side-effects evoked by active site directed compounds.

6.4 Final Conclusions

The findings presented in my thesis suggest a novel endogenous mechanism that can be manipulated in order to promote protection against Aβ aggregation and toxicity, one of the central features for the onset and progression of AD. The small heat-shock protein, Hsp20 has well established cardio-protective functions that include anti-apoptotic effects and protection against ischemia/reperfusion injury. A key aspect of the protective effects of Hsp20 is that they are induced by the phosphorylation of a serine residue within the N-terminal domain. The phosphorylation of this residue is essential for the anti-apoptotic functions; however, we have uncovered for the first time that phosphorylation at this site also regulates the binding of Hsp20 with the Aβ peptide, and can attenuate Aβ-induced cytotoxicity, which is in agreement with our original hypothesis.

Hsp20 has previously been described by us as a multi-functional protective agent (Edwards, Cameron et al. 2011). Throughout the testing of our hypothesis we have shown that even within the context of AD, Hsp20 is functioning at multiple levels (Fig. 6.1). Firstly, through our NMR (Fig 3.6) and co-immunoprecipitation (Fig. 3.3 & 3.7) experiments I have shown that Hsp20 functions to stabilise Aβ in its monomeric conformation by acting as a classical chaperone to prevent protein mis-folding. Furthermore we demonstrated that this binding/stabilisation can be enhanced through the use of our phospho-mimetic Hsp20-S16D mutant. Secondly, both our peptide array (Fig. 3.2) and NMR (Fig. 3.5) revealed that Hsp20 is interacting with domains involved in the self-association of Aβ, a process that precedes the structural conversion of Aβ into a β-hairpin structure which is essential for fibril elongation. Hsp20 also completely blocked Aβ aggregation into fibrils (Fig 3.9A) and the phospho-mimetic form was able to significantly inhibit oligomeric-like growth (Fig. 3.9B), demonstrating that it is an effective Aβ aggregation inhibitor, that is effective in two distinct Aβ aggregation pathways. Thirdly, we have shown that Hsp20 can attenuate Aβ-induced neuronal cell-death when over-

expressed in neuronal-like SH-SY5Y cells. We suggest that this is mediated through both Hsp20's direct interaction with Aβ and subsequent inhibition of Aβ toxicity and through the activation of Hsp20's potent anti-apoptotic properties. This was particularly evident when we showed that the phospho-mimetic Hsp20 mutant but not the non-phosphorylatable S16A mutant was able to significantly attenuate Aβ-induced cytotoxicity when measured using an MTT based cell viability assay (Fig. 3.11A). Lastly, I developed a novel real-time Aβ toxicity assay which helped to also demonstrate that increasing intracellular levels of phospho-Hsp20 increases protection against Aβ-induced cytotoxicity (Fig. 3.14). Using this platform allowed me to test several compounds which induce Hsp20 phosphorylation resulting in increased cytoprotection. This also demonstrated, for the first time that selective inhibition of PDE9 can significantly induce Hsp20 phosphorylation in neuronal-like cells. To conclude, I believe targeting Hsp20 phosphorylation represents a novel approach to treating AD, through the activation of this endogenous neuroprotective mechanism.

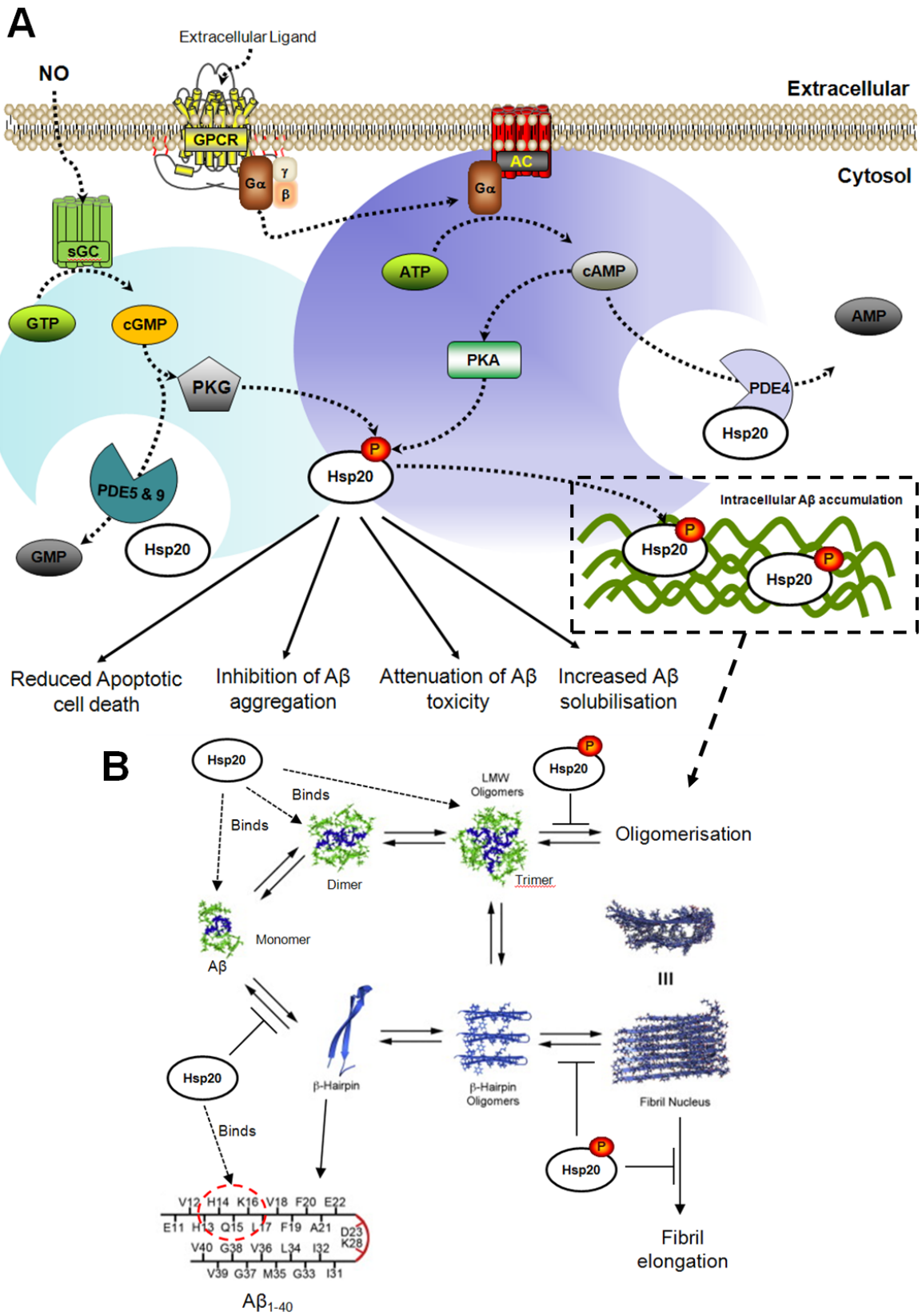

Figure 6.1 – A mechanism by which Hsp20 inhibits Aβ aggregation and attenuates subsequent toxicity.

Cartoon diagram for the mechanism for targeting Hsp20 phosphorylation and its effect on the aggregation dynamics of the Aβ peptide. A - Under normal physiological conditions Hsp20 can be phosphorylated through both cAMP and cGMP second messenger signalling pathways to promote processes such as smooth muscle relaxation and cardiac contractility. I have also demonstrated that increasing Hsp20 phosphorylation either through overexpression or through selective inhibition of PDE4,5 & 9 can significantly attenuate Aβ-induced cytotoxicity. B - Using a variety of protein-protein interaction and Aβ aggregation assays we have shown that Hsp20 binds to monomeric and low molecular weight species of Aβ and functions to keep Aβ in solution and prevent it from

aggregating. Hsp20 binds proximal to the site responsible for the self association of Aβ which is required for oligomerisation and fibril elongation. Using a phospho-mimetic mutant in these various aggregation assays we highlighted how phosphorylation of Hsp20 may improve Hsp20's ability to bind Aβ, inhibit aggregation of Aβ under fibril growing conditions and significantly reduce Aβ oligomerisation. (Figure 6.1B adapted from (Doran, Anderson et al. 2012).

6.5 Limitations & Future Directions

There are several aspects of this thesis that point to limitations within the data/model systems and possible avenues of research that should be pursued further. One of the major limitations was the inability to knock-down Hsp20 using siRNA. I found only one other paper that had managed to accomplish this and it reported an adenovirus containing anti-sense Hsp20 cDNA, which only reduced Hsp20 expression by 40% (Wang, Zingarelli et al. 2009). The recalcitrance to silencing may be due to the high stability of Hsp20, and its ability to exist as high molecular weight aggregates within cells, only to be released upon phosphorylation (van de Klundert, Smulders et al. 1998). Developing viral vectors to knock-down and to over express Hsp20 would also be advantageous given that neuronal-like cells are notoriously difficult to transfect.

Another limitation of the work presented here was the method for aggregating Aβ. I used the ADDL method described by Lambert et al. (1998). The term ADDL is a rather non-specific term and pools together various Aβ species and the exact species which is responsible for toxicity is unknown. However, this is an issue that has plagued the field in general. In this regard, my main priority was to achieve reproducible toxicity between different experimental replicates, a goal which I managed to reach. Ideally, I would have tested the various protocols that exist for aggregating Aβ and validated their toxicity on the xCELLigence platform. The xCELLigence system also provides a co-culture system were effector cells can secrete factors onto underlying target cells. In this type of setup, one could have cells overexpressing APP secreting Aβ onto underlying neurons and monitor the effects in real-time. This would more closely depict what is happening *in vivo*, as opposed to treating cells with micromolar quantities of Aβ.

Another limitation in this body of work was the cell-line that I used. Although SH-SY5Y cells have been utilised extensively in neuronal research, they are a mixed population of cells derived from neuroblastoma cell-lines. Therefore, whether Hsp20 is expressed as abundantly in normal neurons is not known. With the onset of induced pluripotent stem cells, it is now possible to differentiate human neurons from the skin of patients and

undertake cellular assays on them. This system would constitute a highly apt model for testing Hsp20's neuro-protective abilities, though would be beset by numerous ethical and technical difficulties. Another aspect I did not investigate is the effect Hsp20 phosphorylation has on it being secreted from cells. Given that Hsp20 has been shown to co-localise extracellularly with diffuse plaques, it is not know whether this is a result of Hsp20/Aβ complexes being released following necrosis of neurons or whether Hsp20 is being actively secreted as part of a protection mechanism. Hsp20 is known to act extracellularly in response to endothelial injury to regulate platelet function (Kozawa, Matsuno et al. 2002) and more recently Hsp20 has been shown to be secreted via exosomes and promote angiogenesis via activation of VEGFR2 (Zhang, Wang et al. 2012). The latter finding could be particularly significant, as insoluble fibrils are thought to induce hypoxic conditions in underlying neurons. Therefore, mechanisms that increase circulating Hsp20 levels in the brain may also be advantageous.

Having previously mentioned the selective disruption of Hsp20/PDE4D5, it is worthwhile mentioning that I have recently developed a high-throughput screening platform to screen for small molecules that disrupt this interaction. Using fluorescence polarisation I have recently screened a 10,000 compound library and are currently in pursuit of several hits. Albeit, the primary aim of this is to develop a compound that can activate the anti-hypertrophic properties by inducing Hsp20 phosphorylation in the heart. However, if we develop a compound that is able to cross the blood-brain barrier then we would also look to test it in transgenic mouse models of AD, with the expectation that it may prevent progression of the disease.

Another aspect that should be investigated is whether there is a direct interaction between Hsp20 and PDE5 or Hsp20 and PDE9, similar to what we see with PDE4. Hsp20 binds directly to the catalytic domain of PDE4s (Sin, Edwards et al. 2011) and given even across PDE subfamilies there is good conservation it may be possible that Hsp20 binds directly with other PDEs. It would also be worthwhile testing whether there is a synergistic effect of inducing Hsp20 phosphorylation when activating both cAMP and cGMP second messenger pathways. Previous studies have shown that sildenafil can reduce Aβ levels *in vivo* (Puzzo, Vitolo et al. 2005) while rolipram has no effect on Aβ plaque load (Gong, Vitolo et al. 2004). Therefore it would be interesting to note if these PDE inhibitors are activating discrete pools of Hsp20 or the same pool. Finally our studies with PDE9 inhibitors demonstrated for the first time that these compounds can potently induce Hsp20 phosphoryaltion. Given that Hsp20 phosphorylation has recently been shown to protect

against in vitro ischemia/reperfusion injury of mouse neuroblastoma cells and could potentially be targeted therapeutically to treat ischemic stroke (Zeng, Tan et al. 2010; Zeng, Tan et al. 2013) may make PDE9 inhibitors of therapeutic value for other indications requiring Hsp20's protective effects.

7 Appendices

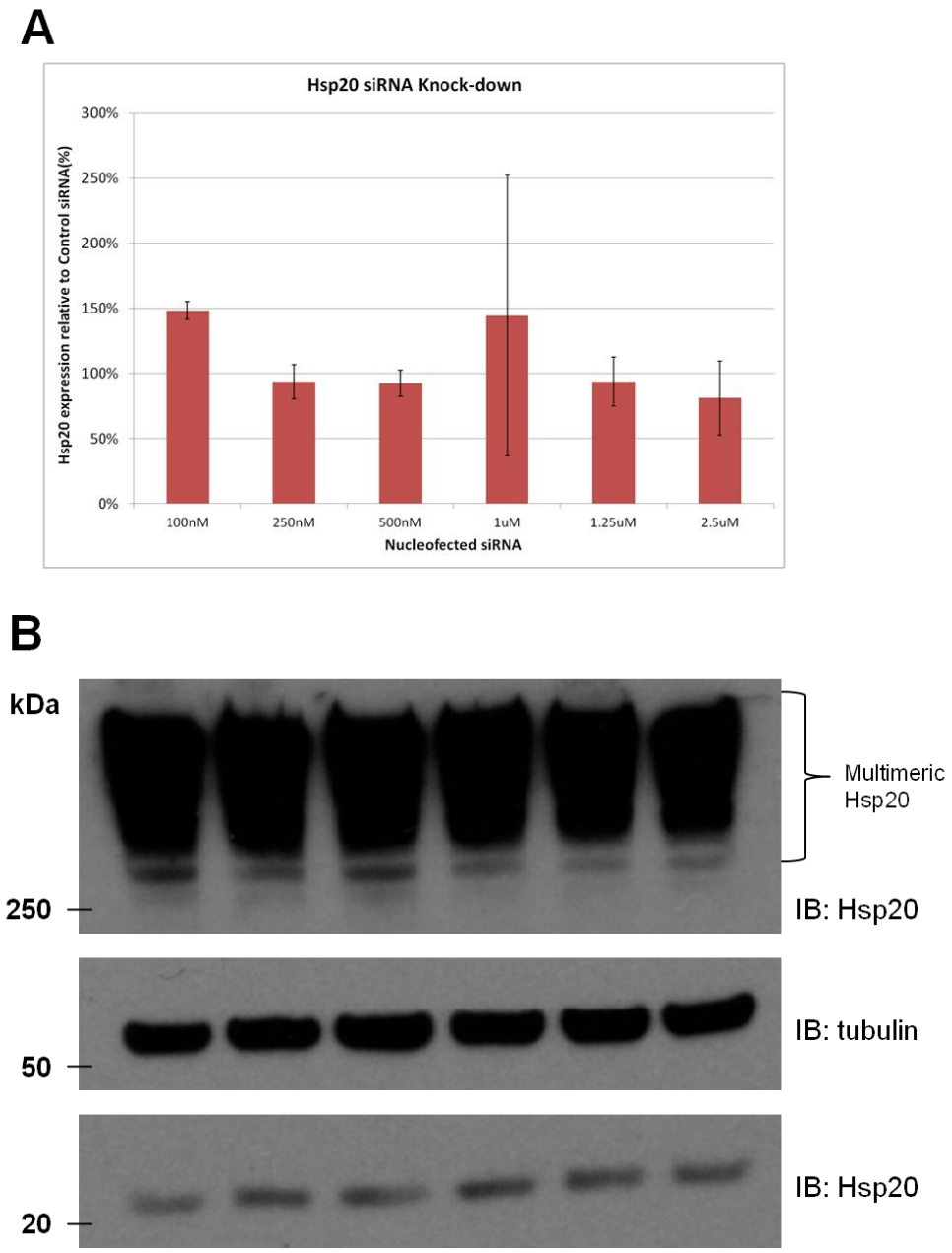

Appendix 1 – siRNA Knock-down of Hsp20 expression
SH-SY5Y cells nucleofected with various concentrations of siRNA that target Hsp20 and incubated for 72 hours. Hsp20 expression was analysed using densitometry with tubulin serving as a loading control. Hsp20 expression was then normalised to SH-SY5Y cells treated with same concentration of control siRNA. A – None of the concentrations of siRNA tested resulted in effective reduction in Hsp20 protein levels. Mean values ±SEM, n = 2. B – In a typical Hsp20 blot high molecular weight bands are always present which are thought to represent large, SDS-stable multimers of Hsp20.

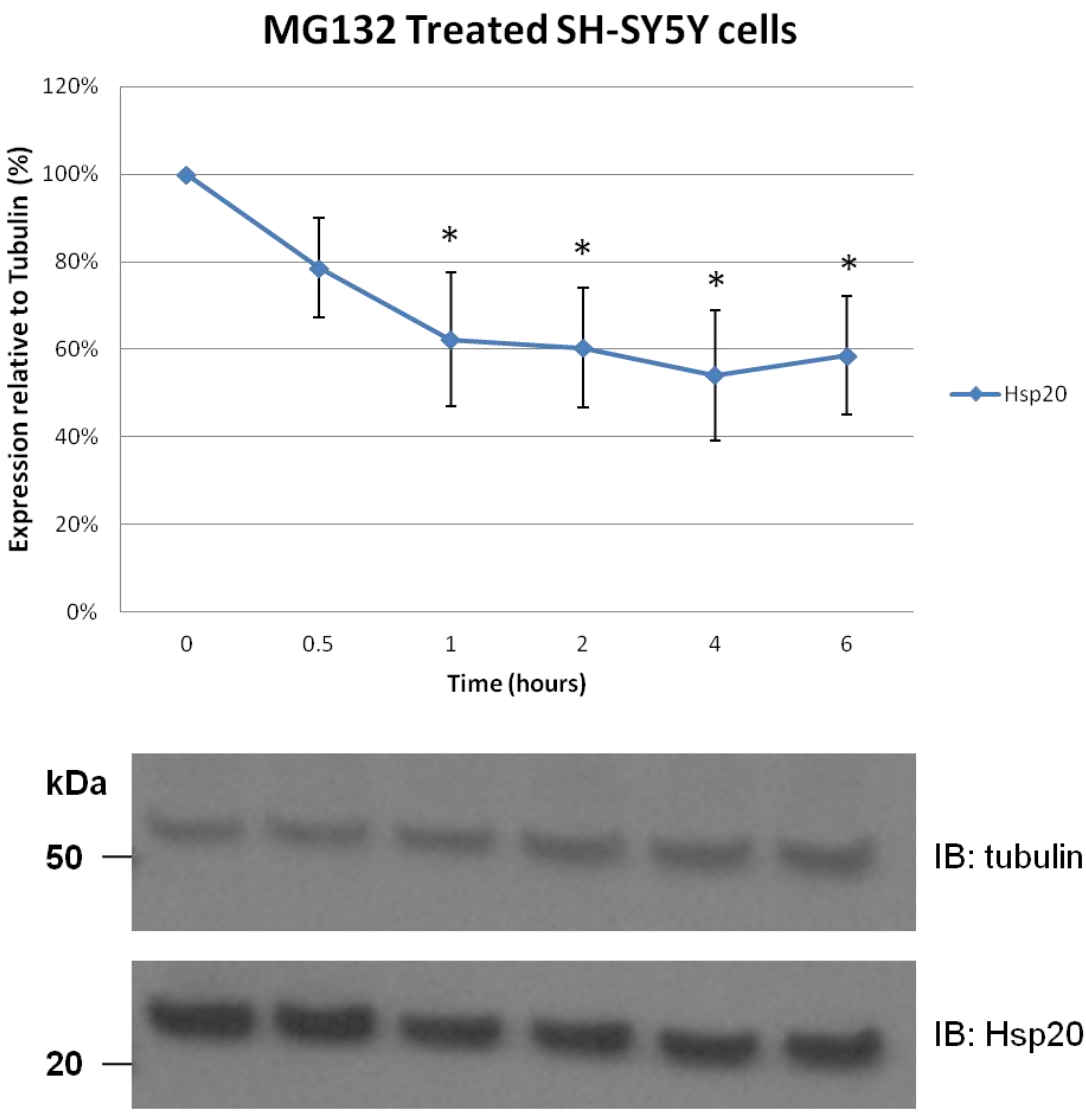

Appendix 2 – MG132 treatment of SH-SY5Y cells
SH-SY5Y cells were treated with 3uM of MG132 over a 6 hour timecourse. MG132 is a 26s proteasome inhibitor which typically leads to a rise in protein levels for proteins regulated via the ubiquitin/proteosomal pathway. I found that Hsp20 levels were in fact significantly reduced after 1 hour of treatment with MG132 and this reduction was sustained over 6 hours. Therefore it is unlikely that Hsp20 levels are regulated via the ubiquitin/proteosomal pathway. Mean values ±SEM, * = *p-value* < 0.05, ANOVA, n = 3.

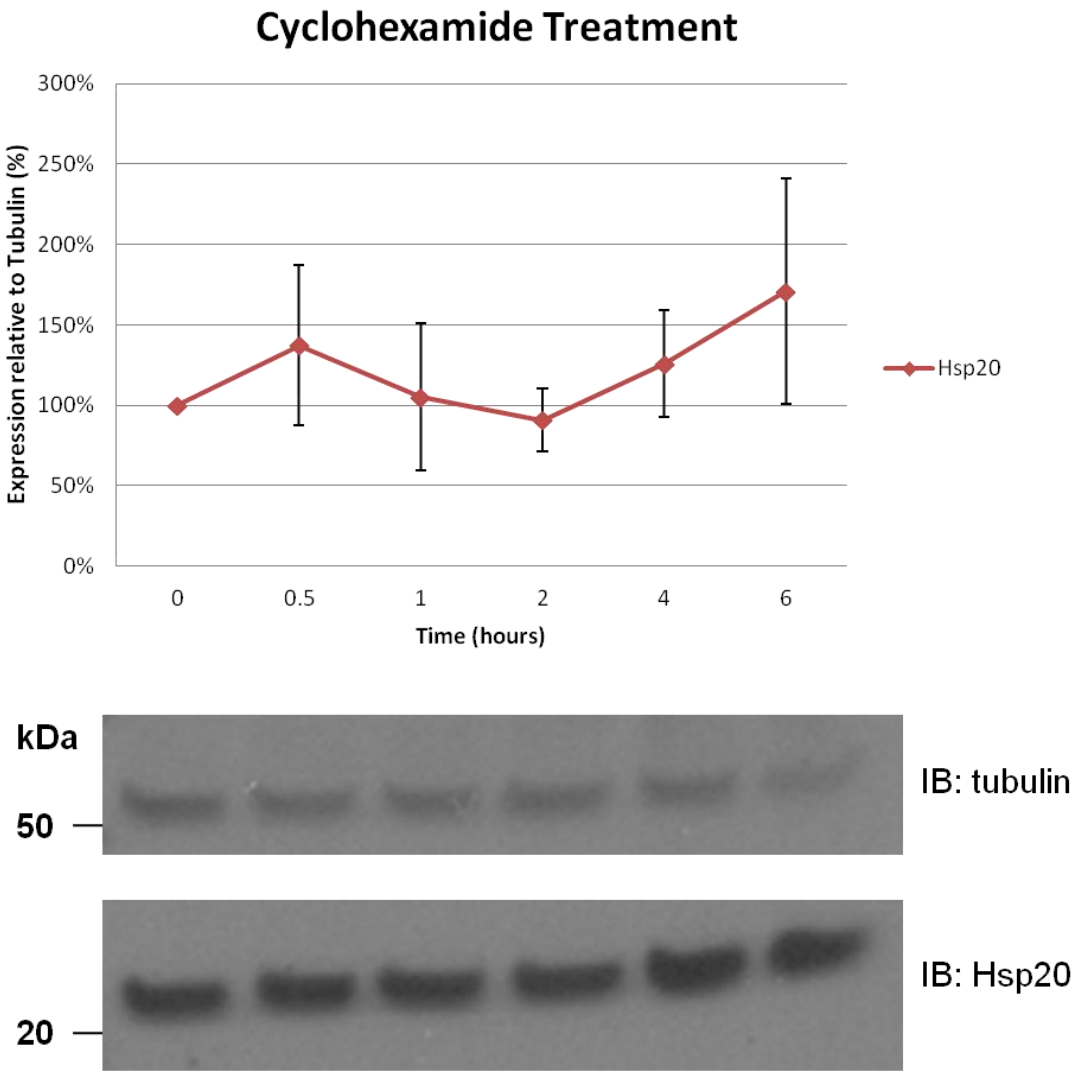

Appendix 3 – Cyclohexamide treatment of SH-SY5Y cells
SH-SY5Y cells were treated with 100uM of cyclohexamide over a 6 hour timecourse. Cyclohexamide is an inhibitor of protein biosynthesis and prevents the expression of new proteins. As there were no significant changes in Hsp20 expression over the 6 hour window suggests that Hsp20 expression is relatively stable. Mean values ±SEM, n = 3.

8 References

Agholme, L., T. Lindstrom, K. Kagedal, J. Marcusson and M. Hallbeck (2010). "An in vitro model for neuroscience: differentiation of SH-SY5Y cells into cells with morphological and biochemical characteristics of mature neurons." J Alzheimers Dis **20**(4): 1069-82.

Ahmed, M., J. Davis, D. Aucoin, T. Sato, S. Ahuja, S. Aimoto, J. I. Elliott, W. E. Van Nostrand and S. O. Smith (2010). "Structural conversion of neurotoxic amyloid-beta(1-42) oligomers to fibrils." Nat Struct Mol Biol **17**(5): 561-7.

Allcock, R. W., H. Blakli, Z. Jiang, K. A. Johnston, K. M. Morgan, G. M. Rosair, K. Iwase, Y. Kohno and D. R. Adams (2011). "Phosphodiesterase inhibitors. Part 1: Synthesis and structure-activity relationships of pyrazolopyridine-pyridazinone PDE inhibitors developed from ibudilast." Bioorg Med Chem Lett **21**(11): 3307-12.

Andreeva, S. G., P. Dikkes, P. M. Epstein and P. A. Rosenberg (2001). "Expression of cGMP-specific phosphodiesterase 9A mRNA in the rat brain." J Neurosci **21**(22): 9068-76.

Ashburn, T. T. and K. B. Thor (2004). "Drug repositioning: identifying and developing new uses for existing drugs." Nat Rev Drug Discov **3**(8): 673-83.

Ashe, K. H. (2005). "Mechanisms of memory loss in Abeta and tau mouse models." Biochem Soc Trans **33**(Pt 4): 591-4.

Baillie, G. S. (2009). "Compartmentalized signalling: spatial regulation of cAMP by the action of compartmentalized phosphodiesterases." FEBS J **276**(7): 1790-9.

Bales K. R., P. N., Svenstrup N., Menniti F.S. (2010). "Phosphodiesterase Inhibition to Target the
Synaptic Dysfunction in Alzheimer's Disease."

Bales, K. R., N. Plath, N. Svenstrup and F. S. Menniti (2010). "Phosphodiesterase Inhibition to Target the
Synaptic Dysfunction in Alzheimer's Disease."

Barad, M., R. Bourtchouladze, D. G. Winder, H. Golan and E. Kandel (1998). "Rolipram, a type IV-specific phosphodiesterase inhibitor, facilitates the establishment of long-lasting long-term potentiation and improves memory." Proc Natl Acad Sci U S A **95**(25): 15020-5.

Baratti, C. M. and M. M. Boccia (1999). "Effects of sildenafil on long-term retention of an inhibitory avoidance response in mice." Behav Pharmacol **10**(8): 731-7.

Beall, A., D. Bagwell, D. Woodrum, T. A. Stoming, K. Kato, A. Suzuki, H. Rasmussen and C. M. Brophy (1999). "The small heat shock-related protein, HSP20, is phosphorylated on serine 16 during cyclic nucleotide-dependent relaxation." J Biol Chem **274**(16): 11344-51.

Beall, A. C., K. Kato, J. R. Goldenring, H. Rasmussen and C. M. Brophy (1997). "Cyclic nucleotide-dependent vasorelaxation is associated with the phosphorylation of a small heat shock-related protein." J Biol Chem **272**(17): 11283-7.

Beavo, J. A. and L. L. Brunton (2002). "Cyclic nucleotide research -- still expanding after half a century." Nat Rev Mol Cell Biol **3**(9): 710-8.

Bender, A. T. and J. A. Beavo (2006). "Cyclic nucleotide phosphodiesterases: molecular regulation to clinical use." Pharmacol Rev **58**(3): 488-520.

Benesch, J. L., M. Ayoub, C. V. Robinson and J. A. Aquilina (2008). "Small heat shock protein activity is regulated by variable oligomeric substructure." J Biol Chem **283**(42): 28513-7.

Bentahir, M., O. Nyabi, J. Verhamme, A. Tolia, K. Horre, J. Wiltfang, H. Esselmann and B. De Strooper (2006). "Presenilin clinical mutations can affect gamma-secretase activity by different mechanisms." J Neurochem **96**(3): 732-42.

Berchtold, N. C. and C. W. Cotman (1998). "Evolution in the conceptualization of dementia and Alzheimer's disease: Greco-Roman period to the 1960s." Neurobiol Aging **19**(3): 173-89.

Beyreuther, K., T. Dyrks, C. Hilbich, U. Monning, G. Konig, G. Multhaup, P. Pollwein and C. L. Masters (1992). "Amyloid precursor protein (APP) and beta A4 amyloid in Alzheimer's disease and Down syndrome." Prog Clin Biol Res **379**: 159-82.

Boncoraglio, A., M. Minoia and S. Carra (2012). "The family of mammalian small heat shock proteins (HSPBs): implications in protein deposit diseases and motor neuropathies." Int J Biochem Cell Biol **44**(10): 1657-69.

Bourtchuladze, R., B. Frenguelli, J. Blendy, D. Cioffi, G. Schutz and A. J. Silva (1994). "Deficient long-term memory in mice with a targeted mutation of the cAMP-responsive element-binding protein." Cell **79**(1): 59-68.

Braak, H. and E. Braak (1991). "Neuropathological stageing of Alzheimer-related changes." Acta Neuropathol **82**(4): 239-59.

Bradford, M. M. (1976). "A rapid and sensitive method for the quantitation of microgram quantities of protein utilizing the principle of protein-dye binding." Anal Biochem **72**: 248-54.

Brownell, S. E., R. A. Becker and L. Steinman (2012). "The protective and therapeutic function of small heat shock proteins in neurological diseases." Front Immunol **3**: 74.

Busciglio, J., A. Lorenzo and B. A. Yankner (1992). "Methodological variables in the assessment of beta amyloid neurotoxicity." Neurobiol Aging **13**(5): 609-12.

Byrne, J. H. and E. R. Kandel (1996). "Presynaptic facilitation revisited: state and time dependence." J Neurosci **16**(2): 425-35.

Calabrese, V., C. Mancuso, M. Calvani, E. Rizzarelli, D. A. Butterfield and A. M. Stella (2007). "Nitric oxide in the central nervous system: neuroprotection versus neurotoxicity." Nat Rev Neurosci **8**(10): 766-75.

Cameron, R. T., R. G. Coleman, J. P. Day, K. C. Yalla, M. D. Houslay, D. R. Adams, B. K. Shoichet and G. S. Baillie (2013). "Chemical informatics uncovers a new role for moexipril as a novel inhibitor of cAMP phosphodiesterase-4 (PDE4)." Biochem Pharmacol **85**(9): 1297-305.

Card, G. L., B. P. England, Y. Suzuki, D. Fong, B. Powell, B. Lee, C. Luu, M. Tabrizizad, S. Gillette, P. N. Ibrahim, D. R. Artis, G. Bollag, M. V. Milburn, S. H. Kim, J. Schlessinger and K. Y. Zhang (2004). "Structural basis for the activity of drugs that inhibit phosphodiesterases." Structure **12**(12): 2233-47.

Carra, S., J. F. Brunsting, H. Lambert, J. Landry and H. H. Kampinga (2009). "HspB8 participates in protein quality control by a non-chaperone-like mechanism that requires eIF2{alpha} phosphorylation." J Biol Chem **284**(9): 5523-32.

Carter, M. D., G. A. Simms and D. F. Weaver (2010). "The development of new therapeutics for Alzheimer's disease." Clin Pharmacol Ther **88**(4): 475-86.

Chen, J., M. J. Feige, T. M. Franzmann, A. Bepperling and J. Buchner (2010). "Regions outside the alpha-crystallin domain of the small heat shock protein Hsp26 are required for its dimerization." J Mol Biol **398**(1): 122-31.

Chen, R. W., A. J. Williams, Z. Liao, C. Yao, F. C. Tortella and J. R. Dave (2007). "Broad spectrum neuroprotection profile of phosphodiesterase inhibitors as related to modulation of cell-cycle elements and caspase-3 activation." Neurosci Lett **418**(2): 165-9.

Cheng, Y. F., C. Wang, H. B. Lin, Y. F. Li, Y. Huang, J. P. Xu and H. T. Zhang (2010). "Inhibition of phosphodiesterase-4 reverses memory deficits produced by Abeta25-35 or Abeta1-40 peptide in rats." Psychopharmacology (Berl) **212**(2): 181-91.

Chiti, F. and C. M. Dobson (2006). "Protein misfolding, functional amyloid, and human disease." Annu Rev Biochem **75**: 333-66.

Christensen, S. B., A. Guider, C. J. Forster, J. G. Gleason, P. E. Bender, J. M. Karpinski, W. E. DeWolf, Jr., M. S. Barnette, D. C. Underwood, D. E. Griswold, L. B. Cieslinski, M. Burman, S. Bochnowicz, R. R. Osborn, C. D. Manning, M. Grous, L. M. Hillegas, J. O. Bartus, M. D. Ryan, D. S. Eggleston, R. C. Haltiwanger and T. J. Torphy (1998). "1,4-Cyclohexanecarboxylates: potent and selective inhibitors of phosophodiesterase 4 for the treatment of asthma." J Med Chem **41**(6): 821-35.

Chrysant, S. G. and G. S. Chrysant (2003). "Pharmacological profile and clinical use of moexipril." Expert Rev Cardiovasc Ther **1**(3): 345-52.

Citron, M., C. Vigo-Pelfrey, D. B. Teplow, C. Miller, D. Schenk, J. Johnston, B. Winblad, N. Venizelos, L. Lannfelt and D. J. Selkoe (1994). "Excessive production of amyloid beta-protein by peripheral cells of symptomatic and presymptomatic patients carrying the Swedish familial Alzheimer disease mutation." Proc Natl Acad Sci U S A **91**(25): 11993-7.

Citron, M., D. Westaway, W. Xia, G. Carlson, T. Diehl, G. Levesque, K. Johnson-Wood, M. Lee, P. Seubert, A. Davis, D. Kholodenko, R. Motter, R. Sherrington, B. Perry, H. Yao, R. Strome, I. Lieberburg, J. Rommens, S. Kim, D. Schenk, P. Fraser, P. St George Hyslop and D. J. Selkoe (1997). "Mutant presenilins of Alzheimer's disease increase production of 42-residue amyloid beta-protein in both transfected cells and transgenic mice." Nat Med **3**(1): 67-72.

Conti, M. and J. Beavo (2007). "Biochemistry and physiology of cyclic nucleotide phosphodiesterases: essential components in cyclic nucleotide signaling." Annu Rev Biochem **76**: 481-511.

Costa, D. A., J. R. Cracchiolo, A. D. Bachstetter, T. F. Hughes, K. R. Bales, S. M. Paul, R. F. Mervis, G. W. Arendash and H. Potter (2007). "Enrichment improves cognition in AD mice by amyloid-related and unrelated mechanisms." Neurobiol Aging **28**(6): 831-44.

Cullen, W. K., Y. H. Suh, R. Anwyl and M. J. Rowan (1997). "Block of LTP in rat hippocampus in vivo by beta-amyloid precursor protein fragments." Neuroreport **8**(15): 3213-7.

Datki, Z., A. Juhasz, M. Galfi, K. Soos, R. Papp, D. Zadori and B. Penke (2003). "Method for measuring neurotoxicity of aggregating polypeptides with the MTT assay on differentiated neuroblastoma cells." Brain Res Bull **62**(3): 223-9.

David, J. C., W. C. Boelens and J. F. Grongnet (2006). "Up-regulation of heat shock protein HSP 20 in the hippocampus as an early response to hypoxia of the newborn." J Neurochem **99**(2): 570-81.

De Jonghe, C., C. Esselens, S. Kumar-Singh, K. Craessaerts, S. Serneels, F. Checler, W. Annaert, C. Van Broeckhoven and B. De Strooper (2001). "Pathogenic APP mutations near the gamma-secretase cleavage site differentially affect Abeta secretion and APP C-terminal fragment stability." Hum Mol Genet **10**(16): 1665-71.

De Jonghe, C., C. Zehr, D. Yager, C. M. Prada, S. Younkin, L. Hendriks, C. Van Broeckhoven and C. B. Eckman (1998). "Flemish and Dutch mutations in amyloid beta precursor protein have different effects on amyloid beta secretion." Neurobiol Dis **5**(4): 281-6.

DeGraw, A. J., M. J. Keiser, J. D. Ochocki, B. K. Shoichet and M. D. Distefano (2010). "Prediction and evaluation of protein farnesyltransferase inhibition by commercial drugs." J Med Chem **53**(6): 2464-71.

DeKosky, S. T. and S. W. Scheff (1990). "Synapse loss in frontal cortex biopsies in Alzheimer's disease: correlation with cognitive severity." Ann Neurol **27**(5): 457-64.

Deshpande, A., E. Mina, C. Glabe and J. Busciglio (2006). "Different conformations of amyloid beta induce neurotoxicity by distinct mechanisms in human cortical neurons." J Neurosci **26**(22): 6011-8.

Diaz, J. C., J. Linnehan, H. Pollard and N. Arispe (2006). "Histidines 13 and 14 in the Abeta sequence are targets for inhibition of Alzheimer's disease Abeta ion channel and cytotoxicity." Biol Res **39**(3): 447-60.

Dickson, D. W., H. A. Crystal, C. Bevona, W. Honer, I. Vincent and P. Davies (1995). "Correlations of synaptic and pathological markers with cognition of the elderly." Neurobiol Aging **16**(3): 285-98; discussion 298-304.

Diemert, S., A. M. Dolga, S. Tobaben, J. Grohm, S. Pfeifer, E. Oexler and C. Culmsee (2012). "Impedance measurement for real time detection of neuronal cell death." J Neurosci Methods **203**(1): 69-77.

Doran, T. M., E. A. Anderson, S. E. Latchney, L. A. Opanashuk and B. L. Nilsson (2012). "Turn nucleation perturbs amyloid beta self-assembly and cytotoxicity." J Mol Biol **421**(2-3): 315-28.

Dostmann, W. R., C. Nickl, S. Thiel, I. Tsigelny, R. Frank and W. J. Tegge (1999). "Delineation of selective cyclic GMP-dependent protein kinase Ialpha substrate and inhibitor peptides based on combinatorial peptide libraries on paper." Pharmacol Ther **82**(2-3): 373-87.

Dreiza, C. M., C. M. Brophy, P. Komalavilas, E. J. Furnish, L. Joshi, M. A. Pallero, J. E. Murphy-Ullrich, M. von Rechenberg, Y. S. Ho, B. Richardson, N. Xu, Y. Zhen, J. M. Peltier and A. Panitch (2005). "Transducible heat shock protein 20 (HSP20) phosphopeptide alters cytoskeletal dynamics." FASEB J **19**(2): 261-3.

Dudai, Y., Y. N. Jan, D. Byers, W. G. Quinn and S. Benzer (1976). "dunce, a mutant of Drosophila deficient in learning." Proc Natl Acad Sci U S A **73**(5): 1684-8.

Ecroyd, H. and J. A. Carver (2009). "Crystallin proteins and amyloid fibrils." Cell Mol Life Sci **66**(1): 62-81.

Edwards, H. V., R. T. Cameron and G. S. Baillie (2011). "The emerging role of HSP20 as a multifunctional protective agent." Cell Signal **23**(9): 1447-54.

Edwards, H. V., J. D. Scott and G. S. Baillie (2012). "The A-kinase-anchoring protein AKAP-Lbc facilitates cardioprotective PKA phosphorylation of Hsp20 on Ser(16)." Biochem J **446**(3): 437-43.

Edwards, H. V., J. D. Scott and G. S. Baillie (2012). "PKA phosphorylation of the small heat-shock protein Hsp20 enhances its cardioprotective effects." Biochem Soc Trans **40**(1): 210-4.

Eyles, S. J. and L. M. Gierasch (2010). "Nature's molecular sponges: small heat shock proteins grow into their chaperone roles." Proc Natl Acad Sci U S A **107**(7): 2727-8.

Fabbri, L. M., B. Beghe, U. Yasothan and P. Kirkpatrick (2010). "Roflumilast." Nat Rev Drug Discov **9**(10): 761-2.

Fan, G. C., G. Chu, B. Mitton, Q. Song, Q. Yuan and E. G. Kranias (2004). "Small heat-shock protein Hsp20 phosphorylation inhibits beta-agonist-induced cardiac apoptosis." Circ Res **94**(11): 1474-82.

Fan, G. C. and E. G. Kranias (2010). "Small heat shock protein 20 (HspB6) in cardiac hypertrophy and failure." J Mol Cell Cardiol.

Fan, G. C. and E. G. Kranias (2011). "Small heat shock protein 20 (HspB6) in cardiac hypertrophy and failure." J Mol Cell Cardiol **51**(4): 574-7.

Fan, G. C., X. Ren, J. Qian, Q. Yuan, P. Nicolaou, Y. Wang, W. K. Jones, G. Chu and E. G. Kranias (2005). "Novel cardioprotective role of a small heat-shock protein, Hsp20, against ischemia/reperfusion injury." Circulation **111**(14): 1792-9.

Fan, G. C., Q. Yuan, G. Song, Y. Wang, G. Chen, J. Qian, X. Zhou, Y. J. Lee, M. Ashraf and E. G. Kranias (2006). "Small heat-shock protein Hsp20 attenuates beta-agonist-mediated cardiac remodeling through apoptosis signal-regulating kinase 1." Circ Res **99**(11): 1233-42.

Fan, G. C., X. Zhou, X. Wang, G. Song, J. Qian, P. Nicolaou, G. Chen, X. Ren and E. G. Kranias (2008). "Heat shock protein 20 interacting with phosphorylated Akt

reduces doxorubicin-triggered oxidative stress and cardiotoxicity." Circ Res **103**(11): 1270-9.
Fisher, D. A., J. F. Smith, J. S. Pillar, S. H. St Denis and J. B. Cheng (1998). "Isolation and characterization of PDE9A, a novel human cGMP-specific phosphodiesterase." J Biol Chem **273**(25): 15559-64.
Flynn, C. R., C. M. Brophy, E. J. Furnish, P. Komalavilas, D. Tessier, J. Thresher and L. Joshi (2005). "Transduction of phosphorylated heat shock-related protein 20, HSP20, prevents vasospasm of human umbilical artery smooth muscle." J Appl Physiol **98**(5): 1836-45.
Fonte, V., W. J. Kapulkin, A. Taft, A. Fluet, D. Friedman and C. D. Link (2002). "Interaction of intracellular beta amyloid peptide with chaperone proteins." Proc Natl Acad Sci U S A **99**(14): 9439-44.
Fonte, V., D. R. Kipp, J. Yerg, 3rd, D. Merin, M. Forrestal, E. Wagner, C. M. Roberts and C. D. Link (2008). "Suppression of in vivo beta-amyloid peptide toxicity by overexpression of the HSP-16.2 small chaperone protein." J Biol Chem **283**(2): 784-91.
Francis, S. H., J. L. Busch, J. D. Corbin and D. Sibley (2010). "cGMP-dependent protein kinases and cGMP phosphodiesterases in nitric oxide and cGMP action." Pharmacol Rev **62**(3): 525-63.
Frank, R. (2002). "The SPOT-synthesis technique. Synthetic peptide arrays on membrane supports--principles and applications." J Immunol Methods **267**(1): 13-26.
Frey, U., Y. Y. Huang and E. R. Kandel (1993). "Effects of cAMP simulate a late stage of LTP in hippocampal CA1 neurons." Science **260**(5114): 1661-4.
Friedrich, R. P., K. Tepper, R. Ronicke, M. Soom, M. Westermann, K. Reymann, C. Kaether and M. Fandrich (2010). "Mechanism of amyloid plaque formation suggests an intracellular basis of Abeta pathogenicity." Proc Natl Acad Sci U S A **107**(5): 1942-7.
Fuchs, M., D. J. Poirier, S. J. Seguin, H. Lambert, S. Carra, S. J. Charette and J. Landry (2010). "Identification of the key structural motifs involved in HspB8/HspB6-Bag3 interaction." Biochem J **425**(1): 245-55.
Furnish, E. J., C. M. Brophy, V. A. Harris, S. Macomson, J. Winger, G. A. Head and E. G. Shaver (2010). "Treatment with transducible phosphopeptide analogues of the small heat shock-related protein, HSP20, after experimental subarachnoid hemorrhage: prevention and reversal of delayed decreases in cerebral perfusion." J Neurosurg **112**(3): 631-9.
Garrido, C., C. Paul, R. Seigneuric and H. H. Kampinga (2012). "The small heat shock proteins family: the long forgotten chaperones." Int J Biochem Cell Biol **44**(10): 1588-92.
Gaulton, A., L. J. Bellis, A. P. Bento, J. Chambers, M. Davies, A. Hersey, Y. Light, S. McGlinchey, D. Michalovich, B. Al-Lazikani and J. P. Overington (2011). "ChEMBL: a large-scale bioactivity database for drug discovery." Nucleic Acids Res **40**(Database issue): D1100-7.
Ge, J. F., J. P. Qiao, C. C. Qi, C. W. Wang and J. N. Zhou (2012). "The binding of resveratrol to monomer and fibril amyloid beta." Neurochem Int **61**(7): 1192-201.
Gibson, L. C., S. F. Hastings, I. McPhee, R. A. Clayton, C. E. Darroch, A. Mackenzie, F. L. Mackenzie, M. Nagasawa, P. A. Stevens and S. J. Mackenzie (2006). "The inhibitory profile of Ibudilast against the human phosphodiesterase enzyme family." Eur J Pharmacol **538**(1-3): 39-42.
Giembycz, M. A. (2001). "Cilomilast: a second generation phosphodiesterase 4 inhibitor for asthma and chronic obstructive pulmonary disease." Expert Opin Investig Drugs **10**(7): 1361-79.
Gilbert, B. J. (2013). "The role of amyloid beta in the pathogenesis of Alzheimer's disease." J Clin Pathol **66**(5): 362-6.

Glenner, G. G. and C. W. Wong (1984). "Alzheimer's disease and Down's syndrome: sharing of a unique cerebrovascular amyloid fibril protein." Biochem Biophys Res Commun **122**(3): 1131-5.

Glenner, G. G. and C. W. Wong (1984). "Alzheimer's disease: initial report of the purification and characterization of a novel cerebrovascular amyloid protein." Biochem Biophys Res Commun **120**(3): 885-90.

Goate, A., M. C. Chartier-Harlin, M. Mullan, J. Brown, F. Crawford, L. Fidani, L. Giuffra, A. Haynes, N. Irving, L. James and et al. (1991). "Segregation of a missense mutation in the amyloid precursor protein gene with familial Alzheimer's disease." Nature **349**(6311): 704-6.

Goedert, M., C. M. Wischik, R. A. Crowther, J. E. Walker and A. Klug (1988). "Cloning and sequencing of the cDNA encoding a core protein of the paired helical filament of Alzheimer disease: identification as the microtubule-associated protein tau." Proc Natl Acad Sci U S A **85**(11): 4051-5.

Goldgaber, D., M. I. Lerman, O. W. McBride, U. Saffiotti and D. C. Gajdusek (1987). "Characterization and chromosomal localization of a cDNA encoding brain amyloid of Alzheimer's disease." Science **235**(4791): 877-80.

Goldsbury, C., U. Baxa, M. N. Simon, A. C. Steven, A. Engel, J. S. Wall, U. Aebi and S. A. Muller (2011). "Amyloid structure and assembly: insights from scanning transmission electron microscopy." J Struct Biol **173**(1): 1-13.

Gong, B., O. V. Vitolo, F. Trinchese, S. Liu, M. Shelanski and O. Arancio (2004). "Persistent improvement in synaptic and cognitive functions in an Alzheimer mouse model after rolipram treatment." J Clin Invest **114**(11): 1624-34.

Gouras, G. K., J. Tsai, J. Naslund, B. Vincent, M. Edgar, F. Checler, J. P. Greenfield, V. Haroutunian, J. D. Buxbaum, H. Xu, P. Greengard and N. R. Relkin (2000). "Intraneuronal Abeta42 accumulation in human brain." Am J Pathol **156**(1): 15-20.

Grabowski, T. J., H. S. Cho, J. P. Vonsattel, G. W. Rebeck and S. M. Greenberg (2001). "Novel amyloid precursor protein mutation in an Iowa family with dementia and severe cerebral amyloid angiopathy." Ann Neurol **49**(6): 697-705.

Gu, L. and R. G. Strickley (1987). "Diketopiperazine formation, hydrolysis, and epimerization of the new dipeptide angiotensin-converting enzyme inhibitor RS-10085." Pharm Res **4**(5): 392-7.

Gupta, S. (2012). "Side-effects of roflumilast." Lancet **379**(9817): 710-1; author reply 711-2.

Haass, C., A. Y. Hung, D. J. Selkoe and D. B. Teplow (1994). "Mutations associated with a locus for familial Alzheimer's disease result in alternative processing of amyloid beta-protein precursor." J Biol Chem **269**(26): 17741-8.

Haass, C., C. A. Lemere, A. Capell, M. Citron, P. Seubert, D. Schenk, L. Lannfelt and D. J. Selkoe (1995). "The Swedish mutation causes early-onset Alzheimer's disease by beta-secretase cleavage within the secretory pathway." Nat Med **1**(12): 1291-6.

Halene, T. B. and S. J. Siegel (2007). "PDE inhibitors in psychiatry--future options for dementia, depression and schizophrenia?" Drug Discov Today **12**(19-20): 870-8.

Hardy, J. (2009). "The amyloid hypothesis for Alzheimer's disease: a critical reappraisal." J Neurochem **110**(4): 1129-34.

Hardy, J. and D. Allsop (1991). "Amyloid deposition as the central event in the aetiology of Alzheimer's disease." Trends Pharmacol Sci **12**(10): 383-8.

Hardy, J. and D. J. Selkoe (2002). "The amyloid hypothesis of Alzheimer's disease: progress and problems on the road to therapeutics." Science **297**(5580): 353-6.

Harrison, R. S., P. C. Sharpe, Y. Singh and D. P. Fairlie (2007). "Amyloid peptides and proteins in review." Rev Physiol Biochem Pharmacol **159**: 1-77.

Haslbeck, M. (2002). "sHsps and their role in the chaperone network." Cell Mol Life Sci **59**(10): 1649-57.

Haslbeck, M., T. Franzmann, D. Weinfurtner and J. Buchner (2005). "Some like it hot: the structure and function of small heat-shock proteins." Nat Struct Mol Biol **12**(10): 842-6.
He, P., X. Cheng, M. Staufenbiel, R. Li and Y. Shen (2013). "Long-term treatment of thalidomide ameliorates amyloid-like pathology through inhibition of beta-secretase in a mouse model of Alzheimer's disease." PLoS One **8**(2): e55091.
Hendriks, L., C. M. van Duijn, P. Cras, M. Cruts, W. Van Hul, F. van Harskamp, A. Warren, M. G. McInnis, S. E. Antonarakis, J. J. Martin and et al. (1992). "Presenile dementia and cerebral haemorrhage linked to a mutation at codon 692 of the beta-amyloid precursor protein gene." Nat Genet **1**(3): 218-21.
Hert, J., M. J. Keiser, J. J. Irwin, T. I. Oprea and B. K. Shoichet (2008). "Quantifying the relationships among drug classes." J Chem Inf Model **48**(4): 755-65.
Hilbich, C., B. Kisters-Woike, J. Reed, C. L. Masters and K. Beyreuther (1991). "Human and rodent sequence analogs of Alzheimer's amyloid beta A4 share similar properties and can be solubilized in buffers of pH 7.4." Eur J Biochem **201**(1): 61-9.
Hilbich, C., B. Kisters-Woike, J. Reed, C. L. Masters and K. Beyreuther (1992). "Substitutions of hydrophobic amino acids reduce the amyloidogenicity of Alzheimer's disease beta A4 peptides." J Mol Biol **228**(2): 460-73.
Hlaing, S. M., L. A. Garcia, I. Kovanecz, R. A. Martinez, S. Shah, J. N. Artaza and M. G. Ferrini (2012). "Sildenafil promotes neuroprotection of the pelvic ganglia neurones after bilateral cavernosal nerve resection in the rat." BJU Int **111**(1): 159-70.
Holtmann, G., N. J. Talley, T. Liebregts, B. Adam and C. Parow (2006). "A placebo-controlled trial of itopride in functional dyspepsia." N Engl J Med **354**(8): 832-40.
Horwitz, J. (2003). "Alpha-crystallin." Exp Eye Res **76**(2): 145-53.
Hoshi, M., M. Sato, S. Matsumoto, A. Noguchi, K. Yasutake, N. Yoshida and K. Sato (2003). "Spherical aggregates of beta-amyloid (amylospheroid) show high neurotoxicity and activate tau protein kinase I/glycogen synthase kinase-3beta." Proc Natl Acad Sci U S A **100**(11): 6370-5.
Hou, L., H. Shao, Y. Zhang, H. Li, N. K. Menon, E. B. Neuhaus, J. M. Brewer, I. J. Byeon, D. G. Ray, M. P. Vitek, T. Iwashita, R. A. Makula, A. B. Przybyla and M. G. Zagorski (2004). "Solution NMR studies of the A beta(1-40) and A beta(1-42) peptides establish that the Met35 oxidation state affects the mechanism of amyloid formation." J Am Chem Soc **126**(7): 1992-2005.
Houslay, M. D. (2009). "Underpinning compartmentalised cAMP signalling through targeted cAMP breakdown." Trends Biochem Sci **35**(2): 91-100.
Houslay, M. D., G. S. Baillie and D. H. Maurice (2007). "cAMP-Specific phosphodiesterase-4 enzymes in the cardiovascular system: a molecular toolbox for generating compartmentalized cAMP signaling." Circ Res **100**(7): 950-66.
Houslay, M. D., P. Schafer and K. Y. Zhang (2005). "Keynote review: phosphodiesterase-4 as a therapeutic target." Drug Discov Today **10**(22): 1503-19.
Howie, A. J. and D. B. Brewer (2009). "Optical properties of amyloid stained by Congo red: history and mechanisms." Micron **40**(3): 285-301.
Hsu, Y. Y., C. M. Liu, H. H. Tsai, Y. J. Jong, I. J. Chen and Y. C. Lo (2010). "KMUP-1 attenuates serum deprivation-induced neurotoxicity in SH-SY5Y cells: roles of PKG, PI3K/Akt and Bcl-2/Bax pathways." Toxicology **268**(1-2): 46-54.
Hu, X., S. L. Crick, G. Bu, C. Frieden, R. V. Pappu and J. M. Lee (2009). "Amyloid seeds formed by cellular uptake, concentration, and aggregation of the amyloid-beta peptide." Proc Natl Acad Sci U S A **106**(48): 20324-9.
Huai, Q., Y. Sun, H. Wang, D. Macdonald, R. Aspiotis, H. Robinson, Z. Huang and H. Ke (2006). "Enantiomer discrimination illustrated by the high resolution crystal structures of type 4 phosphodiesterase." J Med Chem **49**(6): 1867-73.

Ingolia, T. D. and E. A. Craig (1982). "Four small Drosophila heat shock proteins are related to each other and to mammalian alpha-crystallin." Proc Natl Acad Sci U S A **79**(7): 2360-4.
Irwin, J. J., B. K. Shoichet, M. M. Mysinger, N. Huang, F. Colizzi, P. Wassam and Y. Cao (2009). "Automated Docking Screens: A Feasibility Study." Journal of Medicinal Chemistry **52**(18): 5712-5720.
Irwin, J. J., B. K. Shoichet, M. M. Mysinger, N. Huang, F. Colizzi, P. Wassam and Y. Cao (2009). "Automated docking screens: a feasibility study." J Med Chem **52**(18): 5712-20.
Irwin, J. J., T. Sterling, M. M. Mysinger, E. S. Bolstad and R. G. Coleman (2012). "ZINC: A Free Tool to Discover Chemistry for Biology." Journal of Chemical Information and Modeling **52**(7): 1757-1768.
Itoh, A., T. Akaike, M. Sokabe, A. Nitta, R. Iida, A. Olariu, K. Yamada and T. Nabeshima (1999). "Impairments of long-term potentiation in hippocampal slices of beta-amyloid-infused rats." Eur J Pharmacol **382**(3): 167-75.
Iwaki, T., A. Iwaki, J. Tateishi and J. E. Goldman (1994). "Sense and antisense modification of glial alpha B-crystallin production results in alterations of stress fiber formation and thermoresistance." J Cell Biol **125**(6): 1385-93.
Iwata, N., M. Higuchi and T. C. Saido (2005). "Metabolism of amyloid-beta peptide and Alzheimer's disease." Pharmacol Ther **108**(2): 129-48.
Jakob, U., M. Gaestel, K. Engel and J. Buchner (1993). "Small heat shock proteins are molecular chaperones." J Biol Chem **268**(3): 1517-20.
Jan, A., D. M. Hartley and H. A. Lashuel (2010). "Preparation and characterization of toxic Abeta aggregates for structural and functional studies in Alzheimer's disease research." Nat Protoc **5**(6): 1186-209.
Kamino, K., H. T. Orr, H. Payami, E. M. Wijsman, M. E. Alonso, S. M. Pulst, L. Anderson, S. O'Dahl, E. Nemens, J. A. White and et al. (1992). "Linkage and mutational analysis of familial Alzheimer disease kindreds for the APP gene region." Am J Hum Genet **51**(5): 998-1014.
Kampinga, H. H. and C. Garrido (2012). "HSPBs: small proteins with big implications in human disease." Int J Biochem Cell Biol **44**(10): 1706-10.
Kang, J., H. G. Lemaire, A. Unterbeck, J. M. Salbaum, C. L. Masters, K. H. Grzeschik, G. Multhaup, K. Beyreuther and B. Muller-Hill (1987). "The precursor of Alzheimer's disease amyloid A4 protein resembles a cell-surface receptor." Nature **325**(6106): 733-6.
Kappe, G., E. Franck, P. Verschuure, W. C. Boelens, J. A. Leunissen and W. W. de Jong (2003). "The human genome encodes 10 alpha-crystallin-related small heat shock proteins: HspB1-10." Cell Stress Chaperones **8**(1): 53-61.
Kappe, G., P. Verschuure, R. L. Philipsen, A. A. Staalduinen, P. Van de Boogaart, W. C. Boelens and W. W. De Jong (2001). "Characterization of two novel human small heat shock proteins: protein kinase-related HspB8 and testis-specific HspB9." Biochim Biophys Acta **1520**(1): 1-6.
Kato, K., S. Goto, Y. Inaguma, K. Hasegawa, R. Morishita and T. Asano (1994). "Purification and characterization of a 20-kDa protein that is highly homologous to alpha B crystallin." J Biol Chem **269**(21): 15302-9.
Katz, C., L. Levy-Beladev, S. Rotem-Bamberger, T. Rito, S. G. Rudiger and A. Friedler (2011). "Studying protein-protein interactions using peptide arrays." Chem Soc Rev **40**(5): 2131-45.
Katzman, R. (1986). "Alzheimer's disease." N Engl J Med **314**(15): 964-73.
Kayed, R., E. Head, J. L. Thompson, T. M. McIntire, S. C. Milton, C. W. Cotman and C. G. Glabe (2003). "Common structure of soluble amyloid oligomers implies common mechanism of pathogenesis." Science **300**(5618): 486-9.

Keiser, M. J., B. L. Roth, B. N. Armbruster, P. Ernsberger, J. J. Irwin and B. K. Shoichet (2007). "Relating protein pharmacology by ligand chemistry." Nat Biotechnol **25**(2): 197-206.

Keiser, M. J., V. Setola, J. J. Irwin, C. Laggner, A. I. Abbas, S. J. Hufeisen, N. H. Jensen, M. B. Kuijer, R. C. Matos, T. B. Tran, R. Whaley, R. A. Glennon, J. Hert, K. L. Thomas, D. D. Edwards, B. K. Shoichet and B. L. Roth (2009). "Predicting new molecular targets for known drugs." Nature **462**(7270): 175-81.

Kemp, B. E., D. J. Graves, E. Benjamini and E. G. Krebs (1977). "Role of multiple basic residues in determining the substrate specificity of cyclic AMP-dependent protein kinase." J Biol Chem **252**(14): 4888-94.

Kirbach, B. B. and N. Golenhofen (2011). "Differential expression and induction of small heat shock proteins in rat brain and cultured hippocampal neurons." J Neurosci Res **89**(2): 162-75.

Klein, W. L., W. B. Stine, Jr. and D. B. Teplow (2004). "Small assemblies of unmodified amyloid beta-protein are the proximate neurotoxin in Alzheimer's disease." Neurobiol Aging **25**(5): 569-80.

Kleppisch, T. and R. Feil (2009). "cGMP signalling in the mammalian brain: role in synaptic plasticity and behaviour." Handb Exp Pharmacol(191): 549-79.

Klutchko, S., C. J. Blankley, R. W. Fleming, J. M. Hinkley, A. E. Werner, I. Nordin, A. Holmes, M. L. Hoefle, D. M. Cohen, A. D. Essenburg and et al. (1986). "Synthesis of novel angiotensin converting enzyme inhibitor quinapril and related compounds. A divergence of structure-activity relationships for non-sulfhydryl and sulfhydryl types." J Med Chem **29**(10): 1953-61.

Kozawa, O., H. Matsuno, M. Niwa, D. Hatakeyama, Y. Oiso, K. Kato and T. Uematsu (2002). "HSP20, low-molecular-weight heat shock-related protein, acts extracellularly as a regulator of platelet functions: a novel defense mechanism." Life Sci **72**(2): 113-24.

Kudva, Y. C., H. J. Hiddinga, P. C. Butler, C. S. Mueske and N. L. Eberhardt (1997). "Small heat shock proteins inhibit in vitro A beta(1-42) amyloidogenesis." FEBS Lett **416**(1): 117-21.

Kumar-Singh, S., J. Theuns, B. Van Broeck, D. Pirici, K. Vennekens, E. Corsmit, M. Cruts, B. Dermaut, R. Wang and C. Van Broeckhoven (2006). "Mean age-of-onset of familial alzheimer disease caused by presenilin mutations correlates with both increased Abeta42 and decreased Abeta40." Hum Mutat **27**(7): 686-95.

Kwan, A. H., M. Mobli, P. R. Gooley, G. F. King and J. P. Mackay (2011). "Macromolecular NMR spectroscopy for the non-spectroscopist." FEBS J **278**(5): 687-703.

Lakics, V., E. H. Karran and F. G. Boess (2010). "Quantitative comparison of phosphodiesterase mRNA distribution in human brain and peripheral tissues." Neuropharmacology **59**(6): 367-74.

Lambert, M. P., A. K. Barlow, B. A. Chromy, C. Edwards, R. Freed, M. Liosatos, T. E. Morgan, I. Rozovsky, B. Trommer, K. L. Viola, P. Wals, C. Zhang, C. E. Finch, G. A. Krafft and W. L. Klein (1998). "Diffusible, nonfibrillar ligands derived from Abeta1-42 are potent central nervous system neurotoxins." Proc Natl Acad Sci U S A **95**(11): 6448-53.

Landry, J., P. Chretien, H. Lambert, E. Hickey and L. A. Weber (1989). "Heat shock resistance conferred by expression of the human HSP27 gene in rodent cells." J Cell Biol **109**(1): 7-15.

Lanneau, D., G. Wettstein, P. Bonniaud and C. Garrido (2010). "Heat shock proteins: cell protection through protein triage." ScientificWorldJournal **10**: 1543-52.

Lavoie, J. N., G. Gingras-Breton, R. M. Tanguay and J. Landry (1993). "Induction of Chinese hamster HSP27 gene expression in mouse cells confers resistance to heat

shock. HSP27 stabilization of the microfilament organization." J Biol Chem **268**(5): 3420-9.
Lee, M. E., J. Markowitz, J.-O. Lee and H. Lee (2002). "Crystal structure of phosphodiesterase 4D and inhibitor complex." FEBS Letters **530**(1‚Äì3): 53-58.
Lee, M. E., J. Markowitz, J. O. Lee and H. Lee (2002). "Crystal structure of phosphodiesterase 4D and inhibitor complex(1)." FEBS Lett **530**(1-3): 53-8.
Lee, S., K. Carson, A. Rice-Ficht and T. Good (2006). "Small heat shock proteins differentially affect Abeta aggregation and toxicity." Biochem Biophys Res Commun **347**(2): 527-33.
Lesne, S., M. T. Koh, L. Kotilinek, R. Kayed, C. G. Glabe, A. Yang, M. Gallagher and K. H. Ashe (2006). "A specific amyloid-beta protein assembly in the brain impairs memory." Nature **440**(7082): 352-7.
LeVine, H., 3rd (1993). "Thioflavine T interaction with synthetic Alzheimer's disease beta-amyloid peptides: detection of amyloid aggregation in solution." Protein Sci **2**(3): 404-10.
Li, Y. F., Y. F. Cheng, Y. Huang, M. Conti, S. P. Wilson, J. M. O'Donnell and H. T. Zhang (2011). "Phosphodiesterase-4D knock-out and RNA interference-mediated knock-down enhance memory and increase hippocampal neurogenesis via increased cAMP signaling." J Neurosci **31**(1): 172-83.
Liang, J. J. (2000). "Interaction between beta-amyloid and lens alphaB-crystallin." FEBS Lett **484**(2): 98-101.
Lincoln, T. M. and J. D. Corbin (1977). "Adenosine 3':5'-cyclic monophosphate- and guanosine 3':5'-cyclic monophosphate-dependent protein kinases: possible homologous proteins." Proc Natl Acad Sci U S A **74**(8): 3239-43.
Liu, S., J. Li, Y. Tao and X. Xiao (2007). "Small heat shock protein alphaB-crystallin binds to p53 to sequester its translocation to mitochondria during hydrogen peroxide-induced apoptosis." Biochem Biophys Res Commun **354**(1): 109-14.
Lobner, D. (2000). "Comparison of the LDH and MTT assays for quantifying cell death: validity for neuronal apoptosis?" J Neurosci Methods **96**(2): 147-52.
Lu, Y. F., E. R. Kandel and R. D. Hawkins (1999). "Nitric oxide signaling contributes to late-phase LTP and CREB phosphorylation in the hippocampus." J Neurosci **19**(23): 10250-61.
Lugnier, C. (2006). "Cyclic nucleotide phosphodiesterase (PDE) superfamily: a new target for the development of specific therapeutic agents." Pharmacol Ther **109**(3): 366-98.
MacKenzie, S. J., G. S. Baillie, I. McPhee, C. MacKenzie, R. Seamons, T. McSorley, J. Millen, M. B. Beard, G. van Heeke and M. D. Houslay (2002). "Long PDE4 cAMP specific phosphodiesterases are activated by protein kinase A-mediated phosphorylation of a single serine residue in Upstream Conserved Region 1 (UCR1)." Br J Pharmacol **136**(3): 421-33.
Maddala, R. and V. P. Rao (2005). "alpha-Crystallin localizes to the leading edges of migrating lens epithelial cells." Exp Cell Res **306**(1): 203-15.
Mao, Y. W., J. P. Liu, H. Xiang and D. W. Li (2004). "Human alphaA- and alphaB-crystallins bind to Bax and Bcl-X(S) to sequester their translocation during staurosporine-induced apoptosis." Cell Death Differ **11**(5): 512-26.
Marchmont, R. J. and M. D. Houslay (1980). "A peripheral and an intrinsic enzyme constitute the cyclic AMP phosphodiesterase activity of rat liver plasma membranes." Biochem J **187**(2): 381-92.
Masters, C. L., G. Multhaup, G. Simms, J. Pottgiesser, R. N. Martins and K. Beyreuther (1985). "Neuronal origin of a cerebral amyloid: neurofibrillary tangles of Alzheimer's disease contain the same protein as the amyloid of plaque cores and blood vessels." EMBO J **4**(11): 2757-63.

Masters, C. L., G. Simms, N. A. Weinman, G. Multhaup, B. L. McDonald and K. Beyreuther (1985). "Amyloid plaque core protein in Alzheimer disease and Down syndrome." Proc Natl Acad Sci U S A **82**(12): 4245-9.

Mastrangelo, I. A., M. Ahmed, T. Sato, W. Liu, C. Wang, P. Hough and S. O. Smith (2006). "High-resolution atomic force microscopy of soluble Abeta42 oligomers." J Mol Biol **358**(1): 106-19.

McLean, C. A., R. A. Cherny, F. W. Fraser, S. J. Fuller, M. J. Smith, K. Beyreuther, A. I. Bush and C. L. Masters (1999). "Soluble pool of Abeta amyloid as a determinant of severity of neurodegeneration in Alzheimer's disease." Ann Neurol **46**(6): 860-6.

Millar, J. K., B. S. Pickard, S. Mackie, R. James, S. Christie, S. R. Buchanan, M. P. Malloy, J. E. Chubb, E. Huston, G. S. Baillie, P. A. Thomson, E. V. Hill, N. J. Brandon, J. C. Rain, L. M. Camargo, P. J. Whiting, M. D. Houslay, D. H. Blackwood, W. J. Muir and D. J. Porteous (2005). "DISC1 and PDE4B are interacting genetic factors in schizophrenia that regulate cAMP signaling." Science **310**(5751): 1187-91.

Morgan, C., M. Colombres, M. T. Nunez and N. C. Inestrosa (2004). "Structure and function of amyloid in Alzheimer's disease." Prog Neurobiol **74**(6): 323-49.

Mori, C., E. T. Spooner, K. E. Wisniewsk, T. M. Wisniewski, H. Yamaguch, T. C. Saido, D. R. Tolan, D. J. Selkoe and C. A. Lemere (2002). "Intraneuronal Abeta42 accumulation in Down syndrome brain." Amyloid **9**(2): 88-102.

Mosse, Y. P., M. Laudenslager, L. Longo, K. A. Cole, A. Wood, E. F. Attiyeh, M. J. Laquaglia, R. Sennett, J. E. Lynch, P. Perri, G. Laureys, F. Speleman, C. Kim, C. Hou, H. Hakonarson, A. Torkamani, N. J. Schork, G. M. Brodeur, G. P. Tonini, E. Rappaport, M. Devoto and J. M. Maris (2008). "Identification of ALK as a major familial neuroblastoma predisposition gene." Nature **455**(7215): 930-5.

Mozes, E., A. Hunya, A. Posa, B. Penke and Z. Datki (2012). "A novel method for the rapid determination of beta-amyloid toxicity on acute hippocampal slices using MTT and LDH assays." Brain Res Bull **87**(6): 521-5.

Mullan, M., F. Crawford, K. Axelman, H. Houlden, L. Lilius, B. Winblad and L. Lannfelt (1992). "A pathogenic mutation for probable Alzheimer's disease in the APP gene at the N-terminus of beta-amyloid." Nat Genet **1**(5): 345-7.

Murrell, J., M. Farlow, B. Ghetti and M. D. Benson (1991). "A mutation in the amyloid precursor protein associated with hereditary Alzheimer's disease." Science **254**(5028): 97-9.

Narberhaus, F. (2002). "Alpha-crystallin-type heat shock proteins: socializing minichaperones in the context of a multichaperone network." Microbiol Mol Biol Rev **66**(1): 64-93; table of contents.

Natesh, R., S. L. Schwager, H. R. Evans, E. D. Sturrock and K. R. Acharya (2004). "Structural details on the binding of antihypertensive drugs captopril and enalaprilat to human testicular angiotensin I-converting enzyme." Biochemistry **43**(27): 8718-24.

Nichols, M. R., M. A. Moss, D. K. Reed, S. Cratic-McDaniel, J. H. Hoh and T. L. Rosenberry (2005). "Amyloid-beta protofibrils differ from amyloid-beta aggregates induced in dilute hexafluoroisopropanol in stability and morphology." J Biol Chem **280**(4): 2471-80.

Nicolaou, P., R. Knoll, K. Haghighi, G. C. Fan, G. W. Dorn, 2nd, G. Hasenfub and E. G. Kranias (2008). "Human mutation in the anti-apoptotic heat shock protein 20 abrogates its cardioprotective effects." J Biol Chem **283**(48): 33465-71.

Nikolaev, V. O., M. Bunemann, L. Hein, A. Hannawacker and M. J. Lohse (2004). "Novel single chain cAMP sensors for receptor-induced signal propagation." J Biol Chem **279**(36): 37215-8.

Nikulina, E., J. L. Tidwell, H. N. Dai, B. S. Bregman and M. T. Filbin (2004). "The phosphodiesterase inhibitor rolipram delivered after a spinal cord lesion promotes

axonal regeneration and functional recovery." Proc Natl Acad Sci U S A **101**(23): 8786-90.
Niwa, M., A. Hara, A. Taguchi, H. Aoki, O. Kozawa and H. Mori (2009). "Spatiotemporal expression of Hsp20 and its phosphorylation in hippocampal CA1 pyramidal neurons after transient forebrain ischemia." Neurol Res **31**(7): 721-7.
Nomura, I., H. Takechi and N. Kato (2012). "Intraneuronally injected amyloid beta inhibits long-term potentiation in rat hippocampal slices." J Neurophysiol **107**(9): 2526-31.
Nussbaum, R. L. and C. E. Ellis (2003). "Alzheimer's disease and Parkinson's disease." N Engl J Med **348**(14): 1356-64.
Oddo, S., A. Caccamo, M. Kitazawa, B. P. Tseng and F. M. LaFerla (2003). "Amyloid deposition precedes tangle formation in a triple transgenic model of Alzheimer's disease." Neurobiol Aging **24**(8): 1063-70.
Oddo, S., A. Caccamo, J. D. Shepherd, M. P. Murphy, T. E. Golde, R. Kayed, R. Metherate, M. P. Mattson, Y. Akbari and F. M. LaFerla (2003). "Triple-transgenic model of Alzheimer's disease with plaques and tangles: intracellular Abeta and synaptic dysfunction." Neuron **39**(3): 409-21.
Olofsson, A., M. Lindhagen-Persson, M. Vestling, A. E. Sauer-Eriksson and A. Ohman (2009). "Quenched hydrogen/deuterium exchange NMR characterization of amyloid-beta peptide aggregates formed in the presence of Cu2+ or Zn2+." FEBS J **276**(15): 4051-60.
Orr, H. T. (2012). "Polyglutamine neurodegeneration: expanded glutamines enhance native functions." Curr Opin Genet Dev **22**(3): 251-5.
Osborne, B. W., J. Wu, C. J. McFarland, C. K. Nickl, B. Sankaran, D. E. Casteel, V. L. Woods, Jr., A. P. Kornev, S. S. Taylor and W. R. Dostmann (2011). "Crystal structure of cGMP-dependent protein kinase reveals novel site of interchain communication." Structure **19**(9): 1317-27.
Outeiro, T. F., J. Klucken, K. E. Strathearn, F. Liu, P. Nguyen, J. C. Rochet, B. T. Hyman and P. J. McLean (2006). "Small heat shock proteins protect against alpha-synuclein-induced toxicity and aggregation." Biochem Biophys Res Commun **351**(3): 631-8.
Page, C. P. and D. Spina (2012). "Selective PDE inhibitors as novel treatments for respiratory diseases." Curr Opin Pharmacol **12**(3): 275-86.
Paul, S. M., D. S. Mytelka, C. T. Dunwiddie, C. C. Persinger, B. H. Munos, S. R. Lindborg and A. L. Schacht (2010). "How to improve R&D productivity: the pharmaceutical industry's grand challenge." Nat Rev Drug Discov **9**(3): 203-14.
Penke, B., Z. Datki, C. Hetenyi, Z. Molnar, I. Lengyel, K. Soos and M. Zarandi (2003). "Molecular pathomechanisms of Alzheimer’s disease." Journal of Molecular Structure (Theochem)(666-667): 507-513.
Perez-Torres, S., R. Cortes, M. Tolnay, A. Probst, J. M. Palacios and G. Mengod (2003). "Alterations on phosphodiesterase type 7 and 8 isozyme mRNA expression in Alzheimer's disease brains examined by in situ hybridization." Exp Neurol **182**(2): 322-34.
Perez-Torres, S., X. Miro, J. M. Palacios, R. Cortes, P. Puigdomenech and G. Mengod (2000). "Phosphodiesterase type 4 isozymes expression in human brain examined by in situ hybridization histochemistry and[3H]rolipram binding autoradiography. Comparison with monkey and rat brain." J Chem Neuroanat **20**(3-4): 349-74.
Pike, C. J., A. J. Walencewicz, C. G. Glabe and C. W. Cotman (1991). "In vitro aging of beta-amyloid protein causes peptide aggregation and neurotoxicity." Brain Res **563**(1-2): 311-4.
Podlisny, M. B., G. Lee and D. J. Selkoe (1987). "Gene dosage of the amyloid beta precursor protein in Alzheimer's disease." Science **238**(4827): 669-71.
Ponsioen, B., J. Zhao, J. Riedl, F. Zwartkruis, G. van der Krogt, M. Zaccolo, W. H. Moolenaar, J. L. Bos and K. Jalink (2004). "Detecting cAMP-induced Epac

activation by fluorescence resonance energy transfer: Epac as a novel cAMP indicator." EMBO Rep **5**(12): 1176-80.
Prasher, V. P., M. J. Farrer, A. M. Kessling, E. M. Fisher, R. J. West, P. C. Barber and A. C. Butler (1998). "Molecular mapping of Alzheimer-type dementia in Down's syndrome." Ann Neurol **43**(3): 380-3.
Prickaerts, J., A. Sik, W. C. van Staveren, G. Koopmans, H. W. Steinbusch, F. J. van der Staay, J. de Vente and A. Blokland (2004). "Phosphodiesterase type 5 inhibition improves early memory consolidation of object information." Neurochem Int **45**(6): 915-28.
Prickaerts, J., W. C. van Staveren, A. Sik, M. Markerink-van Ittersum, U. Niewohner, F. J. van der Staay, A. Blokland and J. de Vente (2002). "Effects of two selective phosphodiesterase type 5 inhibitors, sildenafil and vardenafil, on object recognition memory and hippocampal cyclic GMP levels in the rat." Neuroscience **113**(2): 351-61.
Puzzo, D., A. Staniszewski, S. X. Deng, L. Privitera, E. Leznik, S. Liu, H. Zhang, Y. Feng, A. Palmeri, D. W. Landry and O. Arancio (2009). "Phosphodiesterase 5 inhibition improves synaptic function, memory, and amyloid-beta load in an Alzheimer's disease mouse model." J Neurosci **29**(25): 8075-86.
Puzzo, D., O. Vitolo, F. Trinchese, J. P. Jacob, A. Palmeri and O. Arancio (2005). "Amyloid-beta peptide inhibits activation of the nitric oxide/cGMP/cAMP-responsive element-binding protein pathway during hippocampal synaptic plasticity." J Neurosci **25**(29): 6887-97.
Qian, J., X. Ren, X. Wang, P. Zhang, W. K. Jones, J. D. Molkentin, G. C. Fan and E. G. Kranias (2009). "Blockade of Hsp20 phosphorylation exacerbates cardiac ischemia/reperfusion injury by suppressed autophagy and increased cell death." Circ Res **105**(12): 1223-31.
Qin, L., J. Vastl and J. Gao (2010). "Highly sensitive amyloid detection enabled by thioflavin T dimers." Mol Biosyst **6**(10): 1791-5.
Quinn, S. D., P. A. Dalgarno, R. T. Cameron, G. J. Hedley, C. Hacker, J. M. Lucocq, G. S. Baillie, I. D. Samuel and J. C. Penedo (2014). "Real-time probing of beta-amyloid self-assembly and inhibition using fluorescence self-quenching between neighbouring dyes." Mol Biosyst **10**(1): 34-44.
Rabe, K. F., E. D. Bateman, D. O'Donnell, S. Witte, D. Bredenbroker and T. D. Bethke (2005). "Roflumilast--an oral anti-inflammatory treatment for chronic obstructive pulmonary disease: a randomised controlled trial." Lancet **366**(9485): 563-71.
Raman, B., T. Ban, M. Sakai, S. Y. Pasta, T. Ramakrishna, H. Naiki, Y. Goto and M. Rao Ch (2005). "AlphaB-crystallin, a small heat-shock protein, prevents the amyloid fibril growth of an amyloid beta-peptide and beta2-microglobulin." Biochem J **392**(Pt 3): 573-81.
Ravati, A., V. Junker, M. Kouklei, B. Ahlemeyer, C. Culmsee and J. Krieglstein (1999). "Enalapril and moexipril protect from free radical-induced neuronal damage in vitro and reduce ischemic brain injury in mice and rats." Eur J Pharmacol **373**(1): 21-33.
Reifert, J., D. Hartung-Cranston and S. C. Feinstein (2011). "Amyloid beta-mediated cell death of cultured hippocampal neurons reveals extensive Tau fragmentation without increased full-length tau phosphorylation." J Biol Chem **286**(23): 20797-811.
Reinke, A. A. and J. E. Gestwicki (2007). "Structure-activity relationships of amyloid beta-aggregation inhibitors based on curcumin: influence of linker length and flexibility." Chem Biol Drug Des **70**(3): 206-15.
Reitz, C. (2012). "Alzheimer's disease and the amyloid cascade hypothesis: a critical review." Int J Alzheimers Dis **2012**: 369808.

Relkin, N. R., P. Szabo, B. Adamiak, T. Burgut, C. Monthe, R. W. Lent, S. Younkin, L. Younkin, R. Schiff and M. E. Weksler (2009). "18-Month study of intravenous immunoglobulin for treatment of mild Alzheimer disease." Neurobiol Aging **30**(11): 1728-36.

Rembold, C. M., D. B. Foster, J. D. Strauss, C. J. Wingard and J. E. Eyk (2000). "cGMP-mediated phosphorylation of heat shock protein 20 may cause smooth muscle relaxation without myosin light chain dephosphorylation in swine carotid artery." J Physiol **524 Pt 3**: 865-78.

Reneerkens, O. A., K. Rutten, H. W. Steinbusch, A. Blokland and J. Prickaerts (2009). "Selective phosphodiesterase inhibitors: a promising target for cognition enhancement." Psychopharmacology (Berl) **202**(1-3): 419-43.

Rentero, C., A. Monfort and P. Puigdomenech (2003). "Identification and distribution of different mRNA variants produced by differential splicing in the human phosphodiesterase 9A gene." Biochem Biophys Res Commun **301**(3): 686-92.

Reyes-Irisarri, E., M. Markerink-Van Ittersum, G. Mengod and J. de Vente (2007). "Expression of the cGMP-specific phosphodiesterases 2 and 9 in normal and Alzheimer's disease human brains." Eur J Neurosci **25**(11): 3332-8.

Ritossa, F. M. (1964). "Behaviour of Rna and DNA Synthesis at the Puff Level in Salivary Gland Chromosomes of Drosophila." Exp Cell Res **36**: 515-23.

Robakis, N. K., N. Ramakrishna, G. Wolfe and H. M. Wisniewski (1987). "Molecular cloning and characterization of a cDNA encoding the cerebrovascular and the neuritic plaque amyloid peptides." Proc Natl Acad Sci U S A **84**(12): 4190-4.

Rogalla, T., M. Ehrnsperger, X. Preville, A. Kotlyarov, G. Lutsch, C. Ducasse, C. Paul, M. Wieske, A. P. Arrigo, J. Buchner and M. Gaestel (1999). "Regulation of Hsp27 oligomerization, chaperone function, and protective activity against oxidative stress/tumor necrosis factor alpha by phosphorylation." J Biol Chem **274**(27): 18947-56.

Roher, A. E. and Y. M. Kuo (1999). "Isolation of amyloid deposits from brain." Methods Enzymol **309**: 58-67.

Rosales, J. L., K. Sarker, N. Ho, M. Broniewska, P. Wong, M. Cheng, F. A. van der Hoorn and K. Y. Lee (2007). "ODF1 phosphorylation by Cdk5/p35 enhances ODF1-OIP1 interaction." Cell Physiol Biochem **20**(5): 311-8.

Rubbo, S. D. and J. Cymerman-Craig (1955). "Anti-tuberculous activity of verazide (1-isonicotinoyl-2-veratrylidene hydrazine)." Nature **176**(4488): 887.

Sa, M. S., M. N. de Menezes, A. U. Krettli, I. M. Ribeiro, T. C. Tomassini, R. Ribeiro dos Santos, W. F. de Azevedo, Jr. and M. B. Soares (2011). "Antimalarial activity of physalins B, D, F, and G." J Nat Prod **74**(10): 2269-72.

Salomon, A. R., K. J. Marcinowski, R. P. Friedland and M. G. Zagorski (1996). "Nicotine inhibits amyloid formation by the beta-peptide." Biochemistry **35**(42): 13568-78.

Santhoshkumar, P. and K. K. Sharma (2004). "Inhibition of amyloid fibrillogenesis and toxicity by a peptide chaperone." Mol Cell Biochem **267**(1-2): 147-55.

Schaal, S. M., M. S. Garg, M. Ghosh, L. Lovera, M. Lopez, M. Patel, J. Louro, S. Patel, L. Tuesta, W. M. Chan and D. D. Pearse (2012). "The therapeutic profile of rolipram, PDE target and mechanism of action as a neuroprotectant following spinal cord injury." PLoS One **7**(9): e43634.

Schudt, C., S. Winder, B. Muller and D. Ukena (1991). "Zardaverine as a selective inhibitor of phosphodiesterase isozymes." Biochem Pharmacol **42**(1): 153-62.

Schwabe, U., M. Miyake, Y. Ohga and J. W. Daly (1976). "4-(3-Cyclopentyloxy-4-methoxyphenyl)-2-pyrrolidone (ZK 62711): a potent inhibitor of adenosine cyclic 3',5'-monophosphate phosphodiesterases in homogenates and tissue slices from rat brain." Mol Pharmacol **12**(6): 900-10.

Selkoe, D. J. (1991). "The molecular pathology of Alzheimer's disease." Neuron **6**(4): 487-98.

Selkoe, D. J. (2002). "Alzheimer's disease is a synaptic failure." Science **298**(5594): 789-91.
Selkoe, D. J., C. R. Abraham, M. B. Podlisny and L. K. Duffy (1986). "Isolation of low-molecular-weight proteins from amyloid plaque fibers in Alzheimer's disease." J Neurochem **46**(6): 1820-34.
Selkoe, D. J. and D. Schenk (2003). "Alzheimer's disease: molecular understanding predicts amyloid-based therapeutics." Annu Rev Pharmacol Toxicol **43**: 545-84.
Shemetov, A. A., A. S. Seit-Nebi and N. B. Gusev (2008). "Structure, properties, and functions of the human small heat-shock protein HSP22 (HspB8, H11, E2IG1): a critical review." J Neurosci Res **86**(2): 264-9.
Shinohara, H., Y. Inaguma, S. Goto, T. Inagaki and K. Kato (1993). "Alpha B crystallin and HSP28 are enhanced in the cerebral cortex of patients with Alzheimer's disease." J Neurol Sci **119**(2): 203-8.
Silva, A. J., J. H. Kogan, P. W. Frankland and S. Kida (1998). "CREB and memory." Annu Rev Neurosci **21**: 127-48.
Simmons, L. K., P. C. May, K. J. Tomaselli, R. E. Rydel, K. S. Fuson, E. F. Brigham, S. Wright, I. Lieberburg, G. W. Becker, D. N. Brems and et al. (1994). "Secondary structure of amyloid beta peptide correlates with neurotoxic activity in vitro." Mol Pharmacol **45**(3): 373-9.
Sin, Y. Y., H. V. Edwards, X. Li, J. P. Day, F. Christian, A. J. Dunlop, D. R. Adams, M. Zaccolo, M. D. Houslay and G. S. Baillie "Disruption of the cyclic AMP phosphodiesterase-4 (PDE4)-HSP20 complex attenuates the beta-agonist induced hypertrophic response in cardiac myocytes." J Mol Cell Cardiol **50**(5): 872-83.
Sin, Y. Y., H. V. Edwards, X. Li, J. P. Day, F. Christian, A. J. Dunlop, D. R. Adams, M. Zaccolo, M. D. Houslay and G. S. Baillie (2011). "Disruption of the cyclic AMP phosphodiesterase-4 (PDE4)-HSP20 complex attenuates the beta-agonist induced hypertrophic response in cardiac myocytes." J Mol Cell Cardiol **50**(5): 872-83.
Smith, D. L., J. Pozueta, B. Gong, O. Arancio and M. Shelanski (2009). "Reversal of long-term dendritic spine alterations in Alzheimer disease models." Proc Natl Acad Sci U S A **106**(39): 16877-82.
Soderling, S. H., S. J. Bayuga and J. A. Beavo (1998). "Identification and characterization of a novel family of cyclic nucleotide phosphodiesterases." J Biol Chem **273**(25): 15553-8.
Soto, C., E. M. Sigurdsson, L. Morelli, R. A. Kumar, E. M. Castano and B. Frangione (1998). "Beta-sheet breaker peptides inhibit fibrillogenesis in a rat brain model of amyloidosis: implications for Alzheimer's therapy." Nat Med **4**(7): 822-6.
Spiecker, M., I. Lorenz, N. Marx and H. Darius (2002). "Tranilast inhibits cytokine-induced nuclear factor kappaB activation in vascular endothelial cells." Mol Pharmacol **62**(4): 856-63.
Spillantini, M. G., R. A. Crowther, R. Jakes, M. Hasegawa and M. Goedert (1998). "alpha-Synuclein in filamentous inclusions of Lewy bodies from Parkinson's disease and dementia with lewy bodies." Proc Natl Acad Sci U S A **95**(11): 6469-73.
Stege, G. J., K. Renkawek, P. S. Overkamp, P. Verschuure, A. F. van Rijk, A. Reijnen-Aalbers, W. C. Boelens, G. J. Bosman and W. W. de Jong (1999). "The molecular chaperone alphaB-crystallin enhances amyloid beta neurotoxicity." Biochem Biophys Res Commun **262**(1): 152-6.
Sticht, H., P. Bayer, D. Willbold, S. Dames, C. Hilbich, K. Beyreuther, R. W. Frank and P. Rosch (1995). "Structure of amyloid A4-(1-40)-peptide of Alzheimer's disease." Eur J Biochem **233**(1): 293-8.
Sun, Y. and T. H. MacRae (2005). "The small heat shock proteins and their role in human disease." FEBS J **272**(11): 2613-27.

Sunde, M., L. C. Serpell, M. Bartlam, P. E. Fraser, M. B. Pepys and C. C. Blake (1997). "Common core structure of amyloid fibrils by synchrotron X-ray diffraction." J Mol Biol **273**(3): 729-39.

Tallot, P., J. F. Grongnet and J. C. David (2003). "Dual perinatal and developmental expression of the small heat shock proteins [FC12]aB-crystallin and Hsp27 in different tissues of the developing piglet." Biol Neonate **83**(4): 281-8.

Tanzi, R. E., J. F. Gusella, P. C. Watkins, G. A. Bruns, P. St George-Hyslop, M. L. Van Keuren, D. Patterson, S. Pagan, D. M. Kurnit and R. L. Neve (1987). "Amyloid beta protein gene: cDNA, mRNA distribution, and genetic linkage near the Alzheimer locus." Science **235**(4791): 880-4.

Tasken, K. and E. M. Aandahl (2004). "Localized effects of cAMP mediated by distinct routes of protein kinase A." Physiol Rev **84**(1): 137-67.

Tegge, W., R. Frank, F. Hofmann and W. R. Dostmann (1995). "Determination of cyclic nucleotide-dependent protein kinase substrate specificity by the use of peptide libraries on cellulose paper." Biochemistry **34**(33): 10569-77.

Terry, R. D., E. Masliah, D. P. Salmon, N. Butters, R. DeTeresa, R. Hill, L. A. Hansen and R. Katzman (1991). "Physical basis of cognitive alterations in Alzheimer's disease: synapse loss is the major correlate of cognitive impairment." Ann Neurol **30**(4): 572-80.

Tessier, D. J., P. Komalavilas, E. McLemore, J. Thresher and C. M. Brophy (2004). "Sildenafil-induced vasorelaxation is associated with increases in the phosphorylation of the heat shock-related protein 20 (HSP20)." J Surg Res **118**(1): 21-5.

Tissieres, A., H. K. Mitchell and U. M. Tracy (1974). "Protein synthesis in salivary glands of Drosophila melanogaster: relation to chromosome puffs." J Mol Biol **84**(3): 389-98.

Tjernberg, L. O., J. Naslund, F. Lindqvist, J. Johansson, A. R. Karlstrom, J. Thyberg, L. Terenius and C. Nordstedt (1996). "Arrest of beta-amyloid fibril formation by a pentapeptide ligand." J Biol Chem **271**(15): 8545-8.

Treweek, T. M., H. Ecroyd, D. M. Williams, S. Meehan, J. A. Carver and M. J. Walker (2007). "Site-directed mutations in the C-terminal extension of human alphaB-crystallin affect chaperone function and block amyloid fibril formation." PLoS One **2**(10): e1046.

Triner, L., Y. Vulliemoz, I. Schwartz and G. G. Nahas (1970). "Cyclic phosphodiesterase activity and the action of papaverine." Biochem Biophys Res Commun **40**(1): 64-9.

Tully, T., R. Bourtchouladze, R. Scott and J. Tallman (2003). "Targeting the CREB pathway for memory enhancers." Nat Rev Drug Discov **2**(4): 267-77.

Van Broeckhoven, C., J. Haan, E. Bakker, J. A. Hardy, W. Van Hul, A. Wehnert, M. Vegter-Van der Vlis and R. A. Roos (1990). "Amyloid beta protein precursor gene and hereditary cerebral hemorrhage with amyloidosis (Dutch)." Science **248**(4959): 1120-2.

van de Klundert, F. A., R. H. Smulders, M. L. Gijsen, R. A. Lindner, R. Jaenicke, J. A. Carver and W. W. de Jong (1998). "The mammalian small heat-shock protein Hsp20 forms dimers and is a poor chaperone." Eur J Biochem **258**(3): 1014-21.

van der Staay, F. J., K. Rutten, L. Barfacker, J. Devry, C. Erb, H. Heckroth, D. Karthaus, A. Tersteegen, M. van Kampen, A. Blokland, J. Prickaerts, K. G. Reymann, U. H. Schroder and M. Hendrix (2008). "The novel selective PDE9 inhibitor BAY 73-6691 improves learning and memory in rodents." Neuropharmacology **55**(5): 908-18.

van Montfort, R. L., E. Basha, K. L. Friedrich, C. Slingsby and E. Vierling (2001). "Crystal structure and assembly of a eukaryotic small heat shock protein." Nat Struct Biol **8**(12): 1025-30.

Van Nostrand, W. E., J. P. Melchor, H. S. Cho, S. M. Greenberg and G. W. Rebeck (2001). "Pathogenic effects of D23N Iowa mutant amyloid beta -protein." J Biol Chem **276**(35): 32860-6.

Van Staveren, W. C., H. W. Steinbusch, M. Markerink-Van Ittersum, D. R. Repaske, M. F. Goy, J. Kotera, K. Omori, J. A. Beavo and J. De Vente (2003). "mRNA expression patterns of the cGMP-hydrolyzing phosphodiesterases types 2, 5, and 9 during development of the rat brain." J Comp Neurol **467**(4): 566-80.

Vasudevan, S. R., J. B. Moore, Y. Schymura and G. C. Churchill "Shape-based reprofiling of FDA-approved drugs for the H(1) histamine receptor." J Med Chem **55**(16): 7054-60.

Vasudevan, S. R., J. B. Moore, Y. Schymura and G. C. Churchill (2012). "Shape-based reprofiling of FDA-approved drugs for the H(1) histamine receptor." J Med Chem **55**(16): 7054-60.

Verschuure, P., C. Tatard, W. C. Boelens, J. F. Grongnet and J. C. David (2003). "Expression of small heat shock proteins HspB2, HspB8, Hsp20 and cvHsp in different tissues of the perinatal developing pig." Eur J Cell Biol **82**(10): 523-30.

Vitolo, O. V., A. Sant'Angelo, V. Costanzo, F. Battaglia, O. Arancio and M. Shelanski (2002). "Amyloid beta -peptide inhibition of the PKA/CREB pathway and long-term potentiation: reversibility by drugs that enhance cAMP signaling." Proc Natl Acad Sci U S A **99**(20): 13217-21.

Vos, M. J., M. P. Zijlstra, B. Kanon, M. A. van Waarde-Verhagen, E. R. Brunt, H. M. Oosterveld-Hut, S. Carra, O. C. Sibon and H. H. Kampinga (2010). "HSPB7 is the most potent polyQ aggregation suppressor within the HSPB family of molecular chaperones." Hum Mol Genet **19**(23): 4677-93.

Walsh, D. M., A. Lomakin, G. B. Benedek, M. M. Condron and D. B. Teplow (1997). "Amyloid beta-protein fibrillogenesis. Detection of a protofibrillar intermediate." J Biol Chem **272**(35): 22364-72.

Walsh, D. M. and D. J. Selkoe (2007). "A beta oligomers - a decade of discovery." J Neurochem **101**(5): 1172-84.

Wang, C., X. M. Yang, Y. Y. Zhuo, H. Zhou, H. B. Lin, Y. F. Cheng, J. P. Xu and H. T. Zhang (2012). "The phosphodiesterase-4 inhibitor rolipram reverses Abeta-induced cognitive impairment and neuroinflammatory and apoptotic responses in rats." Int J Neuropsychopharmacol **15**(6): 749-66.

Wang, J., D. W. Dickson, J. Q. Trojanowski and V. M. Lee (1999). "The levels of soluble versus insoluble brain Abeta distinguish Alzheimer's disease from normal and pathologic aging." Exp Neurol **158**(2): 328-37.

Wang, J., K. Ono, D. L. Dickstein, I. Arrieta-Cruz, W. Zhao, X. Qian, A. Lamparello, R. Subnani, M. Ferruzzi, C. Pavlides, L. Ho, P. R. Hof, D. B. Teplow and G. M. Pasinetti (2010). "Carvedilol as a potential novel agent for the treatment of Alzheimer's disease." Neurobiol Aging **32**(12): 2321 e1-12.

Wang, X., B. Zingarelli, M. O'Connor, P. Zhang, A. Adeyemo, E. G. Kranias, Y. Wang and G. C. Fan (2009). "Overexpression of Hsp20 prevents endotoxin-induced myocardial dysfunction and apoptosis via inhibition of NF-kappaB activation." J Mol Cell Cardiol **47**(3): 382-90.

Weller, A. (2006). "The ontogeny of postingestive inhibitory stimuli: examining the role of CCK." Dev Psychobiol **48**(5): 368-79.

Wilhelmus, M. M., W. C. Boelens, M. Kox, M. L. Maat-Schieman, R. Veerhuis, R. M. de Waal and M. M. Verbeek (2009). "Small heat shock proteins associated with cerebral amyloid angiopathy of hereditary cerebral hemorrhage with amyloidosis (Dutch type) induce interleukin-6 secretion." Neurobiol Aging **30**(2): 229-40.

Wilhelmus, M. M., W. C. Boelens, I. Otte-Holler, B. Kamps, R. M. de Waal and M. M. Verbeek (2006). "Small heat shock proteins inhibit amyloid-beta protein

aggregation and cerebrovascular amyloid-beta protein toxicity." Brain Res **1089**(1): 67-78.
Wilhelmus, M. M., W. C. Boelens, I. Otte-Holler, B. Kamps, B. Kusters, M. L. Maat-Schieman, R. M. de Waal and M. M. Verbeek (2006). "Small heat shock protein HspB8: its distribution in Alzheimer's disease brains and its inhibition of amyloid-beta protein aggregation and cerebrovascular amyloid-beta toxicity." Acta Neuropathol **111**(2): 139-49.
Wilhelmus, M. M., I. Otte-Holler, P. Wesseling, R. M. de Waal, W. C. Boelens and M. M. Verbeek (2006). "Specific association of small heat shock proteins with the pathological hallmarks of Alzheimer's disease brains." Neuropathol Appl Neurobiol **32**(2): 119-30.
Wischik, C. M., M. Novak, P. C. Edwards, A. Klug, W. Tichelaar and R. A. Crowther (1988). "Structural characterization of the core of the paired helical filament of Alzheimer disease." Proc Natl Acad Sci U S A **85**(13): 4884-8.
Wischik, C. M., M. Novak, H. C. Thogersen, P. C. Edwards, M. J. Runswick, R. Jakes, J. E. Walker, C. Milstein, M. Roth and A. Klug (1988). "Isolation of a fragment of tau derived from the core of the paired helical filament of Alzheimer disease." Proc Natl Acad Sci U S A **85**(12): 4506-10.
Wisniewski, T., J. Ghiso and B. Frangione (1991). "Peptides homologous to the amyloid protein of Alzheimer's disease containing a glutamine for glutamic acid substitution have accelerated amyloid fibril formation." Biochem Biophys Res Commun **180**(3): 1528.
Wunder, F., A. Tersteegen, A. Rebmann, C. Erb, T. Fahrig and M. Hendrix (2005). "Characterization of the first potent and selective PDE9 inhibitor using a cGMP reporter cell line." Mol Pharmacol **68**(6): 1775-81.
Wyvratt, M. J. and A. A. Patchett (1985). "Recent developments in the design of angiotensin-converting enzyme inhibitors." Med Res Rev **5**(4): 483-531.
Xu, Y., H. T. Zhang and J. M. O'Donnell (2011). "Phosphodiesterases in the central nervous system: implications in mood and cognitive disorders." Handb Exp Pharmacol(204): 447-85.
Zagorski, M. G. and C. J. Barrow (1992). "NMR studies of amyloid beta-peptides: proton assignments, secondary structure, and mechanism of an alpha-helix----beta-sheet conversion for a homologous, 28-residue, N-terminal fragment." Biochemistry **31**(24): 5621-31.
Zeng, H., Y. Zhang, L. Peng, H. Shao, N. K. Menon, J. Yang, A. R. Salomon, R. P. Freidland and M. G. Zagorski (2001). "Nicotine and amyloid formation." Biol Psychiatry **49**(3): 248-57.
Zeng, L., J. Tan, Z. Hu, W. Lu and B. Yang (2010). "Hsp20 protects neuroblastoma cells from ischemia/reperfusion injury by inhibition of apoptosis via a mechanism that involves the mitochondrial pathways." Curr Neurovasc Res **7**(4): 281-7.
Zeng, L., J. Tan, W. Lu and Z. Hu (2013). "Blockade of Ser16-Hsp20 Phosphorylation Attenuates Neuroprotection Dependent Upon Bcl-2 and Bax." Curr Neurovasc Res.
Zhang, J., J. Guo, X. Zhao, Z. Chen, G. Wang, A. Liu, Q. Wang, W. Zhou, Y. Xu and C. Wang (2013). "Phosphodiesterase-5 inhibitor sildenafil prevents neuroinflammation, lowers beta-amyloid levels and improves cognitive performance in APP/PS1 transgenic mice." Behav Brain Res **250**: 230-7.
Zhang, K. Y., P. N. Ibrahim, S. Gillette and G. Bollag (2005). "Phosphodiesterase-4 as a potential drug target." Expert Opin Ther Targets **9**(6): 1283-305.
Zhang, R., Y. Wang, L. Zhang, Z. Zhang, W. Tsang, M. Lu and M. Chopp (2002). "Sildenafil (Viagra) induces neurogenesis and promotes functional recovery after stroke in rats." Stroke **33**(11): 2675-80.

Zhang, X., X. Wang, H. Zhu, E. G. Kranias, Y. Tang, T. Peng, J. Chang and G. C. Fan (2012). "Hsp20 functions as a novel cardiokine in promoting angiogenesis via activation of VEGFR2." PLoS One **7**(3): e32765.

Zheng, H. and E. H. Koo (2006). "The amyloid precursor protein: beyond amyloid." Mol Neurodegener **1**: 5.

Zourlidou, A., M. D. Payne Smith and D. S. Latchman (2004). "HSP27 but not HSP70 has a potent protective effect against alpha-synuclein-induced cell death in mammalian neuronal cells." J Neurochem **88**(6): 1439-48.